Optimization of Recombinant Protein Production by a Fungal Host

by

Reza Gheshlaghi

A thesis
presented to the University of Waterloo
in fulfillment of the
thesis requirement for the degree of
Doctor of Philosophy
in
Chemical Engineering

Waterloo, Ontario, Canada, 2007

I hereby declare that I am the sole author of this thesis. This is a true copy of the thesis, including any required final revisions, as accepted by my examiners.

I understand that my thesis may be made electronically available to the public.

Reza Gheshlaghi

ABSTRACT

The natural ability of filamentous fungi to synthesize, glycosylate, and secrete high levels of protein products has made them potentially attractive hosts for heterologous protein production. Advances in fungal genetics enabled the expression of several high value proteins in filamentous fungi. Particularly the genus, *Aspergillus* has proven to be potentially useful for the expression of eukaryotic gene products. This thesis pertains to the optimization of recombinant protein production by the fungal host, *Aspergillus n*iger. The target recombinant protein of interest is hen's egg white lysozyme (HEWL). This protein encoded in the genome resulting in relatively stable gene construct; however, it is subject to extracellular protease attack.

The objective of the proposed research is the development and application of engineering methodology for the analysis and optimization of a fungal bioprocess for recombinant protein production. The underlying hypothesis is that a significant improvement of target protein productivity is achievable by using appropriate optimization techniques.

To accomplish this, during the first phase of this study a statistically based experimental method was used to systematically elucidate the effect of medium components (starch, peptone, ammonium sulfate, yeast extract, and $CaCl_2.2H_2O$) on hen's egg white lysozyme production by *Aspergillus niger* HEWL WT-13-16. A 2^{5-1} fractional factorial design augmented with center points revealed that peptone, starch, and ammonium sulfate were the most significant factors, whereas the other medium components were not important within the levels tested. Then, the method of steepest ascent was employed to approach the proximity of optimum. This task was followed by a central composite design to develop a response surface for medium optimization. The optimum medium composition for lysozyme production was found to be: starch 34 gL^{-1}, peptone 34 gL^{-1}, ammonium sulfate 11.9 gL^{-1}, yeast extract 0.5 gL^{-1}, and $CaCl_2.2H_2O$ 0.5 g L^{-1}. This medium was projected to produce theoretically 212 mgL^{-1} lysozyme. Using this optimized medium, an experimentally observed maximum lysozyme concentration of 209 ± 18 mgL^{-1} verified the applied methodology.

A second optimization approach was based on metabolic flux analysis (MFA). A comprehensive metabolic network comprising three intracellular compartments (cytoplasm, mitochondrion and peroxisome) was developed for *Aspergillus niger*. The metabolic flux network included carbohydrate and amino acid metabolism in both anabolic and catabolic reactions. According to experimental observations, the time course of fermentation was divided into five phases, each with unique physiological properties. The network was used to form a set of linear algebraic equations based on the stoichiometry of the reactions by assuming pseudo-steady state for intracellular metabolites. The metabolic flux model consists of 137 metabolites and 287 processes, of which 181 represent biochemical conversions and 106 represent transport processes between the different compartments and the extracellular environment. In addition, due to the physiological evidence some biochemical reactions considered to be active only in one direction. Linear programming was used for optimizing of the specific growth rate as the objective function in combination with 37 measured input and output fluxes of the key metabolites to evaluate corresponding intracellular flux distributions throughout the batch fermentations. The general applicability of the methodology was evaluated by establishing commonality to optimize recombinant HEWL production. The proposed model was able to predict correctly the specific growth rate, oxygen uptake rate, and carbon dioxide evolution rate with good precision.

The results of the metabolic flux and sensitivity analysis were employed for medium design. Growth was biphasic; glucose was utilized initially as the carbon source and was followed by its oxidation product, gluconate, later. Logarithmic sensitivity analysis revealed that the addition of proline, alanine and glutamate benefited growth in defined media. The experimental observations and flux analysis showed that tyrosine was a potential candidate for biomass production improvement. The two amino acids, namely proline and tyrosine benefited biomass production during the initial growth phases. Glutamate and alanine were particularly important during the latter stages of the batch process.

A series of growth studies were conducted with the identified amino acids added in the medium. In these preliminary nutritional experiments the contribution to growth enhancement was 46% for proline, 23% for glutamate, and 22% for tyrosine. Model

predictions were further verified by conducting batch and fed-batch fermentations in a 7- liter bioreactor. The programmed addition of four amino acids (proline, glutamate, alanine, and tyrosine) according to a predetermined schedule resulted in a 44% improvement in biomass and 41% improvement in recombinant protein production. The experiments also confirmed the model prediction that extra amount of amino acids besides the identified ones would not significantly enhance biomass and the recombinant protein production.

A computer-based control system was developed for the on-line monitoring and control of the major state variables (e.g., temperature, pH, and DO) during the time course of fermentation. The graphical programming environment, LabVIEW was used to acquire and integrate these variables in a supervisor computer. The temperature of the bioreactor during sterilization and fermentation was controlled using a cascade methodology. The controller parameters of the master and slave loops were determined experimentally to yield a smooth response with minimum overshoot of both the bioreactor and jacket temperatures. The program scheduled various required steps in an established order during the fermentation. This feature of the software guarantees that every necessary operation will be met. The graphical representation of the process is displayed on the screen and helps the user to follow the process and perform the required adjustments. Furthermore, different variables can be observed simultaneously and saved in text or spreadsheet files for further analysis.

ACKNOWLEDGEMENTS

I would like to express my deep gratitude and appreciation to my supervisors, Professor Jeno M. Scharer, Professor Murray Moo-Young, and Professor Peter L. Douglas for their valuable guidance, support and encouragement in both my academic work and life in general. I consider myself fortunate to have had the chance to learn from such excellent mentors.

I would also like to thank Professor Owen P. Ward, Professor Ali Elkamel, and Professor C. Perry Chou for serving as my committee members and providing me with constructive comments for this thesis.

My appreciations go to external examiner Professor Alain Garnier for his guidance and valuable comments.

I would like to extend my special thanks to Ms. Jana Otruba, technician of the biotechnology laboratory, Mrs. Patricia Anderson graduate administrative assistant in the Department of Chemical Engineering for clerical helps as well as, Mr. Bert Habischer, Mr. Ralph Dickhout, Mr. Dennis Herman, and Mr. Rick Hecktus for their various technical supports throughout the duration of this research. My thanks extend to Mr. Joseph S. Clifford and Mr. Dominik J. Lohmann for explaining the use of the Varian ProStar HPLC system.

My sincere gratitude goes to those friends I have made during the course of my studies in Waterloo, many thanks to Drs. Mazda Biglari, Zairossani Nor, Ali Nowruzian and Sam Guo, Keyvan Nowruzi, Nima Rezaei, Saeid Mehdiabadi, and Yali Xu for their advice, comments and moral support.

I appreciate the Ministry of Science, Research, and Technology of Iran for the sponsorship of my PhD studies as well as NSERC and CellNet for their financial support.

I would like to express my deepest gratitude and love to my parents for their love and constant encouragement throughout my life. I am extremely grateful for the support of my wife, Maryam Khandandel Moghani for her love, patience, and sacrifice. Finally, I would like to extend my special love to my son, Hooman and daughter Melika who fill my life with joy and happiness.

TABLE OF CONTENTS

LIST OF TABLES

LIST OF FIGURES

CHAPTER 1

INTRODUCTION

1.1 Recombinant Protein Over-expression

The over-expression of a recombinant cell product is the primary goal in any biopharmaceutical process. In this regard, several strategies such as strain development, medium optimization, bioprocess optimization, and mathematical modeling have been widely used. A wide range of parameters can effect growth and product formation in a fungal fermentation process, including medium composition, pH, temperature, dissolved oxygen, shear stress, and fungal morphology (Xu et al., 2000). Extra care must be applied when the fermentation process employs a recombinant host. Medium development is of outmost importance when developing an industrial fermentation, because cell growth and metabolite production are strongly influenced by medium composition (e.g., carbon, organic nitrogen, and inorganic salts) and environmental conditions (e.g., temperature, agitation, and pH) (Wang et al., 2003a). Traditional method of optimization involves varying one factor at a time, while keeping the others constant. This strategy is simple and easy to implement with no need for statistical analysis; although, it may require a relatively large number of experiments and frequently fails to achieve optimal conditions (Kalil et al., 2000). This important shortcoming is due to the inability of the approach to consider the effect of possible interactions between factors. This deficiency can be overcome by applying more efficient, statistically based experimental design (Rathi et al., 2002).

In this regard, factorial experimental design and response surface analysis are important tools to determine optimal process conditions. Statistical optimization not only allows quick search of a large experimental domain with considerably fewer trials, but also reflects the role of a given factor in medium. Moreover, the interaction between different variables can be estimated. Basically, this optimization procedure involves: experimentation based on a statistical design, parameter estimation for the mathematical model, checking the adequacy of the model, and estimating the levels of the variables giving the optimum response. Using computing software, these statistical methods have been employed with more or less success for medium optimization by several researchers (e.g., Adinarayana and Ellaiah, 2002; Abdel-Fattah et al., 2002; Liu et al., 2003).

It appears that besides statistics based medium optimization, more efficient methods are needed which allow better biochemical system modeling (Schugerl, 2001). The development of strains with increased production of a desired product is one of the main tasks in biotechnology (Torres et al., 1997). Traditionally, this task has been carried out by a series of random or targeted mutagenesis in a selective environment, or by the addition of external genetic material followed by selection. These methods have been very successful in the past. Some new strains produce over hundred times more product than the original parent strains; however, progress has slowed down considerably in some cases (Barton and Turelli, 1989). This scenario is changing due to the evolution of a new approach called metabolic engineering (Bailey, 1991). Metabolic engineering is a science that combines the benefits of molecular biology, biochemistry, genetics, chemical engineering, biotechnology, and mathematical modeling (Stephanopoulos and Vallino, 1991). Metabolic engineering has two major components. The first is the development of strategies for better understanding the structure of metabolic systems and intracellular enzymatic reactions. The second component is to apply the results of these strategies in selected organisms (Torres and Voit, 2002). To accomplish the later, current techniques enable the microbiologists not only to change the protein content of a given organism, but also to alter its enzymatic profile.

Regarding the first component of metabolic engineering some theoretical approaches have been developed involving the quantitative understanding of the cellular metabolism. Traditionally, enzyme reactions have been represented within the framework of

Michaelis-Menten formalism, but as the number of components in the system increases the complexity of the Michaelis-Menten based modeling approach becomes overwhelming (Savageau, 1976).

One fruitful method is metabolic flux analysis approach, which is based on network stoichiometry and conservation of mass. Often, this may be formulated as a set of linear ordinary differential equations. The stoichiometric approach focuses on the topology of the system and evaluates the rate by which a given metabolite converts into other metabolites. A great advantage of the stoichiometric approach is that it forms a set of linear algebraic equations at steady state, which makes the method amenable to linear optimization. Examples of this type of approach were employed by Papoutsakis and Meyer (1985), Majewski and Dornach (1990), Savinell and Palsson (1992), and Takac et al. (1998).

1.2 Research Objective

Scientific methods of enhancing gene expression including genomics, proteomics, applied molecular biology, metabolic engineering and combinatorial biosynthesis have been sufficiently developed to make a major impact on recombinant protein production in the pharmaceutical industry. However, process improvements from an operational perspective have been lagging. It appears that the combination of trial-and-error experimentation and molecular biology are not sufficient to design an optimum strategy for the overproduction of recombinant proteins (e.g., Ruijter et al., 1997; Smiths et al., 2000). Process optimization requires a strong theoretical and design framework (Alvarez et al., 2000).

The main objective of this study was to develop and apply the engineering strategies for the analysis and optimization of a bioprocess for *A. niger* producing a recombinant protein (hen's egg white lysozyme HEWL). Special emphasis was placed on the effect of the fermentation medium components.

To accomplish this objective the following major tasks were performed:

- Monitor the concentration profiles of the key metabolites and use this data as input for statistical optimization and mathematical models.
- Search for the most significant medium components for recombinant protein production using fractional factorial design.
- Move along the path of steepest ascent to reach the vicinity of the optimum level of the significant components of the medium.
- Apply response surface methodology to determine the optimum level of the important components for maximum production of the protein.
- Construct a mathematical model to simulate the behavior of biological systems.
- Optimize plausible objective functions for achieving recombinant protein production enhancement.
- Perform batch and fed-batch fermentations to confirm optimality.

Due to their filamentous nature, fungi present special challenges with regard to process optimization from an engineering viewpoint. It is hoped that this research provides a theoretically sound framework that may be used for the optimization of recombinant protein productions by filamentous fungus hosts.

1.3 Research Approach

The primary aim of this research was the development of mathematical models for improving the production of the targeted recombinant protein. Although, there was no unique mathematical model capable of capturing all features of a biochemical system (Voit, 2000), statistical methods and metabolic flux analysis were expected to be promising endeavors for achieving the objective.

1.3.1 Experimental Design Analysis

Statistically based experimental design was applied in a sequential manner to investigate the effect of medium components on HEWL production in shake flask cultures. As a first

stage of the analysis when still far from the optimal solution, a fractional factorial design was performed to assess the local terrain. Based on this design a first order model was evaluated and proved to be adequate to simulate the response of the microorganism to the changes in the key medium components. The fitted first-order model was a plane, from which the direction of steepest ascent was determined. The sequential experiments were carried out along this path until the response (i.e., the recombinant protein concentration) passed through maximum.

Close to the peak, the true response generally exhibited greater curvature, and a first-order regression model became inadequate, exhibiting a lack of fit. To explain the nonlinear behavior of the response at the vicinity of the optimum, central composite design was used to fit a second order model to the observations. Analysis of variance was performed in order to specify the most significant terms in the model and the simplified second order model was derived. Some experiments were performed at the predicted optimal level of the significant medium components and the adequacy of the model to predict the behavior of the microorganism was verified.

1.3.2 Metabolic Flux Analysis (MFA)

A comprehensive metabolic network was proposed based on stoichiometry that simulated the behavior of the metabolic system of *A. niger* producing a given recombinant protein (e.g., HEWL). Metabolic flux analysis based on amino acid metabolism was carried out:

- To evaluate the flux distribution within each metabolic pathway of the microorganism and examine different pathway contributions throughout the fermentation.
- To specify the significant metabolites, particularly amino acids, which benefit growth and the targeted protein production.
- To enhance the target protein productivity by sensitivity analysis using an appropriate schedule.

The following major steps were implemented to attain the above mentioned goals:

1.3.2.1 Metabolic Pathway Construction

A fundamental basis and key step for metabolic flux analysis is a plausible metabolic pathway for a microorganism. It is most important that the reaction sequences along the pathway are accurate since all further analyses depend on it. In this study the basic metabolic pathways, EMP pathway, PP shunt, TCA cycle, and anaplerotic pathways as well as biosynthetic pathways leading to amino acid synthesis and amino acid catabolism were considered. Moreover, an in-depth survey of related literature for *A. niger* was performed to augment more specifically relevant features of the microorganism's metabolism. Since, the resultant metabolic pathway included a fairly large number of metabolites and their corresponding reactions; the network was simplified with some rational assumptions to reduce the complexity without loss of vital information.

1.3.2.2 Experimental Studies

Fermentations were carried out using defined medium in 2 and 7 liter nominal volume bioreactor equipped with a pH probe and a dissolved oxygen analyzer for pH and oxygen control. The off-line extracellular analyses of key metabolites, biomass, and the recombinant protein were carried out throughout the batch fermentations.

1.3.2.3 Optimization and Experimental Verification

The accumulated data from the experimental portion along with the steady state balance equations of fluxes were used to construct a set of linear programming constraints. This set was augmented with a plausible objective function to form a linear programming problem. The metabolic flux distribution was determined using GAMS computer code. The logarithmic sensitivity analysis was used to specify amino acids which had the highest effect on both biomass and the recombinant protein production. Some batch and fed-batch experiments were performed to validate the model predictions.

1.4 Thesis Outline

This thesis comprises 7 chapters and is organized as follows:

Chapter 1 provides introduction, research objective, research approaches.

Chapter 2 provides a comprehensive literature review including filamentous fungal morphology and nutrient requirements, cellular metabolism, factorial design, response surface methodology, metabolic flux analysis, power law approximation, and general features of programming in LabVIEW environment.

Chapter 3 presents the materials and methods applied in this research including microorganism, stock culture preparation, medium components, and the analytical methods performed for the analysis of different metabolites in the fermentation culture.

Chapter 4 provides the application of statistical methods to maximize the production of the recombinant protein using medium composition. A sequential approach comprising fractional factorial design, path of steepest ascent, and central composite design was used. These studies explored the importance of optimum levels of significant constituents of the medium for the protein production.

Chapter 5 describes the development of a comprehensive metabolic network for *Aspergillus niger*. In addition to basic metabolic pathways, the metabolism of amino acids, biosynthesis of macromolecular components of biomass and nucleotides are implemented in the proposed model. The importance of having enough and accurate experimental data are discussed. Logarithmic sensitivities of the specific growth rate with respect to different metabolites are studied.

Chapter 6 presents the applied hardware and software for monitoring and control of a 20 liter MBR fermenter. The application of two algorithms for temperature control of the bioreactor are studied and discussed. The written software in LabVIEW environment is able to control and monitor the principal variables of the fermentation such as temperature, pH, and dissolved oxygen.

Chapter 7 summarizes the significant findings of this research and gives some recommendations for future research.

CHAPTER 2

LITERATURE REVIEW

2.1 Filamentous Fungi

Aspergillus species have been considered previously as alternative hosts to *E.coli,* yeast, and animal cells for expressing recombinant proteins (Ward et al., 2006). Traditionally, recombinant protein products have been produced by the bacterium, *Escherichia coli* and Chinese hamster ovary (CHO) cells. These hosts, however, have several disadvantages as recombinant protein producers. Bacteria and yeasts typically lack the mechanism for performing satisfactory post-translational modifications, such as glycosylation; product authenticity is, therefore, compromised. Mammalian cells may be used to overcome these disadvantages, however, they are relatively fragile, produce low levels of the target proteins, require expensive medium, and often have bioprocessing problems in conventional bioreactors.

Fungi have played an important role in several biotechnological processes and the synthesis of a variety of compounds. Fungi are also the target of many biotechnological applications, ranging from the development and production of various pharmaceuticals (antibiotics, for example) and industrial products to their application in homologous and heterologous gene expression (Arora, 2004). However, the synthesis of heterologous proteins is usually much lower than that of homologous proteins (Wang et al., 2003b). Filamentous fungi are capable of producing large amounts of specific proteins. They have been used in the industrial production of a wide variety of native products such as antibiotics (e.g., penicillin and cephalospherine), organic acids (citric, acetic, and formic acids), and commercial enzymes (e.g., protease, catalase, amylase) (Rawool et al., 2001).

They have a number of attractive features as foreign gene hosts, including the fact that many organisms (such as *Aspergillus niger*) have a long history of industrial usages, which means many already have GRAS (generally regarded as safe) status. Their ability to secrete large quantities of enzymes (e.g., more than 20 g L^{-1} of glucoamylase; Finkelstein 1987) has encouraged their use in the production of recombinant proteins. For most proteins having pharmaceutical potential, correct post-translational modification by N-glycosylation is important. Incorrectly glycosylated proteins are immediately cleared from the bloodstream, making them practically useless for therapeutic purposes (Punt et al., 2002). Non-native (heterologous) protein synthesis in *Aspergillus* hosts has proven to be effective, because the protein products usually fold correctly with efficient formation of disulfide bridges, so a high proportion of the product is in an active conformation (Martinelli and Kinghorn, 1994). Proteins have been proven to be correctly glycosylated by recombinant strains of *Aspergillus niger*. A number of heterologous proteins have already been expressed in *Aspergillus* species such as calf chymosin (Van Hartingsveldt et al., 1990), phytase (Van Gorcom et al., 1990), hen's egg white lysozyme HEWL (Archer et al., 1990), and tissue plasminogen activator t-PA (Wiebe et al., 2001). There are some problems, however, with *Aspergillus* strains as heterologous protein hosts. The most important drawback is intracellular and extracellular protease production in relatively high levels, which typically modify and degrade the recombinant proteins (Ahmed et al., 2005).

2.1.1 Morphology

Filamentous fungi (molds) are composed of aggregated long, branching threads termed hyphae and referred collectively as mycelium. Certain branches of mycelium may grow in the air and form spores called conidia. One particular difficulty with the filamentous fungi centers around their morphological. Filamentous fungi are tip growing systems, which grow by apical elongation, with a flow of cytoplasm toward the hyphal tip (Wessels, 1993). As time progresses, older hyphal regions become progressively more vacuolated (Paul et al., 1994) and may become metabolically less active. Thus, in a submerged fungal culture, a range of types of hyphal compartment, with different metabolic capabilities will normally be present.

The flow and behavior of fermentation broth containing filamentous microorganisms differ considerably from that of bacterial cultures primarily due to the complex morphology of filamentous microorganisms. From a bioprocessing point of view, the growth morphology of filamentous fungi may be classified into two categories: dispersed mycelial and pellet form (Figure 2.1). The dispersed form can be further divided into freely dispersed culture and clumps (Thomas and Paul, 1996). Mycelial pellets are naturally dense, spherical, aggregated cell populations that produce a low viscosity suspension. This form of growth represents an immobilized form of growth, as the mycelium grows in a compact form around the core. The internal mass transport resistances imposed on the diffusion of oxygen and other nutrients as the growing pellets exceed a critical size, lead to progressive cell lysis in the center of the pellets and loss of biosynthetic activity (Wittler et al., 1986). Small pellets are favored over large pellets, because in small pellets the ratio between metabolically active mycelium at the outside of the pellet and inactivated mycelium in the center of the pellet is much higher. The induction of pellet formation is controlled by complex interactions between biological and physical factors present in the culture, such as the genotype of the strain, inoculum level, medium composition, pH, and hydrodynamic shear forces (Braun and Vecht-Lifshitz, 1991). Studies have shown that the broths containing high concentration of mycelial filamentous microorganisms are highly viscous (Olsvik and Kristiansen, 1994; Berovic et al., 1993). The high viscosity of the cultures is associated with bulk mixing and gas-liquid mass transfer problems (Cui et al., 1998).

Recent evidence implies that the morphology affects transport processes in the bioreactor which, in turn, have a strong influence on the efficiency and productivity of the entire fermentation process (Papagianni and Moo-Young, 2002; Xu et al., 2000). They found that the formation and secretion of proteases was related to the morphological development of *Aspergillus niger*, with free filamentous forms of growth being involved with higher extracellular protease activities compared to pelleted forms. In contrast, however, the production of both native and recombinant enzymes in a fungal chemostat culture was observed to be the same, even at significantly different levels of hyphal fragmentation (Amanullah et al., 1999). Process conditions such as turbulent stress, medium composition, pH, ionic strength, and inoculum concentration are reported to

have a certain effect on the fungal morphology (Cui et al., 1998). For instance, different concentrations of oxygen in the gas stream affected the morphological development of the fungal culture in chemostat cultures of *Aspergillus niger* (Wongwicharn et al., 1999). The microorganism developed different growth strategies by undergoing both physiological and morphological changes. The authors found an enhancement of enzyme production by highly active, short mycelia when the oxygen supply was in excess.

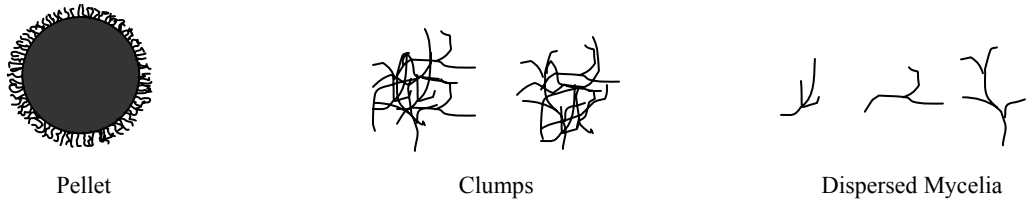

Figure 2.1- Schematic representation of fungal morphology in suspension culture**.**

2.1.2 Chemical Requirements for Growth

Fungi have relatively simple nutritional needs and most species could function quite well under aerobic conditions if supplied with glucose, ammonium salts, inorganic ions, and a few growth factors (Thom and Church, 1926). In their natural habitat, fungi are able to uptake a variety of compounds as nitrogen and/or carbon source. However, not all nitrogen and/or carbon sources support growth and development equally. Macronutrients, supplied in millimolar concentrations, comprise sources of carbon, nitrogen, oxygen, sulfur, phosphorous, potassium and magnesium. Some trace elements are essential for fungal cell growth such as calcium, copper, iron, manganese, molybdenum, and zinc that are provided at micromolar concentrations (Turner, 1971). Carbohydrates are widely used as carbon source for fungal growth. The carbohydrate can be a simple hexose such as glucose or polysaccharides such as starch and cellulose.

Although there are a few reports claiming that some fungi fix nitrogen, most evidence show that fungi can not fix atmospheric nitrogen and need to be supplied with nitrogen containing compounds (Wainwright, 1988) . A nitrogenous compound can be only used

as a nitrogen source if it is convertible to glutamate and glutamine, which in turn serve as nitrogen donors for the synthesis of all other nitrogen-containing compounds in the cell. Both glutamate and glutamine can be synthesized using ammonium ion as the amino group donor. Ammonium salts such as ammonium chloride, ammonium nitrate, and ammonium sulfate can be used as inorganic forms of nitrogen by the great majority of fungi. Ammonium sulfate is a common inorganic source of nitrogen in fungal growth media, because it also supplies utilizable sulfur. Therefore, ammonium salts, glutamate, and glutamine are preferred nitrogen sources (Chang and Todd, 2004). Most fungi can grow on nitrate as a nitrogen source by reducing it first to nitrite and subsequently to ammonia. Although nitrite is toxic to many fungi and bacteria, it can be also used as a nitrogen source by some fungi such as *Aspergillus nidulans*, *A. niger*, and *Neurospora crassa* (Pateman and Kinghorn, 1976). A number of fungi, e.g., *S. cerevisiae*, lack the ability to metabolize nitrate and require reduced nitrogen for growth. The inorganic nitrogen sources can be replaced by a number of organic nitrogen compounds ranging from urea and amino acids to proteins which are good nitrogen and carbon sources for a number of fungi (van Laere, 1995).

Phosphorous is essential for biosynthesis of fungal nucleotides, phospholipids, ATP, and glycophosphates. The phosphate content of fungi is considerable and is mostly in the form of orthophosphates, which acts as a substrate and enzyme effector.

Fungal growth factors are organic compounds occasionally needed in very low concentrations for specific enzymatic or structural roles, but not as energy source. These include vitamins (e.g., thiamine, biotin), purines, pyrimidines, nucleosides, amino acids, fatty acids, and sterols. Some fungi are not able to synthesize the particular growth factor, while *Aspergillus niger* and *Penicillium chrysogenum* are able to synthesize their own growth factor from glucose (Walker and White, 2005).

2.2 Review of Cellular Metabolism

Mathematical formulation of a metabolic pathway is the basis for any quantitative approach of cellular metabolism. This requires some basic information about different major pathways normally present in living cells. Due to the importance of such pathways the basics of glycolysis, pentose-phosphate, tricarboxilic acid, anaplerotic pathways as well as amino acid biosynthesis are reviewed in this section.

2.2.1 Glycolysis

Glycolysis or the Embden-Meyerhof-Parnas (EMP) pathway is a set of biochemical reactions occurring in the cytosol and along which glucose is converted to pyruvate. Figure 2.2 illustrates the enzymatic reactions in the EMP pathway. This pathway can be divided into two major parts. The first part includes six carbon components and does not involve any oxidation-reduction reactions. The reaction sequence comprises two phosphorylation reactions that lead to the production of fructose 1,6 diphosphate.

Then aldolase catalyzes the next cleaving reaction, and two three-carbon molecules, glyceraldehyde-3P and dihydroxyacetone phosphate are formed from fructose 1,6 diphosphate. All components in the second part are three-carbon intermediates. The first oxidation reaction occurs in the second part of the EMP when glyceraldehydes-3P is converted to 1,3 diphosphoglycerate. In this reaction, the coenzyme NAD^+ accepts electron and is reduced to NADH. The final product is pyruvate which is a key intermediate in metabolism. Under certain conditions pyruvate may be converted to lactic acid, ethanol, or other products such as, acetone, butanol, and acetic acid, whereas under aerobic conditions it is converted to CO_2 and NADH through the TCA cycle. The overall stoichiometry for the conversion of glucose to pyruvate in the EMP pathway is:

$$Glu\cos e + 2ADP + 2NAD^+ + 2P_i \rightarrow 2Pyruvate + 2ATP + 2H_2O + 2NADH + 2H^+ \quad (2.1)$$

The major metabolic control site in glycolysis is the phosphorylation of fructose 6-P by phosphofructokinase (3), which is an allosteric enzyme. This enzyme is activated by P_i and ADP, but inhibited by ATP (Shuler and Kargi, 2002). At high ATP/ADP ratios, this enzyme is inactivated, so that the rate of glycolysis and ATP synthesis are reduced.

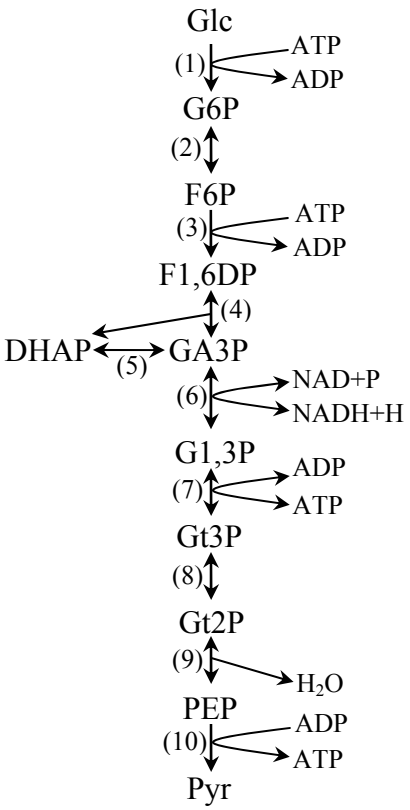

Figure 2.2- Overview of the EMP pathway in fungi. The enzymes are: (1) glucokinase, (2) phosphoglucose isomerase, (3) phosphofruktokinase, (4) aldose, (5) triphospho isomerase, (6) 3-phosphoglyceraldehyde dehydrogenase, (7) 3-hosphoglycerate kinase, (8) phosphoglycerate mutase, (9) enolase, (10) pyruvate kinase.

Glycolysis has three major roles in metabolism (Matthews et al., 1997):

- Production of energy in the form of ATP
- Formation of pyruvate from glucose as a intermediate for final oxidation in the TCA cycle or for fermentation product
- Production of compounds that may be important in biosynthesis of some macromolecules and amino acids.

2.2.2 Pentose-Phosphate Pathway (PPP)

The pentose-phosphate (PP) shunt or hexose monophosphate (HMP) pathway is a sequence of biochemical reactions which provides reducing power for biosynthesis reactions and a group of small organic compounds as shown in Figure 2.3.

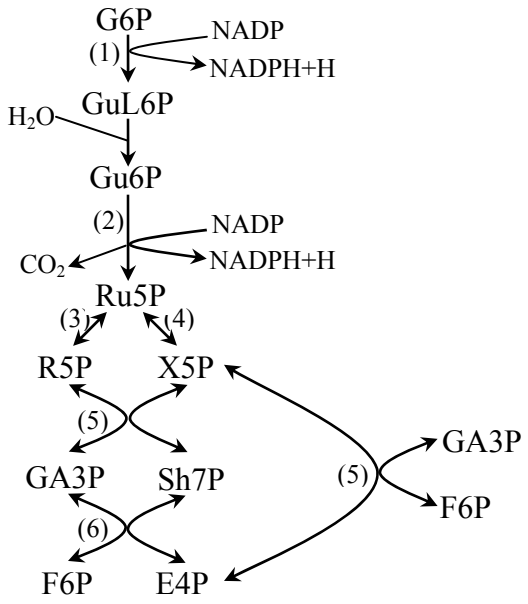

Figure 2.3- Pentose phosphate pathway. The enzymes are (1) Glucose-6P dehydrogenase, (2) 6-Phosphogluconate dehydrogenase, (3) ribosephosphate isomerase, (4) ribosephosphate-3-epimerase, (5) transketolase, (6) transaldolase.

During the oxidative portion of this pathway glucose-6P is converted to ribulose-5P and CO_2 while two molecules of coenzyme $NADP^+$ are reduced to NADPH (Brock and Madigan, 1994). Riboluse-5P is further converted to two other pentose phosphates, xylose-5P and ribose-5P. The reminder of the cycle (i.e. the non-oxidative portion) involves the conversion of the pentose-5P's to 3-, 4-, 5-, and 7- carbon intermediates that finally lead to fructose-6P and/or glyceraldehyde-3P. Since all of the reactions of the non-oxidative portion are freely reversible, it is clear that the operation of the system generates a pool of sugar phosphates. The primary functions of the PP pathway are:

- Generation of reduced coenzyme NADPH, which is extremely important in biosynthetic reactions such as synthesis of lipids, and assimilation of nitrate and ammonia
- production of pentose phosphates which is essential for biosynthesis of nucleic acids, purine, ATP, NAD^+, and other coenzymes
- Formation of erythrose-4P that is a precursor in the synthesis of the aromatic amino acids.

The quantitative importance of the PP pathway appears to be controlled by the demand for NADPH and the increasing demand for NADPH (such as nitrate as nitrogen source) during active growth increases the percentage of glucose metabolized along this pathway (Berry, 1975).

2.2.3 Tricarboxilic Acid cycle (TCA)

Tricarboxylic acid cycle, also known as citric acid cycle or the Krebs cycle is a sequence of biochemical reactions by which the organic product of glycolysis (pyruvate) is completely oxidized to CO_2 (Figure 2.4). Due to the instability of a number of TCA-cycle enzymes, especially α-ketoglutarate dehydrogenase (Meixner-Monori et al., 1985), the operation of a complete TCA cycle has long been in doubt for a number of fungi. However, Kubicek (1988) concluded that the present evidence supports operation of the TCA cycle in fungi.

The first step in the TCA cycle is an oxidative decarboxylation reaction by which pyruvate is converted to an activated form of acetate, known as acetylcoenzyme A, which is a key component in the metabolism of amino acids and fatty acids (Shuler and Kargi, 2002). Acetyl-CoA is an acetyl radical coupled to coenzyme A (Brock and Madigan, 1994). This reaction is catalyzed by a cluster of three enzymes, called collectively as the pyruvate dehydrogenase complex, which in eukaryotes is located in mitochondrion (Stephanopoulos et al., 1998). In this reaction NAD^+ serves as an electron acceptor.

The acetyl group of acetyl-CoA combines with 4-carbon compound oxaloacetate, leading to the eventual formation of citric acid. Citrate is subsequently converted to its isomer, isocitrate. These two molecules are usually regarded as one metabolite.

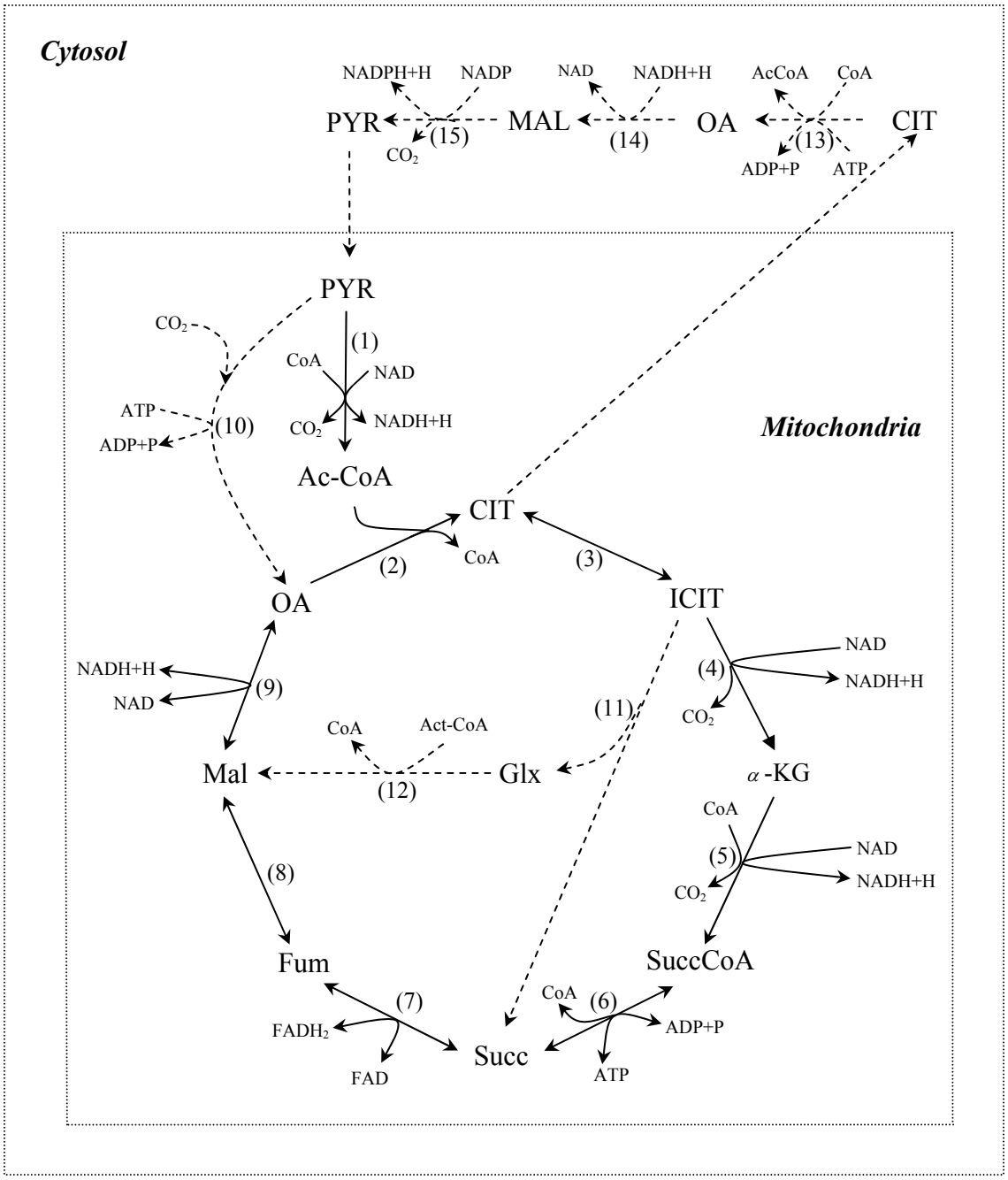

Figure 2.4- TCA cycle and anaplerotic pathways in fungi. The enzymes are: (1) pyruvate dehydrogenase complex, (2) citrate synthase, (3) aconitase, (4) isocitrate dehydrogenase, (5) α- ketoglutarate dehydrogenase, (6) succinate thiokonase, (7) succinate dehydrogenase, (8) fumarase, (9) malate dehydrogenase, (10) pyruvate carboxylase, (11) isocitrate lyase, (12) malate synthase, (13) ATP-citrate lyase, (14) malate dehydrogenase, (15) malic enzyme.

The next two steps of the TCA cycle are oxidative decarboxylation, yielding succinyl-CoA and two molecules of CO_2.

Ultimately, oxaloacetate is regenerated after four further enzymatic reactions, thus completing the cycle. In the mitochondria there are four physiologically irreversible steps in the enzyme cluster consisting of the pyruvate dehydrogenase complex and the TCA cycle, (Matthews et al., 1997). These are pyruvate dehydrogenase (oxydoreductase), citrate synthase, isocitrate dehydrogenase (oxydoreductase), and α-ketoglutarate dehydrogenase (oxydoreductase). These are all metabolic control points in the metabolism. Available evidence from a limited number of fungi suggests that the activity of the cycle is regulated by the NADH/NAD ratio at the level of isocitrate dehydrogenase and α-ketoglutarate dehydrogenase (Stephanopoulos et al., 1998).

The overall stoichiometry for the complete oxidation of pyruvate in the TCA cycle is:

$$Pyruvate + 3H_2O + GDP + P_i + 4NAD^+ + FAD \rightarrow 3CO_2 + GTP + 4NADH + FADH_2 + 4H^+ \qquad (2.2)$$

The major functions of the TCA cycle can be categorized as follows (Shuler and Kargi, 2002):

- Provides electrons (NADH and $FADH_2$) for the electron transport chain and biosynthesis.
- Supplies carbon skeletons for amino acid and nucleotide synthesis, more specifically α-ketoglutarate for glutamate and oxaloacetate for aspartate synthesis.
- Generates energy.

2.2.4 Anaplerotic Pathways

If any metabolite is removed from the TCA cycle for other cellular functions, the cycle cannot continue to operate, because there is no net synthesis of the intermediates in the cycle (Matthews et al., 1997). For instance, some of the compounds in TCA cycle such as succinate, α-ketoglutarate, and oxaloacetate serve as precursors for biosynthesis of some amino acids and nucleotides. The ensuing deficiency is overcome by replacement of oxaloacetate by alternative paths that are not part of the main TCA cycle. These reaction sequences are called *anaplerotic* reactions (Brock and Madigan, 1994). The anaplerotic

pathways are depicted in Figure 2.4 by dashed lines including the glyoxylate shunt, the carboxylation of pyruvate by pyruvate carboxylase, the carboxylation of phosphoenolpyruvate by PEP carboxylase, and the oxidation of malate by the malic enzyme (malate oxydoreductase) (Stephanopoulos et al., 1998).

During metabolism of fat or C_2-compounds, the glyoxylate cycle can also generate C_4 compounds to replenish the TCA cycle. The glyoxylate cycle includes most of the TCA cycle enzymes (2, 3, 11, 12, and 9) and two unique enzymes: isocitrate lyase, which splits isocitrate to succinate, and malate synthase converting glyoxylate and acetyl-CoA to malate (Brock and Madigan, 1994). This pathway occurs in all classes of fungi and does not take place in the mitochondria, but in ultrastructures called glyoxysomes, where there is a net synthesis of succinate from acetyl-CoA (Maxwell et al., 1975).

2.2.5 Amino Acid Biosynthesis

Microorganisms need a large amount of cellular building blocks for the synthesis of amino acids. The 20 amino acids can be categorized into five families with respect to the specific precursor that serves as the starting point. The only exception is histidine biosynthesis that is fairly complicated and cannot be easily grouped with the others (Brock and Madigan, 1994). However, ribose-5P from PP pathway is a key precursor for histidine biosynthesis. The biosynthetic pathways for all 20 amino acids have been elucidated in many eukaryotes and prokaryotes. There are only a few differences in amino acid biosynthesis amongst the various organisms. For example, in bacteria lysine is synthesized from pyruvate, whereas in fungi it is synthesized from α-ketoglutarate. Table 2.1 shows the family and precursors for different amino acid biosynthesis in fungi (Nielsen, 1997).

Table 2.1- Amino acid biosynthesis in eukaryotes.

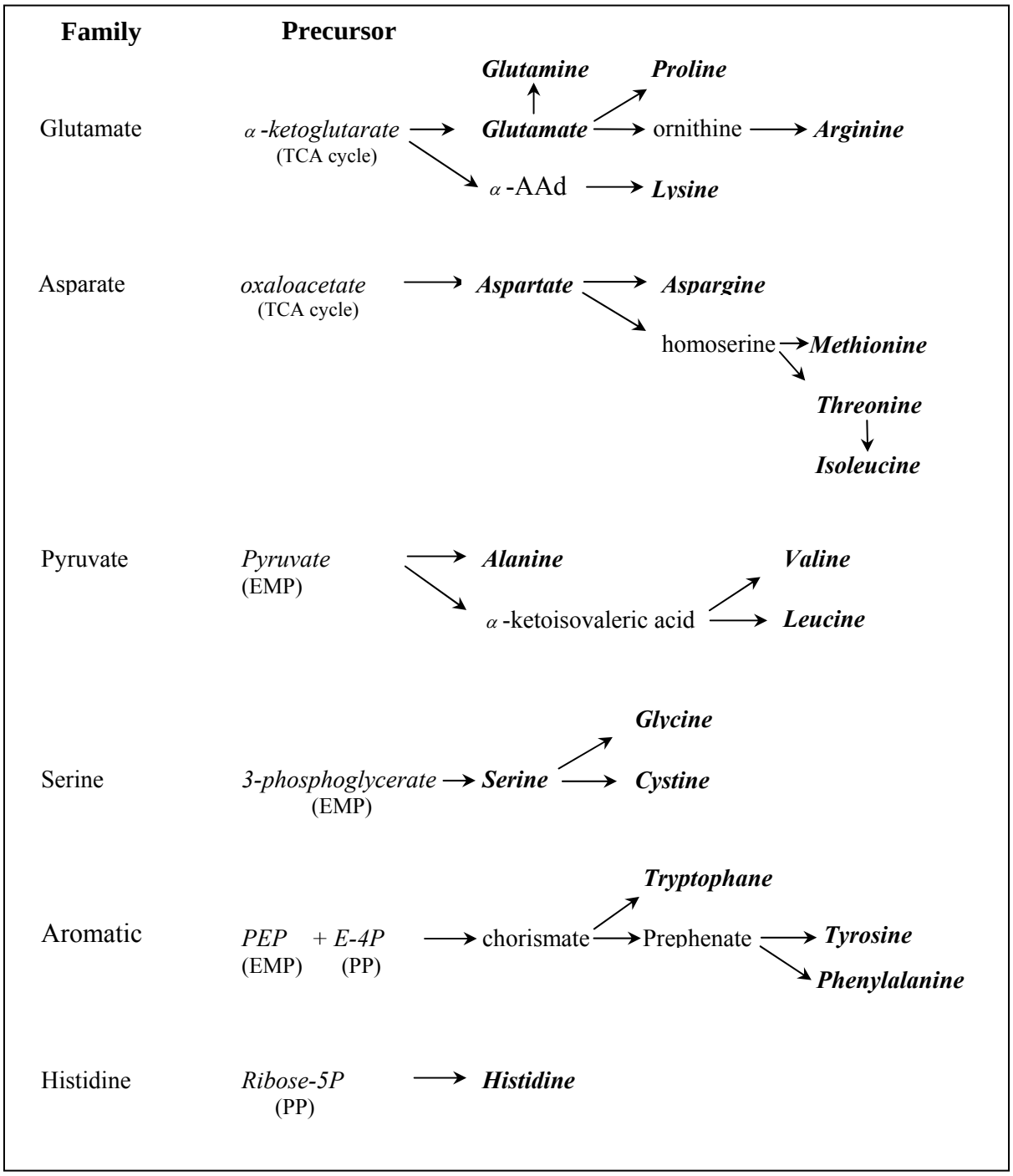

2.3 Factorial Design

In multi-component systems, the effect of two or more variables on the experimental outcome needs to be ascertained. In general, a factorial experimental design is the most efficient statistical tool for this purpose. In each trial or replication of a full factorial design, all possible combinations of the factors levels are investigated. For example, if there are a levels of factor X_1 and b levels of factor X_2, each replicate contains all $a \times b$ treatment combinations.

The effect of a factor in a factorial design is defined as the amount of change in response when the factor level is altered. Since this reflects the change in the primary factors of interest in the experiment; it is called a *main effect*. In some experiments, the response is not a linear combination of the changes in the factors. When this occurs, there is an interaction between factors (Montgomery and Runger, 1994) and the response surface plot may be twisted.

Traditionally, one-factor-at-a-time technique has been used for process optimization. This involves varying one factor while keeping the others at constant levels. Although simple, this often requires a considerable amount of experimental work and may be costly. The major benefit of applying a factorial design is the reduced number of experiments that need be carried out using a choice of the best experimental points to get maximum information (Rajendhran et al., 2002). This results in more efficient experimental design. Furthermore, to avoid misleading conclusions, a factorial design is often necessary when interactions may be present. Finally, the factorial design allows the effect of a given factor to be determined at several levels of the other factors, so the conclusions are valid over a larger range of experimental conditions (Montgomery, 2001).

2.3.1 The 2^K Factorial Design

Factorial designs are very popular in experiments that require the study of the joint effects of the factors on a response. The most important class of the factorial design is to investigate K factors, each at only two levels. The levels may be qualitative, such as two kinds of nutrients, microorganisms, or procedure or they may be quantitative, such as two values of temperature, pressure, concentration.

Since, each factor is considered at high (+) and low (-) levels, a complete replicate of such a design requires 2^K observations and is called a 2^K factorial design. This design enables an experimenter to investigate k factors with relatively small number of runs. Consequently, it is particularly very useful in the early stages of an experiment work when there are usually many factors to be studied. In factorial design, the assumptions that need to be considered (Montgomery, 2001) include fixed factor values, completely randomized design, and the assumption of normality. Since there are only two levels for each factor, the response is assumed to be approximately linear over the range of the chosen factor levels. In many cases, particularly in the early stages of study, this is often a legitimate assumption.

2.3.2 Fractional Factorial Designs

As the number of factors in a *2K* design increases, the number of runs required for a complete replication of the design rapidly increases as well. The complete runs provide an examiner with enough information to evaluate the whole set of main effects as well as all interaction effects. The main effects and lower-order interactions are usually the most significant terms (Mason et al, 1989). In fact, one is capable of determining the main effects and the lower-order interactions by performing a fraction of the complete factorial design without loss of any information. This design is called fractional factorial design (FFD) that contains a $1/2^p$ fraction of the 2^K complete design and is often called a 2^{K-p} fractional factorial design. It is clear that setting the p term equal to zero may refer to a complete two level factorial design. The general approach to the statistical analysis of the 2^{K-p} design is summarized in Table 2.2 (Montgomery, 2001).

The first step is to evaluate factor effects and examine their magnitude and signs. Regarding these preliminary information one can decide about the most important factors and interactions. For example, the effects sign specifies the direction in which these effects can be adjusted to improve the response.

Table 2.2- Analysis procedure for a 2^{K-p} design.

1. Estimate factors effects
2. Form initial model
3. Perform statistical testing
4. refine the model
5. Analyze residuals
6. Interpret results

For a 2^{K-p} fractional factorial design with n_r replications at each treatment combination the effect of X can be quantitatively determined as follows:

$$(Effect)_X = \frac{1}{n_r \times 2^{K-p-1}} \times (Contrast)_X \tag{2.3}$$

Here X is the representative of either a main effect (e.g., X_1 or X_2) or an interaction effect (e.g., $X_1 X_2$). The *contrast* for each term (i.e., main effect or interaction effect) is defined:

$$(Contrast)_X = \sum_{\substack{i=1 \\ X^+}}^{2^{K-p}} \sum_{r=1}^{n_r} Y_{i,r} - \sum_{\substack{i=1 \\ X^-}}^{2^{K-p}} \sum_{r=1}^{n_r} Y_{i,r} \tag{2.4}$$

Where $Y_{i,r}$ is the response at r^{th} replication for i^{th} treatment combination (run number i). X^+ and X^- restrict the summations only for the responses when the effect of X is at its high or low level, respectively.

In step two, one uses all main effects and interactions to form the initial model for the experiment. In the next step, the most significant main effects and interaction effects are examined by applying the analysis of variance (ANOVA). The sum of squares of each effect can be defined as follows:

$$SS_X = n_r \times 2^{K-p-2} (Effect)_X^2 \tag{2.5}$$

The total sum of squares can be defined by:

$$SS_T = \sum_{i=1}^{2^{K-p}} \sum_{r=1}^{n_r} Y_{i,r}^2 - \frac{\left(\sum_{i=1}^{2^{K-p}} \sum_{r=1}^{n_r} Y_{i,r} \right)^2}{n_r \times 2^{K-p}} \tag{2.6}$$

In general, SS_T has $(n_r \times 2^{K-p} - 1)$ degrees of freedom. The error sum of squares with $2^{K-p}(n_r - 1)$ degrees of freedom is usually computed by subtraction:

$$SS_E = SS_T - SS_{Model} \tag{2.7}$$

The model sum of square is defined as the summation of effects sum of squares in the model.

$$SS_{Model} = \sum SS_X \tag{2.8}$$

On the basis of analysis of variance performed in step three, any statistically insignificant term is removed from the initial model in the fourth step. The error or residual sum of squares is now composed of a pure error (in case of full or partial replication of experiment), and a lack of fit component including of sum of squares for all the effects that were dropped from the full model.

The ordinary R^2 for the analysis of a model is defined as follows:

$$R^2 = \frac{SS_{Model}}{SS_{Total}} \tag{2.9}$$

A concern with this statistic is that it always increases as terms are added to the model; although the added terms are often not significant. Consequently, this statistic is usually smaller for the refined model in comparison to the corresponding full model. To negate this drawback, the adjusted coefficient of determination is re-defined as:

$$R^2_{adj.} = 1 - \frac{(SS / d.f.)_{Res.}}{(SS / d.f.)_{Tot.}} \tag{2.10}$$

This statistic is adjusted for the size of the model, more specifically the number of factors. If nonsignificant terms are added to a model, this can usually decrease the $R^2_{adj.}$ value. Obviously, removing the nonsignificant terms from the full model the final model is formulated, by which one can predict the response to new input variables effectively (Montgomery, 2001).

Step five is the usual residual analysis to test for model adequacy and to check for the validity of the assumptions and usually consists of graphical analysis of residuals, effects, response surface, and contour plots. The examination of the residuals is an important part of any analysis of variance. The normality of residuals can be checked by plotting a histogram of the residuals. If the errors are normally distributed with mean zero and constant variance, this plot should look like a sample from a normal distribution centered at zero. Moreover, if the model is adequate then the residuals should contain no patterns.

2.3.3 The Addition of Center Points to the 2^K (2^{K-p}) Design

A potential concern about 2^k (2^{K-p}) design is the assumption of linearity in the factor effects:

$$Y = a_0 + \sum_{k=1}^{K} a_k x_k + \varepsilon \tag{2.11}$$

In the above equation ε represents the noise or error observed in the response Y and x_k is a coded variable**.** The relationship between the coded variable x_k and its natural variable X_k is defined as:

$$x_k = \frac{X_k - (X_{k,high} + X_{k,low})/2}{(X_{k,high} - X_{k,low})/2} \tag{2.12}$$

If the natural variables have only two levels, this coding will generate the values of ± 1 for the levels of the coded variables.

If interaction effects are added to the main effects (first order model) the following result is obtained:

$$Y = a_0 + \sum_{k=1}^{K} a_k x_k + \sum_{k=1}^{K} \sum_{l>k}^{K} a_{kl} x_k x_l + \varepsilon \qquad (2.13)$$

The model is now capable of representing some curvature in the response function. This curvature is introduced into the original linear model by the interaction terms of $a_{kl} x_k x_l$. These terms only twist the response plane slightly, whereas sometimes more curvature is needed. In these situations a higher-order model maybe more appropriate.

Actually, there is a method of replicating certain points in a 2^K (2^{K-p}) design that will allow the examiner to check for the adequacy of curvature expressed in Equation 2.13. Also, this method provides us with an independent estimate of error (Montgomery, 2001). The method involves the addition of center points to the 2^K (2^{K-p}) design. One important reason for adding the replicate runs at the design center is that the center points do not influence the usual effect estimates in a 2^K (2^{K-p}) design. The sum of squares for pure quadratic curvature is given by:

$$SS_{Purequadratic} = \frac{n_f n_c (\overline{Y_f} - \overline{Y_c})^2}{n_f + n_c} \qquad (2.14)$$

Where $\overline{Y_f}$, $\overline{Y_c}$ are the averages of factorial and center point responses, respectively. The design consists of n_f factorial design point and n_c center point runs. This single-degree-of–freedom sum of square may be utilized in an F test by considering the mean square error and check for pure quadratic curvature. Moreover, if there is no replication in the factorial points, one may use the n_c center point runs to estimate the pure error with n_c –1 degrees of freedom.

2.3.4 Response Surface Methodology (RSM)

Often a researcher is interested in a process response, which is influenced by several factors, and the goal is to optimize this response. Response surface methodology that is a combination of mathematical and statistical techniques is useful for the modeling and analysis of this kind of problems (Box et al., 1978).

For instance, suppose the response in a process is a function of several variables as shown below:

$$Y = f(x_1, x_2, \ldots) + \varepsilon \tag{2.15}$$

The expected response is given by:

$$E(Y) = \widehat{Y} = f(x_1, x_2, \ldots) \tag{2.16}$$

The response represented by $\hat{Y}$ is called a response surface. The response surface can be a plane or a twisted plane, such as the models presented by Equations (2.11), (2.13). If the response is moderately nonlinear, a quadratic model may be appropriate:

$$Y = a_0 + \sum_{k=1}^{K} a_k x_k + \sum_{k=1}^{K} \sum_{l>k}^{K} a_{kl} x_k x_l + \sum_{k=1}^{K} a_{kk} x_k^2 + \varepsilon \tag{2.17}$$

Almost all RSM problems utilize one or more of these model features. Undoubtedly, a polynomial model can predict the behavior of a process for a relatively small region of interest accurately, but it is unlikely that the model can provide one with reasonable accuracy over the entire space of independent variables.

One potential method that may be used to determine the quadratic coefficients in the second-order model is to carry out a 3^K factorial design. However, there are two points to be considered with regard to the 3^K design. First, this design is not the most efficient way to model a second-order polynomial. Second, the 2^K design augmented with some center points is a superior way to examine about curvature in the response surface. This augmented 2^K design is relatively simple and efficient in size and simultaneously gives the examiner some protection against curvature (Myers and Montgomery, 2002). If the analysis of variance shows some lack of fit for the linear model, then the model should be augmented with *axial runs* to obtain a *central composite design* (CCD).

The central composite design is one of the most common designs that are utilized for fitting quadratic models and were first described by Box and Wilson in 1951.This is a sequential design strategy and needs fewer experiments than the 3^K factorial design.

At the early stages of an investigation, the response surface is unknown and the initial search may far away from the optimum. Often there is little curvature in the system response and either model 2.11 or 2.13 will be appropriate to predict the behavior of the process, so a factorial (fractional) design is an adequate approximation. The next step is to move rapidly towards the neighborhood of the optimum response. The method of steepest ascent for maximization or steepest descent for minimization is a proper procedure for moving sequentially along the path of steepest direction.

If a first-order model is fitted to the data in a region that is far from optimum, the direction of steepest ascent is the direction along which the response increases rapidly. If one imagines a normal path from the fitted response to the response surface then the direction will be parallel to this normal vector. One usually considers the center of region as the origin for the path of steepest ascent (Montgomery and Runger, 1994). The experiments may be conducted along this path until no more increase in response is observed. The maximum point along the path is in the vicinity of the optimum. Then, a new first-order model can be fitted. If the linear model is adequate and lack of fit analysis is not significant, the optimum will be evaluated by the new surface plane (twisted plane). A common problem is that a linear model usually shows a lack of fit at the neighborhood of the optimum. If so, some axial runs may be performed to augment the model and to allow quadratic terms to be incorporated into the model.

The design of choice to establish a quadratic model is the central composite design (CCD). Each design consists of a standard first order design with n_f factorial points and n_c center points, augmented by n_a axial points. Axial points are also commonly referred to as "star points". Axial points are points located at a specified distance α_{ccd} from the design center in each direction on each axis defined by the coded factor levels (Dean and Voss, 1999). Hence, for a design consists of *K* factor, there will be *2K* distinct axial points. The distance of the axial runs from the design center α_{ccd} and the number of center points n_c must be specified regarding the properties required of the design (Montgomery, 2001). Figure 2.5 shows central composite designs for *K=2* and *K=3* factors.

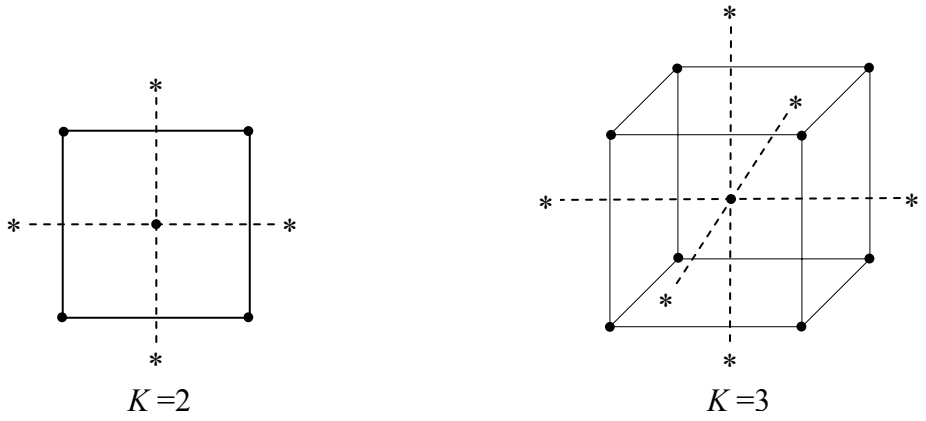

Figure 2.5 - Central composite design for two and three factors.

It is very important that the quadratic model is able to provide the examiner with good predictions throughout the region of interest in the vicinity of optimum. In other words, the model should have a reasonably consistent and stable variance of the predicted response at points of interest (Montgomery, 2001). Since, the purpose of the response surface methodology is optimization and the location of the optimum is unknown prior to performing the experiment, it seems rational to use a design that provides equal precision of estimation in all directions (Box et al., 1978). A design that has this property is called *rotatable* and can be made by selection of appropriate α_{ccd}. This value for a rotatable design is given by $\alpha_{ccd}=(n_f)^{1/4}$. The number of center points for 2 and 3 factors are 5 and 6, respectively.

2.4 Mathematical Modeling of Biochemical Systems

Once sufficient information is obtained about the key components and interactions of a biochemical system, this data become the basis for further analysis. The next step is to translate the metabolic pathway into a mathematical structure that is appropriate and convenient (Voit, 2000). Of course, there are different approaches and approximations for modeling a biochemical system; each approach may have a different context or a different set of goals. Two such approaches are reviewed below. The first class focuses on the stoichiometry of metabolic networks. The second class consists of power-law representations of the system.

2.4.1 Maps

The graphical representation (map) of metabolic pathway is useful and strongly recommended (Voit, 2000). The map consists typically of three main items:

- System components or pool of components
- Flow of material along the pathway
- Flow of information or signals such as feedback inhibition or activation

These schematics serve as bridges between the real system and mathematical model, and should be constructed using the best available information about their components.

2.4.2 Variables and Parameters

Components of a metabolic pathway such as metabolites and enzymes behave in different way in the biochemical system; therefore, their different roles must be reflected in the mathematical representation of the system. In general, three main entities contributing to the dynamics of the biochemical system may be distinguished:

- *Independent variable*: A variable is not affected by the dynamics of the process. Typically, independent variables are either under the control of examiner (e.g., substrates), or without any external controller (enzymes).
- *Dependent variables*: A variable whose value is affected by the dynamics of the system and usually change in value over the course of experiment (e.g., concentration of products and most intermediates along a pathway).

- *Parameter*: A parameter has a constant numerical value and quantifies a property of the system (e.g., kinetic reaction orders and reaction rate constants).

2.4.3 Dynamics of the Biochemical Systems

In general, each metabolite concentration at a point ζ in space at time *t* can be expressed as a unique function of the concentrations of all (bio)chemical compounds that participate at the point ζ and at the time *t*:

$$C_i = C_i\left[\boldsymbol{C}(\zeta,t),\boldsymbol{P},t\right] \tag{2-18}$$

Here $\boldsymbol{C}$ and $\boldsymbol{P}$ are the vectors of metabolite concentrations and parameters, respectively. In most cases explicit time dependency of reaction rate may be ignored without loss of generality. Furthermore, since the volume of living cells is small, the intracellular components are distributed uniformly by diffusion or cytoplasmic streaming in a very short time throughout the space within the cells. This suggests a typical simplification in many biochemical models, namely, a uniform concentration profile for each metabolite within the volume under study (Heinrich and Schuster, 1996). Considering these assumptions, the rate of change of a dependent variable in terms of other variables and parameters may be symbolically represented in form of a differential equation as follows (Voit, 2000):

$$\dot{\boldsymbol{C}}_{(t)} = f\left(\boldsymbol{C}_{(t)},\boldsymbol{P}\right) \tag{2-19}$$

Here, $\boldsymbol{C}_{(t)}$(briefly $\boldsymbol{C}$) is the vector of both dependent (the first m variables) and independent (the following m_1 variables), and $\boldsymbol{P}$ is the vector of parameters. The net change for a compound is composed of two aspects, production and depletion, which reflect two entirely different set of processes. In very general terms, the differential equation taking into account both the production and the depletion can be formulated as (Savageau, 1976):

$$\dot{C}_i = \sum_{j=1}^{q_i} V_{ij}^{+}\left(\boldsymbol{C},\boldsymbol{P}\right) - \sum_{j=1}^{w_i} V_{ij}^{-}\left(\boldsymbol{C},\boldsymbol{P}\right) \qquad i = 1,2,\ldots,m \tag{2-20}$$

In this representation, the index i represents the dependent variables, whereas j symbolizes all processes associated with the variable of interest. The number of these processes, q and w, can be small or large, but is unrelated to m and m_I. The positive-valued functions V_{ij}^{+} and V_{ij}^{-} indicate process(s) that represent the production or consumption (or degradation) of metabolite i, respectively. Since, independent variables are controlled (fixed) at a certain value throughout the experiment; there is no need to be included in the set of differential equations. Nevertheless, they can explicitly impart their influences on the system when appearing on the right-hand side of the system equations.

2.5 Metabolic Flux Analysis (MFA)

In some cases there is insufficient kinetic information on microorganisms under investigation. Therefore, metabolic modeling methods which involve less detailed kinetic information are required. A powerful approach that focuses only on topology of biochemical systems is metabolic flux analysis (Klamt et al., 2002). Using a stoichiometric model for the major intracellular reactions and applying mass balances on the intracellular metabolites under steady state conditions, the intracellular fluxes of the metabolites are calculated. Furthermore, a set of measured extracellular fluxes is used as input to calculations (Aiba and Matsouka, 1979). The measured extracellular fluxes are typically uptake rates of substrates and secretion rates of metabolites (e.g., amino acids, organic acids, carbohydrates). The results consists no information about metabolite concentrations, flow of regulatory signals, or transient behavior (Lee and Papoutsakis, 1999). The final outcome of the flux calculation is a metabolic map, including the metabolic pathway that was considered in the calculation and an estimate of the steady state flux for each reaction in the map (Jeremy and Palsson, 1998).

Since the metabolic fluxes show the contribution of different pathways on the overall metabolic process of substrate uptake and product formation, they have been denoted as a fundamental determinant of cell physiology (Stephanopoulos, 1998). For example, Takac and et al., (1998) showed that throughout the fermentation of L-glutamate production the TCA cycle was utilized in part only, whereas the glyoxylate bypass and pentose phosphate pathways were strongly active.

2.5.1 Elemental Balance

The network consistency with respect to the conservation of atomic mass laws can be checked by defining the reactions in mathematical notation. Let us consider the system of bioreaction network with m distinguishable chemical species and n reactions. If these species are denoted by $M_1, M_2, \ldots, M_m$, the j^{th} biochemical reaction may be symbolized as a linear equation by :

$$\sum_{i=1}^{m} s_{ji} M_i = 0 \tag{2.21}$$

Here, $s_{i,j}$ is the stoichiometric coefficient of metabolite i in the j^{th} reaction. Conventionally, negative values are given to the stoichiometric coefficients of the species that are to be regarded as the reactants and positive values for those of products. If $\boldsymbol{M}$ is considered as the symbolic vector of the species, Equation 2.21 may be written in matrix notation as:

$$\boldsymbol{S}^T \boldsymbol{M} = \boldsymbol{0} \tag{2.22}$$

Each chemical species M_i is composed of atoms. If the set A_l, $l=1,\ldots, L$ includes all the atomic species in the composition of $M_1, M_2, \ldots, M_m$ and e_{il} is the numbers of atom A_l in the species M_i then one may define:

$$\boldsymbol{M} = \boldsymbol{E}.\boldsymbol{A} \tag{2.23}$$

$\boldsymbol{E}$ is the matrix of atomic coefficients e_{il} and $\boldsymbol{A}$ is the symbolic vector of atomic species. Substituting for $\boldsymbol{M}$ in the Equation 2.22 gives:

$$\boldsymbol{S}^T \boldsymbol{E}\, \boldsymbol{A} = \boldsymbol{0} \tag{20-24}$$

The atomic species must be conserved, so that every coefficient of $\boldsymbol{A}$ in these equations is zero:

$$\boldsymbol{S}^T \boldsymbol{E} = \boldsymbol{0} \tag{2.25}$$

2.5.2 Reaction Rates

The rate of a (bio)chemical reaction is defined as the forward velocity v which specifies that a compound with a stoichiometric coefficient s is changed at the rate of sv. The normal unit for reaction rate is (mol/hr), but it is common that the rate is specified regarding a certain reference value such as volume, surface, or mass. For cellular reactions the biomass (dry weight) is considered as the reference parameter to define the so-called *specific rate*, which has the unit ($mol / g_{DW}\ hr$).

In the usual situation when the biochemical system includes more than one reaction, the overall production or consumption of a compound can be calculated by adding up the individual reaction rates v_j as follows:

$$r_i = \sum_{j=1}^{n} s_{ij}\, v_j \qquad i = 1,2,...,m \tag{2.26}$$

The sign of stoichiometric coefficients depends on the chosen direction of reaction. By convention the chemicals on the left-hand side of a reaction are considered as reactants and those on the right-hand side as products. Equation 2.26 can be represented in matrix notation:

$$\boldsymbol{r} = \boldsymbol{S}\boldsymbol{V} \tag{2.27}$$

Where $\boldsymbol{S}$ is the stoichiometric $m \times n$ matrix, $\boldsymbol{V}$ is the vector of n metabolic fluxes, and $\boldsymbol{r}$ is the vector of reaction rates.

2.5.3 Theory

The reaction network, which describes how metabolites are interconnected to each other, is the starting point of metabolic flux analysis (MFA). The basic principle is the conservation of mass. Since one is only interested in flow of materials within the map (topology of biochemical system), usually the map contains no information about flow of information or signals. A cellular metabolic reaction network includes a set of enzymatic reactions and transport processes (Schilling et al., 2000). The transport processes are responsible for passing the relative amounts of certain metabolites into and/or out of the control volume. The enzymatic reactions and transport fluxes are denoted as internal and exchange fluxes, respectively.

The right hand side of Equation 2.20 may be formulated as a flux balance for each metabolite M_i in a metabolic pathway to yield the dynamic mass balance equations. The fluxes with positive stoichiometric coefficients are the processes that increase the concentration of M_i (i.e., V_{ij}^{+} terms) and those with negative stoichiometric coefficients are the processes that decrease the concentration of M_i (i.e., V_{ij}^{-} terms). Considering the

dilution term due to the cell growth (Stephanopoulos et al., 1998), assumption of spatial homogeneity, and the relationship between the reaction rates and terms V_{ij}^{+} and V_{ij}^{-} as explained above, the final form of the dynamic mass balance in terms of fluxes can be written around every metabolite in the system. This generates a system of ordinary differential equations as follows:

$$\frac{d\,C_i}{d\,t} = \sum_{j=1}^{n} s_{i,j}\; v_j - \mu C_i \qquad , \quad i = 1,2,...,m \tag{2.28}$$

Here, v_j represents the flux through the process (e.g., reaction or exchange), and μ is the specific growth rate of the biomass. The last term in Equation 2-28 accounts for dilution due to the cell growth, and is generally negligible because of the low intracellular level of most pathway metabolites (Stephanopoulos et al., 1998). Moreover, it is generally accepted that there is very high turnover rate of most metabolites. Thus, even after a large perturbation in the cellular environment the concentrations of different intracellular metabolites rapidly adjust to new levels. As a result, one can assume that the intracellular metabolites are at a pseudo-steady state (Vallino and Stephanopoulos, 1993). Thus Equation 2.28 can be written in matrix notation as follows:

$$\boldsymbol{S}\boldsymbol{V} = \boldsymbol{0} \tag{2.29}$$

This equation simply states that over long time periods the formation fluxes of a metabolite must be balanced by the degradation fluxes (Lee and Papoutsakis, 1999). Note that this equation is formally analogous to Kirchhoff's current law, used in electrical circuit analysis. An important consequence of the pseudo-steady state assumption is that one can eliminate all pathway intermediates in a linear sequence and just consider the metabolites placed at the branch points of the metabolic pathway (Wiechert, 2002). This results in a significant reduction in the number of equations in the stoichiometry model.

Metabolic flux analysis is based on the knowledge of some fluxes, usually the fluxes of the reactions going into, and out of the cell. Vector $\boldsymbol{V}$ can be partitioned into two vectors, $\boldsymbol{V_u}$ and $\boldsymbol{V_k}$, containing the unknown (unmeasured) and known (measured) elements of $\boldsymbol{V}$, respectively. Upon substitution and rearrangement, Equation 2.29 becomes:

$$\boldsymbol{S}_u \,.\, \boldsymbol{V}_u = -\boldsymbol{S}_k \,.\, \boldsymbol{V}_k \tag{2.30}$$

Here, $\boldsymbol{V_u}$ is the n_u-dimensional unmeasured part and $\boldsymbol{V_k}$ is the n_k-dimensional measured part of $\boldsymbol{V}$. Also, $\boldsymbol{S_u}$ and $\boldsymbol{S_k}$ are the columns of $\boldsymbol{S}$ that corresponds to $\boldsymbol{V_u}$ and $\boldsymbol{V_k}$, respectively.

2.5.4 Classification of Systems and Rates

The following classification of systems and rates is based on the work of van der Heijden et al. (1994). The complete bioreaction network may be classified into two different categories with respect to the *rank* of $\boldsymbol{S_u}$ as follows:

Determinacy:

- *Determined*: *rank* ($\boldsymbol{S_u}$) = n_u; all unknown rates of $\boldsymbol{V_u}$ can be uniquely evaluated.
- *Underdetermined: rank* ($\boldsymbol{S_u}$) < n_u; the number of linearly independent equations are not enough to achieve a unique solution.

Redundancy:

- *Not Redundant: rank* ($\boldsymbol{S_u}$) = m; the rows of the stoichiometric matrix are not linearly dependent; therefore, for any $\boldsymbol{V_k}$ the system is automatically consistent.
- *Redundant: rank* ($\boldsymbol{S_u}$) < m; the rows of the $\boldsymbol{S_u}$ are not linearly independent. That means some of the rows can be expressed as linear combination of the other rows.

Besides, the elements in known and unknown vectors can be classified by the following properties:

Calculability: An element of unknown vector of $\boldsymbol{V_u}$ is called

- *Calculable*: if that specific rate can uniquely be evaluated by Equation 2-30
- *Noncalculable*: if it cannot uniquely be evaluated using Equation 2-30

Balanceability: An element of measured vector of $\boldsymbol{V_k}$ is called

- *Balanceable*: if the consistency of the system 2-30 depends on the value of this rate.
- *Nonbalanceable*: if the consistency of the system 2-30 is independent of the value of this rate.

2.5.5 Determined Systems

In case of determined systems the degrees of freedom of the system is zero. Thus, the solution to Equation 2.30 is unique and the remaining internal fluxes can be easily calculated by standard methods for solving linear algebraic equations. It is necessary for a unique solution that the set of algebraic equations be not redundant (*rank* ($\boldsymbol{S_u}$) = n_u = m). All unmeasured fluxes can be evaluated by using the inverse of the nonsingular matrix $\boldsymbol{S_u}$:

$$\boldsymbol{V_u} = -\boldsymbol{S_u}^{-1} . \boldsymbol{S_k} . V_k \tag{2-31}$$

For example, the metabolism of *Penicillium chrysogenum* has been studied using metabolic flux analysis (Jorgensen et al., 1995). The model included 49 intracellular metabolites, 82 internal fluxes, and 33 fluxes were measured, same as the number of degrees of freedom of their proposed system.

2.5.6 Overdetermined Systems

If there are more measurements available than the degrees of freedom, the system is generally called *overdetermined.* In this case the excess number of measurements can be used to (Stephanopoulos et al., 1998):

- Calculate the remaining internal fluxes
- Apply a least-square type analysis with appropriate criterion to increase the confidence in the measured fluxes
- Specify the main source of measurement errors

The starting point for this analysis is also Equation 2.30 and the solution is determined using a least-square technique to minimize the error between the calculated fluxes and the measured fluxes. Since the matrix $\boldsymbol{S_u}$ is not square, its inverse cannot be calculated, however, if this equation is multiplied by the transpose of $\boldsymbol{S_u}$ the following expression is obtained:

$$\boldsymbol{S_u^T S_u V_u} = -\boldsymbol{S_u^T S_k V_k} \tag{2.32}$$

Matrix $\boldsymbol{S}_u^T \boldsymbol{S}_u$ is certainly square, and if it has a full rank it can be inverted to give the solution for $\boldsymbol{V}_u$ as shown below:

$$\boldsymbol{V}_u = -\boldsymbol{S}_u^{\#} \boldsymbol{S}_k \boldsymbol{V}_k \tag{2.33}$$

Here, $\boldsymbol{S}_u^{\#}$ is the Penrose pseudo-inverse of $\boldsymbol{S}_u$ that is defined as follows (Lee and Papoutsakis, 1999):

$$\boldsymbol{S}^{\#} = \left(\boldsymbol{S}_u^T \boldsymbol{S}_u\right)^{-1} \boldsymbol{S}_u^T \tag{2.34}$$

Equation 2.33 is essentially the least square estimate of the elements on the vector $\boldsymbol{V}_u$, where all balances have been used for their determinations. The above solution is very useful when there is a little noise in the measurements (Vallino and Stephanopoulos, 1993). If a significant amount of noise is present in only some of the measured fluxes, the solution of Equation 2.33 may not satisfy flux conservation around some network nodes.

2.5.7 Underdetermined Systems

If the number of measured internal fluxes is smaller than the degrees of freedom then the system is so-called *underdetermined*. Although the number of solutions for an underdetermined system is infinite, they lie in a restricted region defined as the metabolic genotype of a given organism (Varma and Palsson, 1994), because it defines all the metabolic flux distributions that can be achieved with a particular set of metabolic genes. It is possible to obtain a unique solution for the intracellular fluxes by optimizing an objective function subject to the constraints of the metabolic balances. If the objective function is linear, linear programming could be used to determine the distribution of internal fluxes. Since, all variables in linear programming are required to be nonnegative; one should revise the definition of metabolic fluxes, which may be either positive or negative. Therefore, the model has to be extended in such a way that includes both forward and backward fluxes for each of the n_u reactions in the model, or at least for those reactions that may be reversible. The revised form of Equation 2.30 by considering the individual reaction rates can be written as follows:

$$\boldsymbol{S_{u,ind}}\,\boldsymbol{V_{u,ind}} = -\boldsymbol{S_k}\boldsymbol{V_k} \qquad \text{and} \quad \boldsymbol{V_{u,ind}} \geq \boldsymbol{0} \tag{2.35}$$

Where $\boldsymbol{S_{u,ind.}}$ is the stoichiometric matrix $m \times n_{u,ind}$ including the stoichiometry of both forward and backward reactions and $\boldsymbol{V_{u,ind.}}$ is the corresponding revised unmeasured flux vector with dimension $n_{u,ind.}$.

The next step is to define an objective function that could be a linear function of the elements of vector $\boldsymbol{V_{u,ind.}}$. Then, the optimal solution is found by solving the corresponding maximization or minimization problem:

$$\begin{aligned} &\textit{Max / Min} \quad \boldsymbol{Z} = \boldsymbol{\Omega}.\boldsymbol{V}_{u,ind} \\ &\textit{Subject to} \quad \textit{Equation } 2.35 \end{aligned} \tag{2-36}$$

Here $\boldsymbol{\Omega}$ is a row vector, which specifies the influence of the individual fluxes on the objective function. A number of different objective functions have been used for metabolic flux analysis. These include the following:

1. *Minimize excess ATP production*. This objective is used to determine how energetically efficient metabolism can operate (Majewski and Dornach, 1990).
2. *Minimize nutrient uptake*. This objective function is stated to determine the conditions that cell can perform its metabolism while consuming the minimum amount of available nutrients (Savinell and Palsson, 1992).
3. *Minimize redox potential*. This objective function finds conditions where the cells operate to generate the minimum amount of redox potential (Lee and Papoutsakis, 1999).
4. *Minimize the Euclidean norm*. This objective function has been applied to channel the metabolites as efficiently as possible through the metabolic pathways (Bonarius et al., 1996).
5. *Maximize metabolite production*. This objective has been utilized to determine the biochemical production capabilities of organisms (Varma and Palsson, 1993a; Takac et al., 1998). In this analysis the objective function was defined to maximize the production of a chosen metabolite.

6. *Maximize biomass and metabolite production*. By considering an appropriate weight for these two conflicting objectives, one can specify the trade-off between cell growth and metabolite overproduction (Varma et al., 1993b).

This type of objective function can be stated by Equation 2.36 and it allows the examiner to obtain answers to a number of important questions.

2.5.8 Checking Calculability

The goal of metabolic balancing is the evaluation of as many elements of $\boldsymbol{V_u}$ as possible. An unmeasured rate can sometimes be calculated from the set of independent equations even in an underdetermined system, so it is very important to detect the calculable rates. Singular value decomposition (Van der Heijden et al., 1994) was first introduced in order to address the calculable rates. This method requires the calculation of three matrices. Klamt et al., (2002) determined the possible set of calculable rates by using the null space (kernel) of $\boldsymbol{S_u}$ (*ker* ($\boldsymbol{Su}$)) that is much easier to justify and employ. In their proposed algorithm, such elements $v_{u,j}$ of $\boldsymbol{V_u}$ are determined and therefore calculable, whose corresponding j^{th} row in *ker* ($\boldsymbol{Su}$) is a null row. The values of the detected calculable rates could be obtained by using the general approach of least- square solution by Equation 2-33. It is noteworthy that the non-calculable rates cannot be considered as determined by the least-square solution using the pseudo-inverse method.

2.5.9 Checking Balanceability and Consistency

If a system of equations is not redundant, it will be automatically consistent for any $\boldsymbol{V_k}$, so the balanceable rates are associated with only a redundant system. Substitution of Equation 2.33 into Equation 2.30 yields:

$$\boldsymbol{R}.\boldsymbol{V_k} = \boldsymbol{0} \tag{2.37}$$

Where $\boldsymbol{R}$ is the redundancy matrix and is defined as:

$$\boldsymbol{R} = \boldsymbol{S_k} - \boldsymbol{S_u}.\boldsymbol{S_u^{\#}}.\boldsymbol{S_k} \tag{2.38}$$

Equation 2-37 expresses the relationship between only measured rates. For a non-redundant system, the redundancy matrix is null and therefore Equation 2-37 is consistent for any measured vector. In contrast, due to unavoidable measurement errors, Equation 2-37 is not normally fulfilled in case of a redundant system; hence, the system is inconsistent. Balanceable rates as the main candidate for system inconsistency in the latter case and it can be detected by an inspection of redundancy matrix.

For any null column of $\boldsymbol{R}$, there is no meaningful expression for the corresponding rate in terms of the other measured rates and that rate is not balanceable. Therefore, if j^{th} column of redundancy matrix contains at least one non-zero element, the corresponding measured flux of $v_{b,j}$ is balanceable. The balanceable rates should be adjusted to obtain a consistent system in which the pseudo steady state mass balance set of equations is satisfied. Stephanopoulos et al., (1998) had shown that the variance-covariance matrix of the measurements along with the redundancy matrix can be used to adjust the balanceable rates.

2.6 Power-law Approximations

A number of nonlinear approximations have been utilized successfully to model the rate law of individual enzymatic reactions. The most commonly used mechanistic model is the Michaelis-Menten (1913) model, which is based on earlier ideas of Henri (1903). Although this function along with its derivatives and generalizations (e.g., Cleland, 1967; Koshland and Neet, 1968) reflect the nonlinear nature of the rate law, the expression becomes quite complicated when it involves several substrates and products. In addition, the complexity of the rate law becomes overwhelming if it also involves modulators. Furthermore, rate laws of this type may include a number of parameters when the pathway consists of a reasonable number of metabolites and modulators, so that an extraordinary number of experimental assays need to be carried out (Savageau, 1976).

Consequently, a different approach is required which leads to a simpler mathematical form, but still captures the nonlinear nature of the system. This new approach emphasizes integrated system modeling rather than individual detailed mechanisms. Then again, it may be based on the differential Equation 2-20 in case the functions V_{ij}^{+} and V_{ij}^{-} are specified. The problem is that the exact form of these functions is unknown (Heinrich and Schuster, 1996), but experience of the past three decades confirmed that the power-law approximation of the rate expression, which is equivalent to linear approximation in a logarithmic coordinate system, may be the best choice (Torres and Voit, 2002). There is no mathematical proof that these functions are the best possible descriptions of the exact model; nevertheless, there is considerable evidence supporting the adequacy of these types of functions (e.g., Savageau, 1976; Voit 1991). For instance, the general feature of the power-law representation is similar to the rate law for elemental chemical reactions, in which the original integer kinetic order based on some mechanism is replaced by a real number. Furthermore, a power-law approximation is equivalent to a first-order Taylor approximation in logarithmic space (Savageau, 1969).

2.6.1 Generalized Mass Action (GMA) Systems

Generalized mass action representations are based on power law-functions. In this representation, each process entering or leaving a variable is replaced individually with a

product of power-law functions, applying this approach to the general Equation 2.20 yields (Sierra and Fariren, 2001):

$$\dot{C}_i = \sum_{j=1}^{q_i} \alpha'_{ij} \prod_{l=1}^{m+m_I} C_j^{g'_{ijj}} - \sum_{j=1}^{w_i} \beta'_{ij} \prod_{j=1}^{m+m_I} C_j^{h'_{ilj}} \qquad i = 1,2,...,m \tag{2.39}$$

Where α'_{ij} and β'_{ij} are rate constants and g'_{ilj} and h'_{ilj} are kinetic orders of production and consumption (degradation) of the i^{th} metabolite, respectively. This model is intuitively proper for biochemical systems, because each process is explicitly represented by a separate term in the model (Torres and Voit, 2002). However, this approach has drawbacks, the most important being that the GMA form often does not have an explicit algebraic form for steady state calculations. This drawback becomes of crucial importance for optimization, since a number of equations may need to be solved by trial and error simultaneously.

2.6.2 S-Systems

For this representation within the power-law formalism, elementary fluxes are grouped into aggregated fluxes that pass into and out of metabolic pools. The general Equation 2.20 then can be written as:

$$\dot{C}_i = V_i^+(\boldsymbol{C}, \boldsymbol{P}) - V_i^-(\boldsymbol{C}, \boldsymbol{P}) \qquad i = 1,2,...,m \tag{2.40}$$

Where V_i^+ and V_i^- are all processes that increase the production and degradation of the metabolite *i*, respectively. The multivariable power-law representation of V_i^+ and V_i^- are presented as (Voit, 2000):

$$V_i^+(\boldsymbol{C}, \boldsymbol{P}) = \alpha_i C_1^{g_{i1}} \cdots C_m^{g_{im}} C_{m+1}^{g_{i,m+1}} \cdots C_{m+m_i}^{g_{i,m+m_i}} \tag{2.41}$$

and

$$V_i^-(\boldsymbol{C}, \boldsymbol{P}) = \beta_i C_1^{h_{i1}} \cdots C_m^{h_{i,m}} C_{m+1}^{h_{i,m+1}} \cdots C_{m+m_i}^{h_{i,m+m_i}} \tag{2.42}$$

Where α_i and β_i are the rate constants and determine the speed of production and degradation of metabolite *i*, respectively. The exponents g_{ij} and h_{ij} are the reaction orders

with respect to dependent or independent variables C_j that affect the production or degradation of M_i, respectively. The rate constants may be positive or zero, but cannot be negative, whereas the reaction orders need not be integers. If C_j has a positive effect, the corresponding kinetic order is positive; if it has a negative or inhibitory effect, the corresponding kinetic order is negative. Regarding Equation 2-40 for each dependent variable, the change in time is stated as the difference of two functions, V_i^+ and V_i^-. This equation may depend on some or all dependent and independent variables. Only those variables that directly affect the process under consideration enter the power-law representation. Substituting the functions given by Equation 2-41 and Equation 2-42 into Equation 2.40 and using the usual notation of product yields the biochemical system representation:

$$\dot{C}_i = \alpha_i \prod_{j=1}^{m+m_1} C_j^{g_{ij}} - \beta_i \prod_{j=1}^{m+m_1} C_j^{h_{ij}} \qquad i = 1,2,...,m \tag{2-43}$$

This system of equation is called S-system (Voit, 2000). S-systems have very interesting features for modeling and analysis of biochemical systems, because they can take into account all typical nonlinearities (Savageau and Voit, 1987). In addition, they allow a various algebraic and numerical analyses, and seem to be accurate enough in variety of relevant situations (Voit, 1992).

2.7 Fermentation Control

The control of a fermentation process requires accurate on-line knowledge about the main process variables. For a successful operation more reliable measurements can be achieved by improvements at both the hardware and software level. By combining powerful and flexible software with modular instrumentation hardware, one can create a customized instrument that meets the needs of his/her application. The computer programs can be used for data acquisition, mathematical operations of the control algorithm, communication between different devices, and remote control of bioprocesses. Stoll et al. (1996) developed a system for the independent control of ammonia and glutamine in a hollow-fiber reactor using a fully automated flow injection analysis and a virtual programming language. Kellerhals et al. (1999) developed a closed-loop control system based on on-line gas chromatography to maintain continuously fed substrates at desired level using the graphical programming environment LabVIEW.

2.7.1 LabVIEW Software

National Instrument Corporation's LabVIEW is a leading software tool for designing test, measurement, and control systems in industry and academia. While LabVIEW has the performance and flexibility of general purpose programming languages such as Visual Basic or Visual C^{++}, it is also a high-level rapid development environment used to develop measurement and automation application (National Instrument Measurement and Automation Catalog, 2006). LabVIEW has the same constructs as traditional languages, including variables, data types, looping and sequencing structures, and error handling. In general purpose programming languages, code is as much concern as the application. The user may pay close attention to the syntax (e.g., commas, semicolons, etc.), which is quite tedious. On the other hand, LabVIEW is a higher-level language that uses icons to represent functions, so the user wires icons together to determine the flow of data through the program.

Technically LabVIEW is a dataflow programming language. In other words, program data flows from a data source to one or more data sinks and it propagates through the program in this fashion. Because of dataflow property, LabVIEW is not linear like

conventional development applications and can execute multiple operations in parallel. This property is depicted with a simple example in Figure 2.6.

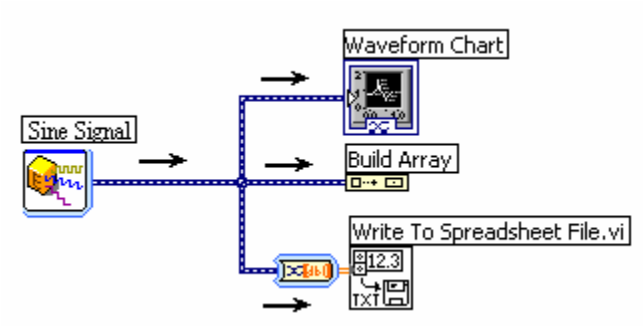

Figure 2.6- Dataflow property of a LabVIEW program.

The sinus waveform is plotted, an array of the data is built, and the waveform is saved to a spread sheet file all in parallel.

2.7.2 Programming Pattern

User-written LabVIEW programs are called Virtual Instruments (VIs). VIs are composed of three main parts: Front Panel window, Block Diagram window, and Icon/Connector.

The Front Panel window serves as the graphical user interface for data inputs and outputs. The user inputs such as knobs, buttons, and switches are displayed on the Front Panel. Inputs on the Front Panel are called Controls. Outputs, such as graphs, LEDs, and meters are called Indicators. The user can use this window to design a user interface that is convenient to use and present the data in the most useful way.

Graphical source code is developed in the Block Diagram window. All of the Controls and Indicators from the Front Panel have an associated terminal that represents them on the Block Diagram. Block Diagram is responsible for the actual data flow between the inputs and outputs. Various operations and analysis on the data may be performed by wiring the terminals to functions in LabVIEW.

After a VI is developed, it may be used as a subroutine for another VIs; which in this case the former VI is called subVI. An Icon is a graphical representation of a VI, which

identifies the subVI when it is called from the Block Diagram of another VI. The user also needs to build a Connector pane to use the VI as subVI. The Connector pane is a set of terminals that corresponds to the inputs and outputs of the VI, similar to the parameter list of a function call in text-based programming languages.

2.7.3 PID Algorithm

Feedback control involves the comparison of the measured value of the controlled variable with its set point and makes adjustments to the manipulated variable in an effort to drive the controlled variable to its setpoint. Currently, the PID (proportional integral differential) algorithm is the most common algorithm used in industry. The PID controller determines a controller output value, such as heater power or control valve position in an analog system and heater or solenoid valve switches in a digital system. In PID control, one must specify a process variable and a set point. The process variable is the system parameter that should be controlled, such as temperature, fluid level, dissolved oxygen and the set point is the desired value for the parameter. The controller applies the controller output value to the system, which in turn drives the process variable toward the set point value. The PID controller compares the set point to the process variable to obtain the error:

$$e(t) = M_{s.p.} - M_{p.v.} \tag{2.44}$$

Controller output is the summation of the proportional, integral, and derivative actions:

$$u(t) = u_P(t) + u_I(t) + u_D(t) \tag{2.45}$$

The different three actions are defined as follows:

$$\begin{aligned} u_P(t) &= K_c\, e(t) \\ u_I(t) &= \frac{K_c}{\tau_I} \int_0^t e(t).d(t) \\ u_D(t) &= K_c\, \tau_D \frac{d\, e(t)}{dt} \end{aligned} \tag{2.46}$$

Where K_c is the controller gain, τ_I is the integral time (rest time) in minutes, and τ_D is the derivative time (rate time) in minutes. Upon substitution of the individual actions into Equation 2.45 it yields:

$$u(t) = K_c\left(e(t) + \frac{1}{\tau_I}\int_0^t e(t).d(t) + \tau_D \frac{de(t)}{dt}\right) \tag{2.47}$$

2.7.4 Tuning Method

Tuning PID loops is one of the major tasks of a control process and the resulting settings have a dominant effect on the performance of a PID control loop. Often, many controllers are poorly tuned. As a result, some controllers are too aggressive and some controllers are too sluggish. Tuning a PID controller needs selecting values for K_c, τ_I, and τ_D . The proper evaluation of the settings will fulfill the operational objectives of the control loop which usually are an appropriate compromise between performance (minimizing deviations from setpoint) and reliability (the controller's ability to remain in service while handling major disturbances) (Riggs, 1999).

Although there are different methods for tuning PID controllers, one of the earliest tuning methods developed by Ziegler-Nichols is presented below. The procedure comprises the following steps (Riggs, 1999):

- With P-only closed-loop control, introduce a set point change and increase the magnitude of the proportional gain until a sustained oscillation is observed.
- The value of controller proportional gain that causes the sustained oscillation is ultimate gain, K_u. Ultimate period, P_u, is the period of the continuous oscillations.
- Regarding the controller chosen, calculate the controller settings using Table 2.3.

Table 2.3- Ziegler-Nichols closed-loop gain settings

Controller	K_c	τ_I	τ_D
P	0.5 K_u	---	---
PI	0.45 K_u	P_u /1.2	---
PID	0.60 K_u	P_u /2.0	P_u /8

For slow response loops (e.g., certain temperature and composition control loops), the aforementioned method of evaluating the ultimate parameters can be a time consuming procedure that leads to less than satisfactory results. Instead, the ATV (autotune variation) method can be used in a manner similar to the ultimate method, but ATV tests can be implemented without upsetting the process. The most common method of ATV utilizes a relay switch to create what is essentially an on-off controller. The resulting oscillatory behavior is analyzed to determine the proper controller settings.

To initiate an ATV test, the system should be at steady state or near steady state conditions. Then the manipulated variable is switched between a maximum and minimum value based on the error as follows:

$$\begin{aligned} &if\ e(t) < 0, then\ u(t) = u_{max} \\ &if\ e(t) > 0, then\ u(t) = u_{min} \end{aligned} \tag{2.48}$$

The allowable input change is h, so $u_{max} = h$ and $u_{min} = -h$. There are two parameters that result from this method. One is the ultimate period of successive peaks, P_u, and the other is the amplitude of the process output, a. The ultimate gain, K_u, is calculated by (Riggs, 1999):

$$K_u = \frac{4h}{\pi a} \tag{2.49}$$

The ultimate parameter values can then be established by one of tuning approaches such as Ziegler-Nichols scheme.

CHAPTER 3

MATERIALS AND METHODS

3.1 Microorganism

A recombinant *Aspergillus niger* strain HEWL WT-13-16 was kindly provided by Dr. Mackenzie of Institute of Food Research, Norwich Research Park, UK. This recombinant strain contains hen egg-white lysozyme cDNA gene which is expressed under the control of *A. niger* glucoamylase promoter (glaA). Although initially introduced as a plasmid, the HEWL gene is incorporated into the host cell genome.

3.2 Stock Culture Preparation

The single cell selection and cloning procedure was performed as outlined by Mc Neil and Harvey (1990). Minimal growth medium was used during the inoculum preparation. First, the fungal culture was grown on agar surface in sterile Petri dishes at 30 ^{o}C for 7 days. The conidia were harvested from the surface by adding 9 ml sterile de-ionized water and scraping the surface with a sterile inoculating loop to obtain a dense suspension of spores. The suspension was then transferred to a 50 ml sterile tube containing 5 sterile spherical glass beads, 4 mm diameter, and vortex mixed to break up spore clumps. Following filtration, several dilution series (10^{-2}- 10^{-8}) of filtrate were prepared in sterile de-ionized water. Then, 100 μl aliquots of the dilution series was spread on the surface of agar in Petri dish and incubated at 30 ^{o}C. After 2 days a plate with a count of 20- 50 colonies (dilution factor 10^{-6}) was chosen for further examination. Three separate colonies with noticeable growth were transferred from the plate onto the surface of an agar slant in 20×150 mm tubes and incubated at 30 ^{o}C for 7 days. The spores were

harvested from the surface of slants, vortex mixed, and filtered. Three flasks, each containing 50 ml of medium ACM/N (Archer et al., 1990) were prepared and inoculated with 40 μl of spore suspension. The slant corresponding to the highest level of protein production was considered as the master culture. To prepare a bank of this single suspension several plates were inoculated with 100 μl of the suspension. After incubation at 30 ^{o}C for 7 days, the conidia were harvested by suspending in 20% (v/v) glycerol solution, vortex mixed, and filtered. Approximately, 1 ml aliquots of the spore suspension were dispensed into 1.5 ml cryogenic vials and stored at -80 ^{o}C as spore stock. The conidium concentration of the spore stock was assessed as approximately 5×10^{7} spores/ml using a hemocytometer.

3.3 Medium Composition

Two types of medium have been used throughout this study, the minimal medium for preparing the spore bank and the complete medium for fermentation.

3.3.1 Minimal Medium

The minimal medium known as AMMN (MacKenzie et al., 1994) was used. The medium contained (per liter): glucose 10 g, salt solution 20 ml, agar 20 g, KNO_3 6 g, and de-ionized water to 1 liter.

3.3.2 Complete Medium

The media were based on ACMS (Archer et al., 1990a) with some modifications according to the applied methods throughout this study. Starch or glucose was used as carbon source and amino acids mixture or peptone (Bacto^{TM}) was supplied as organic nitrogen source in the media. The detailed concentrations of each constituents are presented in each phases of this work. Salt and trace element solutions were basically similar to those described by Cove, 1966 as follows:

Salt solution: KCL 26 g, $MgSO_4.7H_2O$ 26 g, KH_2PO_4 76 g, trace element solution 50 ml, chloroform (as preservative) 2 ml, de-ionized water to 1 liter.

Trace element solution: $Na_2B_4O_7.10H_2O$ 40 mg, $CuSO_4.5H_2O$ 400 mg, ferric phosphate (Sigma F-1523) 646 mg, $MnSO_4.2H_2O$ 800 mg, $Na_2MoO_4.2H_2O$ 800 mg, $ZnSO_4.7H_2O$ 8

g, de-ionized water to 1 liter. In order to dissolve the salts the pH was brought to 4.10 using 2N H_2SO_4.

The amino acid content of the peptone was provided by the supplier (Becton, Dickinson and Company). The composition was (as wt %): Ala 9.2, Arg 5.8, Asp 5.0, Glu 8.1, Gly 15.9, His 0.8, Ileu 2.1, Leu 3.8, Lys 3.4, Met 0.7, Phe 2.8, Pro 8.8, Ser 1.5, Thr 1.1, Tyr 0.6, Val 2.8.

Sodium citrate/citric acid (0.97M, PH 6.5) buffer was used in all shake flask experiments, because biomass increased very fast in un-buffered medium while the pH dropped as low as 2.0. Both growth and protein secretion were reported to be inhibited by acidic conditions (Archer et al., l995). Besides, in their paper on the production of HEWL under the control of *A. niger* glucoamylase promoter, MacKenzie et al. (1994) and Mainwaring et al. (1999) found that initial low pH in batch culture had a negative effect on total HEWL production. For this reason, the initial medium pH was adjusted to 6.00 with either NaOH or H_2SO_4.

3.4 Analytical Procedures

Samples were analyzed for concentrations of cells, glucose, ammonia, organic acids, amino acids, phosphate, and sulfate throughout the fermentation. Each analysis was carried out in triplicate and the average was reported and used in this study. The absorbance of the samples for different assays was measured with a Multiscan Ascent photometer micro plate reader.

3.4.1 Biomass Concentration

Biomass concentration was determined by dry weight measurements. The sampling device was modified to provide representative samples of the culture. 3×5 ml samples were taken at specific time intervals and filtered on predried, preweighed filters (4.25 cm GF/C filter, 1.2 μm, Whantman No. 42) under vacuum. Filter cakes were washed with distilled water twice and dried at 80 ^{o}C for at least 24 hr to constant weight. The filtrate was stored at -35 ^{o}C for further analysis.

3.4.2 Lysozyme Assay

Secreted HEWL were assayed at 30 ^{o}C in 52 mM sodium phosphate buffer (pH 6.24) using the method of Archer et al (1990). Lysis of *Micrococcus luteus* cells (0.25 mg/ml) (Sigma M-3770) was monitored by measuring the decrease in absorbance at 540 nm over a 5-minute period. The standard curve, obtained with authentic HEWL (Sigma L-6876), was linear within the range of 0.6-4.0 (mg lysozyme/L). A typical standard curve is presented in Appendix D Figure D.1. The total volume of 300 μL including 250 μL of *M. luteus* solution and 50 μL of diluted sample solution in sodium phosphate buffer was used for each determination.

3.4.3 Glucose Assay

The glucose content was analyzed enzymatically by a glucose kit (Megazyme Glucose Test Kit). The method is based on the glucose oxidase/peroxidase reaction. The intensity of the formed dye is proportional to glucose concentration when the absorbance of the assay mixture is read at 510 nm against the reagent blank after 20 minutes incubation at 40 ^{o}C.

3.4.4 Organic Acids Assay

Low molecular weight organic acids were measured with a Varian ProStar reverse phase HPLC system (Varian analytical Instruments, USA). The ProStar system consists of an autosampler 410, two 210 solvent delivery system, and a 325 UV-vi detector. Separation was performed on an Inertsil C8-3 column (150 × 4.6 mm, I.D.) with particle size of 5 μm. Star Chromatograph Workstation version 6.0 was used to acquire data from the detector and process data to obtain quantitative and qualitative results.

The organic acid content of the fermentation samples was quantified using the method described by (Gawthray, 2003) with modification of the mobile phase. All the samples and standards were acidified to pH 2.7 with *ortho*-phosphoric acid. He proposed a mobile phase composed of 93% 25 mM KH_2PO_4 and 7% methanol at the total flow rate of 1 ml/min. However, it was found that using a mobile phase of 99.5% 25mM $NH_4H_2PO_4$ and 0.5% methanol at a total flow rate of 0.7 ml/min gave better separation for most of the organic acids under study using the HPLC system outlined in this section.

Accordingly, the concentrations of oxaloacetate, acetate, α-ketoglutarate, citrate, fumarate, malate, pyruvate, oxalate, gluconate, and succinate were determined at 210 nm and temperature of 27 ^{o}C. A typical separation of organic acids is shown in Figure 3.1.

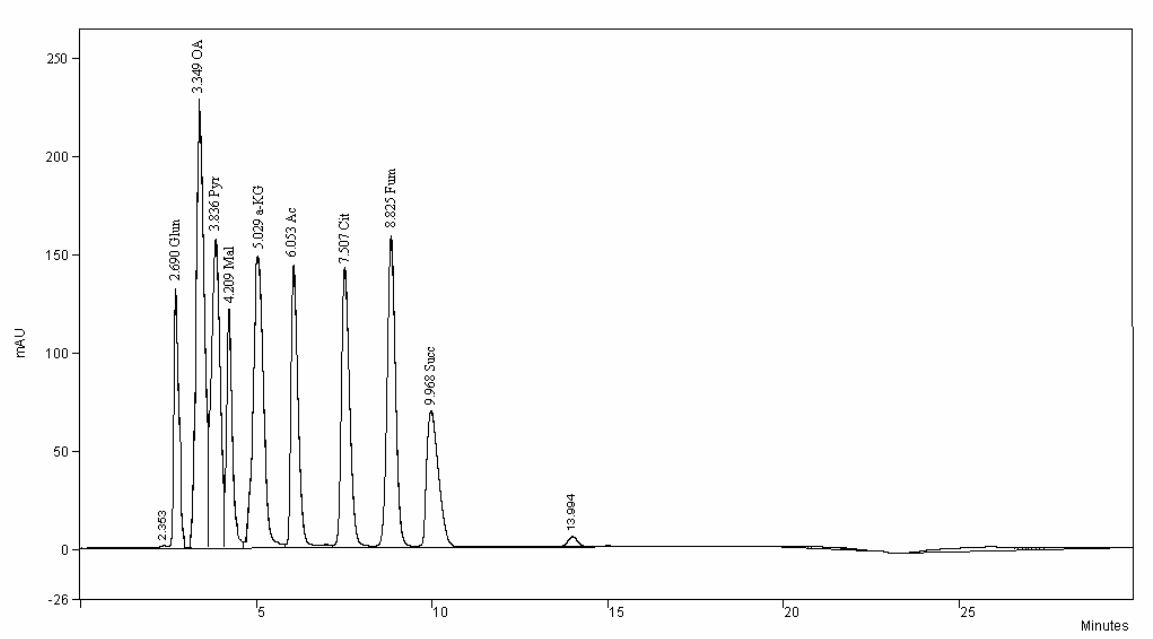

Figure 3.1- Separation of organic acid standards by HPLC with 99.5% 25 mM $NH_4H_2PO_4$ and 0.5% methanol, pH 2.7, 0.7 ml/min, temperature 27 ^{o}C, wavelength 210 nm.

The co-elution between gluconate and oxalate was not prevented by the proposed system, so the first peak in the samples was the sum of absorbance of gluconate and oxalate peaks. Therefore, concentration of gluconic acid in each fermentation sample was determined enzymatically by a specific kit for gluconic acid (Megazyme gluconic acid kit). Since a micro plate reader was used for the analysis, the pipetted volumes of the solutions (i.e., reagents and sample) were reduced ten fold relative to the original assay. The absorbance of each sample solution was monitored over a period of 30 minutes. The conversion of gluconic acid was found to be completed in 15 minutes after the addition of the last reagent. The concentration of gluconic acid and the area of the first peak in the chromatogram of each sample (as the indicator of both acids) along with the calibration

curve of both acids were used for calculating the oxalic acid content of the corresponding sample.

Ultra-pure specimen of the organic acids from Sigma were used to prepare the standard solutions. Calibration curves for the organic acids were determined by at least four different concentrations and are presented in Appendix D Figure D.2. Curves were obtained by plotting the mass of organic acid injected versus peak area. The coefficients of determination (R^2) for all organic acids except gluconate were greater than 0.9998 which showed a perfect linear correlation among the data. Gluconate was the only organic acid with a lower, but still significant coefficient of determination of 0.9871.

3.4.5 Ammonia Assay

Ammonia was measured using a pH/ISE meter model 710A equipped with an ammonia gas-sensing Ion-selective electrode (Beckman). The measurement of ammonium ions with the electrode requires adjustment of the standards and samples to above pH 11 to convert the ammonium ions to ammonia gas. The hydrophobic membrane allows the ammonia gas to pass though the inner chamber of the electrode to be converted back to ammonium ions that is detectable as a pH change in the internal filling solution. The pH adjustment was performed by adding 10M NAOH to the solutions immediately before measurements. The pH change was calibrated against known concentrations of NH_4Cl to cover the ammonia concentration in range of 10-100 ppm.

3.4.6 Inorganic Ion Assay

Phosphate and sulfate were measured using an Ion Chromatography system (Dionex, DX 500 Chromatographic system, USA).

3.4.7 Amino Acids Assay

To determine the free amino acid content of the media, the pre-column derivatization method with phenylisothiocyanate (PITC) (Bidlingmeyer et al., 1984) was used. The samples including up to 50 nmol of each amino acid that resulted a maximum of 975 nmol total amino acid concentration were dried under high vacuum. Then, 20 μl of ethanol: water: triethylamine (TEA) (2:2:1) were added to the samples and dried again

under vacuum. The residual amino acids were ready for derivatization. The derivatization reagent was made fresh and consisted of ethanol: TEA: water: PITC (7:1:1:1) where PITC was added to this solution under nitrogen environment. The derivatized form of amino acids was formed by adding 20 μl of reagent to the dried samples under nitrogen atmosphere and sealing them for 20 minutes at room temperature. The reagents were then removed under vacuum. The derivatized amino acids can be kept dried and frozen for several weeks without significant degradation (Heinrikson and Meredith, 1984).

Reverse phase HPLC was performed at 55 ^{o}C with the same system that was explained for organic acid analysis. The proposed solvent system consisted of two eluents. Solvent A as the aqueous buffer was a solution of 0.14 M sodium acetate containing 0.5 ml/L TEA which titrated to pH 6.35 using glacial acetic acid. Solvent B was a 60% solution of acetonitrile in water.

Different gradient of the solvent system have been performed and checked for optimum resolution of amino acids. The optimum gradient is presented in Figure 3.2.

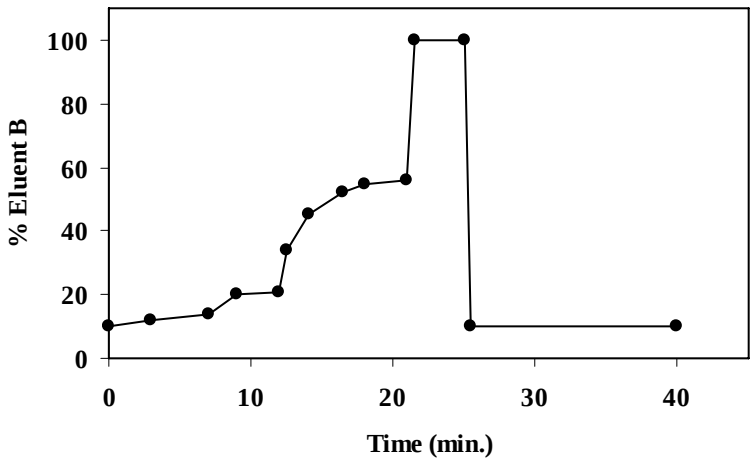

Figure 3.2- Gradient profile for amino acid analysis. Eluent A: 0.14 M sodium acetate, 0.5 ml TEA, pH 6.4; Eluent B: 60% acetonitrile in water. Flow rate 0.6 ml/ min.

Prior to HPLC, the derivatized samples were dissolved in 500 μl of solvent A. Then, 10 μl of the sample solution were injected into the column using the autosampler device. In order to determine the retention time of each amino acid, individual amino acid samples were derivatized and analyzed with the liquid chromatograph. It was observed that the retention times were irregularly shifted when compared with a mixture of the same amino acids. Based on these observations, it was concluded that the individual retention time analysis would not be useful for differentiation between the amino acids in a mixture. To overcome this difficulty a mixture of amino acid standard were analyzed as a basis. Then, an extra amount of each amino acid was added to the same amino acid standard solution and the results were compared to the basis in order to specify the retention time of the individual amino acid. A typical separation of amino acid standards using this protocol is presented in Figure 3.3

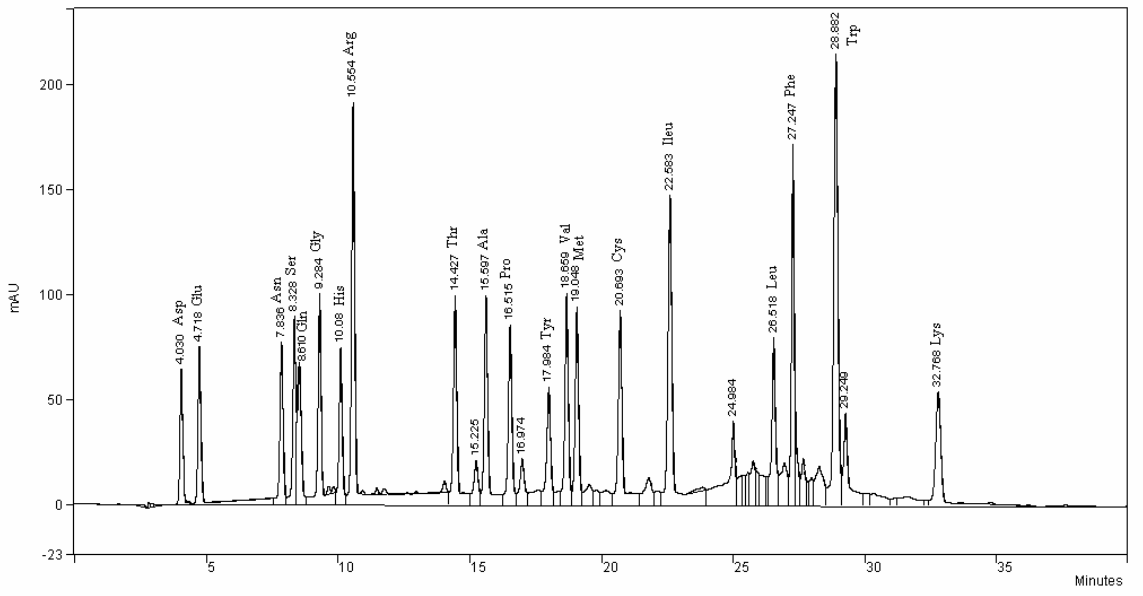

Figure 3.3- Separation of amino acid standards by HPLC. Eluent A: 0.14 M sodium acetate, 0.5 ml TEA, pH 6.4; Eluent B: 60% acetonitrile in water. Flow rate 0.6 ml/ min.

For any chromatographic analysis, it is important to determine the range of the concentration within which the response is linear. Different concentrations varying from

31 to 1000 pmol of amino acid standard mixture were derivatized and analyzed to assess the linear range of the reaction. Samples were run in triplicate, and the average areas were calculated. The data are plotted in Appendix D Figure D.3 and show that linear response is indeed obtained. The coefficient of determination for all amino acids exceeded 0.99 with the exception of tyrosine and cysteine which had the poorest linearity with a coefficient of determination of approximately 0.98.

3.4.8 Protease Assay

Protease activity was determined by the method of Dunn (1989). The substrate solution with a concentration of 2% (w/v) was prepared by dissolving azocasein in 50-100 mM of sodium phosphate buffer. A sample volume of 48 μl of either fresh or frozen culture filtrate was added to 80 μl of substrate solution in a 1.5 ml microcentrifuge tube and mixed gently, but thoroughly. Mixtures were incubated at 25 ^{o}C for 30 minutes before stopping the reaction by adding 384 μl 10% (w/v) trichloroacetic acid. The contents of each microcentrifuge tube was mixed thoroughly and allowed to stand for 15 minutes. One blank was prepared for each individual sample to account for the background effect of the sample color. First trichloroacetic acid was added to each sample and vortex mixed and then the substrate solution was added. This assured that there was no possibility for a reaction between the substrate and enzyme solutions. The samples were centrifuged at 12000 for 5 minutes. Then 384 μl of the resulting supernatant was added to 448 μl of 1 M NaOH and vortex mixed. Finally, 300 μl of the solutions were transferred to plate wells and the absorbance was determined at 450 nm. One unit of enzyme activity was defined as the amount of enzyme necessary to give an absorbance change of 1 under the assay conditions.

3.4.9 Off-Gas Analysis

Carbon dioxide and oxygen concentrations were monitored online at the inlet and outlet of the fermenter with a solid-sate infrared CO_2 sensor and an electrochemical oxygen sensor, respectively (Model 902, Quantek Instruments, USA).

CHAPTER 4

EXPERIMENTAL DESIGN

4.1 Introduction

Growth and metabolism of cells are strongly influenced by medium composition such as the carbon source, nitrogen source, and inorganic salts (Haq et al., 2003; Swift et al., 2000). However, employing factorial design to attempt to obtain optimum levels of all nutritional factors is not an easy task. The traditional one-factor-at-a-time method for optimizing a multivariable problem is not only time and resource consuming, but also might provide the investigator with wrong conclusions (Oh et al., 1995). Response surface methodology (RSM), on the other hand is a powerful tool to deal with these kinds of problems. It provides a methodology to design experiments, build models, evaluate the effective factors, and search for optima in the response variables. Statistics based experimental designs for optimization have been used in many areas of biotechnology such as optimization of a culture medium (Ooijkaas et al., 1999), enzyme production (Ismail et al., 1998; Park et al., 2002), ethanol production (Mübeccel and Mutlu, 2000), and biomass production (Yu et al., 1997). Cortin et al. (2005) employed a multi-step statistical optimization strategy involving factorial design and response surface analysis for the maturation of human megakaryocytes (MK). They found that the combination of the two statistical methods is helpful for optimizing the MK culture system. They argue that the model for cell physiology should be constructed with care and, if necessary, should include the important higher order interactions between medium components (Michaud et al., 2005). To the best of my knowledge, this technique has not been applied for optimization of medium for fungi producing a recombinant protein.

The objective of this study was to evaluate the effects of the medium components for hen egg white lysozyme production by recombinant *A.niger* WT-13-16 and to search for the optimum medium composition for maximizing production. Initially, a fractional factorial design (2^{5-1}) was used to seek for the most important medium ingredients among starch, peptone, ammonium sulfate, yeast extract, and $CaCl_2.2H_2O$. Previously published experimental results on *A.niger* nutrition are conflicting. For example, it has been reported that addition of 10 mM of Ca^{2+} to the growth medium reduces the yield of lysozyme (Spencer et al., 1999). On the other hand, the addition of divalent cations to the medium (Ca^{2+}, Zn^{2+}, and Fe^{2+}) gave loose and frayed mycelial pellets and enhanced growth and product formation (Gyamerah et al., 2002). Consequently, Ca^{2+} was considered as one of the factors to be investigated. In subsequent optimization steps the concentration of the components which have a significant influence on the enzyme production were further optimized using the central composite design and response surface method.

4.2 Materials and Methods

Medium contained the following components (per liter): soluble starch (Difco), peptone (Becto^{TM}), ammonium sulfate, yeast extract (Difco), $CaCl_2.2H_2O$ all as required in the experimental designs (see Tables 4.1, 4.3 , 4.7, and 4.8) as well as salt solution 20 ml, sodium citrate/citric acid (0.97M, PH 6.5) 100 ml.

Media without citrate buffer and $CaCl_2.2H_2O$ were prepared and autoclaved at 121 ^oC for 20 min. Citrate buffer and $CaCl_2.2H_2O$ were autoclaved separately. After autoclaving, the three solutions were mixed to give the final medium. This procedure prevented the formation of precipitate in the medium (Archer et al., 1995).

4.2.1 Inoculation and Incubation

Batch fermentations were carried out in 250 ml Erlenmeyer flasks containing 50 ml medium. The concentration of spore inoculum in each flask was 4×10^4 spores/ml. All fermentations were carried out at 25 ^oC and 150 rpm on an Innova 4330 refrigerated incubator shaker (New Brunswick Scientific Co., USA).

4.2.2 Sampling

Samples of approximately 500 μL were taken aseptically each 24 hr of fermentation. The samples were filtered using Nanosep centrifugal tubes with 10 μm filter pore size to remove cells. The filtrate was then stored at -35^{oC} for later analysis.

4.2.3 Experimental Design and Data Analysis

A three-step experimental design was used in developing a model for lysozyme production. The first step consisted of a fractional factorial design (FFD) to identify which medium ingredients had a significant effect on recombinant protein production. The second set of experiments was then carried out along the path of steepest ascent to ascertain the vicinity of the optimal region. In order to describe the behavior of the response in the optimum region the Box-Wilson experimental design (CCD) (Box et al., 1978) was used. The statistical analysis of the results was performed with the aid of Design Expert version 6.0.4 statistical software (Stat- Ease Inc.).

4.3 Fractional Factorial Design (FFD)

4.3.1 Preliminary FFD

The purpose of the first optimization step was to identify the components of the medium that had a significant effect on lysozyme production within the ranges under study. A wide range of concentrations had been used previously for some medium ingredients of *Aspergillus niger* producing recombinant proteins. For instance, starch concentrations ranging from 10 to 50 g/l have been used for lysozyme production (Archer et al, 1990). Weibe and et al, (2001) supplemented some of their medium with soy peptone (4- 15 g/l) or peptone (100 g/l) and $(NH_4)_2SO_4$ (1.75 to 15 g/l) for t-PA production. The range and the levels of the variables utilized at the preliminary design are given in Table 4.1.

Table 4.1- Applied levels of independent variables in the preliminary FFD

Variable	Component	Applied Levels (g L^{-1})	
		- (Low)	+ (High)
X_1	Starch	10.0	20.0
X_2	Peptone	1.0	5.0
X_3	$(NH_4)_2 SO_4$	1.0	3.0
X_4	Yeast Extract	0.0	1.0
X_5	$CaCl_2.2H_2O$	0.0	1.0

A full factorial design would need 32 experiments, which is a high number. Instead, a 2^{5-1} fractional factorial design consisting of 16 factorial runs along with 3 other experiments at the center of the design for analysis of variance was carried out. The design was constructed by writing down the basic design having 16 runs (a 2^4 design in X_1, X_2,X_3, and X_4), selecting $X_1 X_2 X_3 X_4 X_5$ as the generator, and then setting the levels of the fifth factor $X_5 = X_1 X_2 X_3 X_4$).

The defining relation for 2^{5-1} was $I= X_1 X_2 X_3 X_4 X_5$, where I was the identity matrix. Accordingly, every main effect was aliased with a single four-factor interaction (for example, the effect of X_1 was really the linear combination of the main effect of X_1 and the four-factor interaction of $X_2 X_3 X_4 X_5$), and every two-factor interaction was aliased with a three-factor interaction. Then, the design was of resolution ***V*** and it was impossible to differentiate between the aliased terms. One would expect, however, that the 2^{5-1} design would provide valuable information in reference to the main effects and two-factor interactions.

The lysozyme concentration was taken as the dependent or response variable. The corresponding fractional experimental design and the experimental results are shown in Table 4.2. The normal probability plot of the effect estimates from this experiment is depicted in Figure 4.1. The main factor and their interaction effects were located along the line, which revealed none of the effects were significant in the range proposed in Table 4.1. Despite none of the factors and their interactions were important, peptone had the highest effect on lysozyme production in this design with a P-value of 0.063.

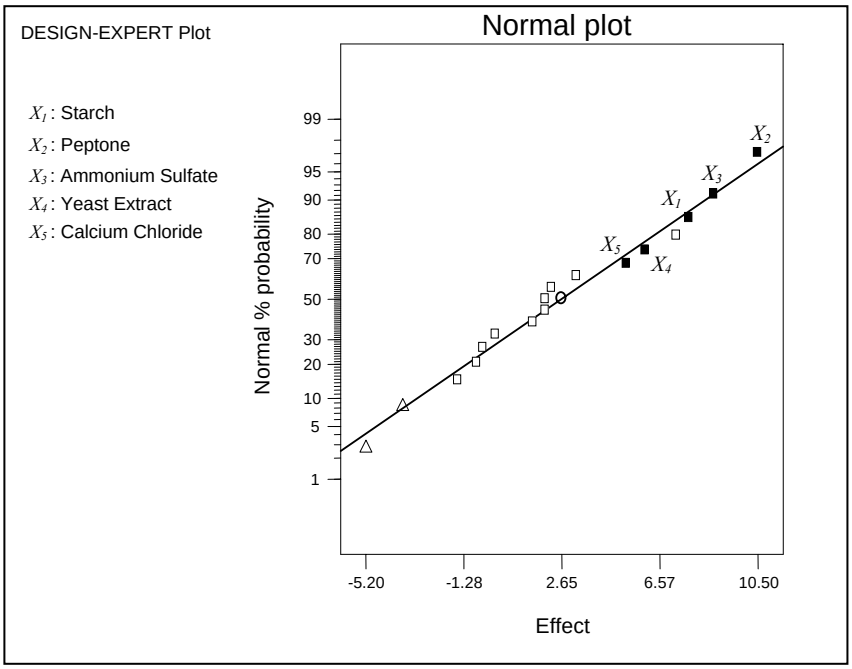

Figure 4.1- Normal probability plot of the effects for the lysozyme concentration in the Preliminary FFD.

Table 4.2- Experimental design and results of preliminary FFD

Run	Natural values (g L^{-1})					Lysozyme (mg L^{-1})
	X_1	X_2	X_3	X_4	X_5	$Y_{experimental}$
1	10	1	1	0	1	22
2	20	1	1	0	0	23
3	10	5	1	0	0	33
4	20	5	1	0	1	42
5	10	1	3	0	0	36
6	20	1	3	0	1	45
7	10	5	3	0	1	38
8	20	5	3	0	0	42
9	10	1	1	1	0	27
10	20	1	1	1	1	41
11	10	5	1	1	1	42
12	20	5	1	1	0	40
13	10	1	3	1	1	31
14	20	1	3	1	0	38
15	10	5	3	1	0	45
16	20	5	3	1	1	65
17	15	3	2	0.5	0.5	58
18	15	3	2	0.5	0.5	52
19	15	3	2	0.5	0.5	63

On the basis of the experimental values, statistical testing was carried out using Fisher's statistical test (not shown). The model P-value of 0.2478 implied that the model was not significant. The curvature F-value of 31.8 unveiled there was significant curvature in the design space and there was only 3% chance that the curvature could occur due to noise.

4.3.2 Revised FFD

To achieve the region where we could determine the significant factors on lysozyme production, a new 2^{5-1} fractional factorial design based on the elevated levels of starch, peptone, and ammonium sulfate was designed (Table 4.3).

Table 4.3- Applied levels of independent variables in the revised FFD

Variable	Component	Applied Levels (g L^{-1})	
		- (Low)	+ (High)
X_1	Starch	20.0	30.0
X_2	Peptone	5.0	15.0
X_3	$(NH_4)_2\ SO_4$	3.3	9.3
X_4	Yeast Extract	0.0	1.0
X_5	$CaCl_2.2H_2O$	0.0	1.0

Similar to the preliminary FFD the new design also consisted of 16 factorial runs, but 5 runs at the center point were considered. The idea was that with the higher number of center points the noise in the analysis could be estimated more accurately. For convenience, the independent variables in the model were utilized in their coded form. The variables were coded as x_i according to Equation 2.12. In this study, more specifically, we have:

$$x_1 = (X_1 - 25.0)/5.0$$

$$x_2 = (X_2 - 10.0)/5.0$$

$$x_3 = (X_3 - 6.3)/3.0$$

$$x_4 = (X_4 - 0.5)/0.5$$

$$x_5 = (X_5 - 0.5)/0.5$$

The corresponding 2^{5-1} fractional experimental design and the experimental results are shown in Table 4.4. The medium with the high level of all factors was associated with the highest concentration of lysozyme of 127 (mg L^{-1}).

Table 4.4- Experimental design and results of the revised FFD

Run	Coded values					Lysozyme (mg L^{-1})
	x_1	x_2	x_3	x_4	x_5	$Y_{experimental}$
20	-	-	-	-	+	60
21	+	-	-	-	-	72
22	-	+	-	-	-	94
23	+	+	-	-	+	92
24	-	-	+	-	-	74
25	+	-	+	-	+	83
26	-	+	+	-	+	105
27	+	+	+	-	-	118
28	-	-	-	+	-	62
29	+	-	-	+	+	76
30	-	+	-	+	+	100
31	+	+	-	+	-	93
32	-	-	+	+	+	67
33	+	-	+	+	-	89
34	-	+	+	+	-	100
35	+	+	+	+	+	127
36	0	0	0	0	0	101
37	0	0	0	0	0	90
38	0	0	0	0	0	87
39	0	0	0	0	0	101
40	0	0	0	0	0	85

4.3.2.1 Analysis of Variance of the Revised FFD (Full Model)

Table 4.5 illustrates the estimates of the effects and the analysis of variance for this experiment. The model F-value of 6.30 implied that the model was significant. The P-value of 0.3127 for the curvature showed that the curvature was not important in the design space, so a linear model was adequate to explain the response.

Table 4.5- Analysis Of Variance (ANOVA) for revised FFD (full model)

Source of Variation	$Effect_i$	SS_i	$d.f.$	MS_i	F	$p > F$
Model	11.00	5597.00	15	373.13	6.30	0.0440
X_1	30.75	484.00	1	484.00	8.18	0.0460
X_2	14.25	3782.25	1	3782.25	63.89	0.0013
X_3	2.00	812.25	1	812.25	13.72	0.0208
X_4	1.00	16.00	1	16.00	0.27	0.6306
X_5	-3.25	4.00	1	4.00	0.07	0.8077
$X_1 X_2$	6.75	42.25	1	42.25	0.71	0.4458
$X_1 X_3$	3.00	182.25	1	182.25	3.08	0.1542
$X_1 X_4$	0.50	36.00	1	36.00	0.61	0.4791
$X_1 X_5$	3.50	1.00	1	49.00	0.02	0.9029
$X_2 X_3$	0.75	49.00	1	49.00	0.83	0.4144
$X_2 X_4$	3.75	2.25	1	2.25	0.04	0.8549
$X_2 X_5$	-1.25	56.25	1	56.25	0.95	0.3849
$X_3 X_4$	-0.75	6.25	1	6.25	0.11	0.7615
$X_3 X_5$	5.50	2.25	1	2.25	0.04	0.8549
$X_4 X_5$	2.00	121.00	1	121.00	2.04	0.2260
Curvature	4.44	78.87	1	78.87	1.33	0.3127
Pure error		236.80	4	59.20		
Total		5912.67	20			

In order to approach the proximity of the optimum values, a model including the linear and interaction terms (see Equation 2.13) was fitted to the data obtained from the fractional factorial design experiments. For a region far from the maximum, this model was sufficient. Using this model, the response surface was represented locally by a twisted sloping plane. The values of the regression coefficients were calculated and the following equation was derived using the coefficients of the coded variables:

$$\hat{Y} = 88.25 + 5.5x_1 + 15.38x_2 + 7.13x_3 + 1x_4 + 0.5x_5 - 1.63x_1x_2 + 3.37x_1x_3 + 1.5x_1x_4 + 0.25x_1x_5 + 1.75x_2x_3 + 0.37x_2x_4 + 1.88x_2x_5 - 0.63x_3x_4 - 0.37x_3x_5 + 2.75x_4x_5 \quad (4.1)$$

Figure 4.2 is a normal probability plot of the effects. All the effects that lied along the line were negligible, whereas the large effects were far from the line. Hence, the yeast extract and calcium chloride did not significantly influence lysozyme production within the levels tested, but starch, peptone, and ammonium sulfate were the significant factors.

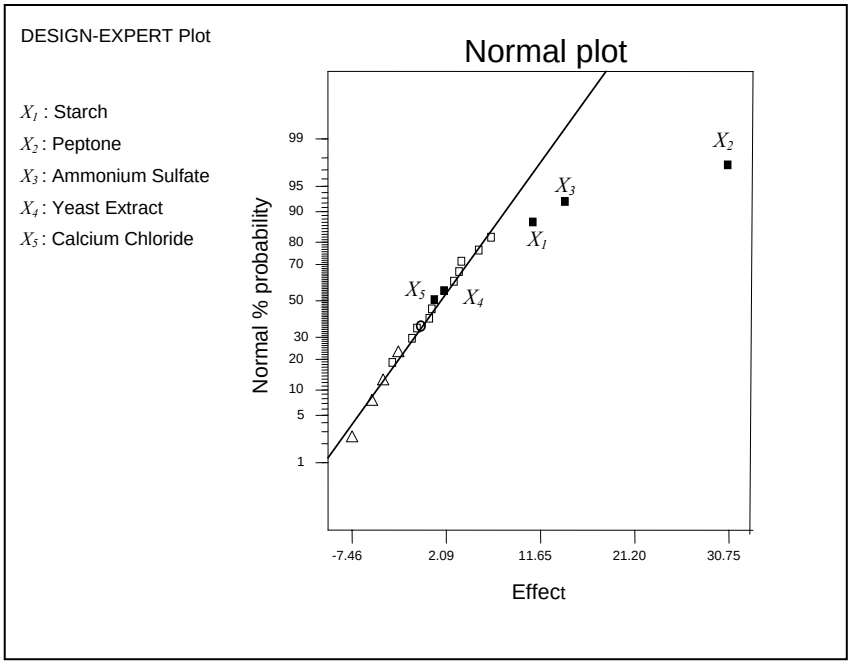

Figure 4.2- Normal probability plot of the effects for the lysozyme concentration in the revised FFD (Full model).

Examining the ANOVA table (Table 4.5) would lead one to identical conclusion. The main effects of X_1, X_2, and X_3 were the only terms with P-values less than 0.05 indicating that they were significant at the probability level of 95%. It is worth to recall that due to aliasing, each main effect was really the linear combination of the main effect and a single four-factor interaction. However, since it was reasonable to assume that high level interactions were negligible, it was concluded that only the main effects were important. The P-value of 0.0013 for peptone showed that it had very noticeable positive effect on lysozyme production. The high level of peptone allowed the strain to produce a higher level of lysozyme than the lower level. Also, increasing levels of starch and ammonium sulfate enhanced the concentration of lysozyme. According to the results shown in Table 4.5, starch, peptone, and ammonium sulfate effects together accounted for nearly 86% of the variability in the lysozyme production. After removing all nonsignificant terms from the model, Equation 4.1 can be reduced as follows:

$$\hat{Y} = 88.25 + 5.5\,x_1 + 15.38\,x_2 + 7.13\,x_3 \tag{4.2}$$

The reduced model should not imply that the eliminated terms from Equation 4.1 would not affect the response; In fact the effects of excluded terms were shown to be not significant by the F-test within the ranges studied. For instance, Figure 4.3 shows the interaction effect of peptone and calcium chloride on the response. It indicated that, at the higher level of peptone, increasing the calcium chloride level would enhance the protein production, whereas at the lower level of peptone any increase in calcium chloride would decrease the response. However, in both scenarios the effect would be very small and negligible in comparison to the more significant effects.

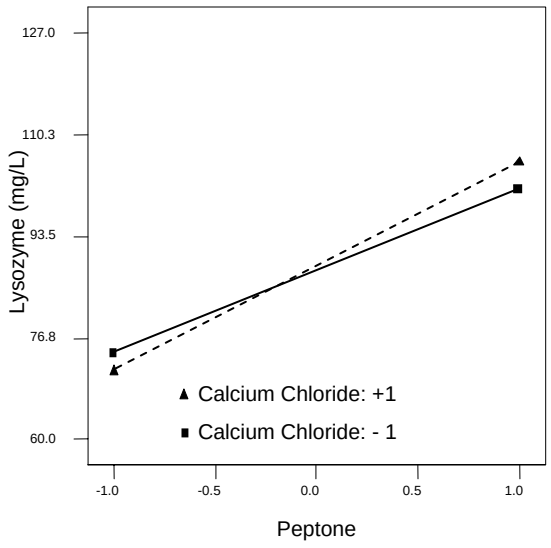

Figure 4.3- The interaction effect of peptone and calcium chloride on the response of the revised FFD (Full model).

4.3.2.2 Adequacy of the Refined Model (FFD)

The analysis of variance for the refined model (Equation 4.2) is summarized in Table 4.6. The curvature F-value of 1.67 indicated that the model curvature was not significant throughout the design space, and there was 21.45% chance that a curvature F-value this large could occur due to noise. This indicates a probable lack of significant curvature. Furthermore, the lack of fit value of 0.73 showed this source of variation was not significant relative to pure error.

The coefficient of determination, R^2, of the model was calculated to be 0.87. This indicated that the model explained 87% of the variability in the data. Although the coefficient of determination of the refined model decreased to 0.87 in comparison to the value of 0.96 for the full model, the adjusted model $R^2_{Adj.}$ = 0.85 was larger than that of the full model ($R^2_{Adj.}$ = 0.81), showing that there was no chance that nonsignificant terms had been included in this model.

Table 4.6- Analysis Of Variance (ANOVA) for refined model

Source of Variation	SS_i	$d.f.$	MS_i	F	$p > F$
Model	5078.50	3	1692.83	35.86	<.0001
X_1	484.00	1	484.00	10.25	0.0056
X_2	3782.25	1	3782.25	80.12	<0.0001
X_3	812.25	1	812.25	17.21	0.0008
Curvature	78.87	1	78.87	1.67	0.2145
Residuals	755.30	16	47.21		
Lack of Fit	518.50	12	43.21	0.73	0.6985
Pure error	236.80	4	59.25		
Total	5912.67	20			

Before adopting the model on the basis of the ANOVA test, the adequacy of the model should be checked. One can use the analysis of the residuals as a primary diagnostic tool for this purpose. The normal probability plot of the studentized residuals for the refined model is displayed in Figure 4.4. The points on this plot lied reasonably close to a straight line, implying that X_1, X_2, and X_3 were the only significant terms in the model. Besides, the plot confirmed that the errors were normally distributed with mean zero and constant but unknown variance as the underlying assumption of the analysis. This figure confirms the model adequacy.

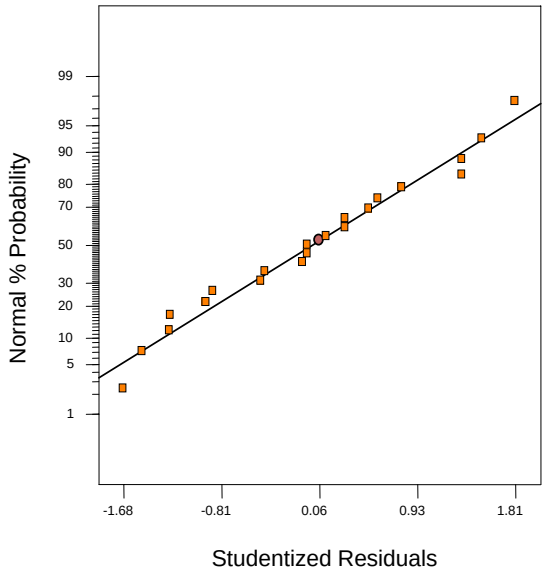

Figure 4.4- Normal probability plot of studentized residuals for the refined model.

The independence of the errors was checked by plotting the residuals versus the different independent variables. In Figure 4.5 the studentized residuals versus the fitted values of the response are plotted. This plot indicated that there was no unusual structure showing a certain pattern for the variance as the lysozyme concentration changed.

Figures 4.6-8 are plots of the studentized residuals versus starch, peptone, and ammonium sulfate levels, respectively. The plots for starch and ammonium sulfate indicated equality of variance between the levels. The display for peptone represented higher variance in the high peptone level. The increase, however, was not severe enough to affect the analysis and conclusions. Thus, all plots appeared satisfactory and there was no reason to reject the conclusions.

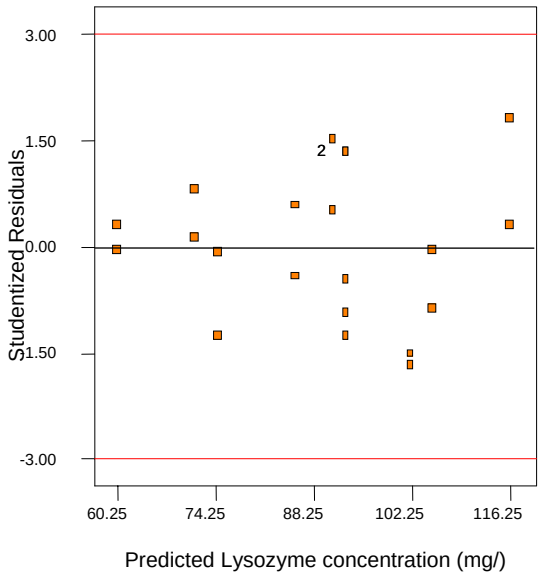

Figure 4.5- Studentized residuals versus predicted response.

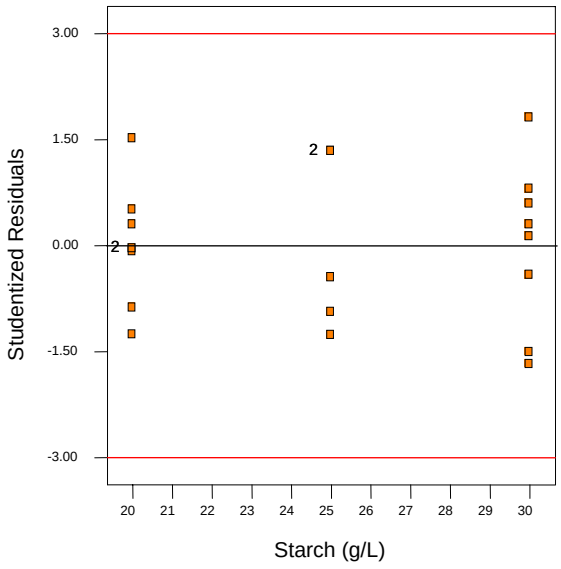

Figure 4.6- Studentized residuals versus Starch levels.

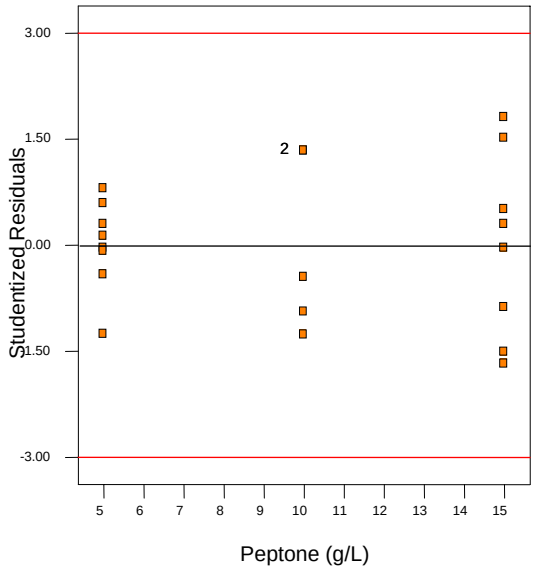

Figure 4.7- Studentized residuals versus Peptone levels.

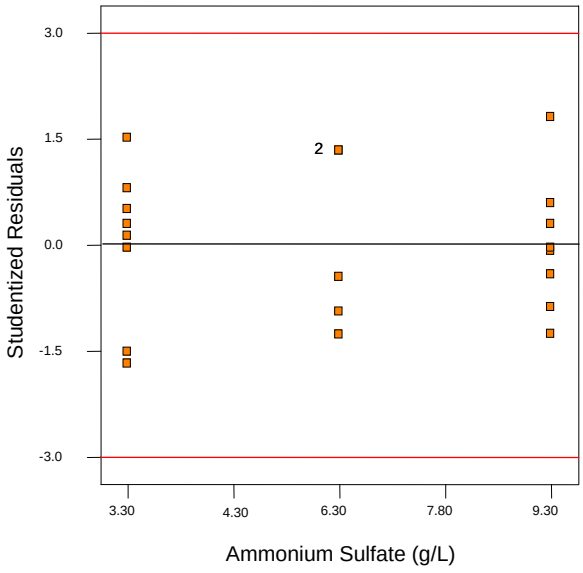

Figure 4.8- Studentized residuals versus Ammonium Sulfate levels.

4.4 The Path of Steepest Ascent

The path of steepest ascent was determined by using Equation 4.2. Yeast extract and calcium chloride were fixed at the center of the fractional factorial design, because they were not significant at the probability level of 95%. Since, the signs of the three significant factors in the refined model were positive, they would have a positive impact for lysozyme production if their concentration into the medium was increased. Table 4.7 illustrates the results of the experiment as well as the directions in which the variables were changed. These were increments of 15.38 units in x_2 and 7.13 units in x_3 for every 5.5 units in x_1 (or 2.8 units of x_2, and 1.3 units of x_3 for each unit of x_1). The center point of the fractional factorial design has been considered as the origin of the path. The response for this point was determined as the average of responses for the runs 35 to 40.

Table 4.7- Experimental design of the steepest ascent and corresponding results

Run	Coded variables			Real variables (g L^{-1})			Lysozyme (mg L^{-1})
	x_1	x_2	x_3	X_1	X_2	X_3	
Origin	0.0	0.0	0.00	25.0	10.0	6.30	93
41	0.5	1.4	0.65	27.5	17.0	8.25	146
42	1.0	2.8	1.30	30.0	24.0	10.20	158
43	1.5	4.2	1.95	32.5	31.0	12.15	198
44	2.0	5.6	2.60	35.0	38.0	14.10	191
45	2.5	7.0	3.25	37.5	45.0	16.05	185
46	3.0	8.4	3.90	40.0	52.0	18.00	182
47	3.5	9.8	4.55	42.5	59.0	19.95	179

Figure 4.9 plots the lysozyme concentration at each step along the path of steepest ascent. Increases in response were observed through the third step; however, all steps beyond this point (Run 43) resulted in a decrease in the response. Therefore, another first-order model was fitted in the general vicinity of the point. For the new first-order model, the region of

exploration for X_1 was [30, 35], and for X_2 and X_3 it was [24, 38] and [10.2, 14.1], respectively.

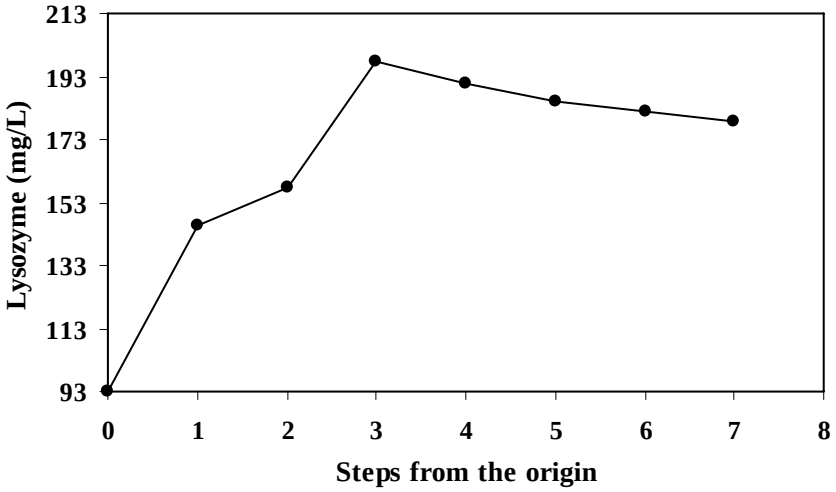

Figure 4.9- Response versus steps along the path of steepest ascent.

For simplicity, the independent variables X_i were coded according to the following equations:

$$x_1 = (X_1 - 32.50)/2.50$$

$$x_2 = (X_2 - 31.00)/7.00$$

$$x_3 = (X_3 - 12.15)/1.95$$

The experimental design of the new first-order design was comprised of a 2^3 full factorial design (Runs 48-55) with six center points (Runs 62-67) as presented in Table 4.9. The analysis of variance of this model was performed (not shown). The curvature F-value of 30.6 indicated that there was a significant curvature in the design space and there was only 0.04% chance that the curvature occurred due to the noise. Because of this curvature, it was appropriate to conclude that a region near the optimum was reached. At this point, additional analysis was performed to locate the optimum more precisely.

4.5 Central Composite Design (CCD)

4.5.1 Full Quadratic Model (CCD)

As seen above, the neighborhood of the optimum response was approached along the path of steepest ascent. In order to explain the nature of the response surface in the optimum region, a central composite design was performed and the level of the three significant variables, starch (x_1), peptone (x_2), and ammonium sulfate (x_3) were further optimized. For the three factors this design was made up of the full 2^3 factors with its 8 cubic points, augmented with 6 replications of the center points, and the 6 axial (star) points. The level of two nonsignificant factors (yeast extract and calcium chloride) was kept at the central point of the fractional factorial design. In order to make the design rotatable, the axial distance α was assigned a value of 1.6818. Table 4.8 shows the different levels of the three variables in the terms of real values.

Table 4.8- Actual levels of the factors for CCD

Independent variables	Real levels (g L^{-1})				
	Star- Low	**Low**	**Center**	**High**	**Star- High**
X_1	28.30	30.0	32.50	35.0	36.70
X_2	19.23	24.0	31.00	38.0	42.77
X_3	8.87	10.2	12.15	14.10	15.43

The 2^3 full factorial design along with the replications at the center point was augmented with the star points (Runs 56-61) to build up the central composite design. The complete experimental design and the measured lysozyme concentrations are presented in Table 4.9 and the CCD for the three independent variables is displayed in Figure 4.10. It is worth mentioning that the experiments associated with the star points were performed at the same time the original 14 runs (48-55 and 62-67) for the first-order model were carried out. The hypothesis was that, if substantial time had elapsed between the two sets

of runs, blocking would have been necessary due to possible changes at the conditions of experiments and lysozyme analysis.

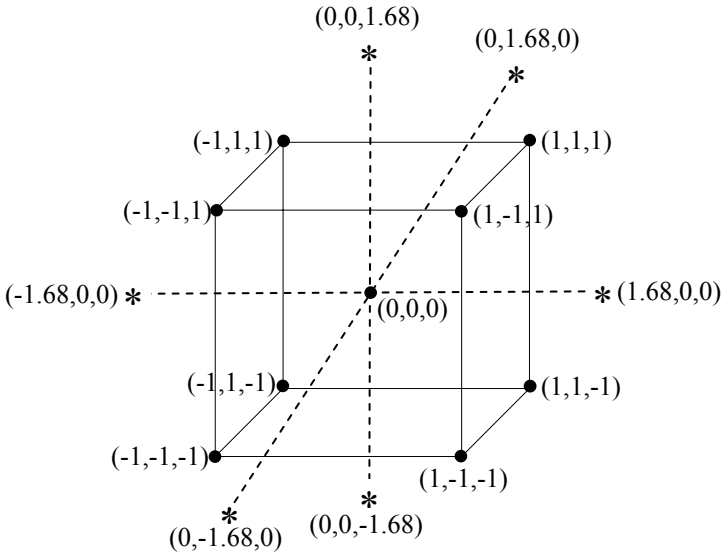

Figure 4.10- Central Composite Design for the three significant factors.

The experimental results of the CCD were fitted with a second-order model. The values of regression coefficients were calculated and the fitted equation (in the terms of coded values) for predicting lysozyme production was as follows:

$$\hat{Y}_{ccd,\,full} = 208.8 + 7.49x_1 + 3.29x_2 + 1.38x_3 - 7.65x_1^2 - 7.65x_2^2 - 8.71x_3^2 + 4.63x_1x_2 - 1.62x_1x_3 - 4.62x_2x_3 \quad (4.3)$$

This equation includes all terms regardless of their significance. Obviously, the relatively high value of $R^2 = 0.89$ means that the full quadratic model is a good fit. The Model F-value of 9.43 was the indicator that the model was significant and there was only 0.08% probability that this level of fit could occur due to random chance. The lack of fit P-value of 0.7949 showed that the lack of fit was not important relative to the pure error.

Table 4.9- Experimental design and results of the 2^3 full factorial central composite design

Run	Coded levels			Lysozyme (mg L^{-1})	
	x_1	x_2	x_3	$Y_{ccd,Exp.}$	$\hat{Y}_{ccd,predicted}$
48	-1	-1	-1	171	174
49	+1	-1	-1	181	180
50	-1	+1	-1	176	181
51	+1	+1	-1	206	205
52	-1	-1	+1	182	183
53	+1	-1	+1	187	189
54	-1	+1	+1	170	171
55	+1	+1	+1	192	196
56	-1.68	0	0	179	175
57	+1.68	0	0	200	200
58	0	-1.68	0	183	182
59	0	+1.68	0	196	193
60	0	0	-1.68	180	184
61	0	0	+1.68	193	184
62	0	0	0	195	209
63	0	0	0	214	209
64	0	0	0	211	209
65	0	0	0	208	209
66	0	0	0	217	209
67	0	0	0	207	209

To determine the significance of each coefficient in the model, the analysis of variance, ANOVA, was performed. Table 4.10 is the summary of the ANOVA for the response surface full quadratic model.

Table 4.10- ANOVA for response surface full quadratic model

Source of Variation	SS_i	$d.f.$	MS_i	F	$p > F$
Model	3627.42	9	403.05	9.43	0.0008
X_1	766.57	1	766.57	17.94	0.0017
X_2	147.38	1	147.38	3.45	0.0930
X_3	26.05	1	26.05	0.61	0.4530
X_1^2	843.95	1	843.95	19.75	0.0012
X_2^2	843.95	1	843.95	19.75	0.0012
X_3^2	1094.10	1	1094.10	25.60	0.0005
$X_1 X_2$	171.13	1	171.13	4.00	0.0733
$X_1 X_3$	21.12	1	21.12	0.49	0.4981
$X_2 X_3$	171.12	1	171.12	4.00	0.0733
Residuals	427.38	10	42.74		
Lack of Fit	134.05	5	26.81	0.46	0.7949
Pure error	293.33	5	58.67		
Total	4054.80	19			

4.5.2 Refined Quadratic Model (CCD)

Recalling that P-value of less than 0.0500 was the indicator of significance, the variable terms X_1, X_1^2, X_2^2, and X_3^2 were significant from a model perspective. After removing all other terms from the full second-order model, the adjusted-R^2 of the new model was less than that of the full model implying that there could be more significant terms in the revised model. Since, the $p > F$ greater than 0.1000 are certainly nonsignificant terms, terms with the $p > F$ less than 0.1000 were considered in seeking a higher value of $R^2_{Adj.}$. The following quadratic surface model was accordingly chosen as the final model:

$$\hat{Y}_{ccd,final} = 208.8 + 7.49x_1 + 3.29x_2 - 7.65x_1^2 - 7.65x_2^2 - 8.71x_3^2 + 4.63x_1x_2 - 4.62x_2x_3 \qquad (4.4)$$

The analysis of variance for the refined quadratic model is presented in Table 4.11. The goodness of fit was expressed by the coefficient of determination R^2, which was calculated to be 0.88, indicating nearly 90% of the variability in the response could be explained by the model. Furthermore, the final model had $R^2_{Adj.}$ equal to 0.82 in comparison to 0.80 calculated for the full quadratic model. This supported the hypothesis that the model equation as expressed by Equation 4.4 was sufficient to describe the response of the experimental observations pertaining to lysozyme production. The *Adequate Precision* statistic was determined to be 9.422. The *Adequate Precision* statistic is a signal to noise ratio. It compares the range of the predicted values at the design points to the average predicted error. Ratios greater than 4 indicate adequate model discrimination. The *Adequate Precision* of 9.422 indicated that the model would give reasonable performance in prediction.

Table 4.11- Analysis of variance of the refined quadratic model

Source of Variation	SS_i	$d.f.$	MS_i	F	$p > F$
Model	3580.24	7	511.46	12.93	<.0001
X_1	766.57	1	766.57	19.38	0.0009
X_2	147.38	1	147.38	3.73	0.0775
X_1^2	843.95	1	843.95	21.34	0.0006
X_2^2	843.95	1	843.95	21.34	0.0006
X_3^2	1094.10	1	1094.10	27.67	0.0002
$X_1 X_2$	171.13	1	171.13	4.33	0.0596
$X_2 X_3$	171.12	1	171.12	4.33	0.0596
Residuals	474.56	12	39.55		
Lack of Fit	181.23	7	25.89	0.44	0.8420
Pure error	293.33	5	58.67		
Total	4054.80	19			

The model F-value of 12.93 implies the model is significant. There is only 0.01% chance that a Model F-value this large could occur by chance. Also, the lack of fit value of 0.44 disclosed that the lack of fit was not significant relative to the pure error. As an additional tool to check the adequacy of the final model, the normal probability plot of the residuals is presented in Figure 4.11. There was no indication of nonnormality, nor was there any evidence pointing to possible outliers, although the singular negative residual of -2.404 (see Run 62) stood out from the others.

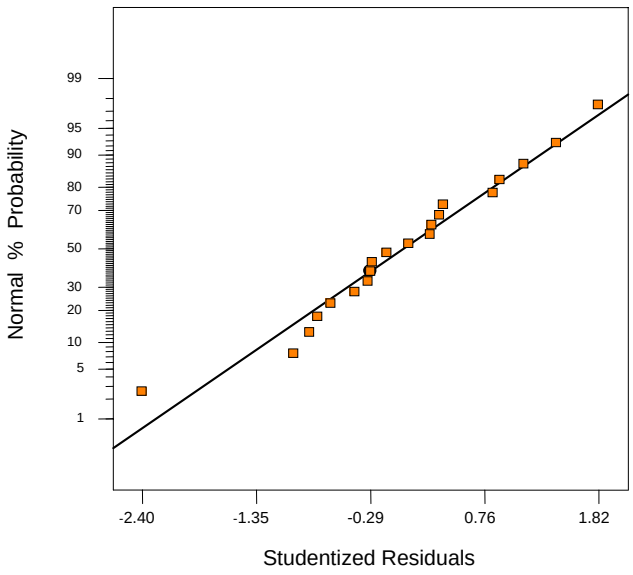

Figure 4.11- Normal probability plot of studentized residuals for refined quadratic model.

Figures 4.12 and 4.13 display residuals versus predicted values and residuals versus run order, respectively. There was no reason to suspect any violation of the independence or constant variance assumption as both figures indicated a nearly constant variance throughout the variable ranges. Similarly to the normal probability plot, the value for Run 62 was far from the others, however, it was not unusual.

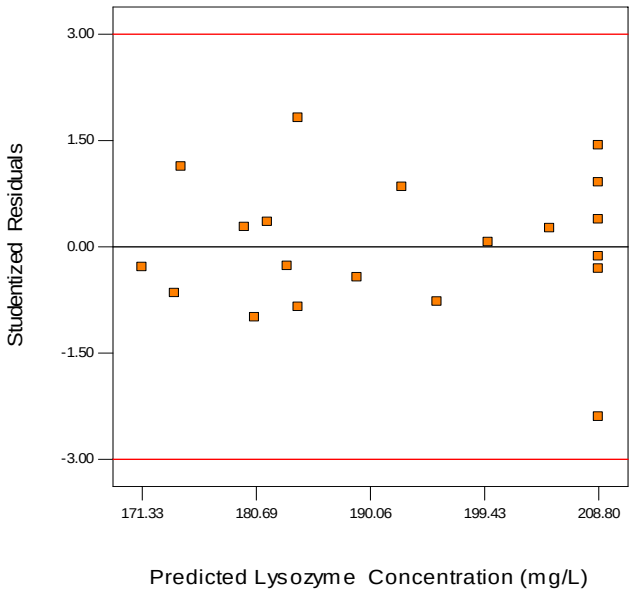

Figure 4.12- Studentized residuals versus predicted response by refined quadratic model.

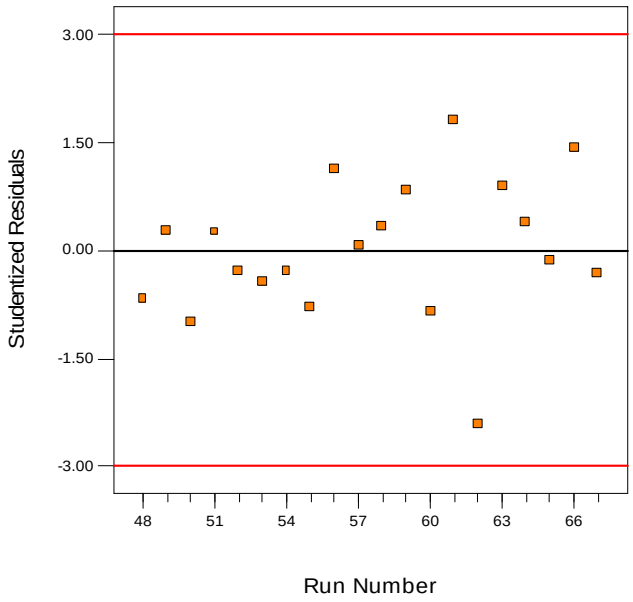

Figure 4.13- Studentized residuals versus run order.

The location of the optimum was determined by solving the set of equations derived by the differentiation of the refined quadratic model. The results are presented in both coded and real values for the independent variables along with the predicted maximum response in Table 4.12. This maximum concentration was the maximum value bounded by the range of experiment values.

Table 4.12- Predicted maximum response and the location of optimum for CCD

	Coded values			**Actual values (g L^{-1})**			**Lysozyme (mg L^{-1})**
	x_1	x_2	x_3	X_1	X_2	X_3	$\widehat{Y}_{Optimum,Pred.}$
Optimum location	0.6222	0.4384	-0.1163	34.06	34.07	11.92	212

The response surface, shown in Figure 4.14, was based on the refined quadratic model. For easy graphical representation one variable was kept constant at optimum level while varying the other two whithin their experimental ranges. Figure 4.14a shows the response surface for the optimum level of starch. The minimum value of the response (141 mg/L) was when both peptone and amonium sulfate were at their lowest level. At the high level of amonium sulfate (15.43 g/L) the response indicated a maximum nearly at the middle of peptone level, whereas the maximum shifts to the higher levels of peptone when amonium sulfate was at the lowest level (8.87 g/L) .

At the optimum level of peptone (Figure 4.14b) , minimum response (143 mg/L) was seen with low level of starch (28.3 g/L) and high level of amonium sulfate. Increases in the response were observed when starch concentration changed from the low level to the high level at any concentration of ammonium sulfate. Figure 4.14c indicates the response at the optimum level of ammonium sulfate. The location of minimum response (146 mg/L) was when starch was at the lowest level and peptone at its highest level.

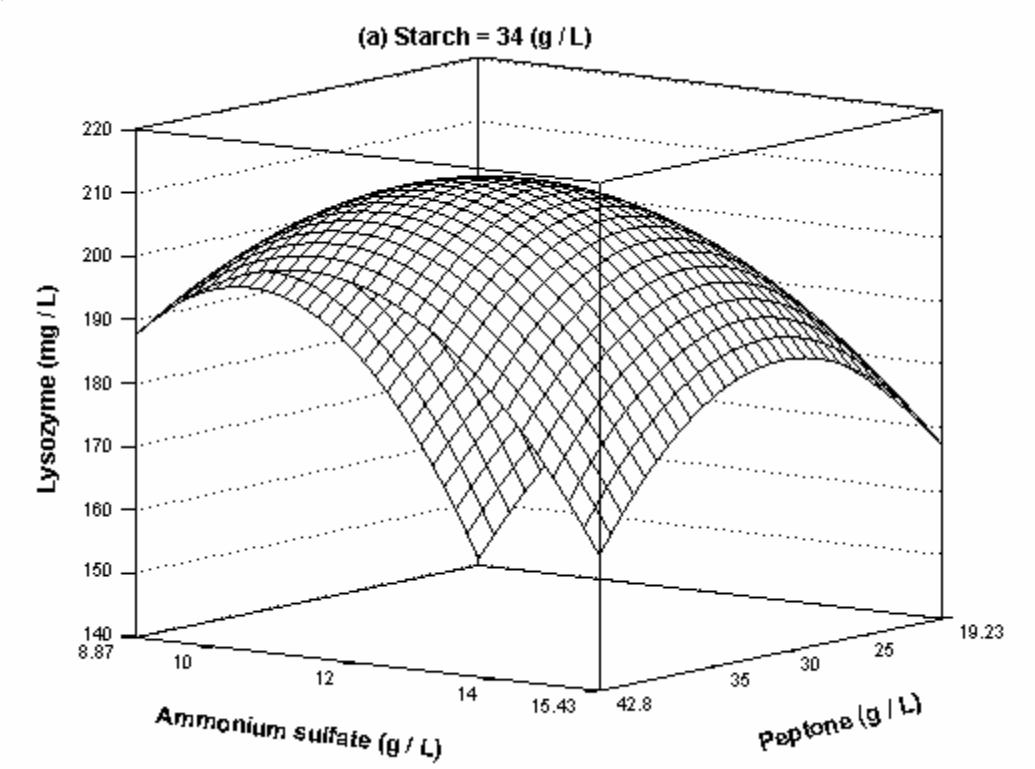
(a) Starch = 34 (g / L)
Lysozyme (mg / L)
220
210
200
190
180
170
160
150
140
8.87
10
12
14
15.43
Ammonium sulfate (g / L)
42.8
35
30
25
19.23
Peptone (g / L)

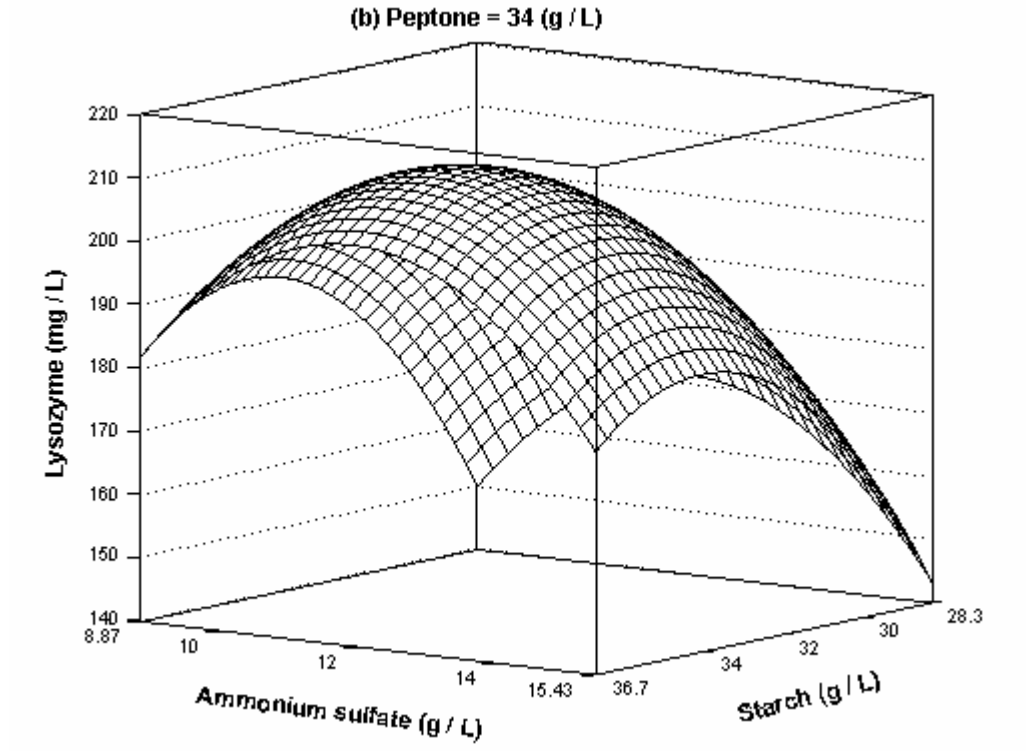
(b) Peptone = 34 (g / L)
Lysozyme (mg / L)
220
210
200
190
180
170
160
150
140
8.87
10
12
14
15.43
Ammonium sulfate (g / L)
36.7
34
32
30
28.3
Starch (g / L)

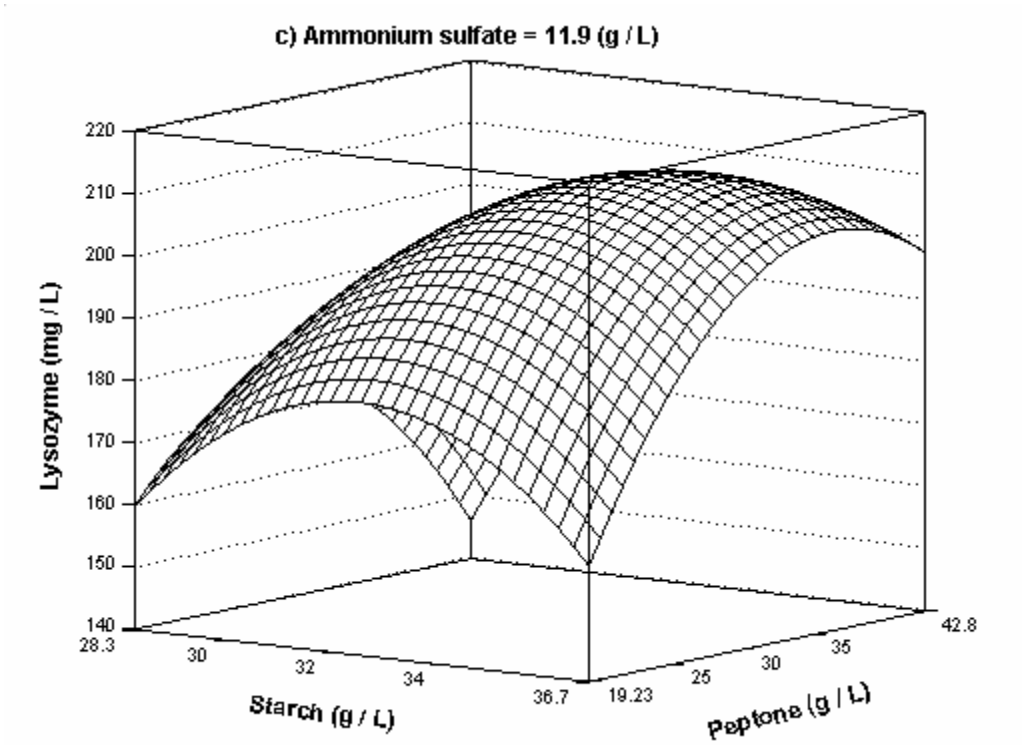

Figure 4.14- Response surface of lysozyme concentration: (a), (b), and (c) fixed starch, peptone, and ammonium sulfate concentrations at their optimum points, respectively.

Figure 4.15 shows the plots of the lysozyme concentration determined by the refined quadratic model against one of the factors for the two levels of the second factor at the optimum level of the third factor. Figure 4.15a illustrates the interaction between peptone and ammonium sulfate for lysozyme production. Response was enhanced 33% with the increase in peptone concentration from low to high level when ammonium sulfate was at the low level, while the response decreased slightly at the high level of ammonium sulfate. In addition, ammonium sulfate had a positive effect on the response at the low level of peptone, while at the high level of peptone its effect was negative. These represented a considerable interaction between ammonium sulfate and peptone.

Analysis of response at the different levels of ammonium sulfate and starch while peptone was at the optimum level revealed that there was no remarkable interaction between these factors (see Figure 4.15b). At diffent levels of starch the response trend was identical along the entire range of ammonium sulfate. This confirms the previous

results from the analysis of variance that the interaction effect between ammonium sulfate and starch was not significant.

The starch and peptone interaction effect are plotted in Figure 4.15c. The plot indicated that starch had little effect at low peptone concentration, but a large positive effect at high peptone level. Furthermore, at the low level of starch peptone showed little negative effect on the response, but at the high level of starch the peptone showed a large positive effect. Based on these observations, one could conclude that there was a significant interaction between starch and peptone levels.

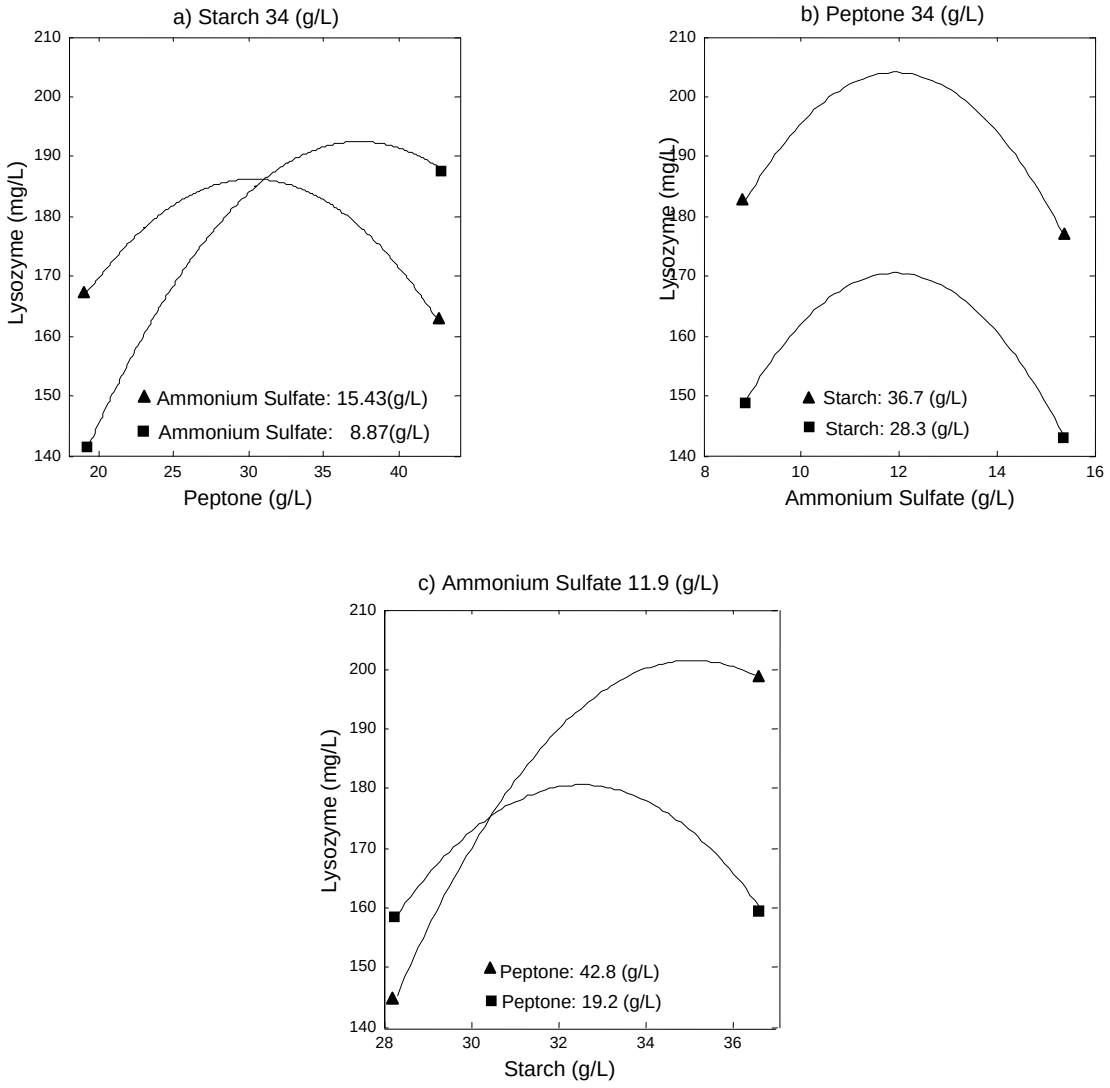

Figure 4.15- The interaction plots at the optimum levels of a) starch, b) peptone, and c) ammonium sulfate.

The predicted values by the refined quardatic model are presented in Table 4.9 along with the corresponding observed values. Comparison of these values indicated that there was an excellent agreement between the model and experimental data for the range of experiment values considered.

In order to confirm the predicted result of the model, experiments using the medium representing the maximum point were performed in triplicate. The maximum lysozyme concentration was experimentally determined to be 209 ± 18 mg L^{-1}, which was in very good agreement with the predicted value.

4.6 Conclusion

The classical method of medium optimization by changing one parameter at a time while keeping the others at fixed levels is laborious and time consuming. This method requires a complete series of experiments for every factor of interest. Moreover, such method does not provide means of observing possible factor interactions. In contrast, factorial experimental designs offer a number of important advantages. For instance, the examiner could easily determine factor effects with considerably less experimental effort, identify factors, find optima, offer greater precision (Leiro et al., 1995) and facilitate system modeling (Miron et al., 1988).

The statistically based experimental design has proven to be a valuable tool in optimizing the medium for lysozyme production (Gheshlaghi et al., 2005). Fractional factorial design used as the first step was efficient to screen which medium components amongst the selected factors were significant. More specifically, the results of this analysis indicated that yeast extract and $CaCl_2.2H_2O$ were not very important parameters with regard to lysozyme production within the levels tested but starch, peptone, and ammonium sulfate were very significant. As the second step, the path of steepest ascent was useful to move toward the vicinity of the optimum.

Finally, the response surface design was found to be very helpful to elucidate the interactions and relationships among the significant components and led to an optimization scheme for lysozyme production. The final quadratic model was accurately able to predict the behavior of the response at the neighborhood of the optima. The linear effects of starch and peptone, quadratic effects of all the three ingredients, and the interaction effects between starch-peptone as well as peptone-ammonium sulfate were the significant terms in the final quadratic model.

The optimum medium composition for the production of lysozyme by *A.niger* was established as follows: starch (34 g/L), peptone (34 g/L), $(NH_4)_2SO_4$ (11.9 g/L), yeast extract (0.5 g/L), and $CaCl_2.2H_2O$ (0.5 g/L). As shown in Table 4-12 this medium was predicted to produce theoretically 212 mg/L lysozyme. This compares with 209 ± 18 mg/L produced experimentally. This was a remarkable improvement in comparison to the results of previous studies. The quadratic model predicted that experiments with the highest (starch: 36.7 g/L, peptone: 42.77 g/L, ammonium sulfate: 15.43 g/L) and lowest

(starch: 28.3 g/L, peptone: 19.23 g/L, ammonium sulfate: 8.87 g/L) levels of these three ingredients would decrease the lysozyme concentration to 159 and 123 mg/L, respectively.

CHAPTER 5

METABOLIC FLUX ANALYSIS

5.1 Introduction

The overproduction of the desired recombinant product is the primary aim of any biotechnology-based industrial process. In this regard, several methods have been applied to increase the level of the desired products including bioprocess optimization (Gyamerah et al., 2002), strain development (Bartsch et al., 2002), medium optimization (Gheshlaghi et al., 2005; Li et al., 2002), and mathematical modeling (Alvarez-Vasquez et al., 2000). Nowadays, it is possible to effect modifications in microorganisms by using recombinant DNA techniques which enable the blocking of byproduct pathways by enzyme deletion or the increase of enzyme levels for the overproduction of the desired product. The problem is, however, to delineate the location and the level of enzyme modifications in the metabolic network, otherwise genetic engineering techniques may not be rewarded with an equivalent improvement in strain enhancement. This shortcoming may be overcome by using a quantitative approach which is able to simulate the behavior of the microorganism before applying any strain modification.

Besides gene modification, metabolic flux analysis can provide important information such as maximal product yields on a substrate, recognize bottlenecks in the overproduction of the desired product, and identify the energetic parameters (Vallino and Stephanopoulos, 1993; Takac et al., 1998; van Gulik et al., 2000; Naeimpoor and Mavituna, 2000). Metabolic flux analysis is based on network stoichiometry and conservation of mass and does not require information regarding enzyme kinetics. Often, it may be formulated as a set of linear ordinary differential equations. The stoichiometric

approach focuses on the topology of the system and evaluates the rate by which a metabolite converts into other metabolites. The great advantage of the stoichiometric approach is that it comprises a set of linear algebraic equations at steady state, which enables linear optimization.

In this work an optimization approach was utilized to obtain the intracellular metabolic flux distribution of an *A.niger* producing the recombinant protein, hen's egg white lysozyme (HEWL). The production of recombinant proteins in aspergilli has been shown to be strictly growth associated (see Appendix D Figure D.4). Therefore, it is convenient to optimize the growth rate in order to optimize recombinant protein productivity. The specific recombinant protein yield, of course, is dependent on cellular metabolism. Using published results, on-line databases, and experimental results, the main objective was to develop an elaborate stoichiometry-based flux model to simulate the behavior of the microorganism, to determine the maximum theoretical specific growth rate and to predict the effect of any change in key fluxes on the behavior of the cells for subsequent experimental perturbation studies.

This *Aspergillus* strain has an absolute requirement for amino acids in the medium. One of the objectives in this work was to replace a complex nitrogen source (peptone) that was used in our previous studies (Gheshlaghi et al., 2005) with a known mixture of amino acids. This enabled one to monitor the concentration of individual amino acids throughout the course of fermentation and use this information as the input for the model.

5.2 Materials and Methods

5.2.1 Medium Composition

The chemically defined medium contained (per liter): glucose 20 g, ammonium sulfate 3.1 g, amino acid mixture 3.20 g, and essential salt solution 20 ml. The amino acid mixture in this study was based on the amino acid content of 0.5% (w/v) peptone (Bacto^{TM}). The amino acid composition of peptone was provided by manufacturer as outlined in materials and methods chapter. Unexpectedly, the glycine content of peptone was 16%, much higher than any of the other amino acid concentrations. The corresponding glycine concentration in the medium was 0.792 g/L. Two experiments with 0.792 and 0.396 g/L glycine were performed while the other amino acids were supplied according to the peptone composition. No significant differences in lysozyme and biomass concentrations were observed. Therefore, for further experiments the concentration of glycine was maintained at 0.4 g/L. Accordingly, the composition of the amino acid mixture in the medium was (%w): Ala 14.3, Arg 8.9, Asp 7.7, Glu 12.5, Gly 12.5, His 1.2, Ileu 3.2, Leu 5.8, Lys 5.1, Met 1.3, Phe 4.3, Pro 13.5, Ser 2.3, Thr 1.7, Tyr 1.4, Val 4.3. Glucose and the inorganic salt solution were autoclaved separately for 20 min at 121 ^{o}C, and were added to filter-sterilized amino acids mixture to give the final medium.

5.2.2 Fermentation

The preparation of inoculum for the bioreactor was carried out in 250 ml Erlenmeyer flasks containing 45 ml of the medium along with 5 ml of sterilized sodium citrate/citric acid (0.97M, pH 6.5) as buffer. The citrate buffer was autoclaved separately and then added to the medium to prevent the formation of a precipitate (Archer et al., 1995). The flasks were inoculated with 40 μL spore stock suspension to give a final concentration of approximately 4×10^4 spores/ml in each flask. These cultures were grown at 27 ^{o}C and 200 rpm for 48 hr on an Innova 4330 refrigerated incubator shaker (New Brunswick Scientific Co., USA). The initial fungal morphology of the preculture was small pellets. In order to promote mycelial growth in the fermenter, these pellets were sheared in a sterile Waring blender for 5 seconds prior to inoculation.

Batch fermentation experiments were performed in either a 2-liter Bioflo fermenter (New Brunswick Scientific Co., NJ) with a working volume of 1.5L, or a 7-liter Applikon bioreactor (Applicon Dependable Instruments, Holland) with a working volume of 4.5L using the medium described above. The bioreactor cultures were inoculated with a mycelial inoculum size of 5% and 3.3% of working volume for 2-liter and 7-liter bioreactors, respectively. The culture temperature was kept at 27 ± 0.5 ^{o}C. The moisture content in the exhaust gas was condensed and returned to the bioreactor by passing it through a vertical condenser mounted on the top of the fermenter. Air was supplied at a rate of 1 vvm and was sterilized through a hydrophobic 0.2 μm (Millipore) membrane filter. The broth was mixed using three six-bladed Rushton turbine impellers rotating at 200-400 rpm. The dissolved oxygen was monitored and kept at above 20% saturation using variable agitation schemes. The initial pH of the broth was adjusted to 6.0 and the fermentations were operated without any pH control until it decreased to a set point of 4.0. After reaching this set point, the pH was maintained at 4.0 ± 0.1 by adding either 2M sodium hydroxide or 2M sulfuric acid by an automatic pH-control system using a sterilizable probe mounted in the reactor. To prevent excessive foaming, antifoam (Sigma 204) was added, as needed.

5.2.3 Analytical Procedures

Samples were analyzed for concentrations of cells, glucose, ammonia, organic acids, amino acids, phosphate, and sulfate throughout the fermentation as described in Chapter 3. Each analysis was carried out in triplicate and the average was reported and utilized in this study. To investigate the accuracy and reproducibility of the HPLC analysis for amino acids, the concentration of each amino acid detected at the beginning of the fermentation was compared with the amount added as stated in the materials and method section. Maximum errors were 18% and 15% for glycine and serine, respectively. The associated error was determined to be 12% for the initial concentration of ammonia.

5.2.4 Model Construction

A stoichiometric model for growth and product formation of *A.niger* has been developed based on the available published information for this microorganism. Moreover, in case there was not specific information for *A.niger*, corresponding data of closely related filamentous fungi (e.g., *A.nidulans*) were included, and, as a last resort, data obtained for yeasts (e.g. *Saccharomyces cerevisiae*) were utilized when data were completely lacking or inadequate. This reaction network includes glycolysis and pentose phosphate (PP) pathways, tricarboxylic acid cycle (TCA), anaplerotic reactions, ammonia and sulfate assimilation, electron transport reactions, biosynthesis and degradation of amino acids, and the biosynthesis of nucleotides and macromolecular components of biomass such as protein, lipid, RNA, DNA, and carbohydrates. Since, several studies failed to produce evidence for the Entener-Doudoroff pathway (EDP) in fungi (Blumenthal 1968; Lakshminarayana et al., 1969) this pathway was not included in the model. In this model three internal cell compartments, the cytosol, mitochondrion, and peroxisome were distinguished. A schematic outline of the major metabolic pathways is depicted in Figure 5.1. The complete set of reactions in the metabolic network with corresponding reaction numbers is given in Appendix C. The subscript *c*, *m*, and *p* denote the location of the species being present in the cytosol, mitochondrial matrix, and peroxisome, respectively. Some assumptions have been made for different parts of the biochemical reaction network, which are given below.

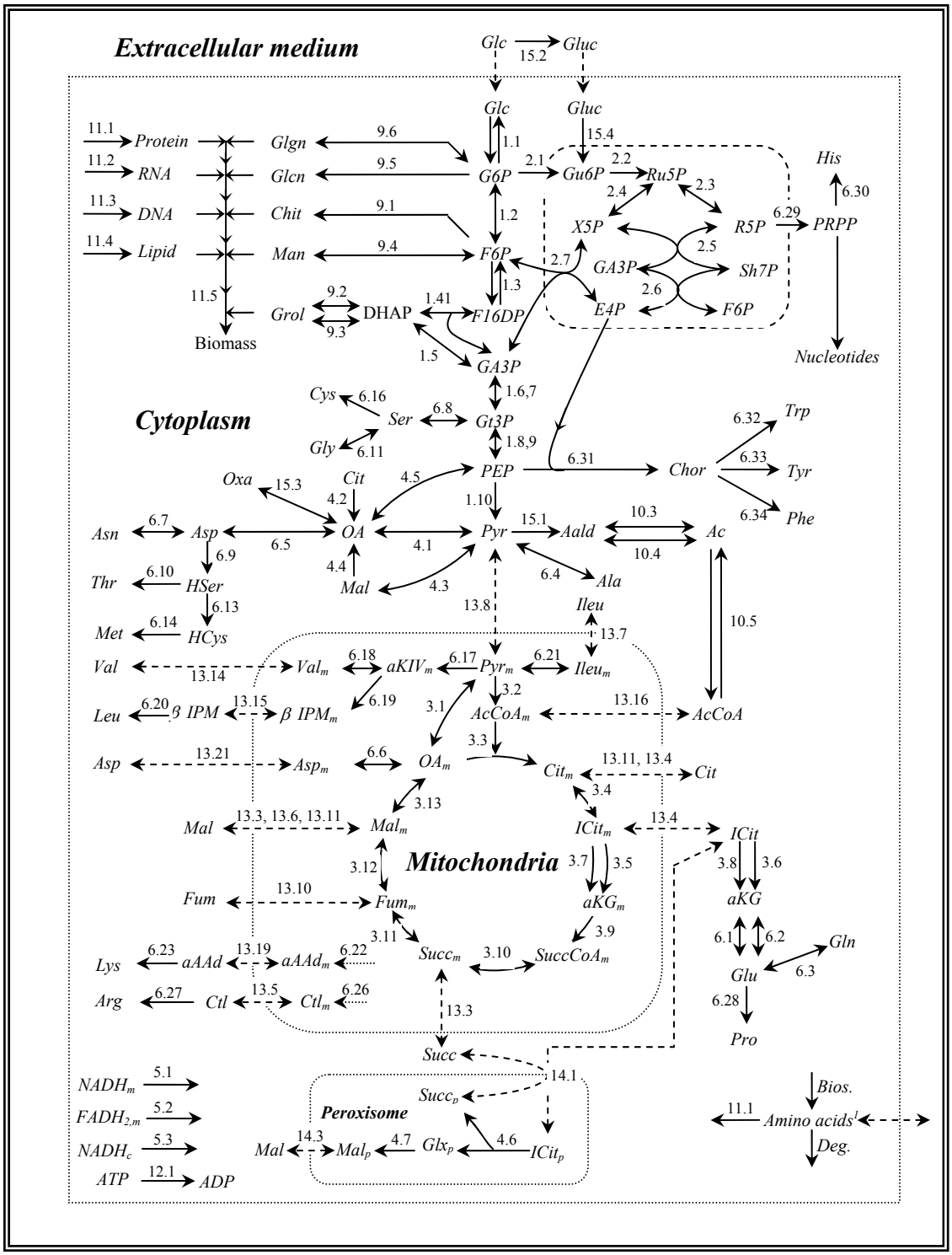

Figure 5.1- The general overview of the proposed metabolic pathways for A.niger (Refer to the appendix B for list of symbols). Three compartments cytoplasm, mitochondria, and peroxisomes are distinguished. The solid and dashed arrows with the reaction numbers next to them represent metabolic reactions and transport processes, respectively. The abbreviations and corresponding reactions are given in the Appendix. For the amino acids four different fluxes have been included in the model: biosynthesis, degradation, transport between cytoplasm and abiotic phase, and for protein biosynthesis; however, for simplicity only the first set is shown in the map.

5.2.4.1 Anabolic Reactions

The anabolic reactions for *A.niger* for protein, lipid, RNA, DNA, and biomass synthesis were taken from the reported information for *A.oryzae* at the specific growth rate of 0.1 h^{-1} (Pedersen et al., 1999). The sensitivity of the biomass yield to perturbations in the biosynthetic demands has been assessed in different studies and some authors concluded that the biomass yield was not sensitive to changes in biosynthetic requirements (Daae and Ison, 1999; Varma and Palsson, 1993a), whereas others emphasized the importance of incorporating changes in biomass composition with growth rate in flux estimation (Pramanik and Keasling, 1997). In this study, one single reaction (*R11.5*) based on a fixed biomass composition was employed for the formation of biomass throughout the fermentation.

5.2.4.2 Intracellular Compartmentation

Intracellular compartmentation plays an important role in the regulation and in the distribution of metabolic fluxes (van de Kamp et al., 1999). Since membranes are impermeable to certain components this compartmentation is necessary to obtain reliable balance of internal fluxes. For instance, NADH and NADPH can not pass the mitochondrial membrane, and separate balances are needed for these cofactors in each compartment.

In eukaryotes most of the central carbon metabolism takes place either in the cytosol or in the mitochondria, however, some unique reactions occur in the microbodies, e.g., peroxisomes and glyoxysomes (Lazarow and Kunau, 1997). In the proposed metabolic model for *A.niger*, the following three compartments have been distinguished. The cytosolic compartment contains the reactions comprising glycolysis, gluconeogenesis, the PP pathway, and the majority of anabolic pathways. The mitochondrial compartment includes the TCA cycle, oxidative phosphorylation, the biosynthesis pathways of the amino acids isoleucine, valine and part of the biosynthesis of leucine, arginine, and lysine; and the peroxisomes fraction, which contains the glyoxylate shunt.

5.2.4.3 Amino Acids Metabolism

The biosynthetic pathways for the twenty common amino acids have been elucidated in filamentous fungi (Jones and Fink 1982; Umbarger 1978). A comparison with similar data for other microorganisms shows that synthesis of amino acids by fungi closely resembles the same by bacteria (Ingraham 1983). However, there are some remarkable exceptions, for instance lysine is synthesized via diaminopimelic acid in bacteria and via α-aminoadiapate acid in filamentous fungi (Lejohn, 1971). Eight steps are involved in biosynthesis of lysine in fungi of which the first five steps take place in the mitochondria to form α-aminoadiapate acid. The last three steps converting α-aminoadiapate acid to lysine are carried out in the cytoplasm (Zabriskie and Jackson, 2000).

In fungi there are two pathways for the biosynthesis of cysteine. The first is the direct sulfhydrylation route in which serine is activated by acetyl-CoA to form *O*-acetylserine which is converted to cysteine by serine transacetylase. The second pathway is more complicated. Here the sulfide group is incorporated into *O*-acetylhomoserine (formed by activation of homoserine by acetyl-CoA) forming homocysteine. This is a branch point for the biosynthesis of methionine and cysteine. In the next step, homocysteine and serine are combined to from cystathionine which in the last reaction is converted to ammonia, cysteine, and α-ketobutyrate. In yeasts both pathways are known to be active (Morzycka and Paszewski, 1982). However, in the fungus, *P. chrysogenum* some investigators have claimed that only the trassulfuration pathway is operative; however, no evidence was presented (Dobeli and Nuesch, 1980; Treichler et al., 1979). The existence of the last enzyme of direct route, *O*-acetylserine sulfhydrylase is more recently demonstrated (Ostergaard et al., 1998). For reason of simplicity, and to avoid the incorporation of dubious path for the recycling of α-ketoglutarate in current model, only the direct sulfhydrylation pathway for *A.niger* was assumed to be operative.

5.2.4.4 Gluconate and Oxalate Metabolisms

The high level production of gluconic acid from glucose in fungal cultures has been known for some time (Cochrane, 1958). Early fungal fermentation processes for gluconic acid production used species of *Penicillium*, however, improved strains of *Aspergillus niger* or *Gluconobacter suboxidans* are now employed in discontinuous submerged

fermentations in industry (Anastassiadis, 2005). Bioconversion of glucose to gluconate is a simple dehydrogenation (oxidation) reaction, which takes place without involvement of complex pathways. The enzyme responsible in *Aspergillus niger* is glucose oxidase (or glucose aerodehydrogenase) that has been extensively studied (Fiedurek and Ilczuk, 1991).

Several strains of *A.niger* are able to catabolize gluconate as the sole source of carbon (Elzainy, 1973). Two pathways for degradation of gluconate by *A.niger* have been proposed. The first mechanism involves phosphorylation of gluconate to gluconate-6-phosphate, which is further metabolized by PP pathway (Lakshminarayana et al., 1969). The second, in contrast, is a completely non-phosphorylative pathway for gluconate metabolism (Elzainy et al., 1973). Gluconate is first dehydrated to 2-keto-3deoxy-gluconate (KDG), which is then cleaved into pyruvate and glyceraldehyde.

Three pathways have been proposed for oxalic acid formation. One requires the operation of NAD-glyoxylate dehydrogenase to oxidize glyoxylate to oxalate (Balmforth and Thomson, 1984). A NADP-glyoxylate dehydrogenase (EC 1.2.1.17) that produces oxalyl-CoA as the initial product has also been found (Quayle and Taylor, 1961). The third one involves the cleavage of oxaloacetate by the enzyme oxaloacetate hydrolase (oxaloacetase, EC 3.7.1.1) to form oxalic acid and acetate. For *A.niger* it has been demonstrated that oxalate is only produced by the enzyme oxaloacetase which is located in the cytoplasm of *A.niger* (Kubicek et al., 1988). This pathway was included in the current model, accordingly.

5.2.4.5 Anaplerotic Pathways

Some TCA cycle intermediates are withdrawn for the biosynthesis of amino acids and nucleotides. In order to avoid a depletion of the cycle, these compounds must be replenished by alternative means as so-called anaplerotic pathways. Pyruvate carboxylase that converts pyruvate to oxaloacetate appears to be the main anaplerotic reaction in fungi (Gow and Gadd, 1995). In some *Aspergillus* strains, e.g. *A.nidulans* and *A.terreus*, the pyruvate carboxylase is reported to be present only in the cytosol (Osmani and Scrutton, 1983; Jaklitsch et al., 1991). In *A.wentii* the enzyme is exclusively mitochondrial and in *A.oryzae* the enzyme is found in both the cytosol and mitochondria (Bercovitz et al.,

1990). For *A.niger* some researchers claim only mitochondrial localization of pyruvate carboxylase (Purohit and Ratledge, 1988), whereas others find the enzyme in both the cytosolic and mitochondrial fractions (Bercovitz et al., 1990). Considering these findings, pyruvate carboxylase was assumed to be present in both the cytosol and mitochondria.

It was well known that acetyl-CoA, which is a precursor for amino acid and lipid biosynthesis, can not pass the inner mitochondrial membrane, and synthesis of this compound may occur by two different pathways. When growing on acetate, this metabolite is assumed to be synthesized from acetate via cytosolic acetyl-CoA synthase. This enzyme is essential for growth on acetate as the sole carbon source in *P. chrysogenum* (Martinez Blanco et al., 1992) and repressed by glucose in *A.nidulans* (Kelly and Hynes, 1982). In case of growth on glucose cytosolic acetyl-CoA is assumed to be formed via ATP citrate lyase converting citrate into acetyl-CoA and oxaloacetate (Pfitzner et al., 1987). The oxaloacetate formed in cytosol can not cross the mitochondrial membrane, so it is converted to malate via cytosolic malate dehydrogenase. Malate may then either enter the mitochondria or be oxidatively decarboxylated to pyruvate by malic enzyme.

There are two enzymes unique to the glyoxylate shunt: isocitrate lyase and malate synthase. These occur in all classes of fungi and are probably located in the glyoxysome (Martinelli and Kinghorn, 1994). Glyoxysomes take up isocitrate and acetyl-CoA and release succinate and malate.

5.2.4.6 Intracellular Transport

A steady flow of certain metabolites both in and out of the mitochondrial matrix space is necessary for the mitochondrion to perform its functions. Mitochondria have been shown to be either freely permeable or to have specific systems to transport the essential metabolites across the impermeable membrane separating the inner matrix space from cytoplasmic environment. Some uncharged molecules such as water, oxygen, and carbon dioxide pass through the inner membrane by free diffusion, but the transport of hydrophilic compounds including those involved in oxidation phosphorylation and electron transport is mediated by carrier proteins that span the lipid layer. In general, monocarboxylic acids such as acetate, acetoacetate, and pyruvate penetrate the

mitochondrion as the un-ionized acids by free diffusion mechanism (Lanoue and Schoolwerth, 1984). There is good evidence that pyruvate uptake is also mediated by antiport proton mechanism (Darvey, 2000). Fumarate is produced in the cytosol by the reactions involved in the biosynthesis of arginine and degradation of tyrosine as well as biosynthesis of nucleotides of AICAR and ATP. However, fumarate was not detected in the extracellular medium throughout the course of the fermentation in this study which means that it should be transported into the mitochondrion. In the current model, fumarate was carried into mitochondria by a carrier-dependent process assumed to be a fumarate/proton uniport.

Phosphate is transported into the mitochondrion by a carrier-dependent process thought to be phosphate/OH^- antiport (formally equivalent to co-transport with proton mechanism as shown by Ferreira et al., 1989). Two transport pathways have been found for the entry of glutamate into the mitochondrion. The first operates as a glutamate/proton symport mechanism which has a relatively low affinity for glutamate. The second means of importing glutamate is through an exchange with intramitochondrial aspartate (Tzagoloff, 1982). It was thought that ornithine enters the matrix space by an electrogenic uniport mechanism, however, more recent data suggests that this amino acid enters the mitochondria by an electroneutral proton exchange (Walker, 1992). The charge neutrality is preserved through the generation of a proton in the matrix during the excursion of citrulline. The transport of zwitterionic amino acids such as valine, isoleucine, and citrulline is mediated by a carrier-dependent process thought to be a proton antiport (Tzagoloff, 1982). The ADP- ATP translocase transports ADP^{3-} into the matrix space in exchange for ATP^{4-} by a reorienting site mechanism in which a single site can be exposed to either the cytoplasmic side or the matrix side of the membrane (Nicholls and Ferguson, 1992). Ac-CoA is assumed to enter the mitochondria via a carnitine shuttle (Jernejc and Legisam, 1996).

5.2.4.7 Energetic Parameters

In eukaryotes, many compounds (e.g., phosphate, pyruvate) are transported across the mitochondrial membrane by proton symport (Zubay, 1988). As a result, there is an influx of protons into the mitochondria, which in turn leads to the incomplete coupling between

the oxidation and phosphorylation processes. As a result, the so-called operational P/O ratio is much below the corresponding theoretical values (Nielsen et al., 2002). The operational P/O ratio for oxidation processes in *A.niger* is found to be 1.5-1.8 for $FADH_2$, 2.3-2.7 for $NADH_m$, and 1.4-1.8 for $NADH_c$ (Nielsen, 1997). Unless otherwise stated, the operational P/O ratio for oxidation of $NADH_m$, $FADH_2$, and $NADH_c$ in the present simulations were considered to be 2.64, 1.64, and 1.64, respectively.

5.2.5 Mathematical Formulation

5.2.5.1 Metabolite Balancing

If a system boundary around the cells is considered, this boundary is closed to the passage of certain metabolites while others are allowed to enter or exit the system based on external sources or sinks. Should an external source or sink of a metabolite exist, the introduction of an exchange flux will be necessary to allow a metabolite to enter or exit the system boundary. These fluxes have been referred to as pseudo-reactions (Clarke, 1980) and can be thought of as representing the inputs and outputs to the system.

It is possible to reduce the degrees of freedom of the set of algebraic Equation 2-29 by measuring some of these exchange fluxes as it was explained by Equation 2.30 by partitioning the flux vector $\boldsymbol{V}$ into unknown and known vectors. In this study, however, flux vector $\boldsymbol{V}$ was decomposed into three vectors. This enabled to implement the mathematical formulation more easily into GAMS environment. More specifically, the vector of fluxes could be partitioned into unknown internal fluxes $\boldsymbol{V_u^I}$, unknown exchange fluxes $\boldsymbol{V_u^E}$, and known (measured) exchange fluxes $\boldsymbol{V_k^E}$. In the same manner, the matrix $\boldsymbol{S}$ can be partitioned into $\boldsymbol{S}_u^I$, $\boldsymbol{S}_u^E$, and $\boldsymbol{S}_k^E$:

$$\boldsymbol{S} = \begin{pmatrix} \boldsymbol{S}_u^I & \boldsymbol{S}_u^E & \boldsymbol{S}_k^E \end{pmatrix} \quad , \quad \boldsymbol{V} = \begin{pmatrix} \boldsymbol{V}_u^I \\ \boldsymbol{V}_u^E \\ \boldsymbol{V}_k^E \end{pmatrix} \tag{5.1}$$

The equation (2-26) can be now written in the following form:

$$\boldsymbol{S}.\boldsymbol{V} = \boldsymbol{S}_{\boldsymbol{u}}^{\boldsymbol{I}}\boldsymbol{V}_{\boldsymbol{u}}^{\boldsymbol{I}} + \boldsymbol{S}_{\boldsymbol{u}}^{\boldsymbol{E}}\boldsymbol{V}_{\boldsymbol{u}}^{\boldsymbol{E}} + \boldsymbol{S}_{\boldsymbol{k}}^{\boldsymbol{E}}\boldsymbol{V}_{\boldsymbol{k}}^{\boldsymbol{E}} = 0 \tag{5.2}$$

Upon rearrangement this yields:

$$\boldsymbol{S}_{\boldsymbol{u}}^{\boldsymbol{I}}\boldsymbol{V}_{\boldsymbol{u}}^{\boldsymbol{I}} + \boldsymbol{S}_{\boldsymbol{u}}^{\boldsymbol{E}}\boldsymbol{V}_{\boldsymbol{u}}^{\boldsymbol{E}} = -\boldsymbol{S}_{\boldsymbol{k}}^{\boldsymbol{E}}\boldsymbol{V}_{\boldsymbol{k}}^{\boldsymbol{E}} \tag{5.3}$$

The right hand side of the latter equation may be replaced by $\boldsymbol{b}$, which is an $m \times 1$ vector:

$$\boldsymbol{S}_{\boldsymbol{u}}^{\boldsymbol{I}}\boldsymbol{V}_{\boldsymbol{u}}^{\boldsymbol{I}} + \boldsymbol{S}_{\boldsymbol{u}}^{\boldsymbol{E}}\boldsymbol{V}_{\boldsymbol{u}}^{\boldsymbol{E}} = \boldsymbol{b} \tag{5.4}$$

Here $\boldsymbol{S}_{\boldsymbol{u}}^{\boldsymbol{I}}$ and $\boldsymbol{S}_{\boldsymbol{u}}^{\boldsymbol{E}}$ are $m \times n_u^I$ and $m \times n_u^E$ matrices, respectively. The elements of vector $\boldsymbol{b}$ can be evaluated from the slope taken between two consecutive concentration data points. In the model, these elements are defined as outward, thus the numerical value of each element of $\boldsymbol{b}$ is negative when metabolite is entering the system, and positive when it is exiting the system. Equation 5.4 is the fundamental relationship in metabolic balancing.

Figure 5.2a shows a simple example of a hypothetical network consisting of five metabolites and six internal reactions. One of these reactions is reversible, which creates a forward and a reverse flux. Altogether there are seven internal fluxes. Metabolites A and C are allowed to enter the system as substrates, and metabolites B and E to exit as products. Also, the uptake rate of metabolite A and excretion rate of metabolite E have been experimentally measured.

Note that the measured fluxes (members of vector $\boldsymbol{b}$) are defined as outward, thus the numerical value of each element of $\boldsymbol{b}$ is negative, when metabolite is entering the system and positive when it is exiting the system. The steady state mass balance of the hypothetical network along with the flux constraints are provided in Figure 5.2b. Each row of the stoichiometric matrix represents the steady state mass balance of the corresponding metabolite.

a) Example Metabolic network

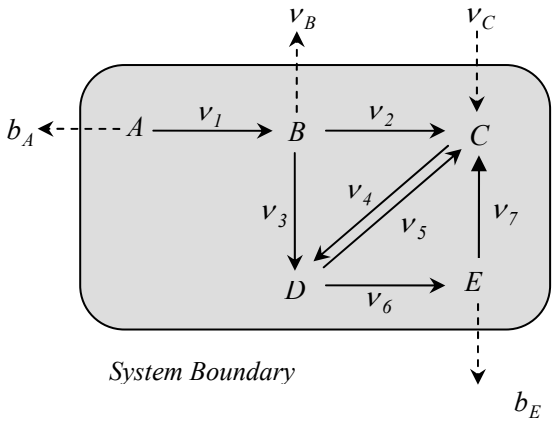

Internal fluxes

$v_1 : A \rightarrow B$

$v_2 : B \rightarrow C$

$v_3 : 2B \rightarrow D$

$v_4 : C \rightarrow D$

$v_5 : D \rightarrow C$

$v_6 : D \rightarrow E$

$v_7 : E \rightarrow 2C$

Exchange fluxes

$b_A : A \dashrightarrow$

$v_B : B \dashrightarrow$

$v_C : C \dashrightarrow$

$b_E : E \dashrightarrow$

b) Mathematical Representation

$$\begin{array}{c} A \\ B \\ C \\ D \\ E \end{array} \begin{bmatrix} -1 & 0 & 0 & 0 & 0 & 0 & 0 \\ 1 & -1 & -2 & 0 & 0 & 0 & 0 \\ 0 & 1 & 0 & -1 & 1 & 0 & 2 \\ 0 & 0 & 1 & 1 & -1 & -1 & -1 \\ 0 & 0 & 0 & 0 & 0 & 1 & 0 \end{bmatrix} \begin{bmatrix} v_1 \\ v_2 \\ v_3 \\ v_4 \\ v_5 \\ v_6 \\ v_7 \end{bmatrix} + \begin{bmatrix} 0 & 0 \\ -1 & 0 \\ 0 & 1 \\ 0 & 0 \\ 0 & 0 \end{bmatrix} \begin{bmatrix} v_B \\ v_C \end{bmatrix} = \begin{bmatrix} b_A \\ 0 \\ 0 \\ 0 \\ b_E \end{bmatrix}$$

Unknown Flux Constraints

$0 \le v_j \le \gamma_j \quad , j = 1,...,7$

$0 \le v_i \le \beta_i \quad , i = B, C$

Known Fluxes

$b_A \le 0$

$b_E \ge 0$

$$S_u^I V_u^I + S_u^E V_u^E = b$$

Figure 5.2- Steady state mass balance of a hypothetical network. (a) Chemical reaction network including 5 metabolites(A and C are substrates, B and E are products), 7 internal fluxes indicated with solid arrows , 2 measured and 2 unknown external fluxes shown with dashed arrows. (b) Mathematical representation of the reaction network in the form of Equation 5.4. All internal and measured fluxes are constrained to be positive as described in the text.

5.2.5.2 Linear Programming

As the number of unknown fluxes n_u is typically greater than the $rank(\boldsymbol{S}_u)$ the system is underdetermined and the degrees of underdeterminacy will increase as the network becomes more complex due to the larger number of branch points in the network.

Consequently, the number of feasible flux distributions allowed by the Equation 5.4 is infinite. The metabolic flux distribution may be estimated by formulating a suitable objective function and using linear programming (Luenberger, 1984). The linear programming can be formulated as follows:

$$
\begin{aligned}
Max \quad & Z = \sum \varpi_j \, v_j \\
subject\ to: \quad & \boldsymbol{S_u^I V_u^I} + \boldsymbol{S_u^E V_u^E} = \boldsymbol{b} \\
& (1-\varepsilon_i) b_i \le b_i \le (1+\varepsilon_i) b_i \\
& 0 \le v_{u,j}^I \le \gamma_j \\
& v_{u,i,\min}^E \le v_{u,i}^E \le v_{u,i,\max}^E
\end{aligned}
\tag{5.5}
$$

Where Z is the objective which is represented as a linear combination of the fluxes v_j. In the present work, the unknown fluxes that are the model variables were expressed in units of ($mmol/g_{DW}\ hr$) and the normalized biomass flux represented the specific growth rate, μ ($1/hr$). In this work, the objective function (Z) was the specific growth rate. The first set of constraints is simply the steady state flux balances (i.e., Equation 5.4).

The second set of constraints introduces the vector of parameters ε_i, which accounts for any possible error involved with the measured fluxes. The introduction of error limits has been proposed by Lee and Papoutsakis (1999), but to our knowledge has not been employed previously.

The solution vector, $v_{u,j}^I$ and $v_{u,i}^E$, of the linear programming problem will be always non-negative due to the characteristics of the Simplex algorithm. Consequently, reversible reactions must be formulated as two separate reactions, one in forward direction, and the other in the reverse direction (e.g., v_4 and v_5 in Figure5.2). This property allows the

incorporation of thermodynamic information by distinguishing between reversible and nearly irreversible reactions in the stoichiometric matrix (Schilling et al. 2000). The third set of constraints simply states this property for unknown internal fluxes. Further, the upper limit of this set could be representative of a maximum allowable flux through a given reaction, resulting from a limited amount of an enzyme being present (Lee and Papoutsakis, 1999).

The last set of constraints implies upper and lower bounds on each exchange flux that represents the corresponding metabolite's potential to enter or exit the system. There can only be one exchange flux per metabolite whose activity subsequently represents the net production or consumption of the metabolite by the system. The activity of these exchange fluxes is considered to be zero if the system is closed to the passage of the metabolite , positive if the metabolite is either exiting or being produced by the system, and negative if the metabolite is entering or being consumed by the system (e.g., metabolite D, B, and C in Figure 5.2, respectively). However, to comply with the Simplex algorithm and make the mathematical procedure more straightforward all exchange fluxes need to be considered non-negative. To overcome this drawback for entering metabolites, one can define all the exchange fluxes as positive and at the same time consider the corresponding member of the entering metabolites in matrix $\boldsymbol{S}_u^E$ positive one instead of negative one (e.g. metabolite C). This convention for reversible reactions and exchange fluxes is used merely for mathematical purposes and does not influence the biological interpretation of metabolic function in any way. Linear programming calculations were performed in a GAMS (General Algebraic Modeling System) environment (Brooke et al., 1998).

5.2.5.3 Sensitivity Analysis

Since any experimental data are subject to analytical errors, the assigned value is only an estimate. This uncertainty necessitates investigating the exchange in the solution if the value assigned to a given observation was adjusted to some other plausible value (Hillier and Lieberman, 2001). The sensitivity of the objective function Z with respect to

the change of the i^{th} measured exchange flux was determined using the shadow price (Pannell, 1997) of the linear programming which is defined as follows:

$$\lambda_i = \partial Z \Big/ \partial b_i \tag{5.6}$$

The shadow price values were computed from the mathematical duality of the primary linear optimization problem. As explained previously, the elements of exchange flux $\boldsymbol{b}$ are defined to be negative for substrates and positive for products and by-products. Thus, the shadow price needs to be considered for improving the optimal solution with respect to the sign of the corresponding exchange flux. For instance, one can ameliorate the optimal solution by increasing substrate uptake rates and/or by decreasing by-product excretion rates of the metabolite with negative shadow prices.

Moreover, since the absolute value of the exchange fluxes varies substantially, the relative or logarithmic sensitivity was used for comparison purposes. The sensitivity value quantifies the relative change in a calculated variable that is evoked by a relative change in a system parameter (Torres and Voit, 2002; Varma and Palsson, 1993a). The logarithmic sensitivity of the objective function in response to the change in the i^{th} measured flux can be mathematically expressed as follows:

$$\Lambda(Z, b_i) = \frac{\partial Z / Z}{\partial b_i / b_i} = \frac{\partial Ln\, Z}{\partial Ln\, b_i} = \frac{b_i}{Z}\lambda_i \tag{5.7}$$

As shown in Equation 5.7, only shadow price values, the measured exchange fluxes, and the optimal value of the objective function are needed to compute logarithmic sensitivities.

5.3 Results and Discussion

5.3.1 Matrix Calculations

The matrix computations throughout this study were performed in MATLAB 6.5 environment.

5.3.1.1 Elemental Conservation

In order to determine the molecular formula of protein, RNA, DNA, and lipid the atomic conservation Equation 2.25 was applied to their biosynthetic reactions (*R11.1-4*). The evaluated general molecular formulas for these macromolecules are presented in Table 5.1.

Table 5.1- Elemental composition of macromolecules

	C	H	N	O	P	S
Protein	4.828	9.538	1.376	2.526	0.011	0.014
RNA	9.542	15.738	3.822	14.006	3.000	0.000
DNA	9.742	17.484	3.758	14.000	3.000	0.000
LIPID	38.409	75.947	0.400	23.358	0.923	0.000

Then, the same algorithm for biomass formation reaction, *R11.5*, was applied and the general formula for biomass was evaluated as:

$$C_{41.689}\,H_{78.391}\,N_{7.228}\,O_{28.145}\,P_{0.836}\,S_{0.060} \tag{5.8}$$

It is worth mentioning that the numbers of elements in the above formula have the unit of mmol. The normalization of this formula with respect to carbon yields the elemental

composition of $CH_{1.88}N_{0.17}O_{0.68}P_{0.02}$, which is in good agreement with the reported formula for *Aspergillus niger* $CH_{1.72}N_{0.17}O_{0.55}$ (Roels, 1983).

Finally, the whole reaction network was checked for conservation of atomic species and we found that the equality expressed by Equation 2.25 was completely fulfilled.

5.3.1.2 Stoichiometric Matrix and Flux Vectors Analysis

The reaction network includes 137 metabolites. Since, the biomass biosynthesis reaction was considered as the objective function of linear programming the total mass balance equations for matrix analysis became 136 equations. Moreover, the model consists of 287 intracellular reactions and transport processes between different compartments. Aside from the 37 measured metabolites (i.e., 20 amino acids, 10 organic acids, glucose, ammonia, phosphate, sulfate, biomass as well as oxygen and carbon dioxide at the outlet of the bioreactor) the exchange flux of all other metabolites was set to zero with some exceptions as described below. The exchange fluxes of DHF, isocitrate, hydrogen sulfide, acetoacetate, and cytosolic water were allowed to be determined by the program. For the first attempt to analyze the matrix the exchange fluxes of Hcys, Hser, SAH, and SAM were set to zero. The redundancy test revealed that the matrix was non-redundant. Then, calculability analysis was performed by evaluating the null space of the stoichiometric matrix. It was found that some fluxes were calculable, but all had negative values. Since all reversible reactions were already separated into two irreversible reactions the negative flux values were not acceptable. In order to overcome this drawback, the exchange fluxes of these four metabolites were also considered to be unknown. Based on this approach, the stoichiometric matrix of the network had 136 rows and 287 columns. The matrix was found to be non-redundant. Besides, the kernel of the latter matrix did not have any null row, so none of the unknown fluxes was calculable. The system was further analyzed using optimization approaches.

5.3.2 Fermentation

Figure 5.3 shows the recombinant protein concentration along with protease activity for two batch fermentations. The only difference between the two experiments was the organic nitrogen source. The first fermentation medium contained 10 g/L peptone as the

organic nitrogen source, while the second fermentation medium contained 3.2 g/L amino acid mixture with the composition outlined in material and methods section.

The protease activity increased throughout the fermentation when the medium contained peptone. The biomass (not shown) and lysozyme reached their maximum concentrations at approximately the 93rd hour of the fermentation. The activity of protease increased dramatically most likely due to the cell lysis with concomitant reduction in lysozyme concentration. The lysozyme concentration decreased at an average rate of 0.62 mg/hr by the end of fermentation. The rate of lysozyme inactivation further increased to 0.72 mg/h afterwards (not shown).

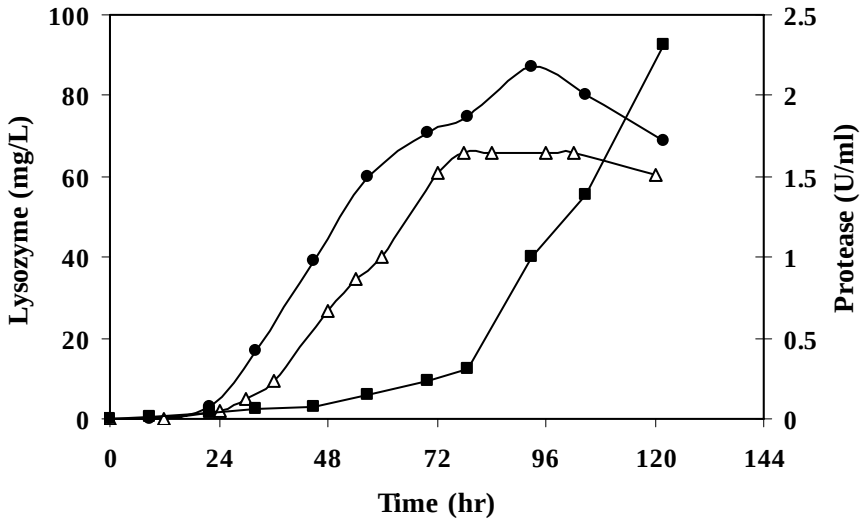

Figure 5.3- The protease activity and lysozyme concentration profiles during the fermentations. T= 27 ^{o}C, N= 400 rpm, and aeration 1 vvm. Peptone as organic nitrogen source: lysozyme (●) and protease (■). Amino acid mixture as nitrogen source: lysozyme (△).

In contrast, protease activity was not detectable in the experiment which contained amino acids as the organic nitrogen source. The maximum biomass concentration was observed at 78 hr and decreased thereafter. In spite of cell lysis, the concentration of recombinant protein remained relatively constant even 24 hours after the cessation of growth and then decreased at a very low rate of 0.13 mg/L at the very end of the fermentation.

Surprisingly, it was found that peptone containing medium with approximately three fold higher amino acid equivalent concentration enhanced recombinant protein production by a factor of only 1.3 over the medium containing amino acids only. The fermentation that contained an amino acid mixture in a defined medium was used for ensuing metabolic flux analysis.

Profiles of the measured extracellular compounds for the lysozyme fermentation of *A.niger* in the 2 liter batch operation are illustrated in Figures 5.4-7 and presented in Appendix D Table D.1. To ensure that all metabolites and cell components are accounted for, detailed overall nitrogen and carbon mass balances were performed using the measured data (not shown). Mass balance calculations included sets of 37 measurements taken at approximately 12-hour intervals for 120 hours of total fermentation time. Both the carbon and nitrogen balances could be closed with a maximum error of 11%. The profiles were found to be reproducible, since fermentation repeats produced almost identical results (data not shown).

Amino acids can be categorized into three groups according to their concentration profiles. The first group consists of alanine, arginine, aspartate, cysteine, glutamate, glycine, and lysine. For sake of clarity only the profiles of three members of the group are given in Figure 5.4. The concentration of these amino acids remained relatively constant or increased slowly during the first 24 hours of fermentation. Then the profiles passed through a maximum and dropped sharply until the concentrations became zero, with the exception of glycine concentration which remained nearly constant after 72 hours of fermentation at 0.45 mmol/L.

The concentration profile of the second group (isoleucine, leucine, phenylalanine, threonine, and tyrosine) decreased throughout the fermentation with particularly high rate during the first 12 hours; then either decreased slowly or remained relatively constant, and finally fell to zero at a relatively high rate. The concentration profile of three members of the second group is given in Figure 5.5. Phenylalanine was the only member whose concentration did not drop to zero but remained constant after 60 hours at a low level of approximately 0.04 g/L which was 4.4% of its initial concentration.

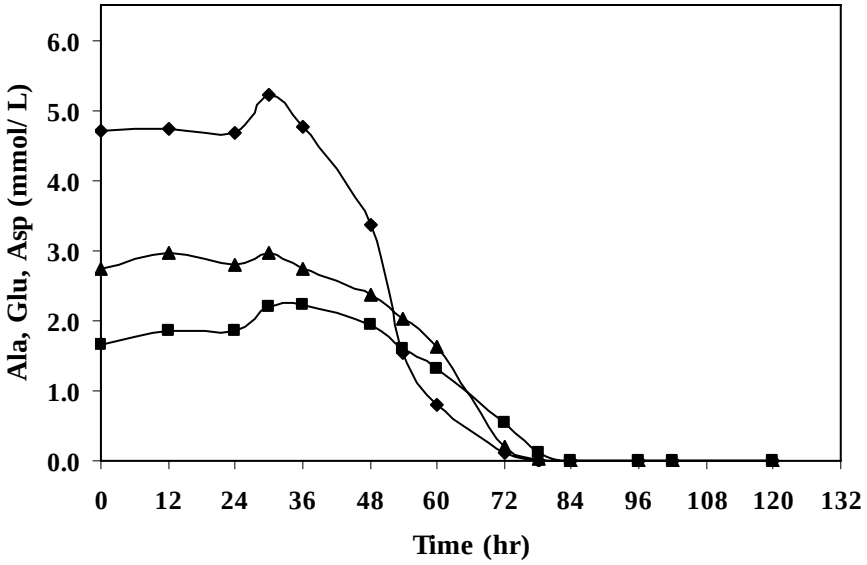

Figure 5.4- The first group amino acids concentration profiles during the fermentation. T= 27 ^{o}C, N= 400 rpm, and aeration 1 vvm. Alanine (◆), glutamate (▲), and aspartate (■).

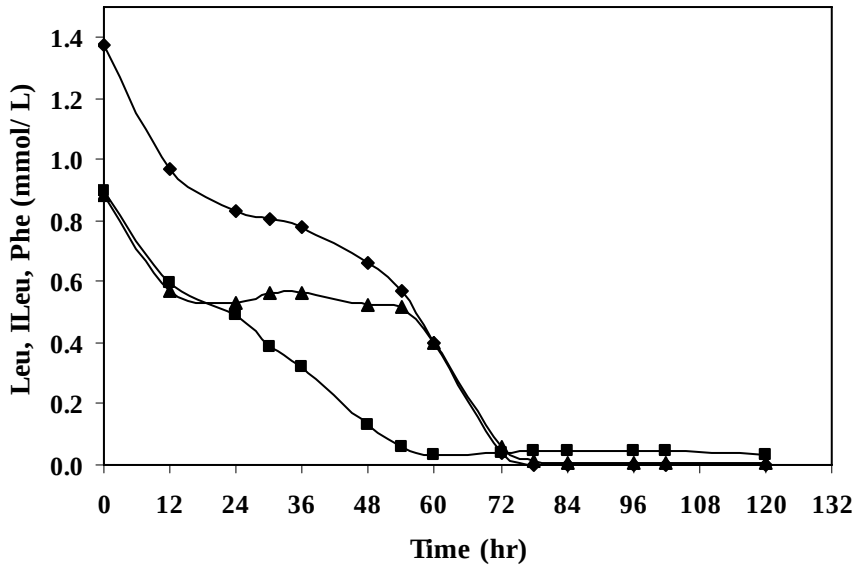

Figure 5.5- The second group amino acids concentration profiles during the fermentation. T= 27 ^{o}C, N= 400 rpm, and aeration 1 vvm. Leucine (◆), isoleucine (▲), and phenylalanine (■).

Proline, histidine, methionine, serine, and valine comprised the third group, which did not possess similar trends as the first two groups (Figure 5.6). For instance, valine and serine were not utilized until late in the fermentation. The utilization of proline, on the other hand, appeared to be biphasic.

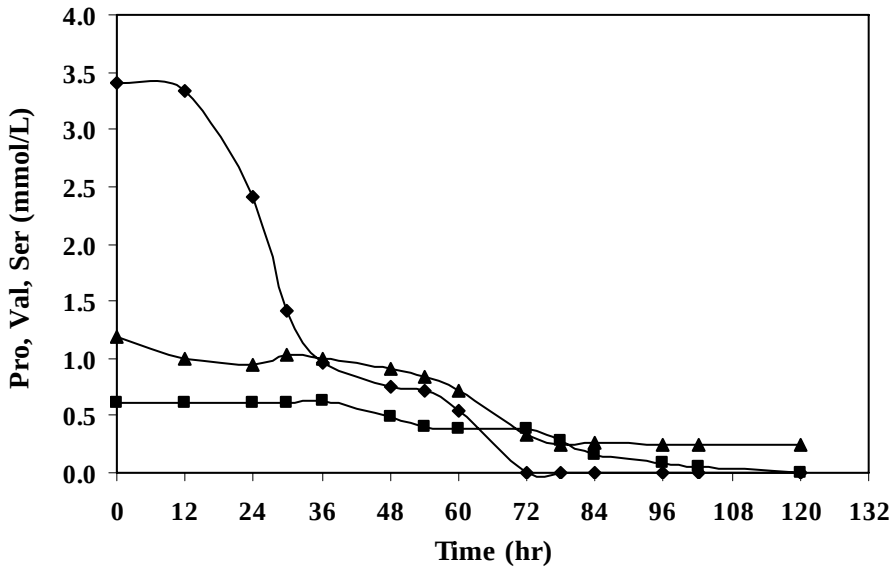

Figure 5.6- The third group amino acids concentration profiles during the fermentation. T= 27 ^{o}C, N= 400 rpm, and aeration 1 vvm. Proline (◆), valine (▲), and serine (■).

Figure 5.7 shows the concentration profiles of glucose, biomass, lysozyme, gluconate, and oxalate throughout the course of the fermentation. Glucose concentration decreased to zero after 30 hours of the fermentation, meanwhile, gluconate reached a maximum concentration of 16.2 g/L.

Considering the total amount of supplied glucose (i.e., inoculum and fermenter) the concentration of gluconate alone accounted for approximately 74% of the converted glucose by the 30th hour of fermentation.

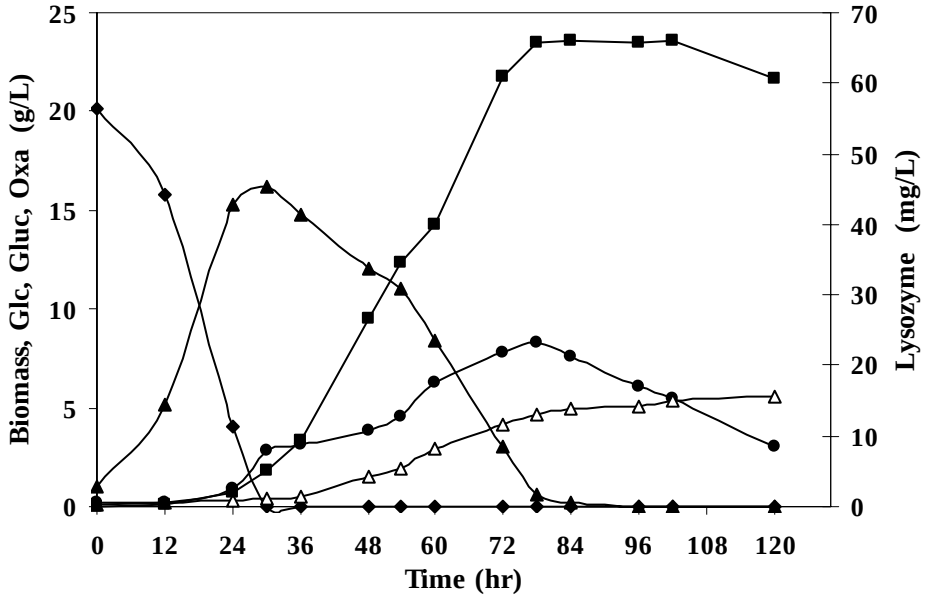

Figure 5.7- Glucose, biomass dry weight, gluconate, oxalate, and lysozyme concentration profiles during the fermentation. T= 27 ^{o}C, N= 400 rpm, and aeration 1 vvm. Glucose (◆), biomass dry weight (●), gluconate (▲), oxalate (△), and lysozyme (■).

The concentration profiles of the other organic acids are depicted in Figure 5.8. Succinate and acetate accumulated during initial 24 to 30 hours of the process to the maximum levels of 0.39 and 0.17 g/L, respectively. The concentration of citrate at the beginning of the fermentation was measured to be 1.3 g/L, which was added as citrate buffer initially. The citrate concentration was nearly constant during the early stage of the fermentation and then dropped to zero by the middle of the process. Pyruvate accumulated during the growth phase and then its concentration declined to zero during the death phase, however, its maximum concentration of 0.075 g/L was very low. Oxaloacetate concentration increased to the maximum level of 0.056 g/L at 36th hour of the fermentation and then fell to zero. Malate and fumarate were not detected in the culture medium during the entire time course of the fermentation.

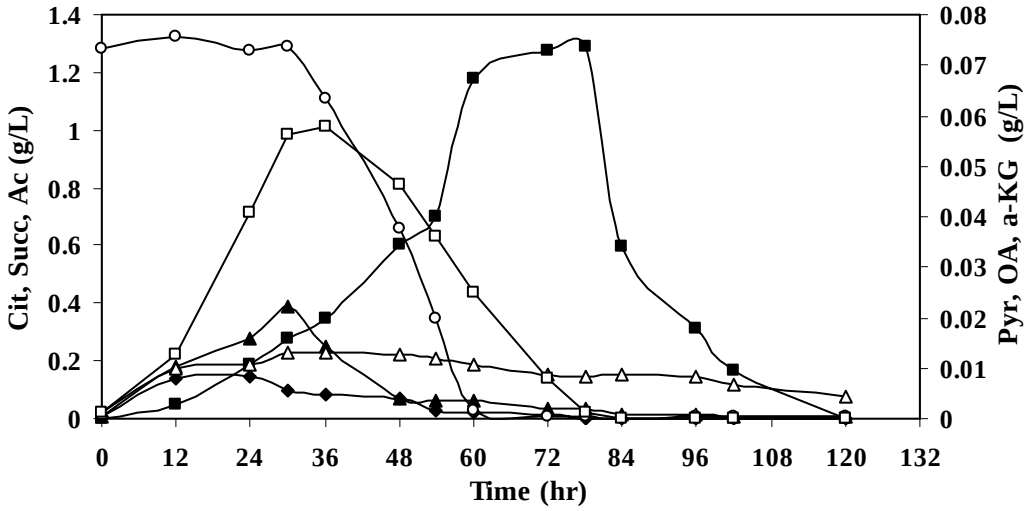

Figure 5.8- Organic acid concentration profiles during the fermentation.
Citrate (○), acetate (◆), succinate (▲), a-ketoglutarate (△), pyruvate (■), oxaloacetate (□).
T= 27 ^{o}C, N= 400 rpm, and aeration 1 vvm.

Considering glucose, biomass, lysozyme, amino acids, organic acids, and other metabolite profiles the fermentation could be conveniently divided into five distinct phases.

Phase I (0< t <12 h), was the early stage of the fermentation, when the culture was in the lag phase and both biomass and lysozyme concentrations were very low. The glucose concentration, however, decreased by 22%. The concentration of gluconate at the end of this phase reached to 5.4 g/L. Based on these observations, gluconate production alone accounted for approximately 93% of glucose consumption. Amongst the amino acids, leucine, isoleucine, and phenylalanine had the highest specific uptake rates of 0.18, 0.14, and 0.13 mmol/g_{DW} hr, respectively. Acetate, oxalate, and succinate excretion rates were determined to be 0.98, 0.70, and 0.66 mmol/g_{DW} hr, respectively. The pH of the culture during this phase was reduced from 6 to 4 and 0.5 ml of 2N sodium hydroxide was added to keep the pH at this point. Although succinate, acetate, and oxalic acid were accumulated in the extracellular medium, the high specific excretion rate of gluconate (10.1 mmol/g_{DW} hr) was the main reason for the pH reduction.

In phase II (12 < t < 24 h), cell concentration commenced to increase, while the lysozyme concentration remained still low. The glucose consumption rate was high and the

concentration decreased to 25% of the initial level while the biomass dry weight level reached nearly 1 g/L by the end of this period. The concentration of gluconate, the main organic acid component in the culture medium increased to 15.3 g/L. From these observations one could conclude that the activity of glucose oxidase enzyme was high during this phase of fermentation. Because of the high secretion rate of gluconate, an average rate of 2.4 ml/hr alkali solution was added to the culture to maintain the pH at 4.0. This was the highest addition rate of the base during the entire time course of the fermentation. Acetate reached its maximum concentration of 0.15 g/L, while the concentrations of oxalate and succinate were still increasing during this period. The concentration of all amino acids decreased during this phase with proline having the highest specific uptake rate. The oxygen consumption rate was approximately three fold higher than during the first period.

During Phase III ($24 < t < 30$ h) glucose was consumed fast and its concentration dropped to essentially zero (i.e., 0.01 g/l) by the end of this period. The gluconate concentration reached its maximum level of 16.2 g/L by the end of this phase. Acetate was the only organic acid with decreasing concentration albeit at a relatively low rate. As the time approached to the end of this phase, succinate concentration increased to its maximum value of 0.4 g/L. The oxygen uptake rate was 1.5 times higher than that of the second phase. The specific carbon dioxide evolution rate peaked during this phase of the fermentation. The first group of the amino acids along with methionine, valine, and serine started to accumulate in the medium, whereas the concentration of the second group decreased. The specific growth rate reached its maximum value of 0.177 hr^{-1} consequently the cells produced the recombinant protein in higher levels than in previous phases.

At the end of Phase IV ($30 < t < 78$), the concentrations of biomass, lysozyme, and pyruvate reached their maximal value. Throughout this period, the glucose concentration was very low. Succinate and acetate concentrations decreased essentially to zero. Gluconate was the main carbon source in the medium and its concentration decreased to 0.6 g/L by the end of this phase showing 96% reduction in the concentration in comparison to its maximum value. Oxalate concentration increased throughout this phase to the final level of 4.6 g/L. Oxaloacetate accumulated since the start of the fermentation

and reached a maximum concentration of 0.056 g/L and then was depleted by the end of this period. This time period is characterized by high amino acid metabolism. Most amino acids were consumed during this phase.

Phase V ($78 < t < 120$ h), is the last phase of the fermentation. Basically, it represents the death phase, when the biomass concentration decreased. With the notable exception of pyruvate, the concentrations of extracellular metabolites showed no significant changes. The pyruvate concentration continued to decrease to zero by the end of this phase. Product formation ceased as the culture entered this phase and the specific growth rate become negative. For these reasons, this phase was not analyzed further.

5.3.3 Model Reconciliation

Some enzymes are known to function with more than one related cofactors. For instance, glutamate oxidoreductase (EC 1.4.1.3) and homoserine oxidoreductase (EC 1.1.1.3) function with both NADH and NADPH. Since the exact cofactor requirements are often not known, in such cases reactions involving both NADH and NADPH were considered in the primary model. For some reversible reactions, however, this would result in an artificial transhydrogenation cycle in which NADH is converted to NADPH without any net formation of other metabolites. However enzyme catalyzing transhydrogenation has not been found in fungi (Stephanopoulos et al., 1998). Therefore, in the present simulation one of the associated reactions was either confined to be irreversible or removed from the model to avoid unrealistic cycling. For example, one can refer to the potential cycle between the reactions catalyzed by the enzyme methylene tetrahydrofolate reductase (EC 1.5.1.20). In this case the transhydrogenation cycle was eliminated by considering NADPH as the only cofactor. A summary of the constraints that were applied to prevent the transhydrogenation cycle in the proposed metabolic network is presented in Table 5.2.

Table 5.2- Additional constraints to eliminate the artificial transhydrogenation cycles

Enzymes	Metabolites	Additional Constraints
Acetaldehyde dehydrogenase (EC 1.2.1.5)	Aald/ Ac	$NAD(H)$ and $NADP(H)$ reactions were considered to be irreversible leading to acetate production when glucose is available in the medium, and considered to be irreversible in the direction of acetate consumption when glucose is depleted.
Acetaldehyde reductase (EC 1.1.1.71)	Aald/ EtOH	$NADP(H)$ reaction is considered to be irreversible leading to acetaldehyde consumption
Glutamate dehydrogenase (EC 1.4.1.3)	α-KG/ Glu	$NADP(H)$ reaction is considered to be irreversible in the direction of glutamate production
Methylene tetrahydrofolate reductase (EC 1.5.1.20)	MnTHF/ MlTHF	$NADP(H)$ reaction is considered to be irreversible in the direction of MlTHF production

Furthermore, considering both reactions involving NADH and NADPH in metabolism of some amino acids would cause the wrong direction of some pathway fluxes and/or a poor prediction of the exchange fluxes. For example, the overall degradation reaction of lysine to α-aminoadiapate acid could involve the formation of either one or two NADPH

(http://kegg.com). The latter case was excluded, because it would result in an inaccurate estimation of the carbon dioxide evolution rate.

The overall degradation reaction of tryptophane gives rise to the formation of alanine as a byproduct. Alanine, however, is mainly metabolized in the reaction catalyzed by the pyruvate transaminase (EC 2.6.1.2). Being a key intermediate; pyruvate is involved in several reactions in the network and plays a significant role in the metabolic network. In the model simulations, however, alanine was considered to be only metabolized by pyruvate transaminase, because by including the degradation of tryptophane the pathway fluxes regarding pyruvate were physiologically unacceptable. Besides, the measured external flux of tryptophane confirmed that the degradation rate of this amino acid is very low in comparison to alanine.

5.3.4 Metabolic Flux Distribution

Using experimental data, the extracellular metabolite fluxes were calculated from the metabolite concentration profiles for each phase. In order to verify the result of each simulation, the oxygen uptake and the carbon dioxide evolution rates were allowed to be determined by the optimization program. It is worth noting that the off-gas analyzer displayed the oxygen content of the air to an accuracy of one significant figure, which, in turn, had a significant effect on the experimental oxygen uptake rate calculations. For example, the reading of 20.5% could be any number within the range of 20.46% to 20.54%. Since the oxygen content of the inlet air was constant during the fermentation, using the lower possible limit of each reading (say 20.46%) for outlet flow would result in a very high oxygen consumption rate. The experimental observations confirmed that the main source of oxygen consumption, especially during the first two phases of the fermentation, was the oxidation of glucose to gluconate. Based on the measured concentration of gluconate, this high oxygen uptake rate was not realistic. On the other hand, when the higher possible limit of each reading (say 20.54%) was used for calculating the experimental oxygen consumption rate, the result was in better agreement with the other measurements (e.g., gluconate production rate). Accordingly, the experimental oxygen uptake rates were calculated based on the higher possible limit of the readings. Using the specific growth rate as the objective of the optimization program,

the predicted specific growth rate, the specific oxygen uptake, and carbon dioxide evolution rates along with the corresponding experimental measurements are presented in Table 5.3. Logarithmic sensitivities of the objective function with respect to amino acids were determined for the various periods of the fermentation and presented in Figure 5.9.

Table 5.3- Experimental and simulation results of specific growth rate, oxygen uptake rate, and carbon dioxide evolution rate at different phases of cultivation

	6 hr		**18 hr**		**27 hr**		**51 hr**	
	Exp.	*Sim.*	*Exp.*	*Sim.*	*Exp.*	*Sim.*	*Exp.*	*Sim.*
$\mu\,(hr^{-1})$	0.014	0.015	0.131	0.128	0.177	0.159	0.029	0.027
$r_{O_2}\,(mmol/g_{DW}.hr)$	8.0	6.9	8.5	6.1	4.4	3.6	0.8	0.7
$r_{CO_2}\,(mmol/g_{DW}.hr)$	0.07	0.04	0.83	0.74	1.50	1.17	0.95	0.76

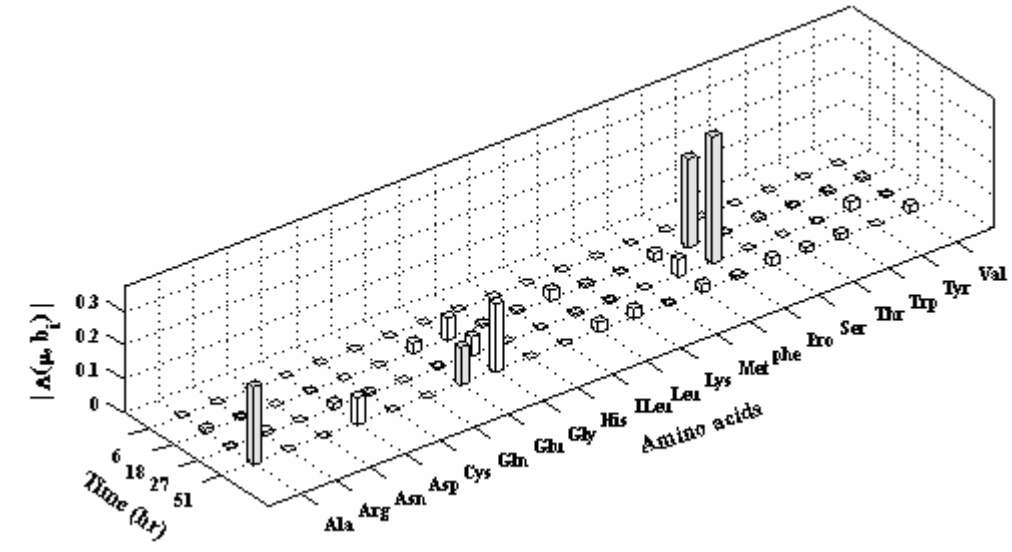

Figure 5.9- Logarithmic sensitivities for amino acids at different phases.

Phase I. Metabolic flux distribution at $t = 6\ hr$ of this period yielded a specific growth rate of 0.015 hr^{-1} that is in good agreement with the measured value (Table 5.3). The specific oxygen uptake rate was determined and showed a 13% error compared with the measured rate. The pentose phosphate pathway (PPP) was active and 12% of the glucose was diverted to this pathway. Approximately 61% of biosynthetic redox potential in cytosol was produced by PPP. The rest of cytosolic NADPH was produced through the conversion of MnTHF to FTHF (*R7.3*) which was further utilized for nucleotide biosynthesis. The NADPH requirement in the mitochondria for the biosynthesis of isoleucine and other amino acid precursors (i.e., ornithine and α-ketoisovalerate) was completely satisfied by mitochondrial NADP-dependent isocitrate dehydrogenase activity (EC 1.1.1.42).

Based on the simulation results, only a minor percentage of the carbon flowed toward the precursors of biomass components (e.g., glycogen, chitin). Using ammonia as the nitrogen source, the NADP-dependent glutamate dehydrogenase enzyme was active leading to glutamate synthesis (*R6.2*). The oxidations of cytosolic and mitochondrial NADH were responsible for 61% and 39% of the oxidative phosphorylation process, respectively. Cytosolic pyruvate carboxylase enzyme was found to be active.

All amino acid fluxes were calculated to have a shadow price of zero (Table 5.4), indicating that they can not be used to improve growth during this period. Among the other measured metabolites, however, phosphate was the only nutrient with nonzero and negative shadow price of -1.27 $(mmol/g_{DW})^{-1}$. Moreover, all nucleotides (e.g., ATP, CTP) had shadow price of -3.81, indicating a necessity to eliminate surplus energy. In one of the runs, the phosphate uptake rate was allowed to be determined by the optimization algorithm; the free uptake rate was more than 4 times higher than the measured value. The sensitivity analysis of the result of this run revealed that the shadow price of the nucleotides were still negative but decreased 97% when compared with the original run. This result indicated that cell growth was limited by phosphate uptake, and not by other measured metabolites including amino acids.

Table 5.4- Shadow prices [a] for amino acids at different culture phases

Amino acids	$\lambda_i\ (g_{DW}\ /\ mmol_i)$			
	6 hr	**18 hr**	**27 hr**	**51 hr**
Ala	0.0000	-0.1393	-0.1384	-0.1557
Arg	0.0000	-0.5571	-0.5534	0.0000
Asn	0.0000	-0.2785	-0.2767	-0.3113
Asp	0.0000	-0.1393	-0.1384	-0.1557
Cys	0.0000	0.0000	-0.1384	0.0000
Gln	0.0000	-0.2785	-0.2767	-0.3113
Glu	0.0000	-0.1393	-0.1384	-0.1557
Gly	0.0000	-0.1393	-0.1384	-0.1557
His	0.0000	-0.4178	-0.4151	-0.4670
Ileu	0.0000	-0.1393	-0.1384	-0.1557
Leu	0.0000	-0.1393	-0.1384	-0.1557
Lys	0.0000	-0.2785	-0.2767	-0.3113
Met	0.0000	-0.1393	-0.1384	-0.1557
phe	0.0000	-0.1393	-0.1384	-0.1557
Pro	0.0000	-0.1393	-0.1384	-0.1557
Ser	0.0000	-0.1393	-0.1384	-0.1557
Thr	0.0000	-0.1393	-0.1384	-0.1557
Trp	0.0000	-0.2785	-0.2767	-0.3113
Tyr	0.0000	-0.1393	-0.1384	-0.1557
Val	0.0000	-0.1393	-0.1384	-0.1557

a: Normal and underlined styles are used for substrates and by-products, respectively.

Phase II. The flux data corresponding to *t = 18 hr* were used to evaluate the metabolic flux distribution of this phase and it is illustrated in Figure 5.10. Since it was not possible to represent all the fluxes, only a summary of the most significant fluxes and those leading to the synthesis of amino acids and organic acids are presented. The optimum specific growth rate was determined to be 0.128 hr^{-1} which was 2.3% less than the measured value.

Both the specific oxygen uptake rate and carbon dioxide evolution rate were underestimated by 28% and 11% in comparison with the measured values. The carbon flux via PPP increased to 19% of the total carbon flux to satisfy the elevated cytosolic NADPH requirements due to the increase in biomass growth rate. Similarly to the first phase, glutamate was produced by NADP-dependent glutamate dehydrogenase enzyme, however, the flux was 2.5 times higher than in Phase I, showing higher requirement of the cells for glutamate. The contribution of $FADH_2$ to generate energy in the form of ATP elevated to 4% of the oxidative phosphorylation process, however it was still small in comparison to 59% contribution of the cytosolic NADH. Unlike the first phase, oxaloacetate was generated mainly by the mitochondrial pyruvate carboxylase. A higher production rate of ATP was possible by the higher flux through the reactions of TCA cycle to generate more redox potentials (i.e., NADH and $FADH_2$). The elevated flux through the TCA cycle produced more carbon dioxide, which, in turn, was more likely favoring carbon dioxide fixation inside the mitochondrion.

Cysteine was the only amino acid with shadow price of zero. Since the shadow price of other amino acids were negative, decrease in secretion rate of the by-products (i.e., arginine and serine) or increase in uptake rate of the other amino acids would improve the optimal specific growth rate. In comparison to the previous phase, the shadow price of nucleotides decreased by a factor of 5 to 10. The shadow price of phosphate was determined to be zero.

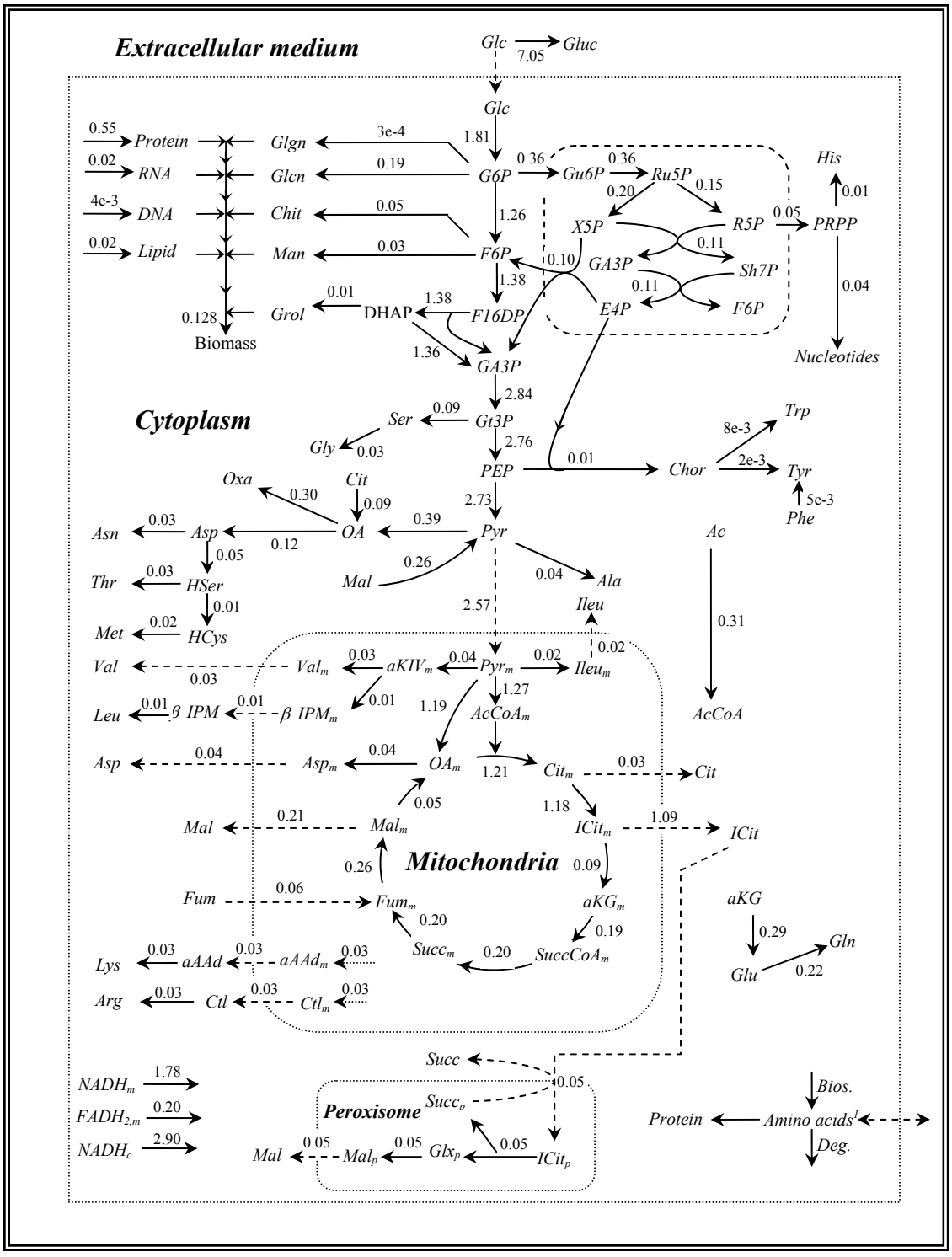

Figure 5.10- Flux distribution map at 18 hr (period II). Not all fluxes are shown. Specific flux estimates from measurements taken at 12.0 hr and 24 hr (mmol/g_{DW} hr).

Furthermore, an examination of the computed logarithmic sensitivities (Figure 5.9) led to some important observations. Although arginine had the highest shadow price amongst the amino acids, its logarithmic sensitivity was very small (less than 0.01), so any change in its exchange flux would not significantly affect the optimal growth rate. On the other hand, proline had only a moderate shadow price but because of its high uptake rate, the optimum value of the objective function was highly sensitive to the proline uptake flux. The highest value of the logarithmic sensitivity among the amino acids was 0.27 for proline. Quantitatively, these values meant that should the uptake rate for this amino acid increases by 10 %, then the specific growth rate would increase by 2.7%.

Finally, among all measured nutrients, ammonia had the highest logarithmic sensitivity of 0.51, indicating ammonia uptake was growth limiting during this early stage of exponential growth.

Phase III. Metabolic flux distribution at the 27^{th} hour of the fermentation was employed as the representative dataset for this phase. The metabolic flux model predicted the specific growth rate reaching a maximum value of 0.159 hr^{-1} which showed 10% error relative to the measured value. The fraction of glucose diverted to the PPP accounted for 20% of the total uptake rate. The biosynthetic redox potential in the cytosol was mainly supplied by the PPP. The contribution of cytosolic NADH to the oxidative phosphorylation process was higher than the mitochondrial one by the factor of 1.7. The mitochondrial pyruvate carboxylase activity was quite significant and accounted for 72% of the total carbon dioxide fixation process. The higher requirement of the cells for ATP caused higher flux through the TCA cycle.

The shadow prices of all amino acids were non-zero and negative. The higher uptake rate of amino acids as energy source (e.g., proline and phenylalanine) and/or lower excretion rate of some (e.g., alanine, aspartate and glycine) would further increase the optimum growth rate. In general, with the exception of ammonia and proline, small logarithmic sensitivities were observed for all measured metabolites. Although, the specific uptake rate of ammonia showed 60% increment relative to the corresponding rate in Phase II it still had the highest logarithmic sensitivity of 0.65 amongst the measured metabolites, and therefore its uptake was the probable limiting factor for growth. Among the amino acids, proline had the highest logarithmic sensitivity of 0.37.

Phase IV. In spite of glucose depletion, the cells continued to grow during this phase but at a lower rate than in the previous phase. The predicted specific growth rate by the simulation was determined to be 0.027 hr^{-1}, which was in excellent agreement with the experimental value of 0.029 hr^{-1}. The error associated with the predicted specific oxygen uptake was 13%. As can be seen from the metabolic flux distribution at $t = 51\ hr$ of the fermentation (Figure 5.11), gluconate was the major source of carbon. Both glucose-6-phosphatase (EC 3.1.3.9) and phosphoenolpyruvate carboxinase (EC 4.1.1.32) that would be active during growth on substrates such as ethanol and acetate were also active. The flux of carbon through the PPP decreased due to the reduced requirement for biomass formation, however; the PPP was responsible for production of 80% of cytosolic NADPH. Excepting cysteine and arginine that had zero shadow prices, all amino acids had non-zero negative shadow prices. The highest logarithmic sensitivities were for alanine, glycine, and glutamate which were computed to be 0.23, 0.20, and 0.11, respectively. The relatively high logarithmic sensitivity of glycine was due to its high degradation rate during this period; however, as it was outlined in the materials and methods section, both the lysozyme and the biomass concentrations were not affected experimentally by changing the glycine concentration even by doubling its concentration for a similar experiment. It could be concluded that glycine catabolism was not coupled directly with biomass formation. Accordingly, glycine was not considered as an important amino acid for further investigations. Interestingly, of all metabolites, ammonia still had the highest logarithmic sensitivity (0.19).

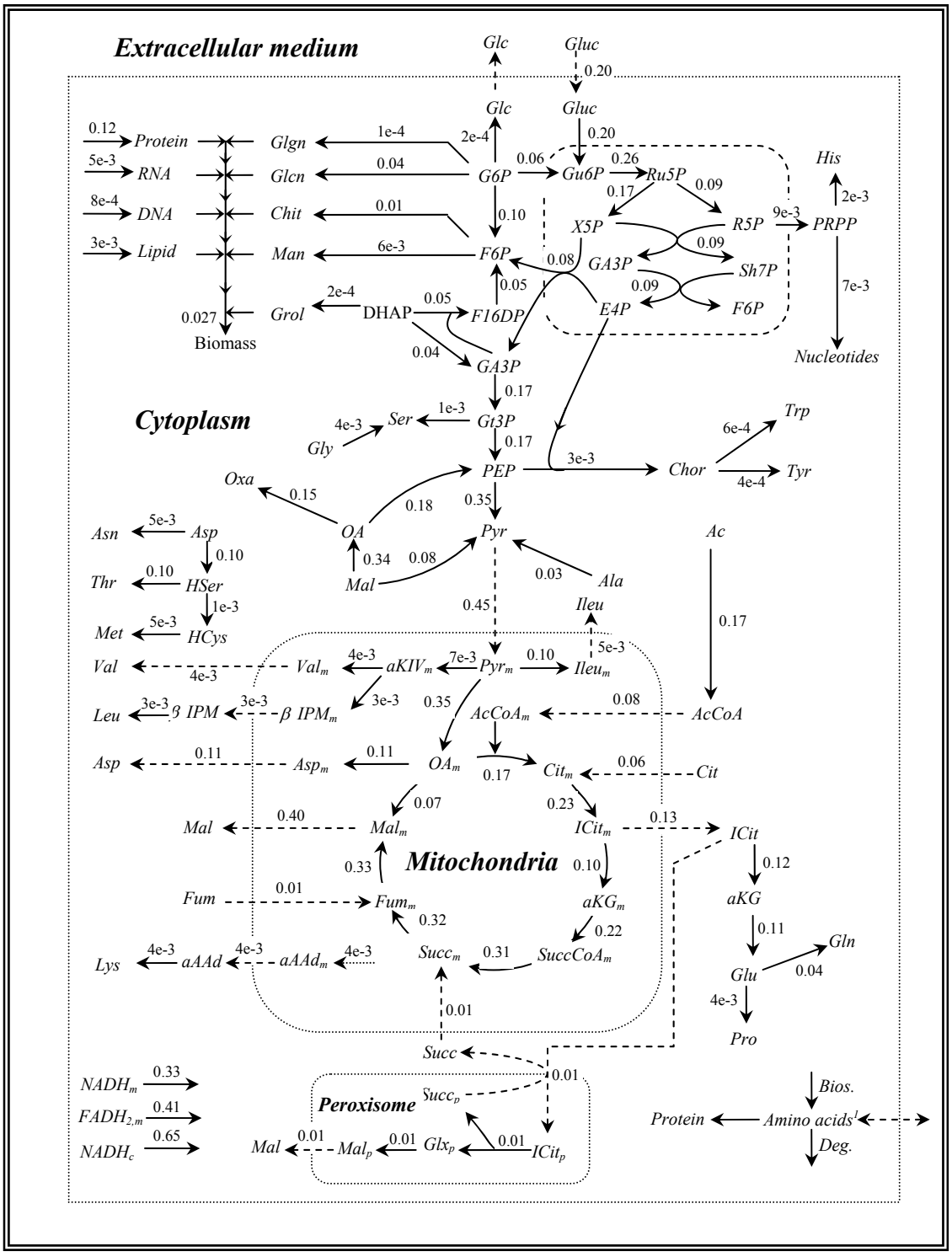

Figure 5.11- Flux distribution map at 51 hr (period IV). Not all fluxes are shown. Specific flux estimates from measurements taken at 48.0 hr and 54.0 hr (mmol/g_{DW} hr).

5.3.5 Overall Remarks

In this study, it was found that tricarboxylic acid cycle was functional throughout the fermentation; however, fluxes were reversed from fumarate to succinate during the lag phase and from oxaloacetate to malate at 27 hr and 51hr. The mitochondrial pyruvate carboxylase was active throughout the growth phase, whereas the cytosolic carboxylase was active during the first three phases of the fermentation. The glyoxylate shunt was active throughout the fermentation; however, the flux through this shunt was low. Acetate was the main product of NADP and NAD-dependent acetaldehyde oxidoreductase (EC 1.2.1.5) and its production was concomitant with the production of homocysteine (*R6.13d*, EC 2.5.1.49), ornithine (*R6.25*), and oxalic acid (*R15.3*, EC 3.7.1.1) in the network. Since, a significant amount of oxalate was accumulated in the extracellular medium the latter was of great importance for the acetate synthesis. The experimental results showed that some of the acetate was secreted into the extracellular medium. In the current model, the rest of the acetate was converted to acetyl-CoA by acetyl-CoA synthase (*R 10.5b*). The acetyl-CoA was either entered into the mitochondrion or the peroxisomes compartments. The peroxisomal glyoxylate and acetyl-CoA reacted by the action of malate synthase to form malate (*R4.7*).

The energy requirement for maintenance was stated in the model as the hydrolysis of ATP (*R.12.1*). The results showed that the maintenance requirements accounted for 33% of the total ATP production during the first phase of the fermentation and dropped to essentially zero afterwards. At low growth rates, the microorganisms did not require large amount of energy for metabolic activities and therefore surplus energy was used as maintenance. According to the model, however, the produced ATP was produced solely for metabolic activities.

The concentration profile of glucose and gluconate as the main carbon sources, total amino acids as the organic nitrogen source, and specific growth rate are depicted in Figure 5.12. The microorganism showed a diauxic growth pattern which was caused by a shift in metabolic pathways in the middle of the growth cycle. The specific growth rate increased rapidly during the first 30 hours of the fermentation when the glucose served as the main carbon source and the total concentration of amino acids were still high.

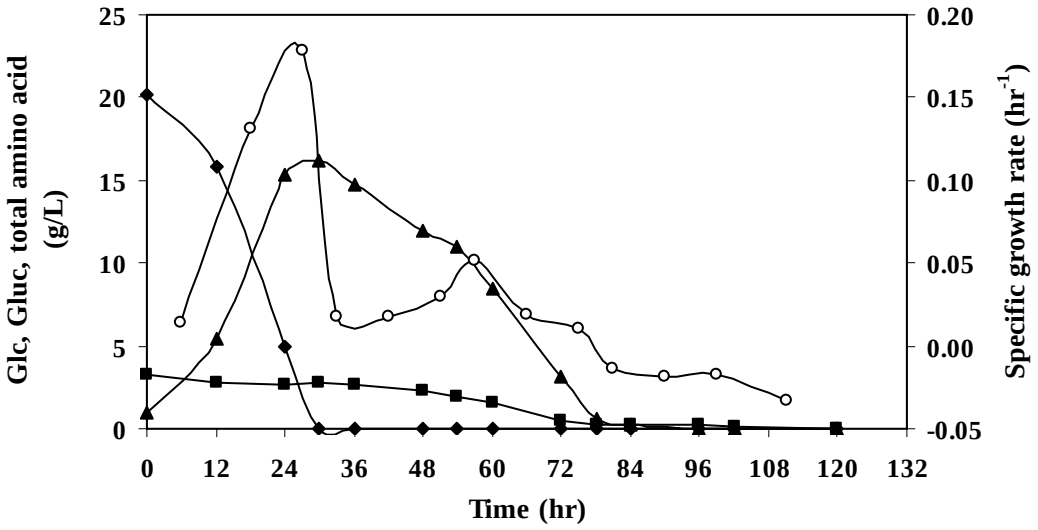

Figure 5.12- Specific growth rate, glucose, gluconate, and total amino acid concentrations as a function of time. Specific growth rate (○), glucose (◆), gluconate (▲), and total amino acid (■). T= 27 ^{o}C, N= 400 rpm, and aeration 1 vvm.

After glucose was exhausted, gluconate was the main carbon source. The specific growth rate dropped during this time. One may conclude that glucose was more readily utilizable than gluconate, and glucose repressed the synthesis of the enzymes (e.g. gluconokinase EC 2.7.1.12) that are required for the metabolism of gluconate. During the next 10 hours cell mass accumulation was only 2% as the cells adapted to the new carbon source. After this adaptation period, the specific growth rate increased approximately 3-fold in comparison to its value at 33 hr. At this time (i.e., 60 hr) the concentration of total amino acids was less than 50% of its initial value, however, the concentration of some amino acids such as alanine, proline, phenylalanine, and cysteine was very low. The concentration of gluconate was still high.

The specific growth rate gradually decreased and reached zero at 78 hr as the cells concentration approached its maximum value. One could conclude that the low concentration of the organic nitrogen sources was the main reason for the slow growth immediately after 60 hr, while the depletion of both gluconate and amino acids were the reason for the cessation of growth at 78 hr. After this time the specific growth rate approached to the small negative values due to cells lysis.

As it was outlined in materials and method section, the effect of biomass composition on the biomass production had been a contentious issue among researchers. Biomass production rate might be affected by its monomeric composition in different ways. The biomass composition of the strain under study might not be available and the information related to the other strains was used. The composition of the biomass also might change slightly during the different phases of fermentation and due to variations in growth conditions such as temperature, dissolved oxygen tension, and medium constituents. The process of evaluating biomass composition of the desired strain could be burdensome and costly. Therefore, before spending time and money on this process, it would be of great importance if the effect of associated error with the level of each constituent was examined. The sensitivity analysis performed in this study allowed the investigation of biomass composition on the predicted specific growth rate.

Table 5.5 shows the calculated logarithmic sensitivity of the specific growth rate with respect to 10% change in the level of each biomass component (*R11.5)*. As can be seen from the results of the analysis, the specific growth rate was not sensitive to the applied perturbation in the composition during the lag phase of the fermentation. During this phase the concentration of different nutrients in the medium was still high and the specific growth rate was small, so demand for higher levels of the monomers for biomass synthesis was possible without any limitation. The specific growth rate was mainly affected by the level of amino acid content of the biomass during the second and the third phases of the fermentation, when the biomass production rate was high and the concentration of the nutrients decreased. For instance, 10% increment in amino acid requirement for biomass biosynthesis would result in 7.8% decline in the specific growth rate during the second phase of the fermentation. RNA and chitin content of the biomass affected the specific growth rate, but their effects were negligible.

Protein content was the only cell component that could have a significant effect on the specific growth rate during the final periods of the active growth. As a result of this analysis, one could conclude that the protein content of the biomass is strain-specific and should be determined with extra precautions and using very accurate methods.

Table 5.5- Logarithmic sensitivity of the specific growth rate to the biomass composition.

Component (M_i)	$\Lambda(\mu, M_i)$			
	6 hr	**18 hr**	**27 hr**	**51 hr**
ATP	0	0	0	0
Protein	0	-0.78	-0.75	-0.74
Glycogen	0	0	0	0
Chitin	0	-0.08	-0.06	0
Glucan	0	0	0	0
RNA	0	-0.08	-0.06	0
DNA	0	0	0	0
Lipid	0	0	0	0
Mannitol	0	0	0	0
Glycerol	0	0	0	0

Evidently, the biomass composition with respect to the other components could be obtained from other strains or even related microorganisms without loss of accuracy in prediction of specific growth rate. Furthermore, since the error associated with each cell component was approximately identical throughout the growth phase; identical biomass composition could be used for the entire culture period.

To investigate the importance of experimental flux measurements on model predictions, four sets of flux measurements obtained in four different simulation runs were compared. Table 5.6 shows the results for the 27th hour of culture. Carbon dioxide evolution rate and oxygen uptake were allowed to be predicted by the model. The experimentally measured fluxes of the specific growth rate, carbon dioxide uptake rate, and oxygen uptake were presented in Table 5.3.

Run-1 is the typical result of the simulation when the exchange flux of amino acids, organic acids, phosphate, ammonia, and sulfate were implemented in the program as the second set of constraints according to Equation 5.5. In Run-2, free uptake rate of amino acids were considered in the simulation. It showed better prediction of the specific growth rate and oxygen uptake rates, whereas the carbon dioxide evolution rate was

predicted with less accuracy compared with the first run. The predicted fluxes of Asn, Gln, His, Leu, Met, and Pro were far from their actual values. Run-3 was performed allowing free uptake rate of amino acids and free excretion rate of organic acids. The same specific growth rate as in Run-2 was observed, while the prediction of carbon dioxide evolution rate was very poor. Besides, the fluxes for Val, His, Pro, OA, Ox, and Glun were not accurately estimated. The last run, Run-4, was performed without applying any constraint in the optimization program. The calculated fluxes were far from the observed values; however, they represented the maximum capability of the microorganism in biomass production based on the present model. Accordingly, in order to move toward this optimum approach, the exchange fluxes of the organic acids should be reduced to low levels.

Based to the simulation results of Run-4, there was no need for providing the medium with sulfate since the cells were allowed to take up methionine without restriction. Although the last three runs (Run-2, 3, 4) predicted higher specific growth rate than the first one, but the exchange fluxes were not generally in agreement with the real values. Hence, one could conclude that the flux distributions of approaches represented in Run-2, 3, 4 would be unreliable for sensitivity analysis and medium optimization purposes, but could be considered for genetic modification of the strain for higher production of biomass.

Table 5.6- The value of exchange fluxes[a,b] between extracellular and intracellular compartments when different set of constraints applied.

Compound	Run-1	Run-2	Run-3	Run-4
μ	0.159	0.175	0.175	0.830
CO_2	1.172	0.878	0.000	11.660
O_2	-3.579	-4.375	-3.310	-15.114
Ala	0.003	-0.000	-0.000	-0.935
Arg	0.003	-0.000	-0.033	-0.000
Asn	-0.000	-1.192	-0.035	-0.000
Asp	0.020	0.000	-0.000	-0.000
Cyc	0.009	-0.008	-0.000	-0.039
Gln	-0.000	-0.154	-0.000	-0.000
Glu	0.007	-0.000	-0.000	-0.338
Gly	0.065	-0.000	-0.000	-0.000
His	-0.000	-0.132	-0.390	-0.000
Ileu	0.001	-0.000	-0.033	-3.012
Leu	-0.009	-1.146	-0.000	-0.246
Lys	0.003	-0.043	-0.043	-0.000
Met	0.000	-0.537	-0.000	-0.050
Phe	-0.059	-0.044	-0.044	-0.111
Pro	-0.430	-0.035	-0.035	-0.168
Ser	0.000	-0.000	-0.000	-0.109
Thr	0.000	-0.000	-0.000	-0.764
Trp	-0.001	-0.000	-0.000	-0.064
Tyr	-0.030	-0.000	-0.000	-0.100
Val	0.005	-0.000	-0.182	-0.000
Ac	-0.050	-0.050	0.000	0.000
a-KG	0.002	0.002	0.000	0.000
Cit	0.002	0.002	0.000	0.000
Fum	0.000	0.000	0.000	0.000
Mal	0.002	0.002	0.000	0.000
OA	0.015	0.015	2.380	0.000
Pyr	0.002	0.002	0.000	0.000
Succ	0.150	0.150	0.073	0.000
Glun	0.338	0.338	0.000	0.000
Ox	0.350	0.350	0.000	0.000
Ammonia	-0.750	-0.750	-0.750	-0.000
Phosphate	-0.126	-0.126	-0.126	-0.654
Sulfate	-0.026	-0.026	-0.026	-0.000

a: All the fluxes are expressed in (mmol/ g_{DW} hr) except the specific growth rate (hr^{-1}).
b: The negative and positive numbers show uptake and secretion rates, respectively.

Figure 5.13 shows the simulated specific production rate of NADPH and the flux through two reactions of the pentose phosphate pathway as a function of specific growth rate. Flux through the pentose phosphate pathway (i.e., flux through reaction producing ribulose-5-P) as well as the fluxes leading to polysaccharides and biomass precursors increased as the specific growth rate increased. This can be explained by an increased demand for NADPH and for PPP intermediates, especially ribose-5-P which is a precursor for nucleotide biosynthesis. The produced NADPH was mainly utilized for synthesis of amino acids, DNA, and lipid. During the first 30 hours of the fermentation when the concentration of amino acids were relatively high, approximately 64% of the produced NADPH was utilized for amino acids synthesis, whereas the percentage increased to 80% at 51 hr showing increased demand for amino acids. Using the data presented in Figure 5.13, the reductive power yield in the form of NADPH ($Y_{X,\ NADPH}$) was estimated to be 6.6 (mmole NADPH/g_{DW}). Furthermore, the specific production rate of ribose-5-P was linearly related to the specific growth rate and $Y_{X,\ R5P}$ was 0.6 (mmole ribose-5-P/ g_{DW}).

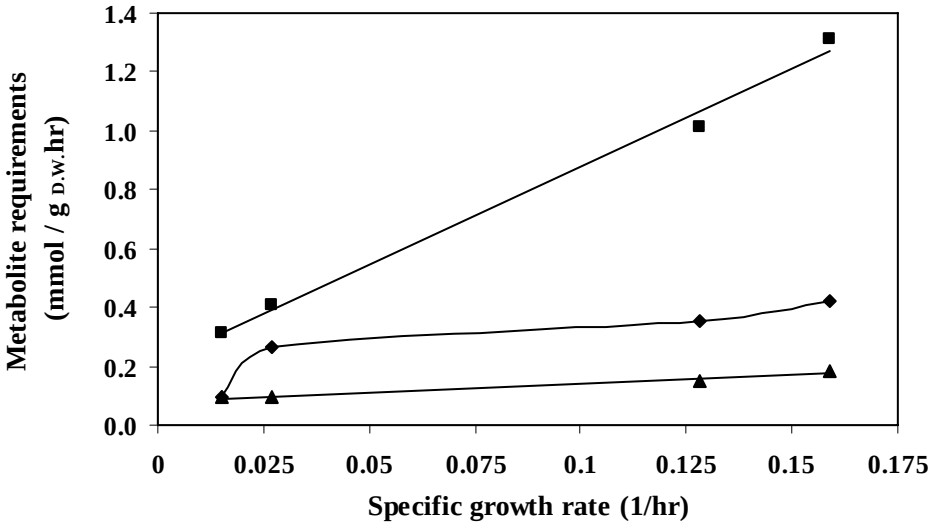

Figure 5.13- Simulation results for the metabolite demands as a function of the specific growth rate. NADPH (■), Riboluse-5-P (◆), ribose-5-P (▲).T= 27 ^{o}C, N= 400 rpm, and aeration 1 vvm.

Experimental measurements showed that isoleucine, leucine, and phenylalanine uptake rates were higher than the uptake rates of the other amino acids during the first phase of the fermentation. The simulations indicated degradative reactions as the cause of the higher uptake. Also, the sensitivity analysis revealed that their level of uptake rate would not affect the value of the objective function, so the cells might have other applications for the products of the reactions than biomass formation during this phase. Upon further look at the catabolic reactions, it was found that glutamate was the common product of the catabolic reactions for leucine and isoleucine, while tyrosine was the product of phenylalanine. Tyrosine, however, converted to glutamate through another degradation reaction. The high flux through this catabolic reaction was verified by simulation. Furthermore, during the second and third phases, proline uptake rate was high due to the high flux through its degradative reaction. Once again, glutamate was the final product of this reaction. In order to investigate which metabolite caused the high demand, one metabolite was eliminated at a time from the proline catabolic pathway in a series of runs with unconstrained uptake rate of proline. It was found that when glutamate was eliminated the flux through the degradation reaction was very low. Moreover, the sensitivity analysis revealed that ammonia had the highest logarithmic sensitivity peaking between 12 hr and 30 hr. The high sensitivity of the objective function to ammonia uptake rate could also be due to the demand of the cells for glutamate. Based on the simulation results, the need for high uptake of proline and ammonia could be replaced by an increase of the uptake rate of glutamate alone. Considering all these observations, one could conclude that during the early stages of fermentation glutamate uptake from the extracellular medium was inhibited while the other amino acids and ammonia were more readily transported.

5.4 Validation of Model Predictions

The definition of the specific growth rate along with the simulation results of the objective function were used to determine the concentration profile of biomass dry weight throughout the fermentation. Based on the pseudo-steady state assumption, the specific growth rate was assumed to be constant between each consecutive measurement. The biomass concentration was expressed by piecewise integration between two consecutive points as follows:

$$C_{D.W.,t+1} = C_{D.W.,t}\, e^{\mu_t \Delta t} \tag{5.9}$$

The predicted and measured biomass concentration profiles are shown in Figure 5.14. The ability of the proposed model to predict the time profile of the cell density provides verification for the validity of the flux balance model and shows its usefulness for bioprocess design.

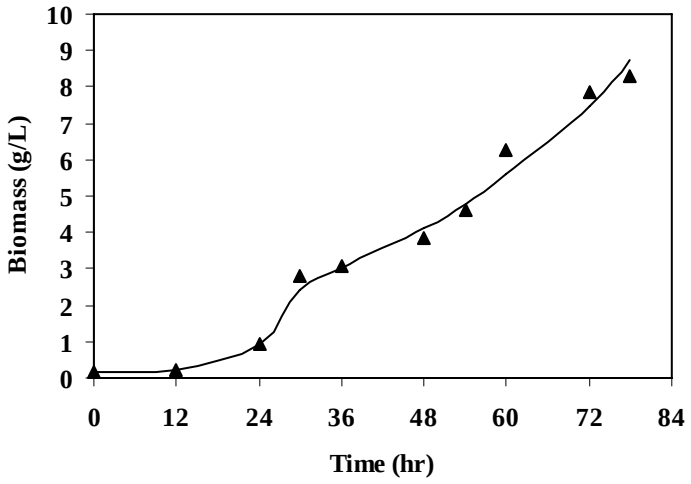

Figure 5.14- The time profile of experimental (▲) and predicted (solid line) biomass concentration. The average relative error between prediction and experimental values was 0.54. T= 27 ^{o}C, N= 400 rpm, and aeration 1 vvm.

The simulation results showed that the higher uptake rate of two amino acids, namely alanine and glutamate benefited biomass production during the last phase, while the higher uptake rate of proline was beneficial during the second and the third phases of the fermentation. Furthermore, the experimental measurements showed that tyrosine was the only amino acid whose concentration decreased approximately to zero after 30 hr of the fermentation. When compared to most amino acids, the catabolic flux of tyrosine was determined to be a small value due to its low initial concentration. It could be the reason why it was not recognized as an important amino acid by logarithmic sensitivity analysis. Being a source of glutamate during the degradation process, it was reasonable to investigate the effect of tyrosine on the growth by further experimentation. Four amino acids, namely proline, glutamate, alanine, and tyrosine were recognized as the significant amino acids and could be expected to have the greatest effect on the biomass production rate.

It is worth to note that higher concentrations of the significant metabolites would not necessarily result in higher uptake rate of these metabolites in real situation, because the microorganism may not be capable to take up at higher rates. Since, the sensitivity analysis revealed that the objective function could be increased by flux alteration through certain processes (i.e., bioconversion reactions or exchange reactions) the following experiments were performed as an initial effort to check the capability of the microorganism for higher uptake rate of the aforementioned amino acids. Consequently, a series of growth studies were conducted in shake flasks and the 7 liter bioreactor with these amino acids added in excess.

In the preliminary nutritional experiments using shake flasks it was found that the apparent contribution to growth enhancement was 46% for proline, 23% for glutamate, and 22% for tyrosine when these amino acids were added in excess.

Four more experiments were carried out in the 7 liter bioreactor with the conditions outlined in the materials and methods section of this chapter with the following modifications. The concentration of glucose and the individual amino acids in the first experiment (E-1) was 50% less than those mentioned in the materials and methods section. The results of this experiment were used as the baseline for comparing results

with other medium combinations. The medium composition of the experiments is presented in Table 5.7.

Table 5.7- Medium Enrichment with Glucose and Amino Acids

Experiment	Glucose (g/L)	Proline, alanine, glutamate, tyrosine (g/L)	The rest of amino acids (g/L)
E-1	10	3	4
E-2	10	8	4
E-3	20	8	4
E-4	20	6	8

The extra amount of proline, alanine, and glutamate for E-2, E-3, and E-4 was added to the medium at certain times determined by the results of the sensitivity analysis. Tyrosine was added at the same time as proline. For instance, based on the sensitivity analysis any increment in proline uptake rate would enhance the biomass production rate during the second (12-24 hr) and the third (24-30 hr) phases of the fermentation. On this account, the excess amount of proline was added in two steps and two hours earlier than the start of each period to make sure that the microorganism had enough time to uptake the amino acid during the upcoming period.

The maximum biomass and lysozyme concentrations observed in each experiment are presented in Figure 5.15 and Figure 5.16, respectively. Comparison between experiments E-1 and E-2 showed that when the concentration of the significant amino acids increased by a factor of 2.7 while the concentration of the other amino acids and glucose were kept constant the biomass and lysozyme concentrations increased 45% and 41%, respectively. Hence, it seems reasonable to hypothesize that the higher concentration of these amino acids increased their uptake rates, which in turn enhanced the biomass and lysozyme concentrations. These results confirmed the simulation predictions that the specific growth rate was sensitive to any change in the uptake rate of these four amino acids.

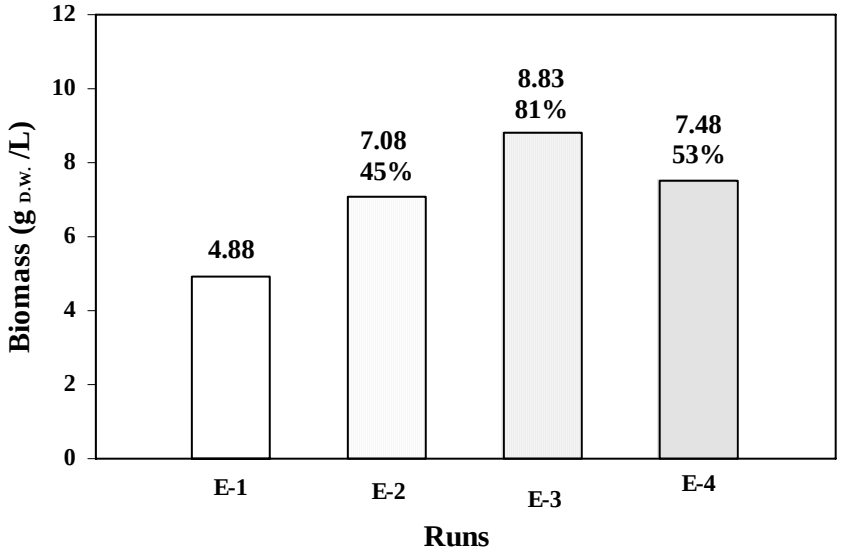

Figure 5.15- The maximum biomass concentration observed in the fermentations with the medium compositions presented in Table 5.7. T= 27 ^{o}C, N= 200 rpm, and aeration 1 vvm.

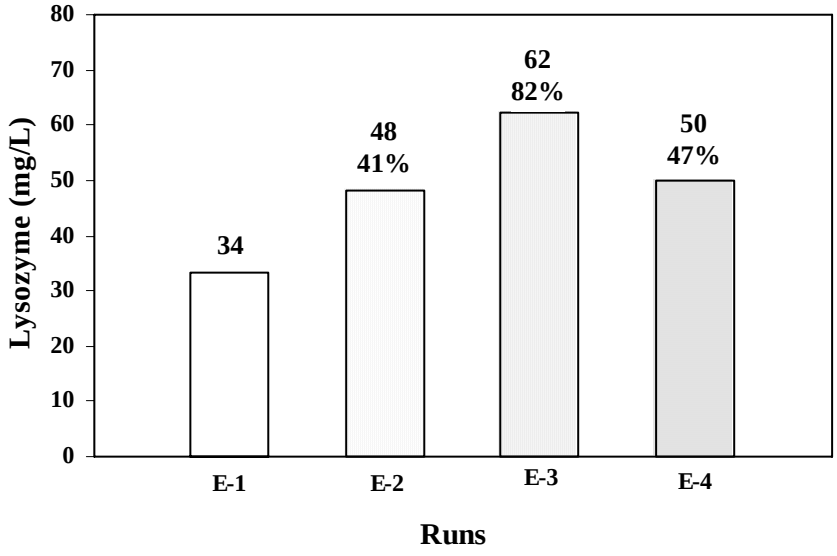

Figure 5.16- The maximum lysozyme concentration observed in the fermentations with the medium compositions presented in Table 5.7. T= 27 ^{o}C, N= 200 rpm, and aeration 1 vvm.

The only difference between experiments E-2 and E-3 was the initial glucose concentration, that was10 and 20 g/L, respectively. In both experiments the concentration of important amino acids were 8 g/L which was the highest level in this series of experiments, while the level of the other amino acids were at the lower level of 4 g/L similar to the basis experiment E-1. It can be seen from the results that the percentage of increment of the biomass concentration increased from 45% to 81% and that of lysozyme concentration from 41% to 82% in comparison to E-2. These observations revealed that when the important organic nitrogen sources were supplied in excess, the higher concentration of glucose had a significant positive effect on both biomass and recombinant protein production.

The initial concentration of the significant amino acids in experiment E-4 was 25% less than in E-2, however, yet it was still high enough to positively affect the production of biomass and recombinant protein. Aside from the concentration of the other amino acids in these two experiments and based on the conclusion in the previous paragraph, one would expect that the biomass and lysozyme concentrations should have been much higher in E-4 than E-2 due to its higher glucose concentration. The experimental results, however, showed that the biomass and lysozyme concentrations in E-4 were only 6% and 4% higher than the corresponding values in E-2. Therefore, one might conclude that the other amino acids not only did not promote the production of biomass and the protein, but most likely had a slightly negative effect on the concentrations.

Figure 5.17 shows biomass yield on glucose, biomass yield on amino acids, and lysozyme yield on biomass. The highest biomass yields on glucose was found for E-2, showing that the yield was affected mainly by the significant amino acids while the higher concentration of glucose and the other amino acids did not have a positive effect on this parameter. The maximum biomass yield on amino acids and the lysozyme yield on biomass were observed in E-3, showing that both glucose and the significant amino acids affected these yields due to a probable significant positive interaction between these two substrates. All the yields were found to be at the minimum levels for E-4, confirming the probable negative effect of the other amino acids in the performed fermentation.

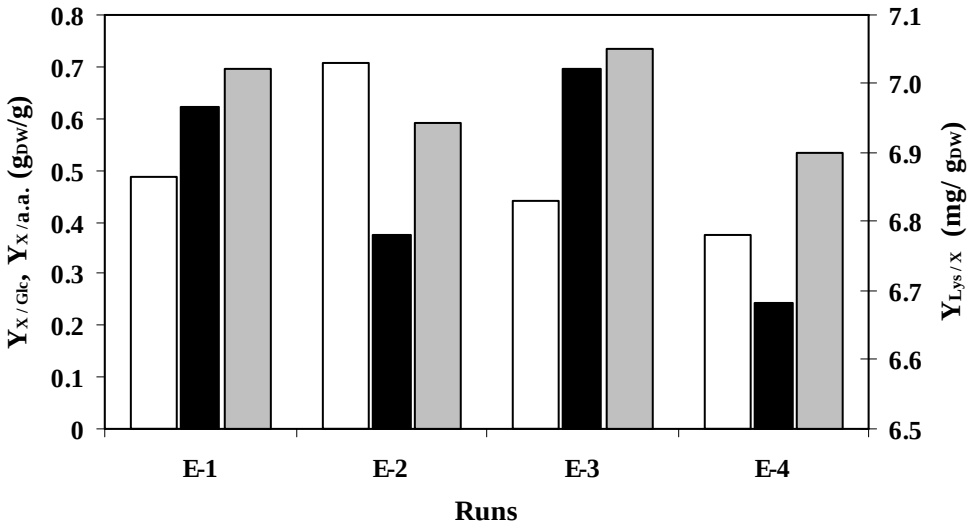

Figure 5.17- Physiological parameters in the four media. Biomass yield on glucose (□), biomass yield on amino acids ( ), and lysozyme yield on biomass (■).

5.5 Conclusion

A flux-based approach was performed for the analysis of the metabolic network of *A.niger*. A unique aspect of the metabolic network was that it included the participation of carbohydrates and amino acids in both degradative and biosynthetic reactions. The network consisted of 181 biochemical reactions (287 processes) and 137 intracellular metabolites which are distributed among three intracellular compartments. It included glycolysis and pentose phosphate (PPP) pathways, the tricarboxylic acid cycle (TCA), anaplerotic reactions, ammonia and sulfate assimilation, electron transport reactions, the metabolism of amino acids, biosynthesis of nucleotides, and the biosynthesis of the macromolecular components of biomass such as protein, lipid, RNA, DNA, and carbohydrates.

The proposed model along with the experimental measurements was used to construct the stoichiometric matrix corresponding to the processes with unknown rates. Implementing the model with experimental data as constraints was proven to be necessary for achieving realistic results. The matrix analysis showed that it was underdetermined and non-redundant, so the system was consistent for any value of the measured vector. The calculability analysis of the null space of the stoichiometric matrix revealed that all of the unknown rates were not calculable. Linear programming with experimental constraints was used to determine the optimized specific growth rate at different phases of the fermentation. Flux distribution maps for two phases of cultivation were also constructed.

The bioreaction network presented in this study is a general pathway which can be valid for any *A.niger* strain or other aspergilli with some minor modifications. This model can be used not only to find the theoretical metabolic flux distribution, but also, with experimental data, it may be employed to clarify the metabolic behavior of the microorganism. In this study, the specific growth rate was considered as the optimization objective, but optimization of different objective functions such as ATP production/consumption, redox potential, and metabolite production can be easily implemented in the model. The model developed in this work was able to predict the specific growth rate very accurately with a maximum error of ±10%. Moreover, oxygen

uptake rate and carbon dioxide evolution rate were evaluated with maximum ±28% and ±22% errors, respectively, during the time course of the fermentation. It should be noted that the off-gas analyzer was not able to display the level of oxygen and carbon dioxide in outlet gas accurately, consequently the corresponding experimentally measured fluxes of these two metabolites were less accurate. This could be the reason for the high error percentage associated with these two fluxes. The biomass concentration profile in each period was determined accurately using the corresponding optimal value of the specific growth rate and the standard differential equation which correlates these two parameters.

The performed sensitivity analysis revealed that phosphate uptake was the growth limiting flux during the early stages of the fermentation. Later, the uptake rate of ammonia had a significant effect on the specific growth rate. Among the amino acids proline, alanine, and glutamate had the highest logarithmic sensitivity. The solution of the flux network was very sensitive to ammonia and to a lesser degree to proline during the early stages of exponential phase when glucose was consumed. During this period 10% increase in ammonia and proline uptake rates would increase the specific growth rate by 5-7% and 3-4%, respectively. Alanine, glutamate, and ammonia were limiting nutrients during the exponential phase with highest logarithmic sensitivities among the measured metabolites at the 51st hour of culture. The sensitivity analysis of the specific growth rate with respect to the biomass components revealed that the solution was only sensitive to its protein content. Besides, the analysis showed that the same biomass biosynthesis reaction could be used throughout the fermentation. The results of the metabolic flux analysis may be employed for medium design in continuous or fed-batch operations involving high density culture.

The experimental observations and simulation results presented in this section could be used for some genetic manipulation processes. For instance, glucose was partially oxidized to form gluconate in addition to entering the glycolytic pathway during the first three phases of the fermentation. The percentage of glucose conversion to gluconate was very high at the start of the fermentation and gradually reduced as the glucose concentration decreased to very low levels. When glucose wad depleted, gluconate was utilized as carbon source by the cells. The experimental results, however, showed that the specific growth rate was higher during growth on glucose. Gene deletion may be applied

to the microorganism in order to inactivate glucose oxidase, which was responsible for the conversion of the more favorable carbon source (glucose) to gluconate. The same technique might be used to eliminate significant amounts of oxalic acid accumulation in the medium that was of approximately 6 g/L by the end of the fermentation.

CHAPTER 6

DATA ACQUISITION

6.1 Introduction

In the development of current industrial fermentation processes, various types of automatic instrumentation and control have become standard. These include temperature, pH, dissolved oxygen, air flow, antifoam, as well as gas stream monitoring devices. Moreover, biochemical processes have generally more exacting control requirements than chemical processes because they are highly sensitive to small changes in operating conditions (Nagy, 1992). For instance, the biocatalyst enzymes usually have narrow temperature and pH range of efficient operation and they may be irreversibility deactivated. The application of computer-based process control makes it easier to maintain the important parameters at their optimal levels.

Using software programs for control and monitoring purposes have some advantages. For example, they need minimum training efforts and are easily understood by users. Furthermore, they have a high degree of flexibility when specifying the different parameters and operational conditions. Conventional data acquisition software is normally built with defined modules and is capable of performing predefined tasks. On the other hand, for research and a variety of small scale applications, more flexible systems such as the LabVIEW development environment are required.

6.2 Materials and Methods

6.2.1 Data Acquisition Hardware System

A key and necessary component of data acquisition hardware is a proper data transfer system. The data are transferred between computer and fermenter through a SC-2345 shielded carrier (Figure 6.1). The carrier consists of 8 sockets for 16 analog inputs, 8 sockets for digital inputs and outputs, and 2 sockets for analog outputs. Signal conditioning component (SCC) modules connect to the carrier sockets to provide custom signal conditioning (i.e., signal amplification, filtering, switching, and isolation) options.

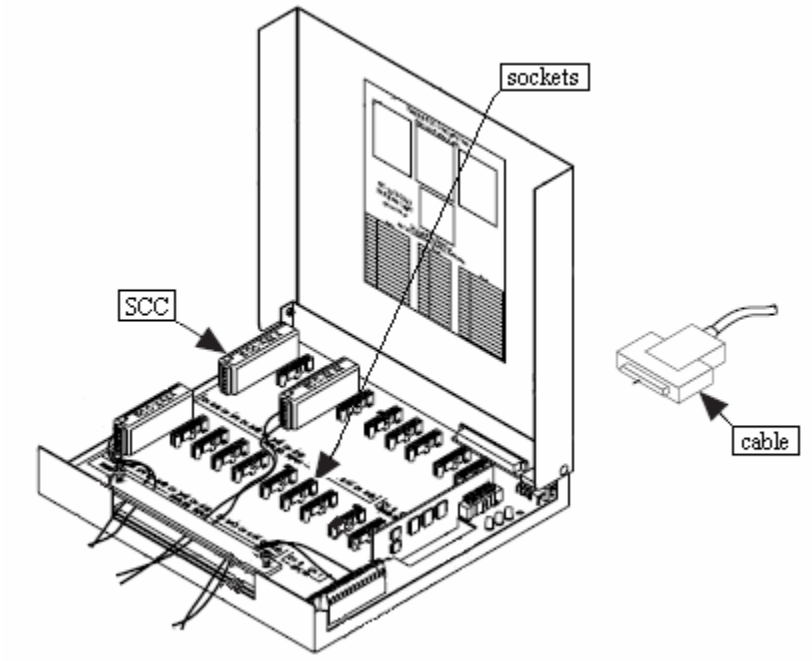

Figure 6.1- SC-2345 carrier and its components (http://www.ni.com/).

A schematic of the whole data acquisition components is depicted in Figure 6.2. Input/output (I/O) signals are transferred between the fermenter and the appropriate SCC modules inside the carrier. A 68-pin shielded cable connects the carrier to a plug-in data acquisition (DAQ) board, which is installed in the computer. LabVIEW and the DAQ

device then communicate with each other through DAQ libraries and then with sensors, transducers, and other fermenter components.

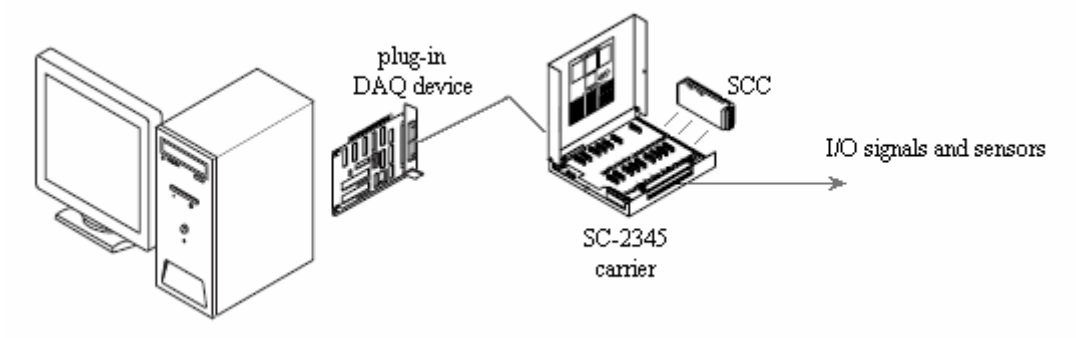

Figure 6.2- Data acquisition system.

In this work, an NI PCI 6040-E data acquisition device along with a Pentium personal computer with Microsoft Windows XP as the DAQ host platform were used. Moreover, the SCC-RTD01 resistance-temperature detector RTD module was used for medium and jacket temperature signals. The SCC-FT01, which is a feed-through module, was used both for analog input and analog output signals. Three modules of SCC-FT01 were plugged into the carrier for dissolved oxygen, pH, and oxygen-carbon dioxide off gas analyzer connections all as analog inputs; two were used as analog outputs for controlling the feed pump and the speed of the stirrer. In addition, seven SCC-DI01 isolated digital input/output modules were utilized for the coolant solenoid valve, three heaters, stirrer motor, acid pump, and base pump. Table 6.1 shows the SCC socket reference, SCC, channel and the associated input or output signal for each variable under supervision. All the mentioned hardware components and LabVIEW software (version 7.1) were provided by National Instruments Corporation.

Table 6.1- SCC modules, channels, and connected signals

SCC Socket Reference	SCC	Channel	Input/output
J01	SCC-RTD01	ACH0	Bioreactor temperature
		ACH8	Jacket temperature
J03	SCC-FT01	ACH2	pH analyzer
J04	SCC-FT01	ACH3	DO analyzer
J06	SCC-FT01	ACH5	O_2 off-gas analyzer
		ACH13	CO_2 off-gas analyzer
J09	SCC-DO01		Solenoid valve
J10	SCC-DO01		XY Heater
J11	SCC-DO01		ZY Heater
J12	SCC-DO01		XZ Heater
J13	SCC-DO01		Impeller motor
J14	SCC-DO01		Acid pump
J15	SCC-DO01		Base pump
J17	SCC-FT01	DAC0	Impeller RPM
J18	SCC-FT01	DAC1	Feed pump

6.2.2 Fermenter and Ancillary Equipment

A 20-Liter MBR bioreactor with the working volume of up to 15 liters equipped with a bottom-driven agitator was used. The medium was mixed using three six-bladed Rushton turbine impellers. The air pressure was adjusted using a pressure reduction valve mounted before the rotameter and the airflow rate was regulated using a needle valve. The airflow then was distributed at the bottom of the bioreactor using a ring sparger. The moisture content of the exhaust gas condensed and returned to the bioreactor by passing it through a vertical stainless steel condenser mounted on the top of the fermenter, before the exhaust air filter.

The pH was measured by a sterilizable Ingold Type 465 pH electrode (Mettler-Toledo Process Analytical, Inc., MA, USA). The pH probe signal was amplified by a pH-40

system (New Brunswick Scientific Co., Inc., NJ) and electrically isolated and filtered using a SSCA 41-03 analog signal conditioner (Dataforth Corporation).Then, the preconditioned signal was directed to the designated SCC-FT01 module installed into the carrier either for calibration or monitoring and control purposes.

The dissolved oxygen was measured by a sterilizable galvanic electrode (Phoenix Electrode Company, USA). The output electrode current in air saturated medium was reported to be 10-15 microamperes by the manufacturer which was not suitable for data acquisition system. Therefore, a dissolved oxygen analyzer model D-40 (New Brunswick Scientific Co., Inc., NJ, USA) was used to convert the electrode output current to voltage. The signal was amplified to a maximum of 1 volt (corresponding to 100% dissolved oxygen). Then, the preconditioned signal was directed to the SC-2345 carrier.

A portable oxygen/carbon dioxide analyzer (Quantek Model 902, MA, USA) used for the measurement of O_2 and CO_2 of the outlet gas from the bioreactor. RTD-PT100 sensors were used for the measurement of medium and jacket temperatures.

6.3 Control of Process Variables

6.3.1 Temperature Control

The objective of this part of the project was to regulate the bioreactor temperature, T, at a desired set point value $T_{s.p.}$ either in the presence of disturbances (e.g., feeding, change in initial operating conditions), or to switch the bioreactor temperature to a new set point value (e.g., sterilization cycle) in a fast and smooth manner. For this task one needed to define a manipulated variable (control variable) and design a controller that could provide the appropriate control action required to achieve the control objectives.

The process graphics for temperature control of the system is shown in Figure 6.3. The 20 liter, jacketed, stirred tank bioreactor was thermally controlled by means of either heated or cooling water circulating in the bioreactor jacket. The water was heated by an in-line heater assembly. A valved flowmeter was provided to change the cooling water flowrate quickly and accurately. The temperature sensor within the bioreactor, the solenoid valve, and the heater box were linked to a 3-term PID controller that was programmed to maintain the desired set-point temperature.

It has been proposed that a combination of a heating and cooling system is effective for reactor control temperature (Liptak, 1986). The heat transmitting fluid is circulated to attain a large heat transfer coefficient. To heat the bioreactor, electrical heaters may be used. Electrical heating may be direct or indirect, and its control can be continuous or discontinuous (on-off). The simplest method of controlling temperature with an on-off system is to install heating resistance elements in groups, while the temperature controller switches one or more elements on or off in a fraction of the previously specified cycle time. The higher the difference between the control variable and its specified set point, the higher is the fraction of cycle time applied by the controller. Uniform heat transfer is achieved by using a heat transfer fluid heated by electrical resistance heaters. Cooling water enters the jacket of the bioreactor through a solenoid valve controlled by the temperature controller.

a) Single-loop feedback control

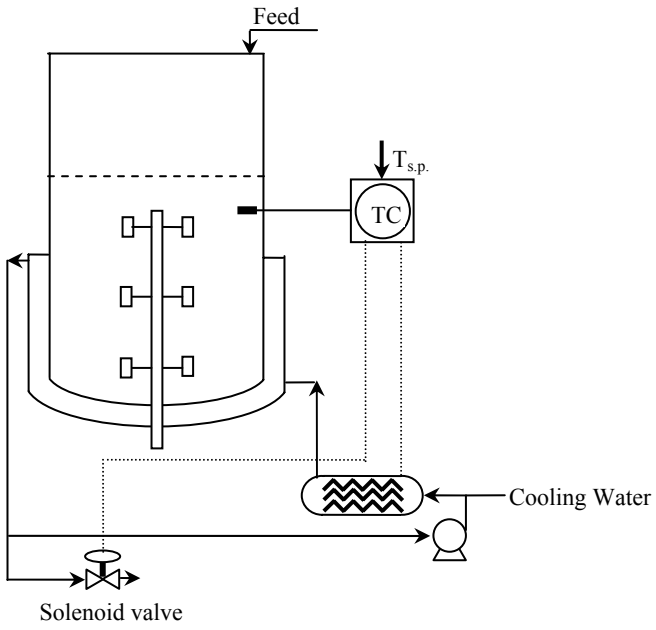

b) Cascade feedback control

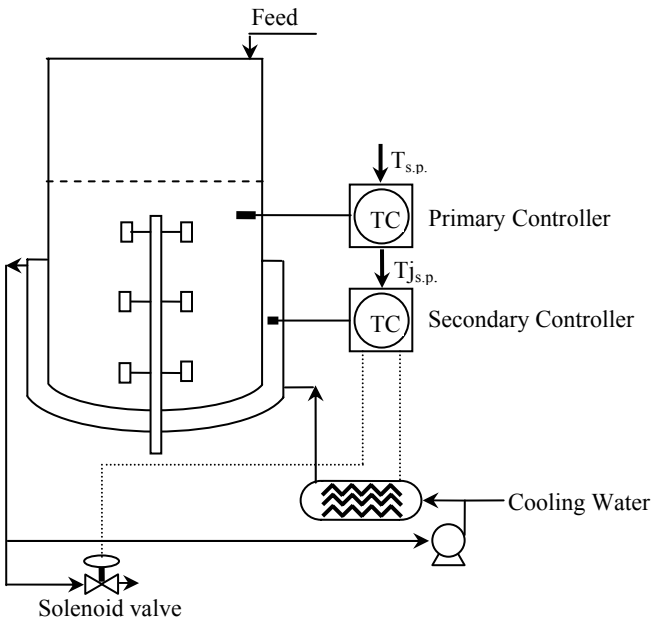

Figure 6.3- Feedback temperature control system of the bioreactor unit.

Based on this scheme, one may consider a linear combination of the heating and cooling actions during each cycle time of the process as follows:

$$u(t) = f_t \sum_i y_i \, P_{H,i} - (y \, F \, C_p \, \rho)_{c.w.} (T_J - T_{c.w.}) \tag{6.1}$$

Where f_t is the fraction of cycle time at time t, during which the heater(s) are on, y is a binary variable that shows the on-off action for each individual heater and the solenoid valve, P_H is the input power of each heater, and F is the flow rate of cooling water. The controller action of $u(t)$ is actually the net rate of heat addition to the jacket circulating system by the heater assembly and the inlet cooling water.

The value of controller action in each cycle time should be specified by the particular controller employed.

6.3.1.1 Single-Loop Controller

Figure 6.3a shows the single-loop control of the bioreactor. The temperature of the medium in the bioreactor was measured by an RTD-PT100 and transmitted to the controller, which in turn manipulated the heaters and the solenoid valve. If the bioreactor temperature is too low, the controller switches the heaters on for a longer fraction of the cycle time and keeps the solenoid valve closed. Consequently, the temperature of the jacket fluid increases, which in turn causes higher heat transfer rate to the medium. On the other hand, if the medium temperature is higher than the set point, the controller opens the solenoid valve to cool down the jacket fluid. A simplified block diagram for the single-loop system is shown in Figure 6.4.

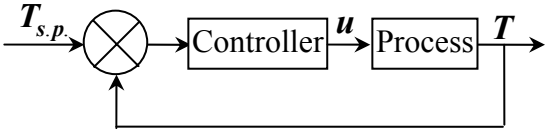

Figure 6.4- Single-loop control block diagram for temperature control.

Since, a direct electrical heating method is utilized in the jacket of the bioreactor, due to high thermal capacity the jacket temperature dynamics are normally significantly faster than the bioreactor temperature dynamics. The time constant of the system is large because of the heat capacity of the medium, the material of the bioreactor itself, the heat transmitting fluid, and the heat resistance of the wall of the bioreactor. Consequently, any temperature change in the jacket fluid will not be realized in the medium for a relatively long time. Hence, the controller does not take any corrective action until the heat transfer between the two fluids brings the bioreactor temperature towards the vicinity of the set point. However, because of this the jacket temperature differs considerably from the medium set point temperature when a new set point is introduced to the system. Ultimately, when the medium temperature approaches the set point, the jacket fluid temperature is too far from the set point, which in turn causes a high deviation of the bioreactor temperature from the specified set point, especially during the first cycle of the controlling process. This could cause a serious problem when the media is not able to tolerate large temperature fluctuations (i.e., enzymes and medium components stabilities). Moreover, during the sterilization when the medium is exposed to high temperature ranges, any high temperature deviation from the set point is undesirable both for media and instruments (e.g., circulating pump, solenoid valve).

Figure 6.5 shows a dynamic temperature test profile resulting from switching the medium set point temperature from 22 ^{o}C up to 27 ^{o}C. The Ziegler-Nichols settings (K_c=41.05, τ_I=2.73, and τ_d=0.53) produced a less desirable response. Therefore, the controller parameters were chosen by trial and error. The response was obtained with K_c=30.75, τ_I=3.86, and τ_d=0.21.

As shown in Figure 6.5, the single PID controller is able to adjust the bioreactor temperature near the set point of 27 ^{o}C, with the deviations ranging as high as 0.5 ^{o}C during the event. However, the jacket temperature reaches 37 ^{o}C which is 37% higher than the set point value of the bioreactor temperature. Theoretically, the use of integral action eliminates the steady state offset of the response, but because of the nature of the utilized cooling process that is based on the on-off action of the solenoid valve the jacket

temperature oscillates around the set point, which in turn causes a steady state off set of $\pm 0.25\ ^{o}C$ for bioreactor temperature.

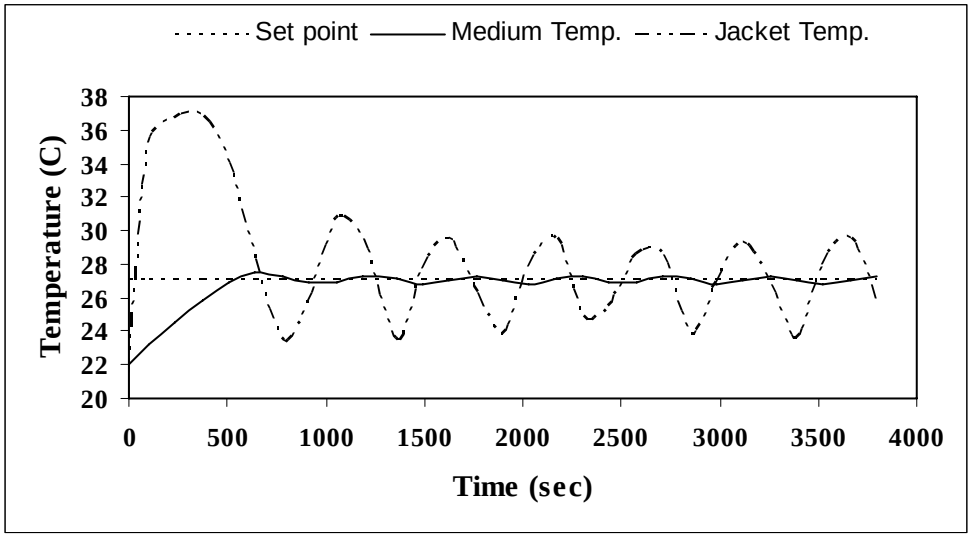

Figure 6.5- Single-loop response to set point change.

6.3.1.2 Cascade Control

Figure 6-3b shows the control configuration for the bioreactor temperature control with a cascade control methodology. Instead of using a single-loop controller for temperature control of the bioreactor, improved performance of the closed loop response can be achieved by employing a cascade scheme. In case where high performance is mandatory or the process has large time constants and frequent disturbances, this method of control is of great value. Cascade control is widely used by chemical process industries to improve the response of a single feedback strategy when the response of the desired variable is sluggish. This control implementation is a familiar task because the architecture is comprised of two ordinary controllers from the PID family. According to this control methodology, one may introduce two nested feedback control loops using two different on line measurements (e.g., T and T_J), which share a common manipulating variable u . The cascade scheme is comprised of a secondary (slave) control loop located inside a primary (master) control loop. With this nested architecture, success in a cascade

implementation requires that the settling time of the inner loop is significantly faster than that of the outer loop. The simplified block diagram of these loops is schematically depicted in Figure 6.6.

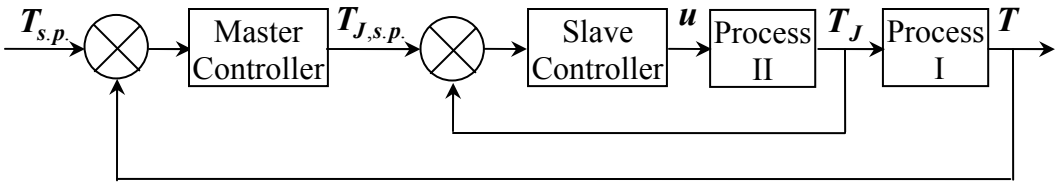

Figure 6.6- Cascade control block diagram for temperature control.

Process-I is the bioreactor and the controller output is the reactor temperature T. Process-II is the jacket whose output, T_J, directly affects process-I and therefore, the bioreactor temperature T. In the primary loop the medium temperature T is measured. Then, it is compared to the desirable set point value $T_{s.p.}$ and the master controller is used to control it. The output from this loop, $T_{J,s.p.}$, becomes the set point for the jacket temperature in the secondary loop. In the secondary loop the measured jacket temperature, T_J, is compared with the output of the primary controller, $T_{J,s.p.}$, that is now viewed as its set point, and the secondary controller is used to manipulate it.

Figure 6.7 is a summary of the implemented cascade temperature control scheme in graphical form. The medium and jacket temperatures were simultaneously acquired (sampling size was 1000 samples with 100 Hz frequency). The average of each sampling data set was determined and assigned to the current temperature, which was directed to the corresponding controller. The output of the secondary controller was the percentage of heating in each cycle time. Based on the experimental observations if the percentage was less than 80%, only one of the heaters was turned on for the period of f milliseconds. If the output was determined to be between 80-99% two heaters and for higher range all the three heaters were being involved with the heating process. These limits were

obtained by trial and errors for an accurate temperature control of the bioreactor including 10-15 liter water, while the cooling water flow rate was adjusted to 1000 ml/min with a cycle time of 3000 milliseconds. Under these conditions, the primary controller adjusted indirectly the jacket temperature.

Because of the introduction of the inner loop, the dynamics of the cascade control system have been changed and it is inevitable to tune the whole system for a good response. The control action for the secondary controller is recommended to be proportional control only (Stephanopoulos, 1984). The rational for the use of proportional control rather than two- or three- mode control is that the tuning is simplified and any offset associated with proportional control of the slave loop can be handled by the presence of the integral action in the master loop. However, it was found that using a PI controller for the slave loop is much favorable for the system under study.

Cascade loop tuning uses the same skills as tuning a regular PID controller. First, both the primary and secondary controllers were put on manual mode. By the use of Ziegler-Nichols tuning method, the proportional gain of the slave loop was determined to be 7.28 and that of integral time was 2.48.

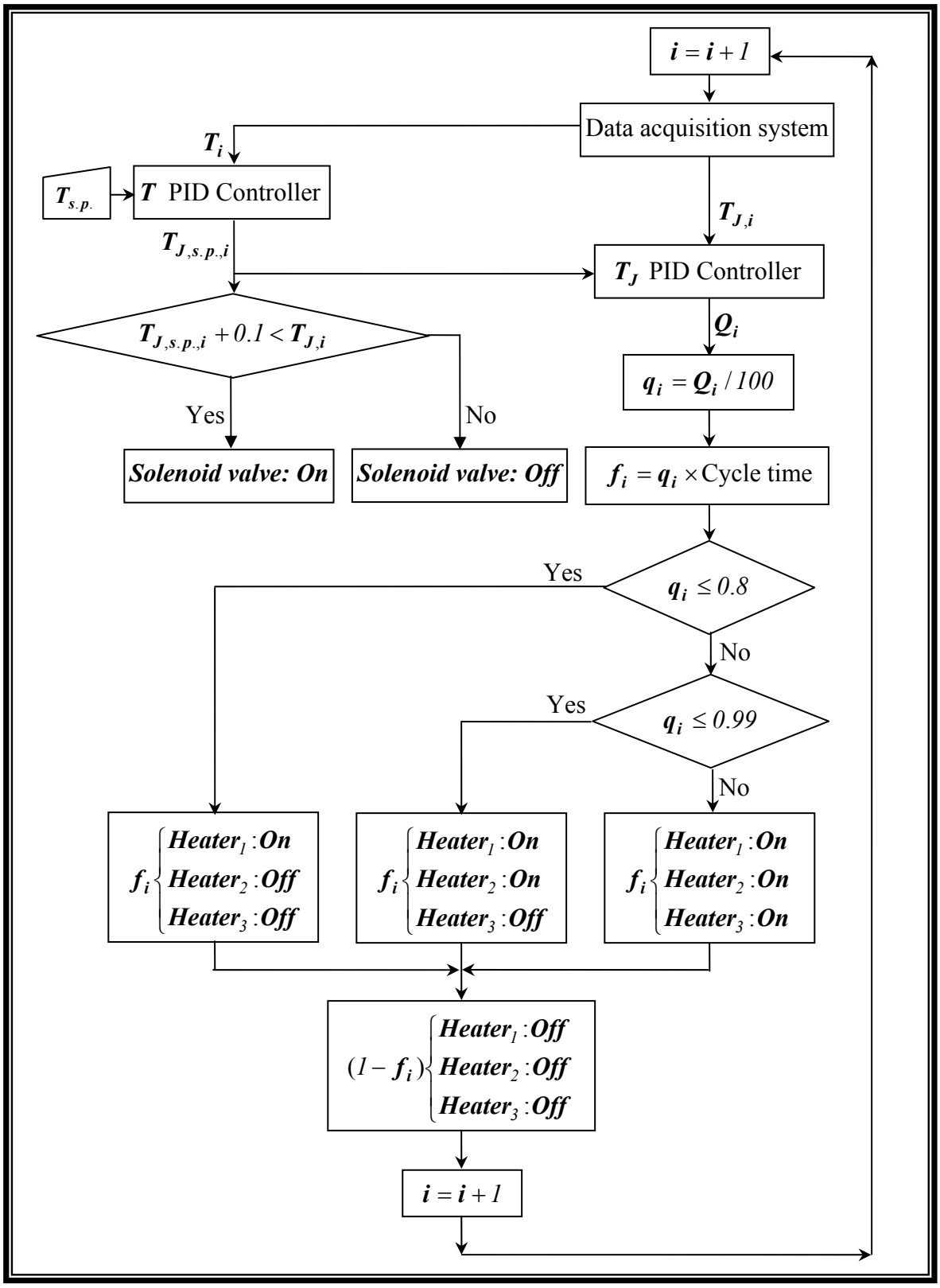

Figure 6.7- Flowchart of temperature control during fermentation process using cascade architecture.

By trial and error, the settings of K_c=6.92, τ_I=3.53 were found to produce a better response. Then, the secondary controller was switched on automatic mode; therefore, it literally became part of the primary process. The controller setting were primarily determined by applying the Ziegler-Nichols algorithm to the system and found to be K_c=13.42, τ_I=4.79, and τ_d=1.57. The above controller settings with cascade scheme gave a very oscillatory response. Because of the oscillatory response, the solenoid valve was switched continuously on and off by the controller. The reason was found to be the noisy signal which was generated by the temperature probe. Although the amplitude of the noise was very small, due to the differential action of the controller the output range of the slave controller switched between the upper and lower limit continuously, causing the oscillatory response. Noises are associated with the probe signals, so the best way to improve the performance of the control system was to eliminate the differential action. By trial and error the PI controller gains of the primary loop were determined to be K_c=10.00 and τ_I=5.60. The same temperature switch trial as employed using the single-loop controller was conducted with the proposed cascade architecture and with experimentally evaluated controller gains. The result is given on Figure 6.8.

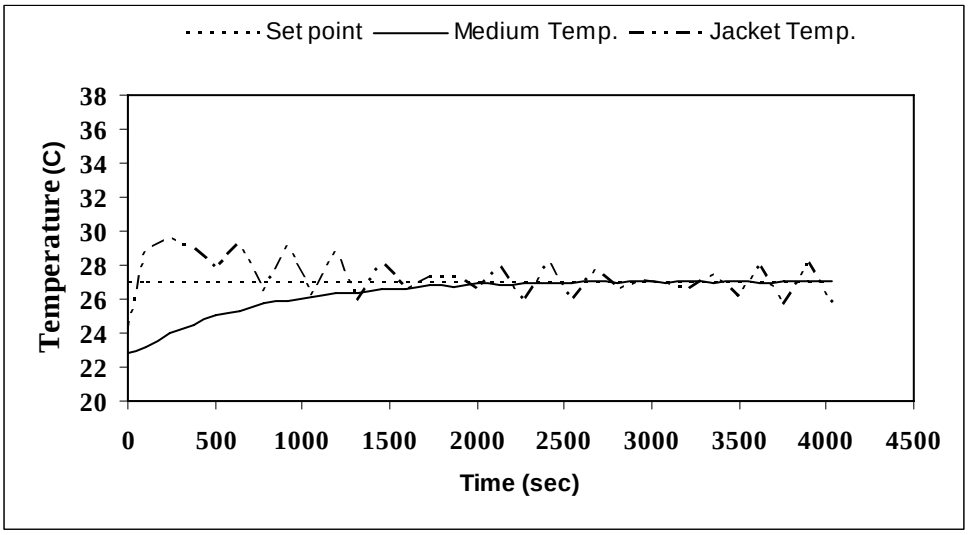

Figure 6.8- Cascade loop response to set point change.

As shown in Figure 6.8, the response of the cascade control system is superior to the response of the conventional single-loop control, both for the bioreactor and the jacket temperature. The maximum bioreactor temperature deviation of 0.07 ^{o}C by the cascade response has been observed. The steady state response of the bioreactor temperature oscillates around the set point with much lower amplitude of $\pm$ 0.02 ^{o}C in comparison to the applied single-loop controller.

The highest value of the jacket temperature was 29.5 ^{o}C, which was much lower than the 37 ^{o}C using the conventional single-loop controller. The lower level of the jacket temperature in this controller is one of the most important advantages of the cascade controller in the system under study during the sterilization process, when the bioreactor contents need to be maintained at 121 ^{o}C for 20 minutes. The rise time and overshoot of the single loop were 533 seconds and 0.0173, while for cascade scheme were 2675 seconds and 0.0001, respectively. The improved performance of the cascade controller prevents the bioreactor from experiencing very high and undesirable temperature levels both in the jacket and inside the bioreactor. This enhanced action of the cascade controller is not free as it requires an additional sensor and controller as well as tuning effort. However, the LabVIEW software environment provides a user with as many controllers as are required without additional costs.

Appendix D Figure D.5 is the block diagram of cascade temperature control during the fermentation process when heating percentage was between 80-99%. The solenoid valve was on automatic mode and the maximum jacket temperature was lower than the specified maximum allowable limit. Figure D.5a represents the first stage during which two heaters were on for *f* milliseconds and Figure D.5b shows the rest of the cycling time with all the heaters at off position. Several case structures and stacked sequence structures were involved in this algorithm, and it was beyond the intent of this discussion to present all cases.

6.3.2 pH Control

The pH is one of the most important biochemical environmental measurements used to indicate the course of the fermentation process. It detects the presence of specific chemical factors that influence growth, metabolism, and the final product. Most industrial

fermentations are batch systems in which control of pH may be difficult, because the amount of acid or base required maintaining a constant pH can increase exponentially with time.

In this work, the bioreactor pH was continuously monitored and controlled by the user written software. Alkali or acid (i.e., NaOH or H_2SO_4) was transferred from sterile vessels to the bioreactor by the use of two peristaltic pumps that were manipulated by the pH feature of the software. During the fermentation the pH was evaluated using the fitted line obtained in calibration section. Working pH range limits are established by high and low set point numeric controls on the front panel. Values exceeding established set points in either direction activate the designated digital I/O modules, for addition of appropriate reagents upon control demand. Adjustable numeric controls enable the user to assign the length of the addition cycle and a delay between the additions to prevent overshooting.

6.3.3 Dissolved Oxygen Control

The dissolve oxygen was continuously monitored and displayed on the screen during the fermentation. The control of dissolve oxygen was implemented in the software by changing the agitation speed. The dissolved oxygen set point is adjusted by using the control variable on the front panel. Set point can be maintained by increasing/decreasing agitation speed under the supervision of a PID control. The maximum and minimum allowable agitation speeds can be established by user.

6.4 Supervisory Software

The program for control and monitoring of bioreactor was build up from different parts, which were written and tested separately before being integrated into one structure. The sections were arranged based on their order in fermentation process on different pages on front panel of the program. The graphical representation of the process is displayed on the screen and helps the user to follow the fermentation. The user can move forward and backward among the pages by pushing the appropriate control tab. The different pages in the software were organized as follows:

6.4.1 Start

The user is asked to set up the pH analyzer before the probe calibration step. In addition, the calibration data of the acid and base pumps are asked to be entered into the provided tables. The pairs of transmitted volume and its corresponding duration time form the calibration data for each pump and the specific tubing size. The data is used by the program to determine the amount of base and/or acid added to the bioreactor during the fermentation.

6.4.2 pH Calibration

The pH probe is calibrated using at least two standard buffers. The pairs of pH and the corresponding voltage signals can be either acquired automatically or entered manually based on the previous observations. Figure 6.9 shows a simplified flowchart of the pH calibration algorithm. In automatic mode, the user places the probe into a standard buffer solution and waits for a stable reading. Ideally these should be at the temperature at which the fermentation will be run. Then the buffer pH is entered in the specified numeric control on the front page and the corresponding voltage signal is acquired by the software. To eliminate the errors due to the inevitable noise, the average of five readings (each including 100 samples) are determined and considered as the voltage signal for each data point. Each pH and its associated voltage are appended into their own one dimensional numerical array. The implemented linear regression analysis determines the slope and intercept of the best fitted line through the data points as well as the mean squared error. The regression data is stored for later applications.

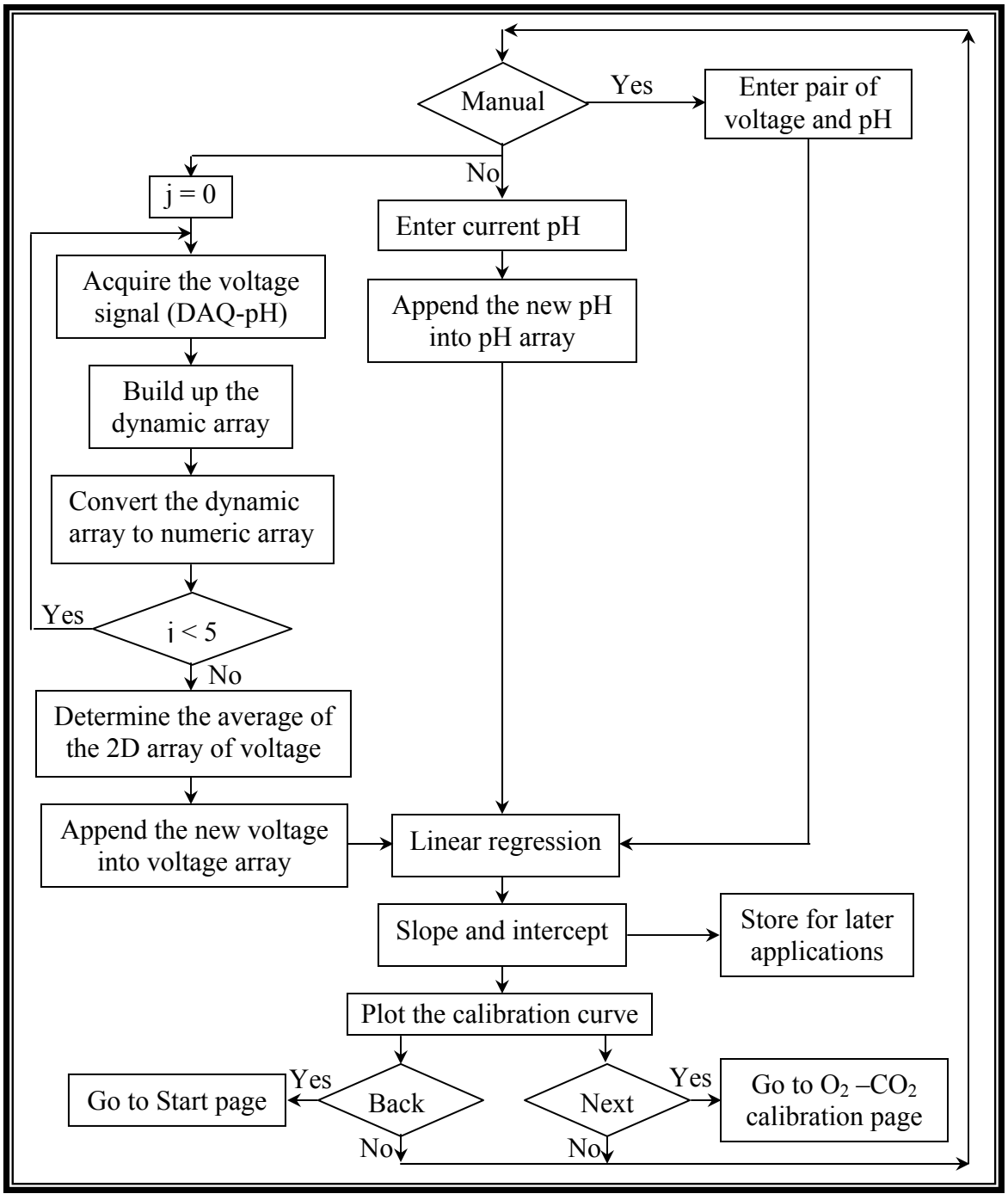

Figure 6.9- Flowchart of pH calibration.

The fitted line and the data points are illustrated on a graph on the front panel of the pH calibration page. A reset button is considered on the screen, so that the user would be able to start over the calibration task in case a mistake occurred during the calibration step. The front panel and the simplified block diagram of the pH calibration section are presented in Appendix D FigureD.6.

6.4.3 O_2-CO_2 Calibration

Similar algorithm as for pH was applied for calibration of the O_2-CO_2 analyzer. At least two data points are required for calibration of the analyzer for each gas. Ultra pure nitrogen may be used for zero set point for both gases. A calibration gas with oxygen and carbon dioxide contents close to the operational levels is preferred for the second data points.

6.4.4 Pre-Sterilization

Before commencing the sterilization process the user is asked to check and install different items. A summary list of the points is as follows:

- Close unused ports with blind plugs.
- Close the condenser cooling water valve.
- Install the temperature probes.
- Install the calibrated pH probe and pressurize it with 1.5 bar.
- Install the dissolved oxygen probe.
- Load the bioreactor.
- Open the main water supply.
- Switch on the heater box.
- Turn on the stirrer box and set the toggle switches to Auto and Run.

This section assures the user that all the required actions have been taken into consideration and the later processes will be carried out without any foreseeable problem.

6.4.5 Sterilization

The sterilization cycle is comprised of four phases: heating, holding, cooling, and normal (operational temperature). The stirrer rotation speed should be high enough to decrease

the internal heat transfer resistance (~ 700 rpm). When in automatic mode, the solenoid valve is kept close during the heating and holding phases, but it is kept open during the cooling phase, and is under the temperature control algorithm of the program during the normal operation. The user is asked to perform the following operations at certain points during the sterilization cycle:

- The air outlet valve on the top of the fermenter is kept open during the heating phase until the medium reaches the boiling point temperature and steam streams out for a few seconds. At this time, the user is asked to close the air outlet valve, so that the contents of the bioreactor can reach higher temperatures.
- At temperature 105 ^{o}C during the cooling phase, the user is asked to connect the air inlet assembly under sterile conditions and open the air inlet valve to prevent a vacuum in the bioreactor.
- When the temperature of the bioreactor contents reaches to the temperature of fermentation operation, the user is asked to:
    - Open the air outlet valve slowly under sterile condition.
    - Set the air inlet flow rate to desired value.
    - Connect the air outlet assembly.
    - Open the condenser valve.

A sound signal and a blinking LED on the screen of the front panel are used to inform the user for the appropriate action. In addition, the appropriate message appears in the provided message box on the front panel.

The front panel of the sterilization process is depicted in Figure 6.10. The default values for maximum allowable jacket temperature, sterilization temperature, sterilization time, culturing temperature, and agitation speed are 140 ^{o}C, 121 ^{o}C, 20 min., 27 ^{o}C, 500 rpm, respectively, but the user can change the set points at any time. It is recommended to place the solenoid valve in automatic mode during the sterilization period. The manual mode should only be used to cool down the system very fast in case of emergency. One round LED is assigned to each phase of sterilization. The set point and current temperatures of both jacket and bioreactor are also displayed on a waveform chart and can be saved along with the corresponding time values to text or spreadsheet files. A graphical representation of the whole process including the bioreactor vessel, stirrer,

sparger, air outlet assembly, cooling water, valves, and heaters are displayed on the front panel that helps user to follow the process. The jacket and bioreactor temperature controller gains are defined as default values based on the controller tuning as explained above. However, they can be adjusted to any new values by user.

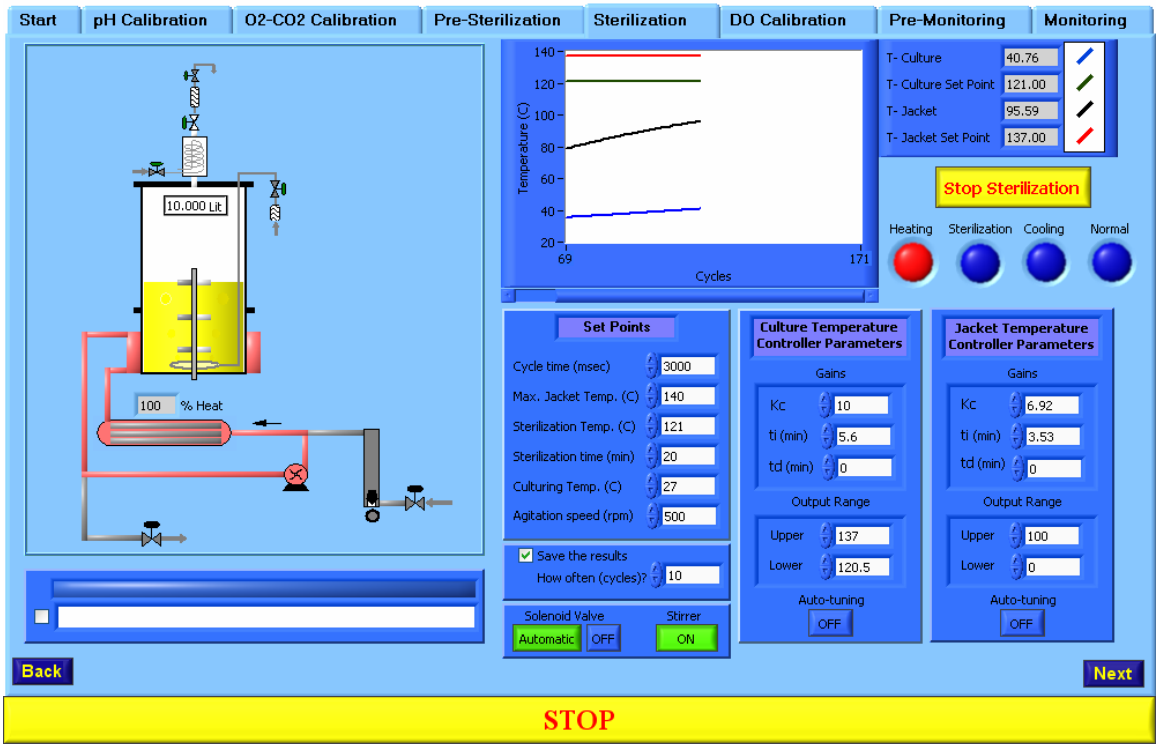

Figure 6.10- Front panel of LabVIEW program for the sterilization cycle.

6.4.6 DO Calibration

The dissolved oxygen probe calibration algorithm is similar to the method that has been used for pH probe. At least two data points are required for calibration purposes. The zero point may be set after extensive gassing of the fermenter with ultra pure nitrogen gas. The second calibration point that determines the slope of the calibration line should be set before inoculation after extensive gassing of the fermenter with air, while stirring and at the temperature of operation.

6.4.7 Pre-Monitoring

The following points need to be performed and checked before commencing the fermentation:

- Set the air flow rate to the desired value, while adjusting the pressure to 1 bar.
- Open the condenser cooling water valve.
- Connect the required tubings under sterile conditions (e.g., acids, base, and feed).
- Add the previously sterilized medium components to the fermenter.
- Inoculate the fermenter.
- Enter the final volume of the culture.
- Enter the initial acid and/or base volumes.
- Unless, all the abovementioned points are performed the user will not be able to proceed to the next step.

6.4.8 Monitoring

The front page of monitoring page is shown in Figure 6.11. The user can monitor and control the essential variables throughout the time course of fermentation using this section of the software. First, the set points for culture temperature, dissolved oxygen (if the user wishes to control it using variable agitation speed), upper and lower limits of pH, agitation speed, maximum allowable agitation speed, and cycle time as well as acid and base addition and delay times are entered. The default values for maximum agitation and cycle time are 750 rpm and 3000 milliseconds, respectively.

The controller gains for culture temperature, jacket temperature are assigned according the values established using the abovementioned tuning methods. The oxygen uptake rate of the microorganism under study and culture properties affect the dissolve oxygen level in the medium. Therefore, the gains for dissolved oxygen should be determined for any microorganism under study during the first series of fermentations using the auto-tuning feature of the dissolve oxygen controller. Then, the gains may be adjusted by trial and error to achieve a smooth and fast response.

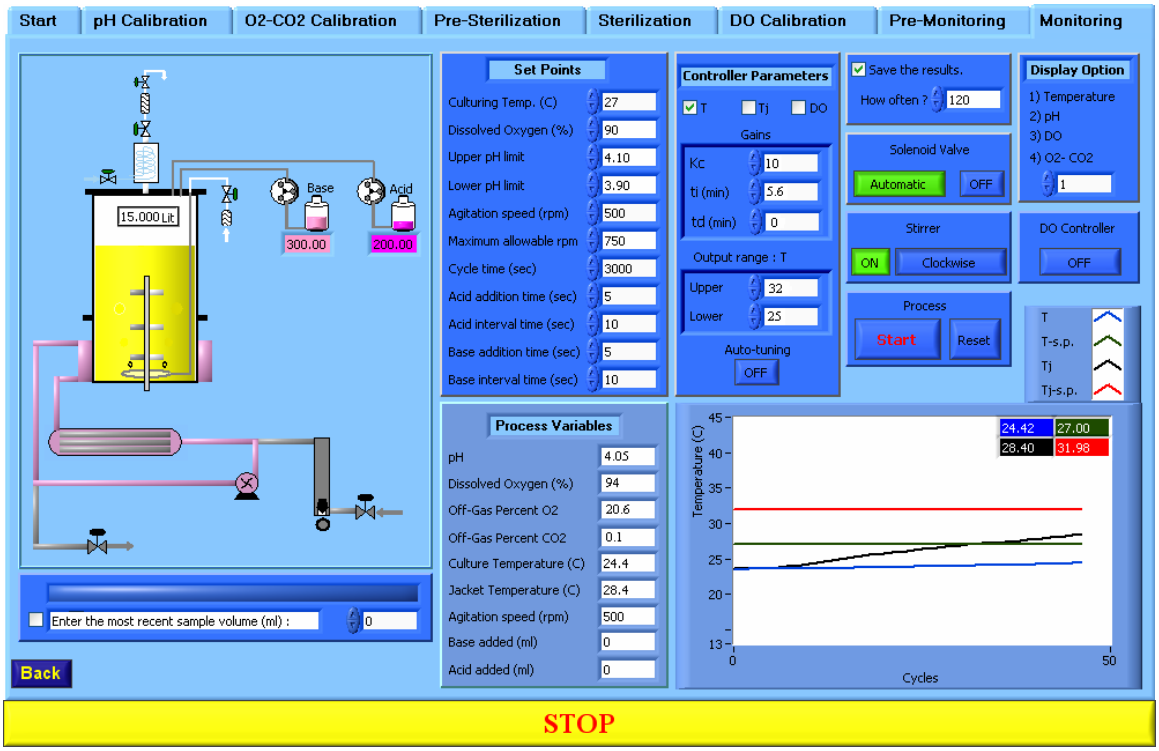

Figure 6.11- Front panel of LabVIEW for monitoring of fermentation processes.

The solenoid valve can be manipulated either manually or automatically during the fermentation. It is recommended to select the automatic mode, unless in case of emergency. The stirrer can be turned on and off by the user. In addition, its direction of rotation can be changed from clockwise to counterclockwise and vice versa during the process. Some microorganisms like many growing filamentous fungi tend to adhere to surfaces (e.g., bioreactor internal wall, probes, stirring shaft, and baffles), which is not desirable in submerged fermentation. The main agitation goal to consider is to detach the attached microorganisms from the surfaces during fermentation by switching the direction of the agitation in certain intervals. To change the rotational direction, however, the stirrer needs to be turned off first.

When all the required inputs are entered by user the monitoring process can be started by pressing the process start button on the screen. The profiles of temperature, pH, and dissolved oxygen as well as the O_2-CO_2 content of the outlet gas are displayed on the screen once at a time using numerical control. Besides, the current values of pH,

dissolved oxygen, the percentages of oxygen and carbon dioxide in the outlet gas, culture and jacket temperatures, agitation speed, and the volumes of acid and base added are shown on the screen and can be saved in text or spreadsheet files along with the time .

The dynamic graphical representation of the process is illustrated on the front panel. It includes the bioreactor, stirrer, air sparger, air inlet and outlet assemblies, solenoid valve, and the acid and base vessels. The reminder volumes of the acid and base are presented under the corresponding vessels in the graphical representation of the process. When either limit is exceeded, the corresponding reagent pump symbol and its line are lit on the front panel, signaling the need for corrective action. The user may enter the volumes of samples taken on the screen. The current volume of culture is adjusted based on the net volume additions to the bioreactor.

CHAPTER 7

CONCLUSIONS AND RECOMMENDATIONS

7.1 Conclusions

This thesis presented the application of two approaches, namely statistical methods and metabolic flux analysis, for maximizing the specific growth rate and the recombinant protein production rate in a model fungal fermentation process. This section summarizes the novel and significant findings of these studies.

- Fractional factorial design (FFD) was efficient to specify the most significant medium components. The analysis of the variance revealed that peptone, ammonium sulfate, and starch were significant factors all with positive effect, whereas yeast extract and $CaCl_2.2H_2O$ were found to be not important with respect to the heterologous lysozyme production. The highest lysozyme concentration of 127 mg/ L was obtained when all factors were at their higher level of the design. The experiment with lower level of the components with the exception of $CaCl_2.2H_2O$ resulted in the lowest lysozyme concentration of 60 mg/L.

- When far from optimal configuration, a first-order model including the main effects of the significant ingredients (peptone, ammonium sulfate, starch) was adequate to predict the behavior of the response. The adequacy of the first-order model was verified by plotting the normal probability plot of the studentized residuals.

- The experiments along the path of steepest ascent resulted in a maximum lysozyme production of 198 mg/L. The concentrations of starch, peptone, and ammonium sulfate at this point were 32.5 g/L, 31.0 g/L, and 12.15 g/L, respectively. Further increase in concentrations of these constituents decreased the recombinant protein concentration.

- Central composite design was used to explain the nature of the response at the vicinity of the maximum. Analysis of variance (ANOVA) revealed that the model was significant and there was no statistically significant lack of fit. According to this analysis, the linear effect of starch and peptone, the quadratic terms of all three significant components, and the starch-peptone as well as peptone-ammonium sulfate interactions were included in the final model. The optimum medium composition within the experimental range was found to be starch 34 g/L, peptone 34 g/L, ammonium sulfate 11.19 g/L, yeast extract 0.5 g/L, and $CaCl_2.2H_2O$ 0.5 g/L. The maximum theoretical lysozyme concentration was 212 mg/L at the optimum levels of the components. An experimental maximum lysozyme concentration of 209 ± 18 mg/L using the optimum medium composition supported the applied methodology.

- Based on the aforementioned results, one may conclude that the statistically based experimental design options when performed sequentially were powerful tools in optimizing a medium for the recombinant protein production by *A.niger*.

- A detailed metabolic network comprising three intracellular compartments (cytoplasm, mitochondrion and peroxisome) was successfully developed for *Aspergillus niger* and could be used in a predictive sense. The model was augmented by the inclusion of amino acid catabolism. Since the biochemical networks were highly underdetermined, the solution space was far too wide. To reduce the solution space, experimental flux measurements of the key metabolites were considered as inputs of the model. This approach was found to be very effective in order to achieve a more realistic model.

- The proposed model was able to predict biomass concentration accurately throughout the fermentation.

- During the early stage (lag phase) of fermentation the glucose concentration dropped 22% without significant production of biomass and lysozyme. The experimental work revealed that the carbon flux was directed mainly toward gluconic acid production. During this period approximately 93% of glucose was utilized for gluconate production, indicating that glucose oxidase was highly functional. Oxidase activity decreased during the next 18 hours of the fermentation when glucose concentration dropped to nearly zero. Approximately 74% of glucose was converted to gluconate during the first 30 hours of the fermentations. Gluconate was then consumed as the carbon source. The maximum specific growth rate during glucose consumption, however, was approximately 3.5 times higher than the maximum value observed for gluconate.

- For accurate analysis of the amino acid fluxes, it was important to use identical concentrations of all amino acids initially and adjust them later according to the mathematical analysis of the uptake rates. Three significant amino acids, proline, alanine, glutamate, were identified by logarithmic sensitivity analysis as having significant effect on growth. In addition, based on the experimental observations tyrosine was a potential candidate to be an effective amino acid. Experimental results confirmed that medium enrichment with proline, alanine, glutamate, and tyrosine benefited both growth and recombinant protein production.

- Sensitivity analysis indicated that the other amino acids were not likely to be important for the recombinant protein and biomass production. This was confirmed by experimental observations.

- From an operational point of view, one may conclude that the amino acid distribution in peptone was suboptimal with regard to both growth and recombinant protein synthesis.

- Glucose was found to benefit significantly both biomass and recombinant protein production, especially when the medium contained the important amino acids at their higher levels.

- Sensitivity of biomass formation reaction with respect to its constituents revealed that during the lag phase when all nutrients were still at high levels, the specific growth rate was not affected by the fungal biomass composition. However, during the active growth period, the protein content of the biomass was a limiting factor for the biomass production rate. This is probably due to the high energy cost of translation for polypeptide synthesis.

- The simulation results showed that the activity of pentose phosphate pathway increased with the specific growth rate increment during the fermentation. Also, a linear behavior was observed between the requirements for NADPH and the specific growth rate of the microorganism.

- The applied statistical analysis revealed that a higher level of nitrogen source enhanced both biomass and the protein production. Central composite design revealed that the interaction between carbon source and nitrogen source was significant with regard to protein production. Metabolic flux analysis also confirmed this finding as biomass and the protein production rates were dramatically higher when both sources were as their higher levels. Moreover, ammonia was found to be a very important inorganic nitrogen source with both methods.

7.2 Recommendations

The studies carried out in this research represent two approaches to identify the key metabolites that enhance the biomass and the recombinant protein productions. Based on this work, the following recommendations for future studies are proposed:

- The proposed metabolic network model for *A.niger* along with the associated experimental flux measurements should be examined with other recombinant fungal systems. This study was limited to recombinant fungal hen egg white lysozyme production only.

- The metabolic flux analysis reveals the topology of the biological system but contains no information about regulatory mechanisms (inhibition or activation). The steady state analysis of network stoichiometry alone ignores valuable information about the kinetic properties and modulations within the system. As an alternative approach which is capable of capturing the modulations and nonlinearity in the system, the S-system representations could be utilized for modeling of biochemical systems. The proposed aspects of this mathematical modeling are:
    - Estimation of the optimum profile of enzyme concentrations contributing to the map to achieve a given goal.
    - Search for a minimum subset of the enzymes which may need to be modified to produce almost the same protein level as the optimal.

- The model could be modified by introducing some integer variables in the optimization program in order to evaluate different set of solutions that have identical objective value and will satisfy the constraints. This methodology can be used to generate potential flux distributions that may be observed from implementing a metabolic engineering strategy.

- Metabolic flux analysis revealed the important components of the medium which significantly affect the biomass production rate are glucose, proline, alanine, glutamate,

tyrosine, and ammonia. With the reduced number of significant metabolites, it is possible to design experiments using statistical methods (for example, factorial design) to determine the optimum level of these ingredients to maximize the biomass and recombinant protein productions.

- Unwanted glucose oxidase activity could be reduced by application of genetic modification techniques. Since, the specific growth rate on glucose was much higher than on gluconate, any reduction in glucose oxidase activity could result in a higher specific growth rate with concomitant higher production of the recombinant protein.

- The concentration of oxalate at the end of fermentations was nearly 25% of the initial concentration of glucose. Oxalate was a terminal acid byproduct. The deletion or reduction of the activity of enzyme oxaloacetate hydrolase (EC 3.7.1.1) which is involved in oxalate formation might result in better usage of the supplied carbon source and increase in the biomass and product levels.

- The MBR reactor should be equipped with an air flow rate control valve which is under the control of LabVIEW software. This enables the user to control the dissolved oxygen both with manipulating the air flow rate and the agitation speed.

- It is recommended that the solenoid valve in the bioreactor be replaced with a water control valve that would be under the supervision of the LabVIEW software. This new arrangement would give smoother temperature profile inside the jacket and prevent the unwanted temperature oscillations in the jacket due to the on-off action of the solenoid valve.

References

Abdel-Fattah Y.R., Abdel-Fattah W.R., Zamilpa R., Pierce J.R. 2002. Numerical modeling of ferrous-ion oxidation rate in Acidithiobacillus ferrooxidans ATCC 23270: optimization of culture conditions through statistically designed experiments. *Acta Microbiol Pol* **51:** 225-235.

Adinarayana K., Ellaiah P. 2002. Response surface optimization of the critical medium components for the production of alkaline protease by a newly isolated Bacillus sp. *J Pharm Pharm Sci* **5:** 272-278.

Ahmed A., Singh, A., Ward, O.P. (2005). Culture-based strategies for reduction of protease activity in filtrates from *Aspergillus niger*. *World J Microbiol Biotechnol* **21**: 1577-1583

Aiba S., Matsouka M. 1979. Identification of metabolic model: Citrate production from glucose by *Candida lipolytica. Biotechnol Bioeng* **21:** 1373-1386.

Alvarez-Vasquez F., Gonzalez-Alcon C., Torres N.V. 2000. Metabolism of citric acid production by *Aspergillus niger*: Model definition, steady state analysis and constrained optimization of the citric acid production rate. *Biotechnol Bioeng* **70:** 82-108.

Ammanullah a., Blair R., Davies A., Riley G.R., Thomas C.R., Nienow A.W. 1999. Effects of agitation intensity on mycelial morphology and protein production in chemostat cultures of recombinant *Aspergillus oryzae*. *Biotechnol Bioeng* **62**: 434-446.

Anastassiadis S., Aivasidis A., Wandrey C., Rehm H.J. 2005. Process optimization of continuous gluconic acid fermentation by isolated yeast-like strains of *Aureobasidium pullulans*. *Biotechnol Bioeng* **91**: 494-501.

Archer D.B., Jeens D.J., Mackenzie D.A., Brightwell G., Lambert N., Lowe G., Radford S.E., Dobson C.M. 1990. Hen egg white lysozyme expressed in, and secreted form, *Aspergillus niger* is correctly processed and folded. *Biotechnology*. **8**: 741-745.

Archer D.B., MacKenzie D.A., Ridout M.J. 1995. Heterologous protein secretion by *Aspergillus niger* growing in submerged culture as dispersed or aggregated mycelia. *Appl Microbiol Biotechnol* **44:** 157-160.

Arora D.K., 2004. Handbook of fungal biotechnology. Mycology series, vol. 20. Marcel Dekker, Inc., NY, USA.

Bailey J. 1991. Toward a science of metabolic engineering. *Science* **252:** 1668-1674.

Balmforth A.J., Thomson A. 1984. Isolation and characterization of glyoxylate dehydrogenase from the fungus *Sclerotium rolfsii*. *Biochem J* **218**: 113-118.

Barton N.H., Turelli M. 1989. Evolutionary quantitative genetics: how little do we know? *Ann Rev Genet* **23**, 337-370.

Bartsch S., Schimek C., Wostemeyer J. 2002. Microprojectile bombardment as a reliable method for transformation of the mucoralean fungus *Absidia glauca*. *Mycoscience* **43**:213-217.

Bercocic M., Koloini T., Olsvic E.S., Kristiansen B. 1993. Rheological and morphological properties of submerged citric acid fermentation broth in stirred-tank and bubble column reactors. *Chem Eng J* **53**, 35-40.

Bercovitz A., Peleg Y., Battat E., Rokem J.S., Goldberg I. 1990. Localization of pyruvate carboxylase in organic acid-producing *Aspergillus* strains. *Applied and Environmental Microbiology* **56**:1594-1597.

Berry D.R. 1975. The environmental control of the physiology of filamentous fungi, in The Filamentous Fungi, Volume 1, Industrial Mycology,(eds. Smith J.E., Berry D.R.) Edward Arnold Ltd. London. 16-32.

Bidlingmeyer B.A., Cohen S.A., Tarvin T.L. 1984. Rapid analysis of amino acids using precolumn derivatization. *Journal of Chromatography* **336**:93-104.

Blumenthal H.J. 1968. Glucose catabolism in fungi. Wallerstein Laboratories Communications. **31**(106):171-191.

Bonarius P.J.B., Hatzimanikatis V., Meesters K.P.H. 1996. Metabolic flux analysis of hybridoma cells in different culture media using mass balances. *Biotechnol Bioeng* **50:** 299-319.

Box G.E.P., Hunter W.G., Hunter J.S. 1978. Statistics for experimenters. New York: John Wiley and Sons.

Box G.E.P., Wilson K.B. 1951. On the experimental attainment of optimum conditions. *Journal of the Royal Statistical Society, Series B* **13**:1-45.

Braun S., Vecht-Lifshitz S.E. 1991. Mycelial morphology and metabolite production .*TIBTECH* **9**:63-68.

Brock T.D., Madigan M.T. 1994. Biology of microorganism. *Prantic Hall, Englewood Cliffs, New Jersey, USA*.

Brooke A., Kendrick D., Meeraus A. 1998. GAMS a user's guide. A tutorial by Rosenthal R.E. GAMS development corporation.http://www.gams.com/.

Chang, P.K., Todd R.B. 2004. Metabolic pathway regulation. In: Arora D.K. (ed.), Handbook of fungal biotechnology (ed.). Mycology series, vol. 20. Marcel Dekker, Inc., NY, USA. 25-37.

Clarke, B.L. 1980. Stability of Complex reaction networks. Adv. Chem. Phys. 43: 1-215.

Cleland WW. 1967. The statistical analysis of enzyme kinetic data. *Advan Enzymol* **29**: 1-32.

Cochrane V.W. 1958. Physiology of Fungi. Wiley, NY/London.

Cortin V., Garnier A., Pineault N., Lemieux R., Boyer L., Proulx C. 2005. Efficient in vitro megakaryocytic maturation using cytokine cocktails optimized by statistical experimental design. *Exp Hematol* **33**: 1182-1191.

Cove D.J. 1966. The induction and repression on nitrate reductase in the fungus *Aspergillus nidulans. Biochim Biophys Acta* **113:** 51-56.

Cui Y.Q., Okkerse W.J., Van der lans J.M., Luyben K.C.H.A.M. 1998. Modeling and measurements of fungal growth and morphology in submerged fermentations. *Biotechnol Bioeng* **60:** 216-229.

Daae E.B., Ison A.P. 1999. Classification and sensitivity analysis of a proposed primary metabolic reaction network for Streptomyces lividans. *Metabolic Engineering* **1**:153-165.

Darvey I.G. 2000. Does the transport of oxaloacetate across the inner mitochondrial membrane during gluconeogenesis require carrier proteins other than those used in the malate-aspartate shuttle? *Biochemical Education* **28**:80-82.

Dean A. and Voss D. 1999. Design and analysis of experiments. Speringer-Verlag New York, Inc.

Dobeli H., Nuesch J. 1980. Regulatory properties of O-acetyl-L- serine sulfhydrylase of *Cephalosporium acremonium*: Evidence of an isoenzyme and its importance in Cephalosporin C biosynthesis. *Antimicrob Agents Chemother* **18**: 111-117.

Dunn B.M. 1989. Determination of protease mechanism. In: Beynon R.J., Bond J.S., eds. Proteolytic Enzymes: A practical Approach. Oxford: Oxford University Press, 57-81.

Elzainy T.A., Hassan M.M., Allam A.M. 1973. New pathway for nonphosphorylated degradation of gluconate by *Aspergillus niger*. *J of Bacheriology* **114**: 457-459.

Ferreira G.C., Pratt R.D., Pedersen P.L. 1989. Energy-linked anion transport. Cloning sequencing, and characterization of a full length cDNA encoding the rat liver mitochondrial proton/ phosphate symporter. *J Biol Chem* **264**:15628-15633.

Fiedurek J., Ilczuk Z. 1991. Glucose oxidase biosynthesis using immobilized mycelium of *Aspergillus niger*. *World J Microbiol Biotechnol* **7**: 379-384.

Finkelstein D.B. 1987. Improvement of enzyme production in Aspergillus. Antonie van Leeuwenhoek **53**: 349-352.

Gawthray G.R. 2003. An improved reversed-phase liquid chromatographic method for the analysis of low-molecular mass organic acids in plant root exudates. *Journal of Chromatography A* **1011**:233-240.

Gheshlaghi R., Scharer J.M., Moo-Young M, Douglas P.L. 2005. Medium Optimization for Hen Egg White Lysozyme production by recombinant *Aspergillus niger* using Statistical methods. Biotechnol Bioeng **90**:754-760.

Gow N.A.R. and Gadd G.M. 1995. The growing fungus. Chapman & Hall, UK.211-238.

Gyamerah M., Merichetti G., Adedayo O., Scharer J.M., Moo-Yang M. 2002. Bioprocessing strategies for improving hen egg-white lysozyme (HEWL) production by recombinant *Aspergillus niger* HEWL WT-13-16. *Appl Microbiol Biotechnol* **60:** 403-407.

Haq I.U., Ali S., Iqbal J. 2003, Effects of volume of culture medium on enhanced citric acid productivity by a mutant culture of *Aspergillus niger* in stirred fermenter. *Letters in Applied Microbiology* **36:** 302-306.

Hatzimanikatis V., Floudas C.A, Bailey J.E. 1996a. Optimization of regulatory architectures in metabolic reaction networks. *Biotechnol Bioeng* **52:** 485-500.

Heinrich R., Schuster S. 1996. The regulation of cellular systems. *Chapman & Hall, USA.*

Heinrikson R.L. and Meredith S.C. 1984. Amino acid analysis by reverse-phase high-performance liquid chromatography: Precolumn derivatization with phenylisothiocyanate. *Analytical Biochemistry* **136:** 65-74.

Henri V. 1903. Lois generales de l'action des diastases. Hermann, Paris.

Hillier F.S., Lieberman G.J. 2001. Introduction to operations research, seventh edition. McGraw-Hill, New York, NY, 10020. 231-262.

Ingraham J.L., Maaloe O., Neidhardt F.C. 1983. Growth of the bacterial cell. Sinnauer Associates, Sunderland.

Ismail A., Soultani S., Ghoul M. 1998. Optimization of the enzymatic synthesis of butyl glucoside using response surface methodology. *Biotechnol Prog* **14:** 874-878.

Jaklitsch W.M., Kubicek C.P., Scrutton M.C. 1991. The sub-cellular organization of itaconate biosynthesis in *Aspergillus terreus*. *Journal of General Microbiology* **137**:533-539.

Jeremy S.E., Palsson B.O. 1998. How will bioinformatics influence metabolic engineering? *Biotechnol Bioeng* **58:** 162-169.

Jernejc K., Legisa M. 1996. purification and properties of carnitine acetyltransferase from citric acid producing *Aspergillus niger*. *Appl Biochem Biotechnol* **60**:151-158.

Jones E.W., Fink G.R. 1982. Regulation of amino acid and nucleotide biosynthesis in yeasts. In The Molecular Biology of the yeast Saccharomyces. Metabolism and Gene Expression. 181-299. Edited by J.N. Starhern, E.W. Jones & J.R. Broach. Cold Spring Harbor, NY: Cold Spring Harbor Laboratory Pres.

Kalil S.J., Maugeri F., Rodrigues MI. 2000. Response surface analysis and simulation as a tool for bioprocess design and optimization. *Proc Biochem* **35:** 539-550.

Kellerhals M.B., Kessler B., Witholt B. 1999. Closed-loop control of bacterial high-cell-density fed-batch cultures: Production of mcl-PHAs by *Pseudomonas putida* KT2442 under single-substrate and cofeeding conditions. *Biotechnol Bioeng* **65**: 306-315.

Kelly J., Hynes M.J. 1982. The regulation of NADP-linked isocitrate dehydrogenase in *Aspergillus nidulans*. *J Gen Microbiol* **128**:23-28.

Klamt S., Schuster S., Gilles E.D. 2002. Calculability analysis in underdetermined metabolic networks illustrated by a model of the central metabolism in purple nonsulfur bacteria. *Biotechnol Bioeng* **77:** 734-751.

Koshland D.E., Neet K.E. 1968. The catalytic and regulatory properties of enzymes. *Ann Rev Biochem* **37:** 359-410.

Kubicek C.P., Schreferl-Kunar G., Wohrer W., Rohr M. 1988. Evidence for a cytoplasmic pathway of oxalate biosynthesis in Aspergillus niger. *Appl Environ Microbiol* **54**:633-637.

Kubicek C.P. 1988. Regulatory aspects of the tricarboxylic acid cycle in filamentous fungi. A review. *Transactions of the British Mycological Society* **90**:339-349.

Lakshminarayana K., Modi V.V., Shah V.K. 1969. Studies of gluconate metabolism in *Aspergillus niger*. *Arch Mikrobiol* **66**:396-405.

Lanoue K.F., Schoolwerth A.C. 1984. Metabolite transport in mammalian mitochondria. In Bioenergetics. Edited by Ernster L. Amsterdam. Elsevier Science Publisher. 221-268.

Lazarow P.B., Kunau W.H. 1997. Peroxisomes. In Pringle J.R., Broach J.R., Jones E.W. (Eds) Molecular Biology of the yeast *Saccharomyces cerevisiae*, Vol III: Cell cycle and cell biology. Cold Spring Harbor Laboratory Press, ColdSpring Harbor NY. 547-606.

Lee S.Y., Papoutsakis E.T. 1999. Metabolic Engineering. New York: Marcel Dekker Inc.

Leiro J., Siso M.I.G., Ortega M., Santamarina M.T., Sanmartin M.L. 1995. A factorial experimental design for investigation of the effects of temperature, incubation time, and pathogen- to- phagocyte ration on *in vivo* phagocytosis by turbot adherent cells. *Comp Biochem Physiol* Vol. 112C, **2:** 215-220.

Lejohn H.B. 1971. Enzyme regulation, lysine pathways and cell wall structures as indicators of major lines of evolution in fungi. *Nature* **231**:164-168.

Li C., Bai J., Cai Z., Ouyang F. 2002. Optimization of a cultural medium for bacteriocin production by *Lactococcus lactis* using response surface methodology. *Journal of Biotechnology* **93**:27-34.

Liptak B.G. 1986. Controlling and optimizing chemical reactors. *Chem Eng* **93**: 69-81.

Liu C., Liu Y., Liao W., Wen Z., Chen S. 2003. Application of statistically-based experimental designs for the optimization of nisin production from whey.*Biotechnol Lett* **25:**877-882.

Mackenzie D.A., Gendron L.C.G., Jeenes D.J., Archer D.B. 1994. Physiological optimization of secreted protein production by *Aspergillus niger. Enz Microb Technol* **16:** 276-280.

Mainwaring D.O., Weibe M.G., Robson G.D., Goldrick M., Jeens D.J., Archer D.B., Trinci A.P.J. 1999. Effect of PH on hen egg white lysozyme production and evolution of a recombinant strain of *Aspergillus niger*. *Journal of Biotechnology* **75:** 1-10.

Majewski R.A., Dornach M.M. 1990. Simple constrained optimization view of acetate overflow in E-*coli. Biotechnol Bioeng* **35:** 732-738.

Martinelli S.D., Kinghorn J.R. 1994. Aspergillus: 50 years on. Progress in industrial microbiology. Volume **29**: 61-140.

Martinez Blanco H., Reglero A., Fernandez-Valverde M., Ferrero M.A., Moreno M.A. Penalvas M.A., Luengo J.M. 1992. Isolation and characterization of the acetyl-CoA synthase from *Penicillium chrysogenum*. *J Biol Chem* **267**:5474-5481.

Mason R.L., Gunst R.F., Hess J.L. 1989. Statistical design and analysis of experiments: with applications to engineering and science. *John Wiley & sons, Inc. USA*.

Matthews H.R., Freedland R., Miesfeld R.L. 1997. Biochemistry a short course. *Willey-Liss, Inc., New York, USA*.

Maxwell D.P., Maxwell M.D., Hancssler G. (1975). Microbodies and glyoxylate-cycle enzyme activities in filamentous fungi. *Planta* **124**: 109-23.

Meixner-Monori B., Kubicek C.P., Habison A. 1985. Presence and regulation of the α-ketoglutarate dehydrogenase multienzyme complex in the filamentous fungus *Aspergillus niger*. *Journal of Bacteriology* **161**: 265-271.

McNeil B., Harvey L.M. 1990. Fermentation: A practical approach. *Oxford University Presss, Oxford, England*.

Michaelis L., Menten M.L. 1913. Die Kinetik der Invertinwirkung. *Biochem Z* **49:** 333-369.

Michaud F.T., Parent V.A., Garnier A., Duchesne C., 2005. Letter to the editor: On the proper use of statistical design of experiments. *Exp Hematol* **33**: 1271-1272.

Miron J., Siso M.I.G., Murado M.A., Gonzalez M.P. 1988. Microfungus- yeast mixed cultures in the degradation of amylaceous wastes. II: An experimental design for optimization of yeast production. *Biotechnol Lett* **2:** 171-176.

Montgomery D.C. 2001. Design and analysis of experiments. *John Wiley & sons, Inc. USA*.

Montgomery D.C., Runger G.C. 1994. Applied statistics and probability for engineers. *John Wiley & sons, Inc. USA*.

Morzycka E., Paszewski A. 1982. Cysteine and homocysteine synthesis in *Sacchoromycopsis lipolytica*. Identification and characterization of two cysteine synthases. *Acta Biochim Pol* **29**:81-93.

Mübeccel E., Mutlu S.F. 2000. Application of a statistical technique to the production of ethanol from sugar beet molasses by *Sacchromyces cerevisiae*. *Bioresource Technology*. **73:** 251-255.

Myers R.H., Montgomery D.C. 2002. Response surface methodology: process and product optimization using designed experiments. John Wiley & Sons, Inc. NY, USA.

Naeimpoor F., Mavituna F. 2000. Metabolic flux analysis in *Streptomyces coelicolor* under various nutrient limitations. *Metabolic Engineering* **2**:140-148.

Nagy I. 1992. Process Measurement and control, Volume 3: Introduction to Chemical Process Instrumentation. Elsevier, NY, USA.

Nicholls D.G., Ferguson S.J. 1992. Bioenergetics 2. Academic Press Limited, UK. 207-234.

Nielsen J., Villadsen J., Cunnar L. 2002. Bioreaction Engineering Principles, 2nd edition. Plenum publishers, New York, USA.

Nielsen, J. 1997. Physiological engineering aspects of *Penicillium chrysogenum*. World Scientific Publishing Co. Pte. Ltd. Singapore.61-138.

Oh S., Rheem S., Sim J., Kim S., Baek Y. 1995. Optimizing conditions for the growth of Lactobacillus casei YIT 9018 in tryptone- glucose medium by using response surface methodology. *Appl Environ Microbiol* **61:** 3809-3814.

Olsvik E.S., Kristiansen B. 1994. Rheology of filamentous fermentations. *Biotechnol Adv* **12**, 1-39.

Ooijkaas L.P., Wilkinson E.C., Tramper J., Buitelaar R.K. 1999. Medium optimization for spore production of *Coniothyrium minitans* using statistically- based experimental designs. *Biotechnol Bioeng* **64:** 92-100.

Osmani S.A., Scrutton C. 1983. The sub-cellular localization of Pyruvate carboxylase and some other enzymes in *Aspergillus nidulans*. *Eur J Biochem* **133**:551-560.

Ostergaard S., Theilgaard H.A., Nielsen J., 1998. Identification and purification of O-acetyl serine sulfhydrylase in *Penicillium chrysogenum*. *Appl Microbiol Biotechnol* **50**: 663- 668.

Pannell D.J. 1997. Introduction to practical linear programming. John Wiley & Sons, Inc. USA.

Papagianni M., Moo-Young M. 2002. Protease secretion in glucoamylase producer *Aspergillus niger* cultures: Fungal morphology and inoculum effects. *Process Biochem* **37**: 1271-1278.

Papoutsakis E.T., Meyer C.L. 1985. Equations and calculations of product yields and preferred pathways for butanediol and mixed-acid fermentations. *Biotechnol Bioeng* **27:** 50-66.

Park Y.S., Kang S.W., Lee J.S., Hong S.I. 2002. Xylanase production in solid state fermentation by *Aspergillus niger* mutant using statistical experimental designs. *Appl. Microbiol Biotechnol* **58:** 761-766.

Pateman J.A., Kinghorn J.R. 1976. Nitrogen metabolism, in the filamentous fungi, Volume 2, Biosynthesis and metabolism (eds. Smith J.E., Berry D.R.) Edward Arnold Ltd. London. 159- 237.

Paul G.C., Kent C.A., Thomas C.R. 1994. Hyphal vacuolation and fragmentation in *Penicillium chrysogenum*. *Biotechnol Bioeng* **44**: 655-660.

Pedersen H., Carlsen M., Nielsen J. 1999. Identification of enzymes and quantification of metabolic fluxes in the wild type and in a recombinant *Aspergillus oryzae* strain. *Appl Environ Microbiol* **65**: 11-19.

Pfitzner A., Kubicek C.P., Rohr M. 1987. Presence and regulation of ATP-citrate lyase from the citric acid producing fungus *Aspergillus niger*. *Arch Microbiol* **147**: 88-91.

Pramanik J., Keasling J.D. 1997. Stoichiometric model of *Escherichia coli* metabolism: incorporation of growth-rate dependent biomass composition and mechanistic energy requirements. *Biotechnol Bioeng* **56**:398- 421.

Punt P.J., van Biezen N., Conesa A., Albers A., Mangnus J., van den Hondel C. 2002. Filamentous fungi as cell factories for heterologous protein production. *Trends in Biotechnology* Vol **5**, No 5, 200-206.

Purohit H.J., Ratledge C. 1988. Mitochondrial location of pyruvate carboxylase in *Aspergillus niger*. *FEMS Microbiology Letters* **55**:129-132.

Quayle J.R., Taylor G.A. 1961. Carbon assimilation by *Pseudomonas oxalaticus* (OXl). *Biochem J* **78**: 611-615.

Rajendhran J., Krishnakumar V., Gunasekaran P. 2002. Optimization of a fermentation medium for the production of penicillin G acylase from *Bacillus sp*. *Letters in Applied Microbiology* **35:** 523-527.

Rathi P., Goswami V.K., Sahai V., Gupta R. 2002. Statistical medium optimization and production of hyperthermostable lipase from *Burkholderia Cepacra* in bioreactor. *J of Applied Microbiology* **93:** 930-936.

Rawool S.B., Sahoo S., Rao K.K., Sureshkumar G.K. 2001. Improvement in enzyme productivities from mold cultivations using the liquid- phase oxygen supply strategy. *Biotechnol Prog* **17:** 832-837.

Riggs J.B. 1999. Chemical process control. Ferret Publishing, USA.

Roels J.A. 1983. Energetics and kinetics in biotechnology. Amsterdam: Elsevier Biomedical Press.

Ruijter G.J., Panneman H., Visser J. 1997. Overexpression of Phosphofructokinase and pyruvate kinase in citric acid producing Aspergillus niger. *Biochim Biophys Acta* **1334:** 317.

Savageau M.A. 1969. Biochemical systems analysis, II. The steady-state solutions for an n-pool system using a power-law approximation. *J Theor Biol* **25:** 370-379.

Savageau M.A. 1976. Biochemical analysis: A study of function and design in molecular biology. *Addison, Wesley, Readind, MA*.

Savageau M.A., Voit E.O. 1987. Recasting nonlinear differential equations as S-system: a canonical nonlinear form. *Mathem Biosci* **87:** 83-115.

Savinell J.M., Palsson B.O. 1992. Network analysis of intermediary metabolism using linear optimization. II. Interpretation of *hybridoma* cell metabolism. *J Theor Biol* **154:** 455-473.

Schilling C.H., Letscher D., Palsson B.O. 2000. Theory for systemic definition of metabolic pathways and their use in interpreting metabolic function from a pathway-oriented perspective. *J Theor Biol* **203:** 229-248.

Schugerl K. 2001. Progress in monitoring, modeling and control of bioprocesses during the last 20 years. *J of Biotechnology* **85:** 149-173.

Shuler M.L., Kargi F. 2002. Bioprocess engineering, Basic concepts, 2nd edition. *Prantice Hall PTR, USA.*

Sierra R.D., Fariren V. 2001. Simplified method for the computation of parameters of power-law rate equations from time-series. *Mathematical Biosciences* **171:** 1-19.

Smiths H.P., HAuf J., Muller S., Hobley T.J., Zimmermann F.K., Hahn-Hagerdal B., Nielsen J., Olsson L. 2000. Simultaneous overexpression of enzymes of the lower part of glycolysis can enhance the fermentative capacity of *Sccharomyces cerevisiae. Yeast* **16:** 1325.

Spencer A., Morozov-Roche L.A., Noppe W., Mackenzie D.A., Jeens D.J., Joniau M., Dobson C.M., Archer D.B. 1999. Expression, purification, and characterization of the recombinant calcium-binding equine lysozyme secreted by the filamentous fungus *Aspergillus niger*: Comparisons with the production of hen and human lysozymes. *Protein Expression and Purification* **16**: 171-180.

Stephanopoulos G., Aristidou A.A., Nielsen J. 1998. Metabolic Engineering: Principles and Methodologies. San Diego, CA: Academic Press 309-351

Stephanopoulos G., Vallino J.J. 1991. Network rigidity and metabolic engineering overproduction. *Science* **252:** 1675-1681.

Stephanopoulos G. 1984. Chemical process control: An introduction to theory and practice. Prentice-Hall Inc. NJ, USA.

Stoll T.S., Ruffieux P.A., von Stocker U., Marison I.W. 1996. Development of an on-line control system for the cultivation of animal cell in a hollow-fiber reactor using flow injection analysis and a visual programming language. *J Biotechnol* **51**: 37-48.

Swift R.J., Karandikar A., Griffen A.M., Punt P.J., Cees A.M.J.J., Hondel V.D., Robson G.D., Trinci A.P.J., Weibe M.G. 2000. The effect of organic nitrogen sources on recombinant glucoamylase production by *Aspergillus niger* in chemostat culture. *Fungal Genetics and Biology* **31:** 125-133.

Takac S., Calik G., Mavituna F., Dervakos G. 1998. Metabolic flux distribution for the optimized production of L- glutamate. *Enzyme and Microbial Technology* **23:** 286-300.

Thom C., Church M.B. 1926. The aspergilli. The Williams & Wilkins Company. UAS.

Thomas C.R., Paul G.C. 1996. Application of image analysis in cell technology. *Curr Opin Biotechnol* **7**:35-45.

Torres N.V., Voit E.O. 2002. Pathway analysis and optimization in metabolic engineering. Cambridge University Press. Cambridge CB2 2RU, UK. 60- 64.

Torres N.V., Voit E.O., Glez-Alcon C., Rodriguez F. 1997. An indirect optimization method for biochemical systems: Description of method and application to the maximization of the rate of ethanol, glycerol, and carbohydrate production in *Saccharomyces cerevisiae*.*Biotechnol Bioeng* **55**: 758-772.

Treichler H.J., Liersch M., Nuesch J., Dobeli H. 1979. Role of sulfur metabolism in cephalosporin C and penicillin biosynthesis. In O.K. Sebek and A.L. Laskin (eds.), Genetics of industrial microorganisms. American Society for Microbiology, Washington, DC.

Turner W.B. 1971. Fungal metabolites. Academic Press Inc. LTD, London.11-24.

Tzagoloff A. 1982. Mitochondria. Plenum Press, New York. 199- 233.

Umbarger H.E. 1978. Amino acid biosynthesis and its regulation. *Annual Reviews in Biochemistry* **47**:1127-1162.

Vallino J.J., Stephanopoulos G. 1993. Metabolic flux distribution in *Corynebacterium glutamicum* during growth and lysine overproduction. *Biotechnol Bioeng* **41:** 633-649.

Van de Kamp M., Driessen A.J.M., Konings W.N. 1999. Compartmentalization and transport in β - lactam antibiotic biosynthesis by filamentous fungi. *Antonie van Leeuwenhoek* **75**:41-78.

Van der Heijden R.T.J.M., Heijan J.J., Hellinga C., Romein B., Luyben K.Ch. M. 1994. Linear constraint relations in biochemical reaction systems: I. Classification of the calculability and the balanceability of conversion rates. *Biotechnol Bioeng* **43**, 3-10.

Van Gorcom R.F.M., Van Hartingsveldt W.L.A., Van Paridon P.A.B., Veenstra A.E.N., Luiten R.G.M.A., Selton G.C.M.S. 1990. Cloning and expression of microbial phytase. *Eur Pat Appl* 0420 358 A1.

Van Gulik W.M. de Laat T.A.M., Vinke J.L., Heijnen J.J. 2000. Application of metabolic flux analysis for the identification of metabolic bottlenecks in the biosynthesis of Penicillin-G. *Biotechnol Bioeng* **68**:602-618.

Van Hartingsveldt W.L.A., Van Zeijl C.M.J., Veenstra A.E.N., Van den Berg J.A., Pouwels P.H., Van Gorcom R.F.M., Van den Hondel C.A.M.J.J. 1990. Heterologous gene expression in *Aspergillus*: Analysis of chymosin production in single-copy transformants of *A.niger*. In: Hesolt H, Davis J, Florent J, Bobichon L, Durand G, Penasse L, editors. Proceedings of the 6th International Symposium on Genetics of Industrial Microorganisms. Societe Francaise de Microbiologie, Strasbourg, France. P 107-116.

Van Laere A. 1995. Intermediary metabolism, in The growing fungus. (eds., Gow N.A.R. and Gadd G.M.). Chapman & Hall, UK.211-238.

Varma A., Palsson B.O. 1993a. Metabolic capabilities of *Escherichia coli*. II. Optimal growth patterns. *J Theor Biol* **165**:503-522.

Varma A., Boech B.W., Palsson B.O. 1993b. Biochemical production capabilities of Escherichia coli. *Biotechnol Bioeng* **42:** 59-73.

Varma A., Palsson B.O. 1994. Metabolic flux balancing: Basic concepts, scientific and practical use. *Bio/Technology* **12:** 994-998.

Voit E.O. 1991. Canonical nonlinear modeling. S-system approach to understanding complexity. *Van Nostrand Reinhold, New York*.

Voit E.O. 1992. Optimization in integrated biochemical systems. *Biotechnol. Bioeng*. **40**, 572-582.

Voit E.O. 2000. Computational analysis of biochemical systems: A Practical Guide for Biochemists and Molecular Biologists. Cambridge University Press, UK.

Wainwright M. 1988. Metabolic diversity of fungi in relation to growth and mineral cycling in soil- a review. *Transactions of the British Mycological Society*. **90**:159-170.

Walker G.M., White N.A. 2005. Introduction to fungal physiology. In Fungi: Biology and applications edited by Kavanagh K. John Wiley & sons Ltd. England.

Walker J.E. 1992. The mitochondria transporter family. *Current Opinion in Structural Biology* **2**:519-526.

Wang L., Ridgway D., Gu T., Moo-Young M. 2003a. Effects of process parameters on heterologous protein production in *Aspergillus niger* fermentation. *J Chem Technol Biotechnol* **78**: 1259-1266.

Wang, Y., Murray-Stewart, T., Devereux, W., Hacker, A., Frydman, B., Woster, P. M. and Casero, Jr, R. A. 2003b. Properties of purified recombinant human polyamine oxidase, PAOh1/SMO. *Biochem Biophys Res Commun* **304:** 605–611.

Ward O.P., Qin Q.M., Dhanjoon J.Y.J., Singh A. 2006. Physiology and biotechnology of Aspergillus. *Advances in Applied Microbiology* **58**:1-75.

Wessels J.G.H. 1993. Wall growth, protein excretion and morphogenesis in fungi. *New phytol* **123**: 397-413.

Wiebe M.G., Karandikar A., Robson G.D., Trinci A.P.J., Canida J.L.F., Trappe S., Wallis G., Rinase U., Derkx P.K.F., Madrid S.M., Sinniega H., Faus I., Montijn R., Van den Hondel C.A.M.J.J., Punt P.J. 2001. Production of tissue plasminogen activator (t-PA) in *Aspergillus niger. Biotechnol Bioeng* **76:** 164-174.

Wiechert W. 2002. Modeling and simulation: tools for metabolic engineering. *Journal of Biotechnology* **94:** 37-63.

Wittler R., Baumgardi H., Lubbers D.W., Schugerl K. 1986. Investigation of oxygen transfer into Penicillium chrysogenum pellets by microprobe measurements. *Biotechnol Bioeng* **28**: 1024-1036.

Wongwicharn A, McNeil B, Harvey LM. 1999. Effect of oxygen enrichment on morphology, growth, and heterologous protein production in chemostat cultures of *Aspergillus niger* B1-D. *Biotechnol Bioeng* **65:** 416-424.

Xu J., Wang L., Ridgway D., Gu T., Moo-Young M. 2000. Increased heterologous protein production in *Aspergillus niger* fermentation through extracellular proteases inhibition by pellet growth. *Biotechnol Prog* **16**: 222-227.

Yu X., Hallet S.G., Sheppard J., Watson A.K. 1997. Application of the Plackett- Burman experimental design to evaluate nutritional requirements for the production of *Colletotrichum coccodes* spores. *Appl Microbiol Biotechnol* **47:** 301-305.

Zabriskie T.M., Jackson M.D. 2000. Lysine biosynthesis and metabolism in fungi. *Nat Prod Rep* **17**: 85-97.

Zubay G. 1988. Biochemistry, 2nd edition. New York: Macmillan.

Appendix A- Nomenclature

a	amplitude of the oscillation peak
a_0	response intercept
a_k	linear coefficients
a_{kk}	quadratic coefficients
a_{kl}	interaction coefficients
A_l	symbol of atomic element of l
$\boldsymbol{A}$	symbolic vector of atomic species
b_i	measured flux of i^{th} metabolite
$\boldsymbol{b}$	vector of measured fluxes
C_i	intracellular concentration of i^{th} metabolite
$\boldsymbol{C}$	vector of metabolite concentrations
$\dot{\boldsymbol{C}}$	vector of concentration changes per unit time
$\dot{\boldsymbol{C}}_i$	concentration change of i^{th} metabolite per unit time
C_P	cooling water heat capacity
$d.f.$	degrees of freedom
$e(t)$	error between set point and process variable at time t
e_{il}	number of atoms of A_l in the species of M_i
$\boldsymbol{E}$	matrix of atomic coefficients of e_{il}
F	cooling water flow rate
f_t	fraction of cycle time at time t
g_{ij}	reaction rate order of the production of metabolite i
$g'_{i,j,l}$	reaction rate order of the production of metabolite i
h	allowable input change
$h_{i,j}$	reaction rate order of the consumption of metabolite i
$h'_{i,j,l}$	reaction rate order of the consumption of metabolite i
I	identity matrix
K	number of factors
K_c	proportional gain
K_u	ultimate gain
L	number of elements in the metabolites
m	number of metabolites
m_I	number of independent variables
M_i	symbol of i^{th} metabolite
M	symbolic vector of species
$M_{p.v.}$	process variable value
$M_{s.p.}$	set point value
MS_i	mean sum of square of effect i
n	number of fluxes
n_a	number of axial runs
n_c	number of center point runs
n_k	number of known fluxes (number of columns of $\boldsymbol{S_k}$)
n_r	number of replications for i^{th} treatment combination

n_u	number of unknown fluxes (number of columns of $\boldsymbol{S_u}$)
n_u^E	number of unknown exchange fluxes
n_u^I	number of unknown intracellular fluxes
$n_{u,ind}$	number of unknown fluxes of $\boldsymbol{V_{u,ind}}$
$\boldsymbol{P}$	vector of parameters
p	an integer that specifies the fraction of a full factorial design
$P_{H,i}$	input power of heater i
P_u	ultimate period
P/O	stoichiometry of the oxidative phosphorylation of $NADH_m$
$(P/O)^*$	stoichiometry of the oxidative phosphorylation of $NADH_c$ and $FADH_{2,m}$
Q	jacket temperature controller output (a number between 0 and 100)
q	percentage of required heating
q_i	number of processes that increase the production of i^{th} metabolite
R	redundancy matrix
R^2	coefficient of determination
R_{adj}^2	adjusted coefficient of determination
r_i	overall reaction rate of metabolite i
$\boldsymbol{r}$	vector of reaction rates
S_{ij}	Stoichiometric coefficient of i^{th} metabolite in j^{th} process
$\boldsymbol{S}$	stoichiometric matrix
$\boldsymbol{S^{-1}}$	stoichiometric matrix inverse
$\boldsymbol{S^{\#}}$	stoichiometric matrix pseudo inverse
$\boldsymbol{S^T}$	transpose of stoichiometric matrix
$\boldsymbol{S_k}$	stoichiometric matrix associated to the known fluxes of $\boldsymbol{V_k}$
$\boldsymbol{S_k^E}$	stoichiometric matrix associated with the known fluxes of $\boldsymbol{V_k^E}$
$\boldsymbol{S_u}$	stoichiometric matrix associated to the unknown fluxes of $\boldsymbol{V_u}$
$\boldsymbol{S_u^E}$	stoichiometric matrix associated with the unknown fluxes of $\boldsymbol{V_u^E}$
$\boldsymbol{S_u^I}$	stoichiometric matrix associated with the unknown fluxes of $\boldsymbol{V_u^I}$
$\boldsymbol{S_{u,ind}}$	stoichiometric matrix associated with the unknown fluxes of $\boldsymbol{V_{u,ind}}$
SS_E	error sum of square
SS_{Model}	model sum of square
SS_X	sum of square of the effect X
SS_T	total sum of square
t	time
T_J	jacket temperature
u	control action
u_D	differential control action
u_I	integral control action
u_{min}	minimum value of set point
u_{max}	maximum value of set point
u_P	proportional control action
v_j	flux through j^{th} individual reaction
$\boldsymbol{V}$	vector of fluxes
$\boldsymbol{V_k}$	vector of known (measured) fluxes

$\boldsymbol{V_k^E}$	vector of known exchange fluxes
$\boldsymbol{V_u}$	vector of unknown fluxes
$\boldsymbol{V_u^E}$	vector of unknown exchange fluxes
$\boldsymbol{V_u^I}$	vector of unknown intracellular fluxes
$\boldsymbol{V_{u,ind}}$	vector of unknown fluxes in a system that each reversible reaction is divided into two individual reactions (revised system)
V_{ij}^+	j^{th} process that increase the production of metabolite i
V_{ij}^-	j^{th} process that increase the consumption of metabolite i
w_i	number of processes that decrease the production of i^{th} metabolite
X_i	variable associated with the i^{th} component
x_i	coded variable associated with the i^{th} component
X^+	factor or factor interaction at high level
X^-	factor or factor interaction at low level
y	binary variable
Y	response
$\widehat{Y} = E(Y)$	expected value of response
$\overline{Y}_C$	average of center point responses
$\overline{Y}_F$	average of the factorial design responses
$Y_{i,r}$	response at r^{th} replication for i^{th} combination
Z	linear objective function

Greek letters

α_{CCD}	distance from the design center of central composite design
α_i, β_i	reaction rate constants of production and consumption of metabolite i in
$\alpha'_{i,j}, \beta'_{i,j}$	reaction rate constants of production and consumption of i^{th} metabolite in j^{th} reaction
$v^E_{i,u,\min}$	lower bound of i^{th} unknown exchange flux
$v^E_{i,u,\max}$	upper bound of i^{th} unknown exchange flux
γ_j	upper limit of j^{th} unknown intracellular flux
ε_i	error associated with the i^{th} measured flux
ε	noise in the response
τ_D	differential time (min)
τ_I	integral time (min)
λ_i	shadow price of i^{th} metabolite
$\Lambda(Z, b_i)$	logarithmic sensitivity of objective function with respect to i^{th} measured flux
μ	specific growth rate (hr^{-1})
ζ	a point in space

$\boldsymbol{\Omega}$	row vector of constants
ϖ_j	coefficient of j^{th} flux in objective function of linear programming
ρ	cooling water density

Subscripts

c	cytosolic compartment
ccd	central composite design
c.w.	cooling water
m	mitochondrial compartment
p	peroxisomal compartment
D.W.	dry weight
s.p.	set point

Appendix B- Abbreviations Used In Metabolic Reactions

αAAd	α-Aminoadipate
Aald	Acetaldehyde
Ac	Acetate
AclHser	O-Acetyl Homoserine
Acact	Acetoacetate
AcCoA	Acetyl Coenzyme A
ADP	Adenosine 5 diphosphate
AICAR	5-Aminoimidazole-4-carboxamide ribotide
αKB	α-Ketobutyrate
αKG	α-Ketoglutarate
αKIV	α-Ketoisovalerate
Ala	L-Alanine
Arg	L-Arginine
Asn	L-Asparagine
Asp	L-Aspartate
ATP	Adenosine-5-triphosphate
βIPM	β-Isopropylmalate
Carp	Carbamoylphosphate
Chit	Chitine
Chor	Chorismate
Cit	Citrate
CO_2	Carbon dioxide
Ctl	Citruline
CTP	Cytidine triphosphate
Cys	L-Cysteine
DHAP	Dihydroxyacetone phosphate
DHF	Dihydrofolate
DNA	Deoxyribonucleic acid
E4P	Erythrose-4-phosphate
EtOH	Ethanol
F1,6DP	Fructose-1, 6-diphosphate
F6P	Fructose-6-phosphate
FAD	Flavine adenine dinucleotide (oxidized)
$FADH_2$	Flavine adenine dinucleotide (reduced)
FTHF	Formyltetrahydrofolate
Fum	Fumarate
G1,3DP	Glycerate-1, 3-diphosphate
G6P	Glucose-6-phosphate
GA3P	Glyceraldehyde-3-phosphate
Glc	Glucose
Glgn	Glycogen
Gln	L-Glutamine
Glu	L-Glutamate

Glcn	Glucan
Gluc	Gluconic acid
Glx	Glyoxylate
Gly	L-Glycine
Grol	Glycerol
Gt2P	Glycerate-2-phosphate
Gt3p	Glycerate-3-phosphate
GTP	Guanosine triphosphate
Gu6P	Gluconate-6-phosphate
GuL6P	Gluconolactone-6-P
H	Proton
H_2O	Water
HCys	Homocysteine
HEWL	Hen egg white lysozyme
His	L-Histidine
HSer	Homoserine
H_2S	Hydrogen sulfide
ICit	Isocitrate
Ileu	L-Isoleucine
IMP	Inosine monophosphate
Leu	L-Leucine
Lys	L-Lysine
Mal	Malate
Man	Mannitol
Met	L-Methionine
MlTHF	Methyltetrahydrofolate
MnTHF	Methylenetetrahydrofolate
NAD	Nicotinamide adenine dinucleotide (oxidized)
NADH	Nicotinamide adenine dinucleotide (reduced)
NADP	Nicotinamide adenine dinucleotide phosphate (oxidized)
NADPH	Nicotinamide adenine dinucleotide phosphate (reduced)
NH_3	Ammonia
O_2	oxygen
Ox	Oxalic acid
OA	Oxaloacetate
Orn	ornithine
P	Inorganic Orthophosphate
PEP	Phosphoenolpyruvate
Phe	L-Phenylalanine
Pro	L-Proline
PRPP	5-Phosphoribosylpyrophosphate
Pyr	Pyruvate
R5P	Ribose- 5- phosphate
RNA	Ribonucleic acid
Ru5P	Ribulose-5-phosphate
SAH	S-Adenosylhomocysteine

SAM	S-Adenosylmethionine
Ser	L-Serine
SH7P	Sedoheptulose-7-phosphate
SO_4	Sulfate
Succ	Succinate
SuccCoA	Succinyl Coenzyme A
THF	Tetrahydrofolate
Thr	L-Threonine
Trp	L-Tryptophane
Tyr	L-Tyrosine
UDP	Uridine-5-diphosphate
UTP	Uridine triphosphate
Val	L-Valine
X5P	Xylulose-5-phosphate

Appendix C- Metabolic Reactions

The letters *b*, *d*, and *g* following the reaction numbers indicate biosynthesis, degradation, and gluconeogenesis reactions.

Glycolysis

$R1.1)\ Glc_c + ATP_c \Rightarrow G6P_c + ADP_c$

$R1.1g)\ G6P_c + H_2O_c \Rightarrow Glc_c + P_c$

$R1.2)\ G6P_c \Leftrightarrow F6P_c$

$R1.3)\ F6P_c + ATP_c \Rightarrow F1,6DP_c + ADP_c$

$R1.3g)\ F1,6DP_c + H_2O_c \Rightarrow F6P_c + P_c$

$R1.4)\ F1,6DP_c \Leftrightarrow DHAP_c + GA3P_c$

$R1.5)\ DHAP_c \Leftrightarrow GA3P_c$

$R1.6)\ GA3P_c + NAD_c + P_c \Leftrightarrow G1,3DP_c + NADH_c + H_c$

$R1.7)\ G1,3P_c + ADP_c \Leftrightarrow Gt3P_c + ATP_c$

$R1.8)\ Gt3P_c \Leftrightarrow Gt2P_c$

$R1.9)\ Gt2P_c \Leftrightarrow PEP_c + H_2O_c$

$R1.10)\ PEP_c + ADP_c \Rightarrow Pyr_c + ATP_c$

Pentose Phosphate Pathway

$R2.1)\ G6P_c + NADP_c + H_2O_c \Rightarrow Gu6P_c + NADPH_c + H_c$

$R2.2)\ Gu6P_c + NADP_c \Rightarrow Ru5P_c + NADPH_c + H_c + CO_{2,c}$

$R2.3)\ Ru5P_c \Leftrightarrow R5P_c$

$R2.4)\ Ru5P_c \Leftrightarrow X5P_c$

$R2.5)\ R5P_c + X5P_c \Leftrightarrow GA3P_c + Sh7P_c$

$R2.6)\ GA3P_c + Sh7P_c \Leftrightarrow E4P_c + F6P_c$

$R2.7)\ E4P_c + X5P_c \Leftrightarrow GA3P_c + F6P_c$

Tricarboxylic Cycle Pathway

$R3.1)\ Pyr_m + ATP_m + CO_{2,m} + H_2O_m \Leftrightarrow OA_m + ADP_m + P_m$

$R3.2)\ Pyr_m + CoA_m + NAD_m \Rightarrow AcCoA_m + NADH_m + H_m + CO_{2,m}$

$R3.3)\ AcCoA_m + OA_m + H_2O_m \Rightarrow Cit_m + CoA_m$

$R3.4)\ Cit_m \Leftrightarrow ICit_m$

$R3.5)\ ICit_m + NAD_m \Rightarrow \alpha KG_m + NADH_m + H_m + CO_{2,m}$

$R3.6)\ ICit_c + NAD_c \Rightarrow \alpha KG_c + NADH_c + H_c + CO_{2,c}$

$R3.7)\ ICit_m + NADP_m \Rightarrow \alpha KG_m + NADPH_m + H_m + CO_{2,m}$

$R3.8)\ ICit_c + NADP_c \Rightarrow \alpha KG_c + NADPH_c + H_c + CO_{2,c}$

$R3.9)\ \alpha KG_m + CoA_m + NAD_m \Leftrightarrow SuccCoA_m + NADH_m + H_m + CO_{2,m}$

$R3.10)\ SuccCoA_m + ADP_m + P_m \Leftrightarrow Succ_m + ATP_m + CoA_m$

$R3.11)\ Succ_m + FAD_m \Leftrightarrow Fum_m + FADH_{2,m}$

$R3.12)\ Fum_m + H_2O_m \Leftrightarrow Mal_m$

$R3.13)\ Mal_m + NAD_m \Leftrightarrow OA_m + NADH_m + H_m$

Anaplerotic Pathways

$R4.1)\ Pyr_c + ATP_c + CO_{2,c} + H_2O_c \Leftrightarrow OA_c + ADP_c + P_c$

$R4.2)\ Cit_c + ATP_c + CoA_c \Rightarrow OA_c + ADP_c + P_c + AcCoA_c$

$R4.3)\ Mal_c + NADP_c \Rightarrow Pyr_c + CO_{2,c} + NADPH_c + H_c$

$R4.4)\ Mal_c + NAD_c \Leftrightarrow OA_c + NADH_c + H_c$

$R4.5)\ PEP_c + ADP_c + CO_{2,c} \Rightarrow OA_c + ATP_c$

$R4.5g)\ OA_c + ATP_c \Rightarrow PEP_c + ADP_c + CO_{2,c}$

$R4.6)\ ICit_P \Rightarrow Glx_p + Succ_p$

$R4.7)\ Glx_p + AcCoA_p + H_2O_c \Rightarrow Mal_p + CoA_p$

Oxidative Phosphorylation

$R5.1)\ NADH_m + H_m + 0.5O_{2,c} + (P/O)ADP_c + (P/O)P_c \Rightarrow NAD_m + (P/O)ATP_c + [(P/O) + 1]H_2O_m$

$R5.2)\ FADH_{2,m} + 0.5O_{2,m} + (P/O)^* ADP_c + (P/O)^* P_c \Rightarrow FAD_m + (P/O)^* ATP_c + [(P/O)^* + 1]H_2O_m$

$R5.1)\ NADH_c + H_c + 0.5O_{2,C} + (P/O)^* ADP_c + (P/O)^* P_c \Rightarrow NAD_c + (P/O)^* ATP_c + [(P/O)^* + 1]H_2O_c$

Amino Acid metabolism

$R6.1)\ \alpha KG_c + NH_{3,c} + NADH_c + H_c \Leftrightarrow Glu_c + NAD_c + H_2O_c$

$R6.2)\ \alpha KG_c + NH_{3,c} + NADPH_c + H_c \Leftrightarrow Glu_c + NADP_c + H_2O_c$

$R6.3)\ Glu_c + NH_{3,c} + ATP_c \Leftrightarrow Gln_c + ADP_c + P_c$

$R6.4)\ Pyr_c + Glu_c \Leftrightarrow Ala_c + \alpha KG_c$

$R6.5)\ OA_c + Glu_c \Leftrightarrow Asp_c + \alpha KG_c$

$R6.6)\ OA_m + Glu_m \Leftrightarrow Asp_m + \alpha KG_m$

$R6.7)\ Asp_c + G\ln_c + 2ATP_c + 2H_2O_c \Leftrightarrow Asn_c + Glu_c + 2ADP_c + P_c$

$R6.8b)\ Glu_c + Gt3P_c + NAD_c + H_2O_c \Rightarrow Ser_c + \alpha KG_c + NADH_c + H_c + P_c$

$R6.8d)\ Ser_c + \alpha KG_c + NADH_c + H_c + ATP_c \Rightarrow Glu_c + Gt3P_c + NAD_c + ADP_c$

$R6.9b1)\ Asp_c + ATP_c + 2NADPH_c + 2H_c \Rightarrow HSer_c + ADP_c + P_c + 2NADP_c$

$R6.9b2)\ Asp_c + ATP_c + NADPH_c + NADH_c + 2H_c \Rightarrow HSer_c + ADP_c + P_c + NADP_c + NAD_c$

$R6.10b)\ HSer_c + ATP_c + H_2O_c \Leftrightarrow Thr_c + ADP_c + P_c$

$R6.10d)\ Thr_c \Rightarrow \alpha KB_c + NH_{3,c}$

$R6.11)\ Ser_c + THF_c \Leftrightarrow Gly_c + MnTHF_c + H_2O_c$

$R6.12)\ SO_{4,c} + 2ATP_c + 4NADPH_c + 4H_c \Rightarrow H_2S_c + 2ADP_c + 2P_c + 4NADP_c + 2H_2O_c$

$R6.13b)\ HSer_c + AcCoA_c \Rightarrow AclHSer_c + CoA_c$

$R6.13d)\ AclHSer_c + H_2S_c \Rightarrow HCys_c + Ac_c$

$R6.14)\ HCys_c + MlTHF_c \Rightarrow Met_c + THF_c$

$R6.15)\ HCys_c + Ser_c \Rightarrow Cys_c + NH_{3,c} + \alpha KB_c$

$R6.16b)\ Ser_c + AcCoA_c + H_2S_c \Rightarrow Cys_c + CoA_c + Ac_c$

$R6.16d)\ Cys_c + AclHSer_c + H_2O_c \Rightarrow HCys_c + NH_{3,c} + Pyr_c$

$R6.17b)\ 2Pyr_m + NADPH_m + H_m \Rightarrow \alpha KIV_m + CO_{2,m} + NADP_m + H_2O_m$

$R6.17d)\ \alpha KIV_m + 3NAD_m + CoA_m + 2H_2O_m + FAD_m \Rightarrow 3NADH_m + 3H_m + SuccCoA_m + CO_{2,m} + FADH_{2,m}$

$R6.18)\ \alpha KIV_m + Glu_m \Leftrightarrow Val_m + \alpha KG_m$

$R6.19)\ \alpha KIV_m + AcCoA_m + H_2O_m \Rightarrow \beta IPM_m + CoA_m$

$R6.20b)\ \beta IPM_c + Glu_c + NAD_c \Rightarrow Leu_c + \alpha KG_c + CO_{2,c} + NADH_c + H_c$

R6.20d) $Leu_c + \alpha KG_c + ATP_m + CoA_m + NAD_m + FAD_m + 2H_2O_m \Rightarrow Glu_c + ADP_m + P_m + AcCoA_m + NADH_m + H_m + FADH_{2,m} + Acact_m$

R6.21b) $Pyr_m + \alpha KB_m + Glu_m + NADPH_m + H_m \Rightarrow ILeu_m + \alpha KG_m + NADP_m + CO_{2,m} + H_2O_m$

R6.21d) $ILeu_m + \alpha KG_m + ATP_m + 2CoA_m + 2NAD_m + FAD_m + 2H_2O_m \Rightarrow Glu_m + SuccCoA_m + AcCoA_m + ADP_m + P_m + 2NADH_m + 2H_m + FADH_{2,m}$

R6.22b) $Glu_m + AcCoA_m + NAD_m + H_2O_m \Rightarrow \alpha AAd_m + CoA_m + NADH_m + H_m + CO_{2,m}$

R6.22d) $\alpha AAd_m + \alpha KG_m + 2CoA_m + 2NAD_m + FAD_m + H_2O_m \Rightarrow Glu_m + 2AcCoA_m + 2NADH_m + 2H_m + FADH_{2,m} + 2CO_{2,m}$

R6.23b) $\alpha AAd_c + Glu_c + 2ATP_c + 2NADPH_c + NAD_c + H_c + H_2O_c \Rightarrow Lys_c + \alpha KG_c + 2ADP_c + 2P_c + 2NADP_c + NADH_c$

R6.23d1) $Lys_c + \alpha KG_c + NADP_c + H_2O_c \Rightarrow \alpha AAd_c + Glu_c + NADPH_c + H_c$

R6.23d2) $Lys_c + \alpha KG_c + NADH_c + 2NADP_c + H_2O_c \Rightarrow \alpha AAd_c + Glu_c + NAD_c + 2NADPH_c + H_c$

R6.24) $Gln_c + 2ATP_c + CO_{2,m} + 2H_2O_m \Rightarrow CarP_m + Glu_m + 2ADP_m + P_m$

R6.25) $2Glu_m + AcCoA_m + ATP_m + NADPH_m + H_m + H_2O_m \Rightarrow Orn_m + \alpha KG_m + CoA_m + ADP_m + P_m + NADP_m + Ac_m$

R6.26) $Carp_m + Orn_m \Leftrightarrow Ctl_m + P_m$

R6.27b) $Asp_c + Ctl_c + 2ATP_c + H_2O_c \Rightarrow Arg_c + Fum_c + 2ADP_c + 2P_c$

R6.27d) $Arg_c + H_2O_c \Rightarrow Orn_c + CO_{2,c} + 2NH_{3,c}$

R6.28b) $Glu_c + ATP_c + 2NADPH_c + 2H_c \Rightarrow Pro_c + ADP_c + P_c + H_2O_c + 2NADP_c$

R6.28d) $Pro_m + 0.5O_{2,m} + NAD_m + H_2O_m \Rightarrow Glu_m + NADH_m + H_m$

R6.29) $R5P_c + 2ATP_c \Leftrightarrow PRPP_c + 2ADP_c$

R6.30b) $Gln_c + PRPP_C + ATP_c + 2NAD_c + 5H_2O_c \Rightarrow His_c + \alpha KG_c + AICAR_c + 2NADH_c + 2H_c + 5P_c$

R6.30d) $His_c + THF_c + 2H_2O_c \Rightarrow Glu_c + NH_{3,c} + FormiTHF_c$

R6.31) $2PEP_c + E4P_c + ATP_c + NADPH_c + H_c \Rightarrow Chor_c + ADP_c + 4P_c + NADP_c$

R6.32b) $G\ln_c + Ser_c + PRPP_c + Chor_c \Rightarrow Trp_c + Glu_c + GA3P_c + Pyr_c + 2P_c + CO_{2,c} + H_2O_c$

R6.32d) $Trp_c + Glu_c + 3O_{2,c} + NADPH_c + H_c + 3H_2O_c \Rightarrow For_c + Ala_c + \alpha KG_c + \alpha AAd_c + CO_{2,c} + NH_{3,c} + NADP_c$

R6.33b) $Glu_c + Chor_c + NAD_c \Rightarrow Tyr_c + \alpha KG_c + NADH_c + H_c + CO_{2,c}$

R6.33d) $Tyr_c + \alpha KG_c + 2O_{2,c} + H_2O_c \Rightarrow Glu_c + Fum_c + CO_{2,c} + Acact_c$

R6.34b) $Glu_c + Chor_c \Rightarrow Phe_c + \alpha KG_c + CO_{2,c} + H_2O_c$

R6.34d1) $Phe_c + O_{2,c} + NADPH_c + H_c \Rightarrow Tyr_c + NADP_c + H_2O_c$

R6.34d2) $Phe_c + O_{2,c} + NADH_c + H_c \Rightarrow Tyr_c + NAD_c + H_2O_c$

R6.35) $\alpha KB_m + ATP_m + H_2O_m + CoA_m + NAD_m \Leftrightarrow SuccCoA_m + ADP_m + P_m + NADH_m + H_m$

R6.36) $Thr_c \Leftrightarrow Gly_c + Aald_c$

Biosynthesis and Interconversion of One-Carbon Units

R7.1) $DHF_c + NADPH_c + H_c \Leftrightarrow THF_c + NADP_c$

R7.2) $Gly_c + THF_c + NAD_c \Rightarrow MnTHF_c + NH_{3,c} + CO_{2,c} + NADH_c + H_c$

R7.3) $MnTHF_c + NADP_c + H_2O_c \Leftrightarrow FTHF_c + NADPH_c + H_c$

R7.4) $MnTHF_c + NADH_c + H_c \Leftrightarrow MlTHF_c + NAD_c$

R7.5) $MnTHF_c + NADPH_c + H_c \Leftrightarrow MlTHF_c + NADP_c$

R7.6) $Met_c + ATP_c + 2H_2O_c + H_c \Rightarrow SAM_c + 3P_c$

R7.7) $SAH_c + 2ATP_c + H_2O_c \Rightarrow HCys_c + 3ADP_c$

Nucleotides Biosynthesis

R8.1) $AICAR_c + FTHF_c \Rightarrow IMP_c + THF_c + H_2O_c$

R8.2) $Asp_c + 3ATP_c + IMP_c \Rightarrow ATP_c^* + Fum_c + 3ADP_c + P_c$

R8.3) $IMP_c + Gln_c + 4ATP_c + NAD_c + 3H_2O_c \Rightarrow GTP_c + Glu_c + 4ADP_c + NADH_c + H_c + 2P_c$

R8.4) $Asp_c + Gln_c + PRPP_c + 4ATP_c + NAD_c + 2H_2O_c \Rightarrow UTP_c + Glu_c + 4ADP_c + NADH_c + H_c + 4P_c$

R8.5) $UTP_c + Gln_c + ATP_c + H_2O_c \Rightarrow CTP_c + Glu_c + ADP_c + P_c$

$R8.6)\ PRPP_c + FTHF_c + Gly_c + Asp_c + 2Gln_c + 4ATP_c + CO_{2,c} + 3H_2O_c \Rightarrow AICAR_c + THF_c + Fum_c + 2Glu_c + 4ADP_c + 6P_c$

$R8.7)\ UDP_c + ATP_c \Leftrightarrow UTP_c + ADP_c$

Biomass Components

$R9.1)\ F6P_c + Gln_c + AcCoA_c + UTP_c + H_2O_c \Rightarrow Chit_c + Glu_c + CoA_c + UDP_c + 2P_c$

$R9.2b)\ DHAP_c + NADH_c + H_c + H_2O_c \Rightarrow Grol_c + NAD_c + P_c$

$R9.2d)\ Grol_c + ATP_c + NAD_c \Rightarrow DHAP_c + ADP_c + NADH_c + H_c$

$R9.3b)\ DHAP_c + NADPH_c + H_c + H_2O_c \Rightarrow Grol_c + NADP_c + P_c$

$R9.3d)\ Grol_c + ATP_c + FAD_m \Rightarrow DHAP_c + ADP_c + FADH_{2,m}$

$R9.4b)\ F6P_c + NADH_c + H_c + H_2O_c \Rightarrow Man_c + NAD_c + P_c$

$R9.4d)\ Man_c + ATP_c + NADP_c \Rightarrow F6P_c + ADP_c + NADPH_c + H_c$

$R9.5)\ G6P_c + UTP_c + H_2O_c \Rightarrow Glcn_c + UDP_c + 2P_c$

$R9.6b)\ G6P_c + UTP_c + H_2O_c \Rightarrow Glgn_c + UDP_c + 2P_c$

$R9.6d)\ Glgn_c + P_c \Rightarrow G6P_c$

C_2 Compounds Metabolism

$R10.1)\ Aald_c + NADPH_c + H_c \Leftrightarrow EtoH_c + NADP_c$

$R10.2)\ Aald_c + NADH_c + H_c \Leftrightarrow EtoH_c + NAD_c$

$R10.3)\ Aald_c + NADP_c + H_2O_c \Leftrightarrow Ac_c + NADPH_c + H_c$

$R10.4)\ Aald_c + NAD_c + H_2O_c \Leftrightarrow Ac_c + NADH_c + H_c$

$R10.5b)\ Ac_c + CoA_c + 2ATP_c + H_2O_c \Rightarrow AcCoA_c + 2ADP_c + 2P_c$

$R10.5d)\ AcCoA_c + H_2O_c \Rightarrow CoA_c + Ac_c$

Polymerization Reactions

$R11.1)\ 0.095Ala_c + 0.044Arg_c + 0.046Asn_c + 0.046Asp_c + 0.011Cyc_c + 0.080Gln_c + 0.080Glu_c + 0.094Gly_c + 0.020His_c + 0.045ILeu_c + 0.069Leu_c + 0.057Lys_c + 0.014Met_c + 0.031Phe_c + 0.047Pro_c + 0.066Ser_c + 0.048Thr_c + 0.018Trp_c + 0.028Tyr_c + 0.064Val_c + 4ATP_c + 4H_2O_c \Rightarrow Protein_c + 4ADP_c + 4P_c$

$R11.2)\ 0.256ATP_c^* + 0.196CTP_c + 0.286GTP_c + 0.262UTP_c + ATP_c + H_2O_c \Rightarrow RNA_c + ADP_c + P_c$

$R11.3)\ 0.242ATP_c^* + 0.258CTP_c + 0.258GTP_c + 0.242UTP_c + 1.242NADPH_c + 0.242MnTHF_c + ATP_c + H_2O_c \Rightarrow DNA + 1.242NADP_c + 0.242DHF_c + ADP_c + P_c$

$R11.4)\ 18.12AcCoA_c + 0.623DHAP_c + 0.3G6P_c + 1.1SAM_c + 0.4Ser_c + 2.6O_{2,c} + 1.7NADH_c + 22.4NADPH_c + 0.623FADH_{2,m} + 18ATP_c + 18H_2O_c \Rightarrow Lipid_c + 18.12CoA + 1.1SAH_c + 3.8CO_{2,c} + 1.7NAD_c + 22.4NADP_c + 0.623FAD_m + 18ADP_c + 18P_c$

$R11.5)\ 4.299Protein_c + 0.194RNA_c + 0.030DNA_c + 0.126Lipid_c + 0.408Chit_c + 1.515Glcn_c + 0.002Glgn_c + 0.213Man_c + 0.090Grol_c + 46.3ATP_c + 46.3H_2O_c \Rightarrow Biomass(1g_{DW}) + 46.3ADP_c + 46.3P_c$

Maintenance Requirements

$R12.1)\ ATP_c + H_2O_c \Rightarrow ADP_c + P_c$

Mitochondrial Membrane Transport Systems

$R13.1)\ ATP_m + ADP_c \Leftrightarrow ADP_m + ATP_c$

$R13.2)\ P_c + H_c \Leftrightarrow P_m + H_m$

$R13.3)\ Succ_c + Mal_m \Leftrightarrow Succ_m + Mal_c$

$R13.4)\ ICit_m + Cit_c \Leftrightarrow ICit_c + Cit_m$

$R13.5)\ Ctl_m + H_c \Leftrightarrow Ctl_c + H_m$

$R13.6)\ Mal_m + P_c \Leftrightarrow Mal_c + P_m$

R13.7) $ILeu_m + H_c \Leftrightarrow ILeu_c + H_m$

R13.8) $Pyr_c + H_c \Leftrightarrow Pyr_m + H_m$

R13.9) $CO_{2,m} \Leftrightarrow CO_{2,c}$

R13.10) $Fum_c + H_c \Leftrightarrow Fum_m + H_m$

R13.11) $Cit_m + Mal_c \Leftrightarrow Cit_c + Mal_m$

R13.12) $Glu_c + H_c \Leftrightarrow Glu_m + H_m$

R13.13) $Gln_c + H_c \Leftrightarrow Gln_m + H_m$

R13.14) $Val_m + H_c \Leftrightarrow Val_c + H_m$

R13.15) $\beta IPM_m + H_c \Leftrightarrow \beta IPM_c + H_m$

R13.16) $AcCoA_c + CoA_m \Leftrightarrow CoA_c + AcCoA_m$

R13.17) $O_{2,c} \Leftrightarrow O_{2,m}$

R13.18) $Ac_m \Leftrightarrow Ac_c$

R13.19) $\alpha AAd_m \Leftrightarrow \alpha AAd_c$

R13.20) $\alpha KB_c + H_c \Leftrightarrow \alpha KB_m + H_m$

R13.21) $Asp_m + Glu_c \Leftrightarrow Asp_c + Glu_m$

R13.22) $Pro_c + H_m \Leftrightarrow Pro_m + H_c$

R13.23) $Acact_c \Leftrightarrow Acact_m$

R13.24) $Orn_c + H_m \Leftrightarrow Orn_m + H_c$

R13.25) $H_2O_m \Leftrightarrow H_2O_c$

Peroxisomal Membrane Transport Systems

R14.1) $Succ_p + ICit_c \Leftrightarrow Succ_c + ICit_p$

R14.2) $ICit_c + Mal_p \Leftrightarrow ICit_p + Mal_c$

R14.3) $Mal_p + H_p \Leftrightarrow Mal_c + H_c$

R14.4) $ATP_c + H_2O_c + H_c \Rightarrow ADP_c + P_c + H_p$

R14.5) $AcCoA_c + CoA_p \Leftrightarrow CoA_p + AcCoA_p$

R14.6) $H_2O_p \Leftrightarrow H_2O_c$

Other Reactions

R15.1) $Pyr_c \Rightarrow Aald_c + CO_{2,c}$

R15.2) $Clc_c + 0.5O_2, c \Rightarrow Gluc_c$

R15.3) $OA_c + H_2O_c \Rightarrow Ox_c + Ac_c$

R15.4) $Gluc_c + ATP_c \Rightarrow Gu6P_c + ADP_c$

Appendix D- Calibration Curves and LabVIEW Diagrams

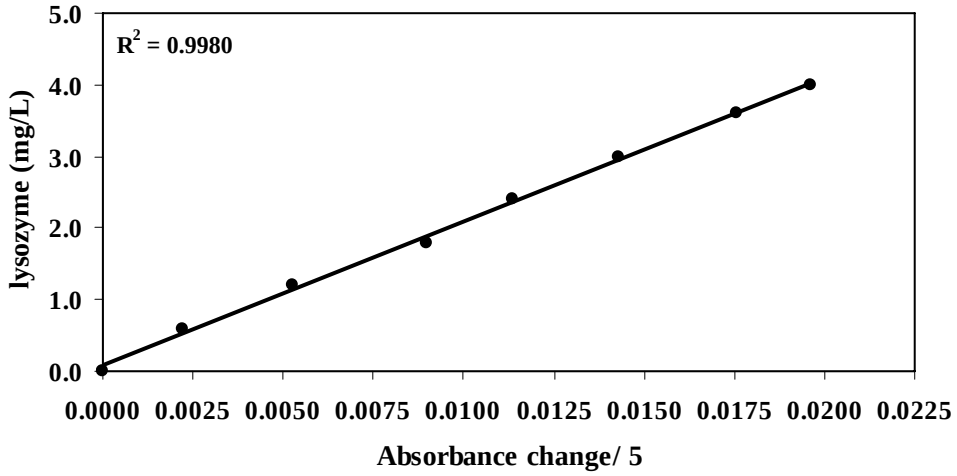

Figure D.1- A typical standard curve for determining lysozyme concentration from the decrease in absorbance over a 5 minutes period.

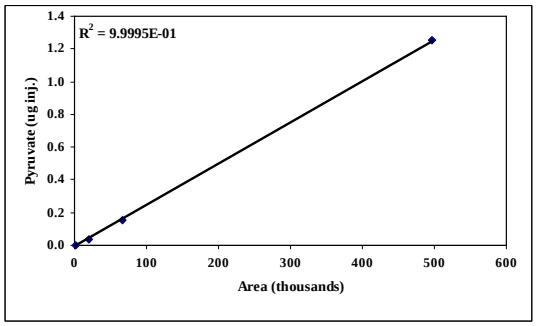

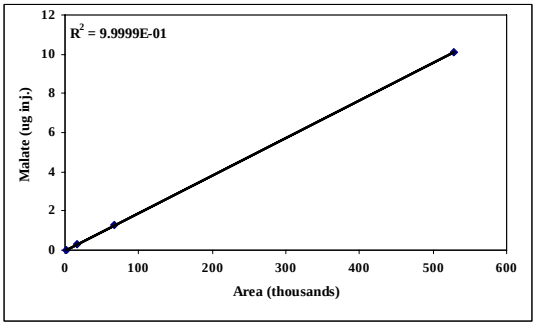

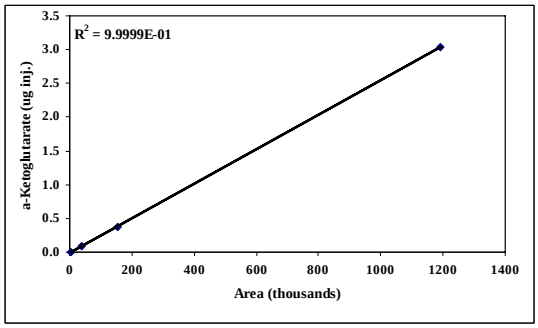

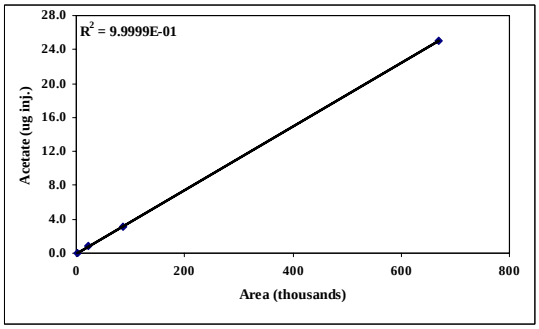

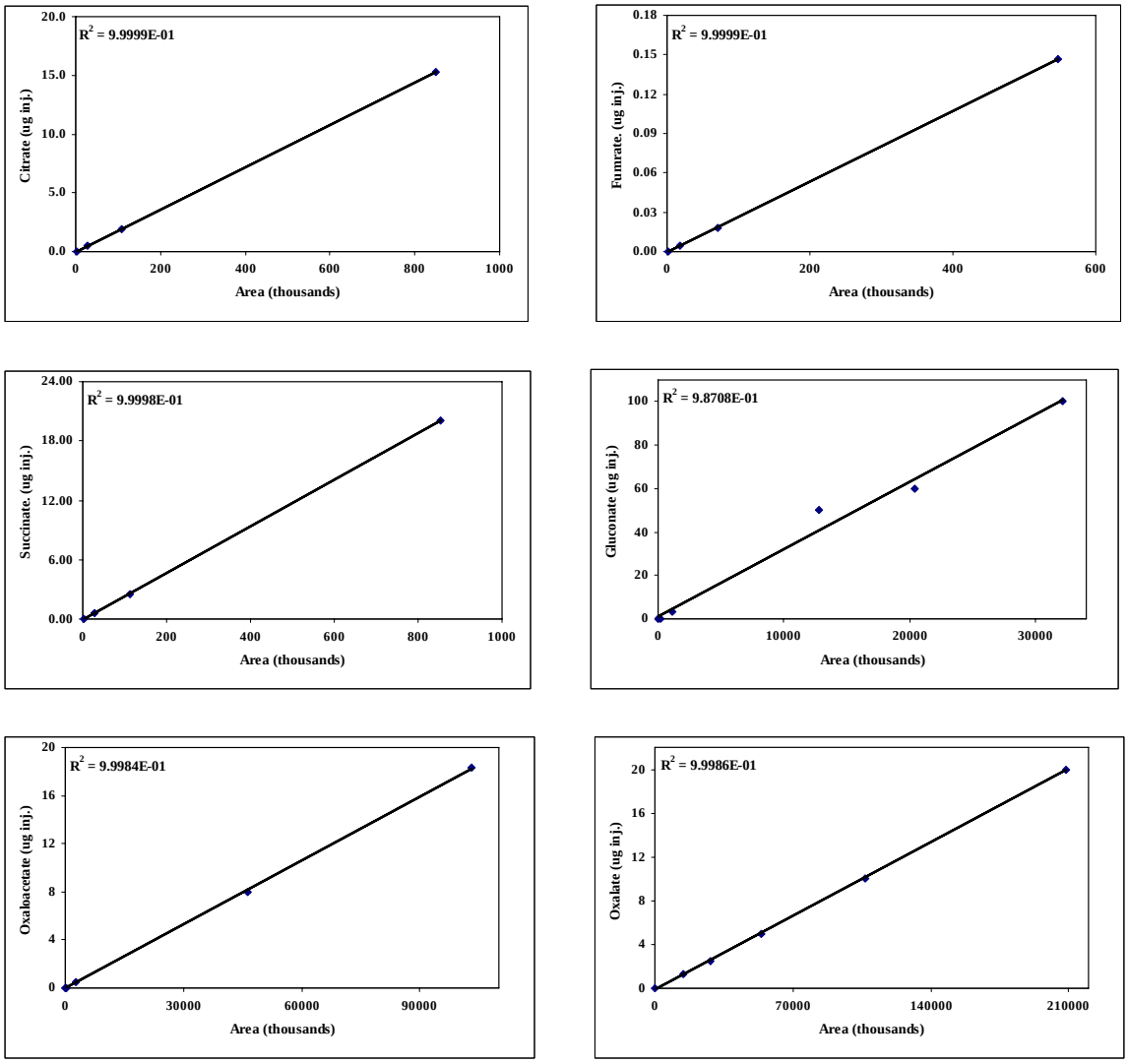

Figure D.2- The typical standard curves of organic acids.

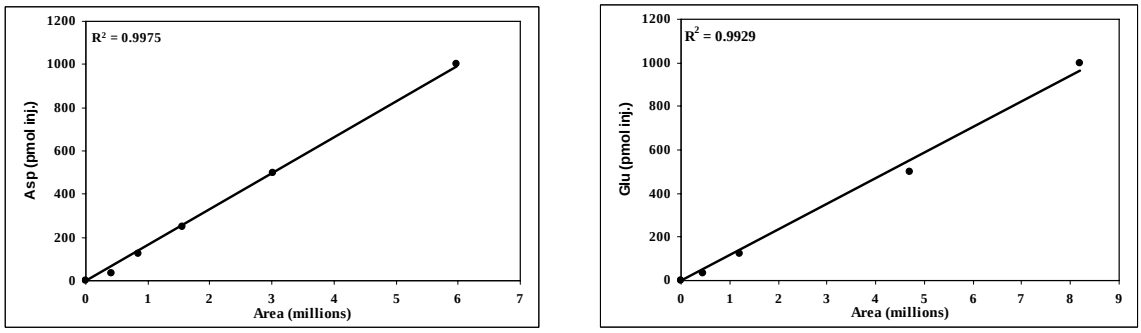

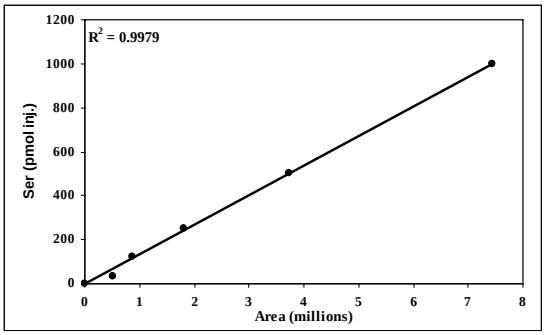
R2 = 0.9979
Ser (pmol inj.)
Area (millions)

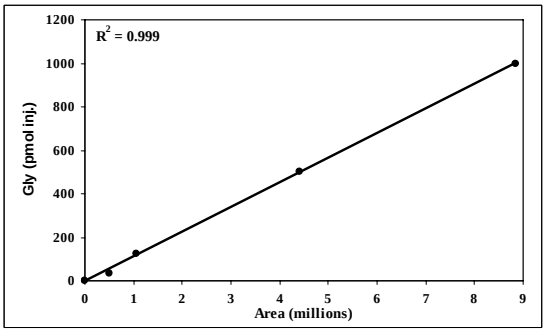
R2 = 0.999
Gly (pmol inj.)
Area (millions)

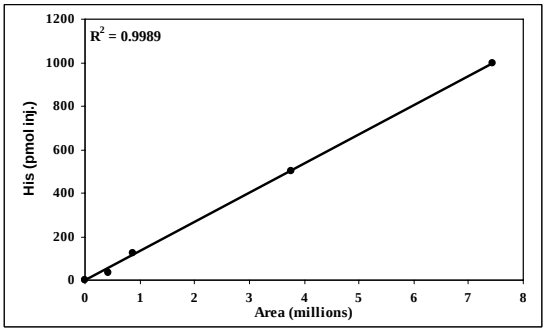
R2 = 0.9989
His (pmol inj.)
Area (millions)

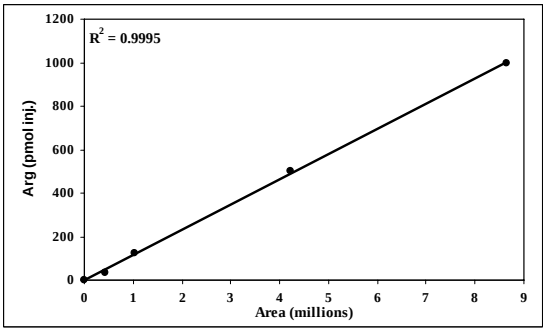
R2 = 0.9995
Arg (pmol inj.)
Area (millions)

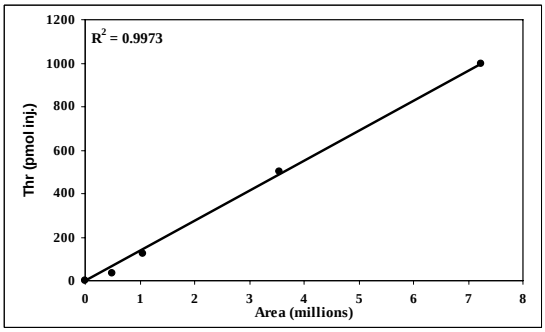
R2 = 0.9973
Thr (pmol inj.)
Area (millions)

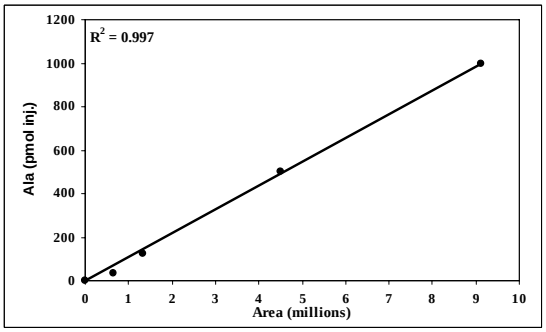
R2 = 0.997
Ala (pmol inj.)
Area (millions)

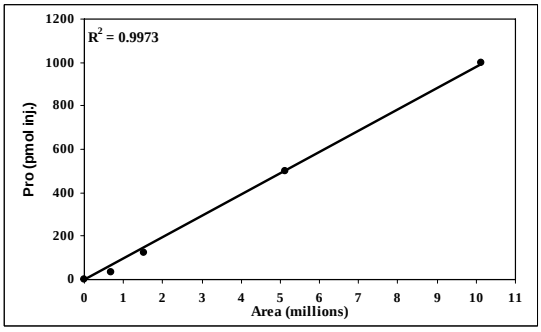
R2 = 0.9973
Pro (pmol inj.)
Area (millions)

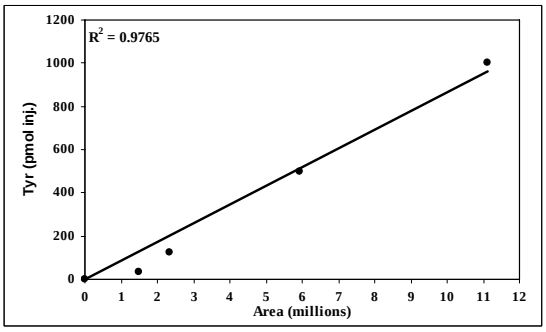
R2 = 0.9765
Tyr (pmol inj.)
Area (millions)

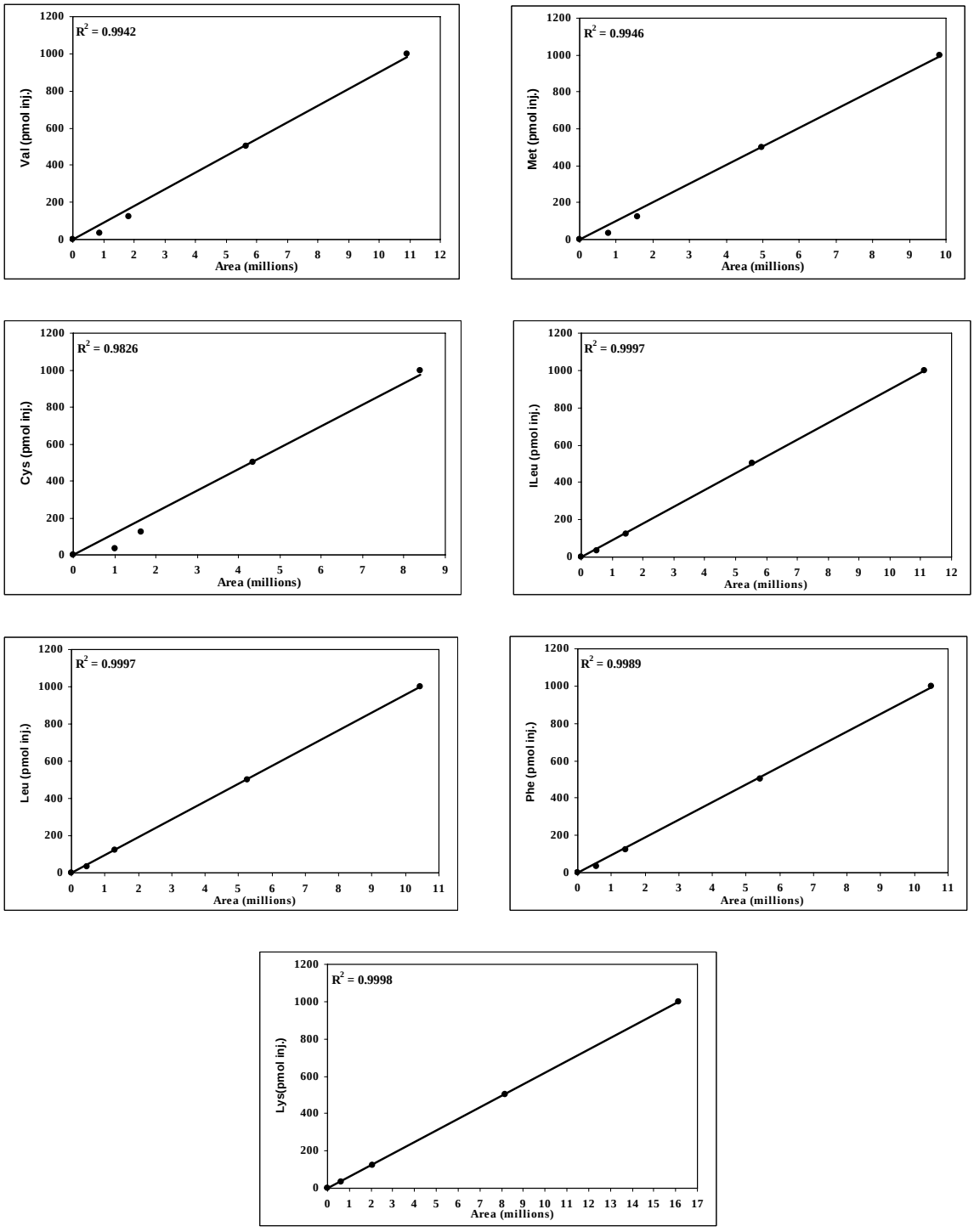

Figure D.3- The typical standard curves of amino acids.

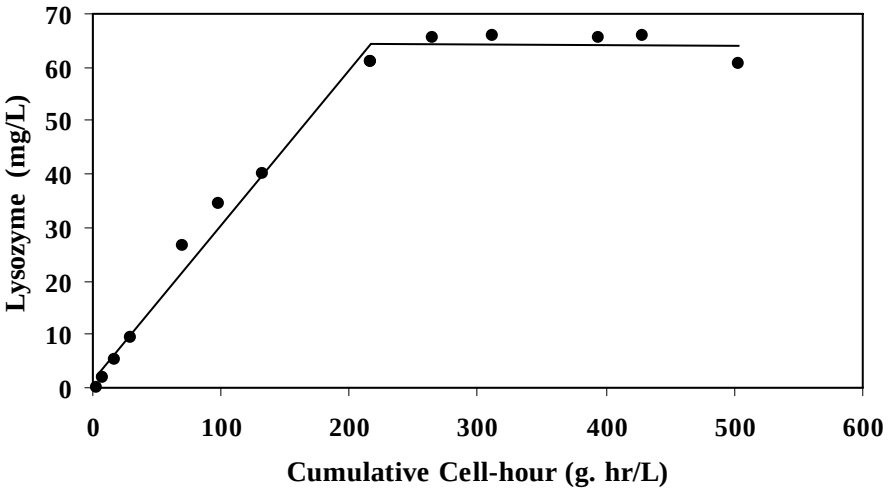

Figure D. 4- Dependence of lysozyme production on cell growth.

a) On time

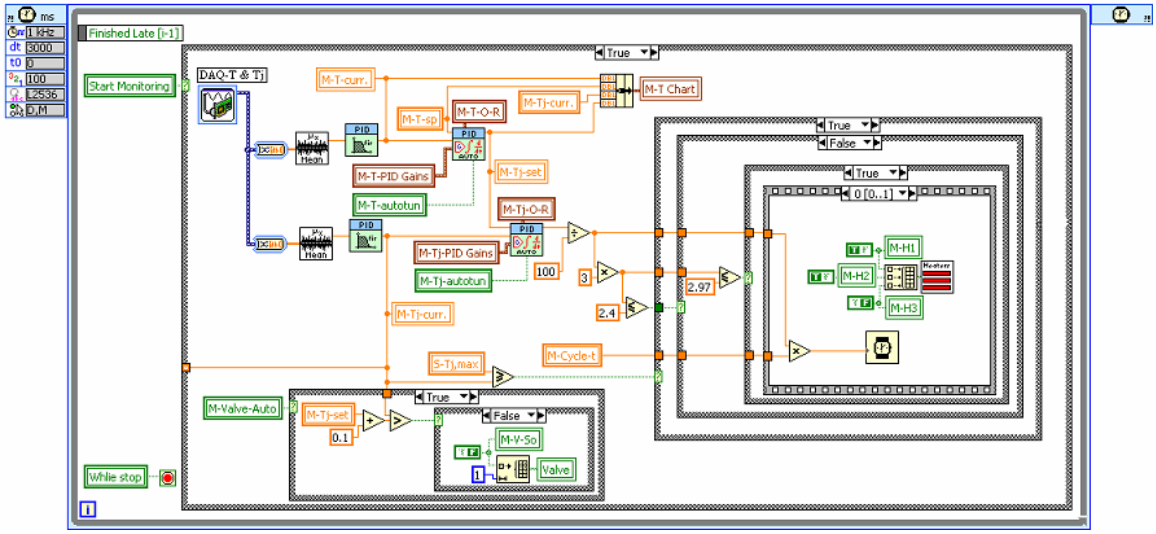

b) Off time

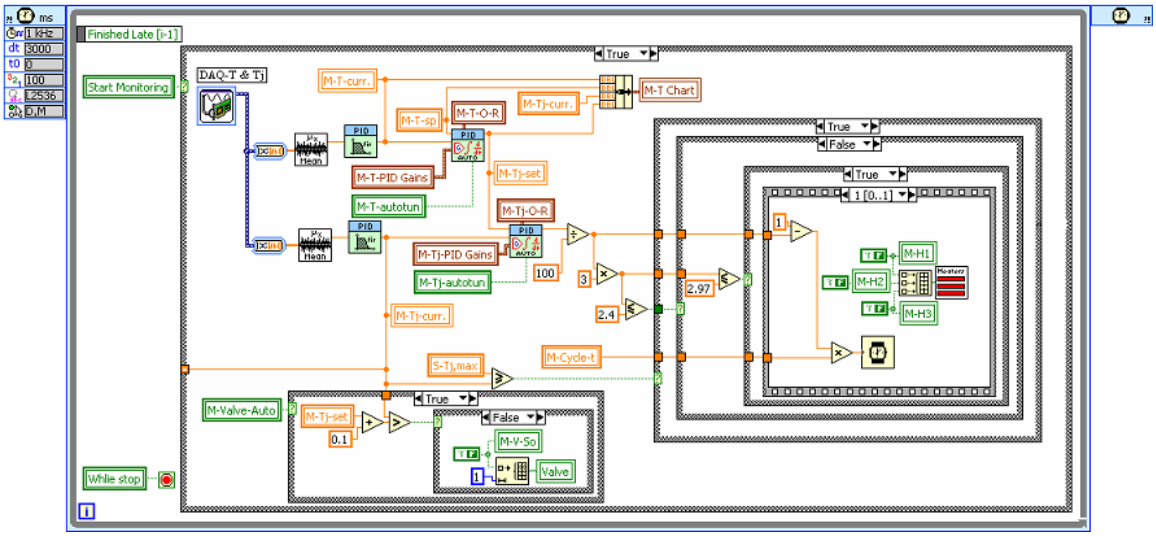

Figure D.5- The block diagram of LabVIEW for cascade temperature control. The fraction of cycle time that the assigned heaters are: a) on and b) off.

a) Front panel

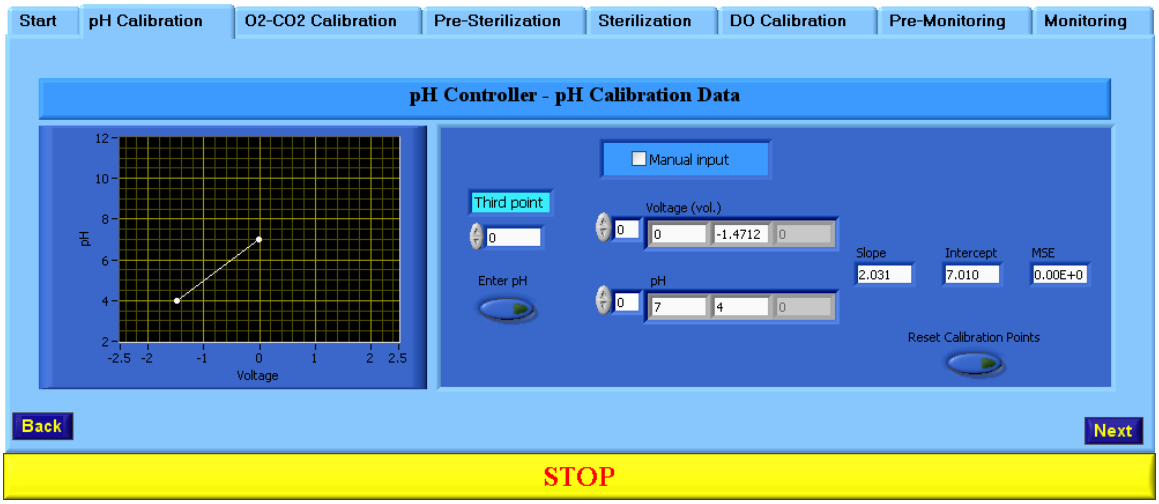

b) Block diagram

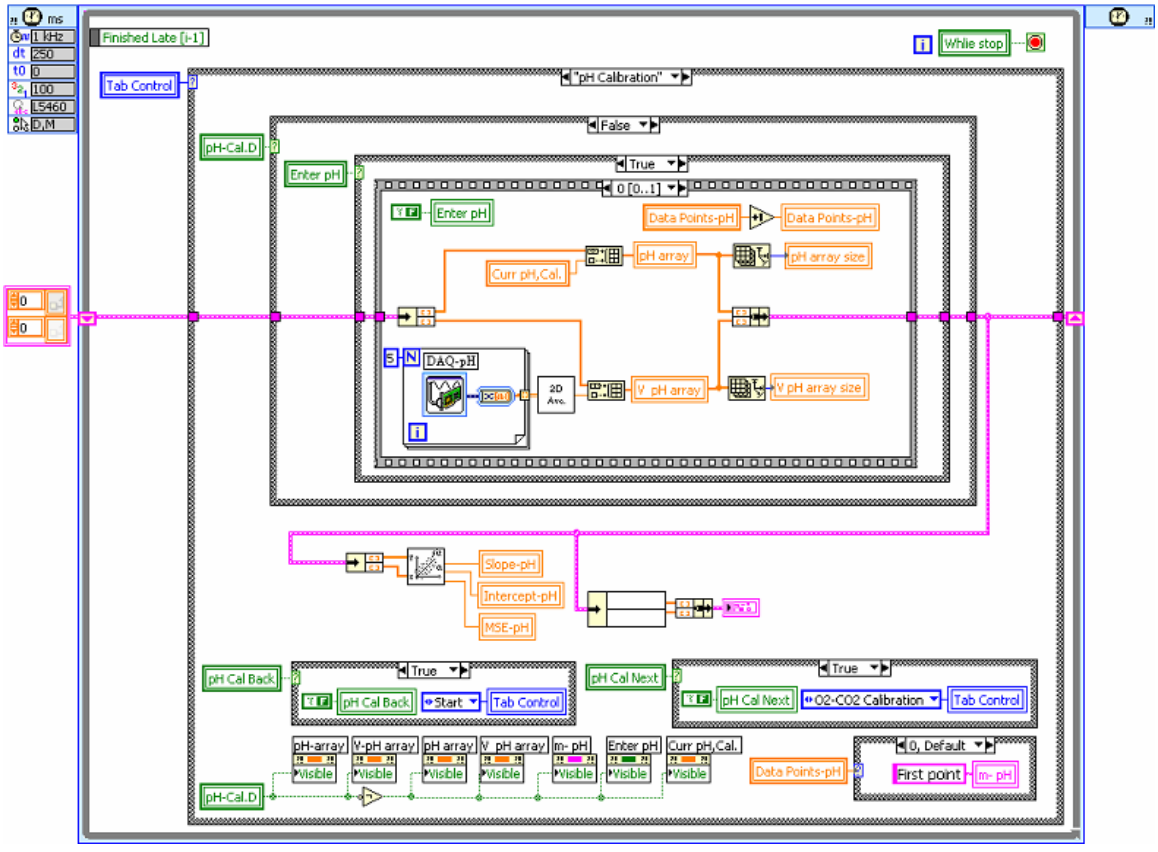

Figure D.6- Front panel and block diagram of LabVIEW program for pH calibration.

Table D. 1.1- Extracellular concentration of measured metabolites during 0-54 hr of the fermentation

Metabolite	Unit	0 hr	12 hr	24 hr	30 hr	36 hr	78 hr	54 hr
Glc	g/L	20.165	15.804	5.00	0.014	0.004	0.007	0.008
Lysozyme	mg/L	0.08	0.17	1.97	5.06	9.4	26.71	34.55
Biomass	g/L	0.17	0.20	0.96	2.79	3.10	3.85	4.59
Glun	g/L	0.97	5.40	15.31	16.20	14.75	12.00	11.00
Ox	g/L	0.07	0.21	0.35	0.44	0.55	1.50	1.93
Pyr	g/L	0.0001	0.0027	0.0108	0.0158	0.0199	0.0344	0.0401
Ac	g/L	0.010	0.140	0.145	0.095	0.080	0.070	0.030
Succ	g/L	0.005	0.178	0.280	0.039	0.248	0.069	0.063
a-KG	g/L	0.0010	0.0100	0.0105	0.0129	0.0132	0.0128	0.0118
Cit	g/L	1.283	1.325	1.276	1.287	1.106	0.657	0.349
OA	g/L	0.0010	0.0125	0.0408	0.0564	0.0580	0.0462	0.0359
Mal	g/L	0.000	0.000	0.000	0.000	0.000	0.000	0.000
Fum	g/L	0.000	0.000	0.000	0.000	0.000	0.000	0.000
Ala	g/L	0.418	0.422	0.417	0.464	0.423	0.299	0.136
Arg	g/L	0.256	0.275	0.279	0.289	0.298	0.277	0.254
Asn	g/L	0.218	0.245	0.244	0.290	0.295	0.256	0.211
Asp	g/L	0.000	0.000	0.000	0.000	0.000	0.000	0.000
Cys	g/L	0.000	0.045	0.039	0.058	0.046	0.032	0.028
Gln	g/L	0.405	0.436	0.413	0.434	0.402	0.350	0.299
Glu	g/L	0.000	0.000	0.000	0.000	0.000	0.000	0.000
Gly	g/L	0.330	0.328	0.307	0.392	0.443	0.397	0.350
His	g/L	0.041	0.037	0.035	0.035	0.035	0.035	0.034
Ileu	g/L	0.116	0.074	0.069	0.074	0.074	0.069	0.068
Leu	g/L	0.181	0.127	0.109	0.106	0.102	0.087	0.075
Lys	g/L	0.150	0.154	0.152	0.162	0.172	0.162	0.155
Met	g/L	0.036	0.019	0.027	0.028	0.033	0.024	0.023
Phe	g/L	0.149	0.098	0.081	0.063	0.053	0.022	0.010
Pro	g/L	0.391	0.383	0.277	0.163	0.111	0.086	0.082
Ser	g/L	0.065	0.063	0.065	0.065	0.067	0.051	0.043
Thr	g/L	0.049	0.040	0.035	0.035	0.034	0.025	0.019
Trp	g/L	0.000	0.000	0.000	0.000	0.000	0.000	0.000
Tyr	g/L	0.043	0.025	0.020	0.002	0.003	0.002	0.002
Val	g/L	0.140	0.117	0.111	0.121	0.117	0.107	0.099
Ammonia	g/L	0.723	0.715	0.662	0.517	0.508	0.487	0.472
Phosphate	g/L	1.155	1.152	1.078	0.931	0.872	0.784	0.725
Sulfate	g/L	2.850	2.846	2.803	2.774	2.765	2.755	2.752

Table D.1.2- Extracellular concentration of measured metabolites during 60-120 hr of the fermentation

Metabolite	Unit	60 hr	72 hr	78 hr	84 hr	96 hr	102 hr	120 hr
Glc	g/L	0.009	0.010	0.011	0.010	0.012	0.013	0.013
Lysozyme	mg/L	39.97	60.97	65.64	66.00	65.64	66.00	60.62
Biomass	g/L	6.27	7.83	8.31	7.63	6.10	5.50	3.03
Glun	g/L	8.40	3.08	0.60	0.23	0.05	0.03	0.02
Ox	g/L	2.95	4.11	4.63	4.95	5.10	5.33	5.57
Pyr	g/L	0.0675	0.0730	0.0735	0.0342	0.0177	0.0094	0.0000
Ac	g/L	0.02	0.016	0.009	0.005	0.000	0.000	0.000
Succ	g/L	0.0622	0.0357	0.0312	0.0108	0.0141	0.0065	0.0094
a-KG	g/L	0.0108	0.0088	0.0083	0.0086	0.0083	0.0068	0.0045
Cit	g/L	0.0299	0.0102	0.0048	0.0034	0.0037	0.0035	0.0039
OA	g/L	0.0250	0.0080	0.0010	0.0008	0.0002	0.000	0.000
Mal	g/L	0.000	0.000	0.000	0.000	0.000	0.000	0.000
Fum	g/L	0.000	0.000	0.000	0.000	0.000	0.000	0.000
Ala	g/L	0.071	0.009	0.000	0.000	0.000	0.000	0.000
Arg	g/L	0.223	0.070	0.000	0.000	0.000	0.000	0.000
Asn	g/L	0.173	0.073	0.013	0.000	0.000	0.000	0.000
Asp	g/L	0.000	0.000	0.000	0.000	0.000	0.000	0.000
Cys	g/L	0.000	0.000	0.000	0.000	0.000	0.000	0.000
Gln	g/L	0.238	0.029	0.003	0.000	0.000	0.000	0.000
Glu	g/L	0.000	0.000	0.000	0.000	0.000	0.000	0.000
Gly	g/L	0.354	0.047	0.049	0.062	0.040	0.033	0.040
His	g/L	0.033	0.052	0.048	0.059	0.051	0.043	0.059
Ileu	g/L	0.052	0.007	0.001	0.001	0.001	0.001	0.001
Leu	g/L	0.052	0.005	0.000	0.000	0.000	0.000	0.000
Lys	g/L	0.157	0.131	0.117	0.110	0.060	0.013	0.000
Met	g/L	0.021	0.000	0.000	0.000	0.000	0.000	0.000
Phe	g/L	0.006	0.006	0.007	0.007	0.007	0.007	0.005
Pro	g/L	0.062	0.000	0.000	0.000	0.000	0.000	0.000
Ser	g/L	0.040	0.041	0.029	0.016	0.009	0.005	0.000
Thr	g/L	0.008	0.002	0.000	0.000	0.000	0.000	0.000
Trp	g/L	0.000	0.000	0.000	0.000	0.000	0.000	0.000
Tyr	g/L	0.000	0.000	0.000	0.000	0.000	0.000	0.000
Val	g/L	0.084	0.038	0.028	0.030	0.028	0.028	0.028
Ammonia	g/L	0.468	0.464	0.459	0.558	0.681	0.758	0.790
Phosphate	g/L	0.706	0.686	0.657	0.735	0.823	0.902	1.029
Sulfate	g/L	2.754	2.756	2.736	2.688	3.072	3.264	3.552